# Influence of pile radius on kinematic and inertial responses of pile groups

（地盤変形と慣性力を受ける群杭基礎の応答特性に及ぼす杭径寸法の影響）

**2018** 年 **03** 月

埼玉大学大学院理工学研究科（博士後期課程）

理工学専攻（主指導教員齊藤正人）

**Mostafa Faghihnia Torshizi**

# Influence of pile radius on kinematic and inertial responses of pile groups

A dissertation submitted for the partial fulfillment of the requirements for the Degree of

Doctor of Philosophy

Submitted by

**Mostafa Faghihnia Torshizi**

Supervised by

Professor Masato Saitoh


Department of Civil and Environmental Engineering

Graduate School of Science and Engineering

Saitama University

Japan

March, 2018

# CHAPTER 1

# INTRODUCTION

During strong earthquakes, propagation of seismic waves through soil medium induces deformations in the soil that excite embedded piles by imposing a spatially-variable displacement field. Such displacement field will then generate, as the result of "kinematic interaction" ([1.1]~[1.3]), bending and shearing along the entire length of the pile. This is different from the bending and shearing generated by the inertial forces produced by the vibrating superstructure (as the result of "inertial interaction"). An increasing number of research contributions estimating the kinematic response of soil-pile-structure systems has become available in recent times ([1.4]~ [1.18]), many of which are based on analytical formulations ([1.4]~ [1.7]).

Previous earthquake events of Mexico City (Mexico) in 1985, Kobe (Japan) in 1995, and Chi Chi (Taiwan) in 1999 have highlighted the sensitivity of pile foundations to damage in dominance of kinematic interaction. Especially, in kinematic interactions, damages appear either at the pile head or deep down the pile where inertial forces are vanishingly small. The observed field data in the past in conjunction with theoretical studies have revealed three possibilities of damage due to kinematic bending along fixed head piles: (1) near restraining pile cap; (2) interfaces between soil layers; and (3) the toe of the pile. Generally, damage due to the kinematic bending occurs at the pile head in homogeneous soil layers and in the presence of a stiff restraining cap [1.11]. However, the possibility of damage at the interface between soil layers will increase in layered soil media with strong discontinuities [1.8]. A number of design-oriented researches ([1.8]~ [1.11]) have contributed to simple solutions, allowing the estimation of kinematic pile moments at the interface between two consecutive layers with significantly differing stiffness. Studies indicate that the kinematic bending strains at these interfaces could exceed the bending strains at the head of the pile depending on the soil layers stiffness contrast, the pile-soil stiffness contrast, and the relative thickness of

the soil layers with respect to the length of the pile. It has been shown that both in homogeneous and layered soils, when the toe is strongly restrained, the kinematic bending strains may dominate [1.12]. Therefore, the importance of kinematic loading on the seismic performance of piles has been recognized by modern seismic codes including Eurocode 8 and the Italian national provisions ([1.19], [1.20]). For example Eurocode 8 states that: 'piles should be designed to resist the following two types of effects: (i) inertia forces from the vibrating superstructure…; (ii) kinematic forces arising from the passage of seismic waves and thereby will impose lateral strain on the piles. Therefore, in seismic design, the kinematic bending and inertial bending must be considered simultaneously when assessing the performance of a pile.

In seismic design, pile radius plays an important role because it directly affects the bending stiffness of a pile ( $EI$) and subsequently seismic performance of a pile. For homogeneous soil it is assumed that piles are not exposed to significant kinematic forces, therefore only inertial forces of a superstructure are considered for design issues. Based on this concept, increasing the pile radius is often an appropriate solution in reducing the bending strains. In contrary to this perception which is reflected in seismic Codes, kinematic bending may not be negligible compared to inertial bending. In soft soils and large pile diameters regardless of seismic intensity, kinematic bending may dominate over inertial one at the pile head. Therefore, under the dominance of kinematic interaction even for homogeneous soil, specific techniques are needed to minimize the bending strains. Also the importance of pile radius in seismic design is not understood well and not covered by seismic codes ([1.5],[1.13]) .

## 1.1 Influence of pile radius in soil-pile interaction

A number of investigators have argued the importance of the pile radius in kinmatically-loaded piles. A simple method for evaluation of the effect of kinematic forces on pile bending developed in the pioneering studies of Margason [1.7] and Margason and Holloway [1.8]. These researches are known as the first to distinguish the significance of pile radius and suggest using large radius piles as they can conform easier to seismically-induced soil deformations. Their method for assessing kinematic pile bending suffers from

several drawbacks. For instance, it is assumed that the pile follows the surrounding soil motion and the interaction between pile and soil is neglected. Moreover it lacks developing rational analysis. Only a few research efforts focused on the effect of pile radius on kinematic bending of piles, most of them conducted in the proximity of deep interfaces separating soil layers of different stiffness ([1.5],[1.10],[1.16]) .

Saitoh [1.14] proposed a technique in order to obtain the optimal pile radius (defined as the radius for which the bending strains in the pile are minimum) of a fixed-head cylindrical vertical single pile embedded in a homogeneous elastic soil layer and supported by a rotationally compliant bedrock. His theoretical model is identical to those described in Tajimi [1.15] and Ohira et al [1.13], and the frequency of excitation is assumed to be equal to the fundamental frequency of the soil medium. In his research, variation in both inertial and kinematic bending strains against the slenderness ratio ($r/H$) (radius) was also investigated individually. It was shown that the normalized inertial bending strain descends rapidly as the slenderness ratio increases. Further, the kinematic bending strains approach zero when the slenderness ratio ($r/H$) tends to zero. The value of the kinematic bending strain increases approximately linearly up to the local maximum ($r/H \approx 0.1$), but gradually decreases afterwards. Kinematic and inertial bending strain were calculated separately and the resultant effects were superimposed into one as the combined total bending strain. The variation of normalized total bending strains with slenderness ratio ($r/H$) implies that a slenderness ratio that minimizes the normalized bending strains at the head of piles may appear. Moreover, in a higher region (larger slenderness ratios) where kinematic bending dominates over inertial bending a local maximum of the normalized total bending strain may also appear (Figure 1.1).

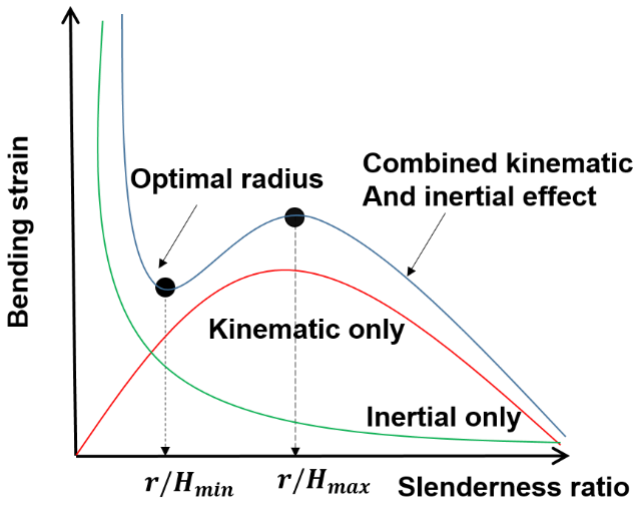


**Figure 1.1:** Kinematic and inertial bending moments as function of pile radius.

Dezi et al [1.16] conducted parametric analysis of single fixed-head piles with consideration of varying the important parameters governing the response of kinematically excited piles. Influence of different parameters such as diameter, bedrock depths and shear wave velocity of the deposit has been taken into account for performing a comprehensive parametric analysis. Furthermore, empirical formulas for design purposes have been proposed to accomplish evaluation of the induced bending moments at the pile head and at the deposit-bedrock interface. They mentioned that the pile radius significantly influences the amplitudes of the bending moments at the pile head and at the interface between soil layers: for a given soil deposit, the bending moment increases while the pile radius increases.

Di Laora et al [1.22] explored the role of pile radius in seismic induced loads at the pile head under a restraining cap, with reference to steel piles in homogeneous soil layer. Their research results indicated that kinematic bending moments at the pile head depend on the fourth power of pile diameter *d*, whereas inertial bending moments are proportional to the second or third power, this shows that kinematic moments will dominate seismic demand with increasing pile diameter and there will exist a maximum diameter beyond which a pile will experience failure. The value of the maximum pile diameter was found to depend on peak ground acceleration, soil stiffness and factor of safety against gravity loading. Also they established the

combined action of kinematic and inertial moments at the pile head, which in reality interact adversely with each other, the simultaneous presence of these actions provides a limited range of permissible radius, with the upper bound (maximum diameter) governed by dominance of kinematic action, and the lower one (minimum diameter) by inertial action. This range is narrower than that obtained for the kinematic and inertial actions considered individually.

Mylonakis et al [1.23] inspected the role of pile diameter in seismically-induced bending for both steel and concrete piles in homogeneous soils as well as soils with stiffness increasing proportionally with depth. A number of closed-form expressions for kinematic and inertial bending moments were presented, based on which minimum and maximum admissible pile diameters were defined, Moreover based on their research results, following points are worthy of mention: (i) for soft soil with constant stiffness, kinematic interaction has a dominant influence and as a result maximum admissible pile size will attain small values. Under these conditions, adding more piles or increasing pile length will not guarantee safety against bending failure; (ii) in stiffer soil deposits, inertial interaction will dominate. Therefore, a minimum admissible pile diameter are provided by inertial interaction which may be quite large for areas vary from moderate to high seismicity; (iii) main important parameters such as ground acceleration, pile length, soil strength, soil stiffness, pile safety factor and amount of reinforcement control the range of admissible pile diameters. Therefore, it could be concluded that pile material strength has insignificant role in controlling pile size. In other words geotechnical and geometrical properties seem to be more significant than the structural properties; (iv) among all diameters which are admissible for a wide range of parameters, always an optimal pile radius that prevent bending failure exists. This diameter will be beneficial as a guidance in designing piles in earthquake prone areas.

## 1.2 Objectives

At present it seems that certain aspects of the pile bending are well understood while others remain unresolved. Yet, there has been no investigation dealing with the effect of pile radius on the bending strains

at the pile head in soil-pile groups systems where kinematic interaction dominates even for the simple case of homogeneous soil layer. The problem appears to be important, because the pile head is stressed by both kinematic and inertial forces. Therefore in order to establish a criteria for optimal pile radius for both inertially and kinematically excited pile groups, it is essential to quantify variations of both inertial and kinematic bending strains with respect to pile radius in a systematic way. This dissertation focuses on obtaining a comprehensive relation between the pile radius and the bending strains at the head of a cylindrical vertical pile groups under kinematic loading. For the sake of simplicity and in order to perceive basic characteristics of the pile groups, piles are considered to be embedded in a homogeneous elastic stratum resting on a rigid bedrock, being the piles length identical to the thickness of the soil stratum. Two different constraint conditions are considered at the pile tip: (a) hinged tip, and (b) end-bearing (fixed) tip.

Nikolaou et al [1.9] performed a parametric investigation on the kinematic bending strains in a single pile embedded in both homogeneous and layered soil deposit and subjected to harmonic steady-state shear waves and proposed a closed-form expression for the evaluation of the maximum bending moment at the interface between layers. One of the most important conclusions that have revealed from their analysis is that in most cases, the maximum bending strain occurs at the fundamental natural period of the soil deposit. The variation of kinematic bending strain with frequency follows, more or less, the amplification of the free-field acceleration. This signifies the influence of the first mode of vibration on the magnitude of bending strain. In fact the curvature is affected by the overall drift between the top and the bottom of the pile. This drift usually becomes maximum at the first mode of vibration, and thereby generates the largest bending moment at the first resonance.Therefore with an understanding that the maximum value of kinematic bending strains at the head of a pile occurs at the fundamental frequency of the soil stratum for most of the soil profiles, such specific frequency is targeted in the present work. Analytical formulations are obtained based on the beam-on-dynamic-Winkler-foundation method.

## 1.3 Organization

**Chapter 1:** A brief introduction to the role pile diameter and optimal pile radius in seismic performance of the piles as well as literature review are presented.

**Chapter 2:** This chapter details the methodology employed for the problem of dynamic pile-soil interaction. Pile-soil interaction is realistically represented through a dynamic Winkler model, frequency-dependent Winkler dashpots and springs are obtained through an improved plain strain model. This model is free of the shortcomings of the two-dimensional plane strain model and it allows for cutoff frequency of the homogeneous soil layer to be incorporated. Pile-to-pile interaction is taken into account through an approximate three-step wave-interference solution in which simple cylindrical wave field originates along each pile shaft and spreads outward. Closed form solutions are obtained for: (i) the complex-valued Winkler modulus, (ii) the displacement field in the soil and the pile in fundamental frequency of the homogeneous soil layer. The simplicity of the approximate method offers an efficient alternative to complex numerical solutions.

**Chapter 3:** In this chapter fixed-head pile groups in a homogeneous viscoelastic soil stratum over a rigid base with different tip conditions are considered to be imposed by inertial head loading. Pile-soil interaction, incorporating group effects in pile groups, is represented through a simplified beam-on-dynamic-Winkler –foundation (BDWF) model with realistic frequency-dependent springs and dashpots. Closed form expressions for inertial interaction factors and curvature ratios atop the pile are presented. On the basis of the three-step methodology of the chapter two, the inertial bending strains at the head of the piles in fundamental frequency of the homogeneous soil layer are derived. The inertial bending strains are normalized with respect to a mean shear strain of the soil medium. The variation of normalized inertial bending strains are expressed by the radius to height ratio of the piles, the ratio of soil to pile stiffness, and a factor representing the relative amplitude and the phase lag between the inertial loading at the head of the

piles and the deformation of the ground. Rigorous numerical solutions based on coupled finite elements-boundary elements (FE-BE) are employed to verify the predictions of the proposed method.

**Chapter 4:** In this chapter fixed-head pile groups in a homogeneous viscoelastic soil stratum over a rigid base with different tip conditions are considered to be provoked by vertical impinging seismic shear waves. Pile-soil interaction, incorporating group effects in pile groups, is represented through a simplified beam-on-dynamic-Winkler –foundation (BDWF) model with realistic frequency-dependent springs and dashpots. Closed form expressions for kinematic interaction factors and curvature ratios atop the pile are presented. On the basis of the three-step methodology of the chapter two, the kinematic bending strains at the head of the piles in fundamental frequency of the homogeneous soil layer are derived. The kinematic bending strains are normalized with respect to a mean shear strain of the soil medium. The variation of normalized kinematic bending strains are expressed by the radius to height ratio of the piles. Rigorous numerical solutions based on coupled finite elements-boundary elements (FE-BE) are employed to verify the predictions of the proposed method. In order to investigate main characteristics of the normalized kinematic bending strains in pile groups, parametric studies which encompass different parameters are carried out.

**Chapter 5:** In this chapter fixed-head pile groups in a homogeneous viscoelastic soil stratum over a rigid base with different tip conditions are considered to be provoked simultaneously by vertical impinging seismic shear waves and inertial head loading. According to chapters three and four, kinematic and inertial bending strain are calculated separately. Afterwards, superposition method are applied readily to determine the combined total normalized bending strains in pile groups. The variation of normalized inertial bending strains are expressed by the radius to height ratio of the piles, the ratio of soil to pile stiffness, and a factor representing the relative amplitude and the phase lag between the inertial loading at the head of the piles and the deformation of the ground. In order to determine the appropriate radius (optimal radius) in pile groups, influence of different parameters (factor of relative amplitude and phase lag between inertial loading and soil deformations, the pile-soil stiffness ratio, pile spacing and the number of piles) are

implemented through parametric studies. Three different methods (average, weighted average and envelope) are introduced for estimating the optimal pile radius in pile groups.

**Chapter6**: Conclusions and recommendations for future research are presented.

## References


[1.1] Roesset, JM., Whitman, RV., Dobry, R. (1973) Modal analysis for structures with foundation interaction. *Journal of the Structural Division*, 99:ST3, 399-416.

[1.2] Wolf, JP. (1985) Dynamic soil-structure interaction. *Prentice-Hall*, New York.

[1.3] Gazetas, G. and Mylonakis, G. (1998) Seismic soil-structure interaction: new evidence and emerging issues. In: Dakoulas P, Yegian EvlK, Holtz RD, editors. *Geotechnical earthquake engineering and soil dynamics*, ASCE.

[1.4] Dobry, R. O'Rourke, MJ. (1983) Discussion on "Seismic response of end-bearing piles" by Flores-Berrons R & Whitman RV". *Journal of the Geotechnical Engineering Division*, 109(5):778-81.

[1.5] Mylonakis, G. (2001) Simplified model for seismic pile bending at soil layer inter-faces. *Soils and Foundations*, 41(4), 47-58.

[1.6] Flores-Berrones, R., Whitman, RV. (1982) Seismic response of end-bearing piles. *Journal of Geotechnical Engineering Division* ASCE, 108(4):554-69.

[1.7] Margason E. Pile bending during earthquake. (1975) Lecture ASCE/UC-Berkeley seminar on *design construction & performance of deep foundation*.

[1.8] Margason E, Holloway DM (1977) Pile bending during earthquakes. In: Sarita Prakashan (ed) *Proceedings of 6$^{th}$ world conference on earthquake engineering*, Meerut, vol II, pp 1690-1696

[1.9] Nikolaou, S., Mylonakis, G., Gazetas, G., Tazoh, T. (2001) Kinematic pile bending during earthquakes: analysis and field measurements. *Géotechnique*; 51(5):425-40.

[1.10] Maiorano, RMS., de Sanctis, L., Aversa, S., Mandolini, A. (2009) Kinematic response analysis of piled foundations under seismic excitations. *Canadian Geotechnical Journal*; 46(5):571-84.

[1.11] Sica, S., Mylonakis, G., Simonelli, AL. (2011) Transient kinematic pile bending in two-layer soil. *Soil Dynamics and Earthquake Engineering*, 31(7):891-905.

[1.12] Di Laora, R., Mandolini, A. and Mylonakis, G. (2012) insight on kinematic bending of flexible piles in layered soil. *Soil Dynamics and Earhquake Engineering*, 43: 309-322.

[1.13] Ohira, A., Tazoh, T., Nakahi, S. and Shimizu, K. (1985) Observation and analysis of earthquake response behaviour of foundation piles in soft soil deposit. *Journal of Structural Mechanics and Earthquake Engineering*, 362/I-4,417-426 (in Japanese).

[1.14] Saitoh, M. (2005) Fixed-head pile bending by kinematic interaction and criteria for its minimization at optimal pile radius. *Journal of Geotechnical and Geoenvironmental Engineering* ASCE,131 (10):1243-1251.

[1.15] Tajimi, H. (1969) Dynamic analysis of a structure embedded in an elastic stratum. In: *proceedings of the 4th world conference on earthquake engineering*, Santiago, Chile.

[1.16] Dezi, F., Carbonari, S., Leoni, G. (2009) Kinematic bending moments in pile foundations. *Soil Dynamics and Earthquake Engineering*, 30(3): 119-132.

[1.17] Kaynia, AM., Kausel, E. (1982) Dynamic stiffness and seismic response of pile groups. Research report no. R82-03. *Cambridge*, MA: Massachusetts Institute of Technology.

[1.18] K, Fan., Gazetas, G., Kaynia, AM., Kausel, E., Ahmad, S. (1991) Kinematic seismic response of single piles and pile groups. *Journal of Geotechnical Engineering*,117 (12):1860-1879.

[1.19] Gazetas, G., K, Fan. (1993) Dynamic response of pile groups with different configurations. *Soil Dynamics and Earthquake Engineering*, (12):239-57.

[1.20] CENT/TC 250. Eurocode 8: Design of structures for earthquake resistance Part 5: Foundations, retaining structures and geotechnical aspects. European Committee for Standardization Technical Committee 250, Brussels, Belgium, Standard EN 1998-5, 2003.

[1.21] Ministero delle Infrastructure. Nuov Norme Tecniche per le Costruzioni. DM 14.01.08. Gazzetta Ufficiale della Repubblica Italiana, No. 29, 4 Febbraio 2008 [in Italian].

[1.22] Di Laora, R. Mylonakis, G. Mandolini, A. (2013) Pile-head kinematic bending in layered soil. *Earthquake Engineering and Structural Dynamics*, 42:319-337.

[1.23] Mylonakis, G., Di Laora, R., Mandolini, A. (2014) The Role of Pile Diameter on Earthquake-Induced Bending. In *Perspective on European Earthquake Engineering and Seismology*,. Springer Vol 1. 533-556.

# CHAPTER 2

# DYNAMIC SOIL-PILE GROUPS INTERACTION

Dynamic soil-pile interaction modeling has received significant research attention over the past four decades. Most studies are based on either purely numerical in nature ([2.1]~[2.3]), or mixed analytical-numerical formulations which have various degrees of complexity ([2.4] ~[2.7] ). Other researches concentrate on experimental aspects of the problem, both in the field ([2.8], [2.9]), and the laboratory ([2.10]~[2.12]). In purely analytical studies two-dimensional idealization for wave propagation in the soil medium has been taken into account, these methods are associated with the approximate model of Baranov and Novak ([2.13],[2.15]). On the other hand, analytical solutions based on three-dimensional wave propagation theory, which are more realistic and have the ability in predicting the main characteristics of dynamic soil-pile interaction, have received less research attention ([2.16]~[2.20]),

Dynamic soil-pile interaction can be modeled efficiently based on engineering approximations in which soil medium is represented by series of independent Winkler springs and dashpots uniformly distributed along the pile axis. Substitution of soil medium by springs and dashpots is convenient, because the multi-dimensional boundary value problem is simplified to a rod subjected to one-dimensional wave propagation in the vertical and lateral direction. Engineers use these simplified Winkler models for a wide range of dynamic soil-pile interaction problems ([2.21]~[2.23]). Their popularities stem from their ability to ([2.24])

(a) Pile response can be predicted in a realistic way

(b) Variable soil properties with depth and radial distance from the pile can be incorporated

(c) Group effects can be modeled by employing pertinent pile-to-pile interaction models

(d) Computational efforts become smaller than more rigorous alternatives.

In general the dynamic behavior of a group of vertical piles in any mode of vibration is basically different from the single pile. Similarly, the dynamic response of a pile group differ from the response of the

individual pile alone, in addition to loading transmitted to piles from the superstructure through the cap pile groups experience additional loading imposed along their shafts, This pile-to-pile interaction is dependent-frequency entity, resulting from waves that are emitted from the periphery of each pile and propagate to strike the neighboring piles.

The scope of this chapter is: (i) to introduce a general approximate method that involves three consecutive steps to solve the problem of dynamic pile-soil-pile interaction for two major types of loading:

(a) Lateral harmonic excitation at the pile head (inertial loading).

(b) Seismic excitation in the form of vertically-propagating harmonic shear waves (kinematic loading).

(ii) to develop a simple method for calculating the lateral soil impedance and attenuation of soil displacement in fundamental frequency of homogeneous soil layer.

## 2.1 Model for dynamic soil-pile interaction

The soil-pile system under consideration is shown in Figurre 2.1: two vertical cylindrical piles each of length $L$, diameter $d$, cross-sectional moment of inertia $I_p$, mass density $\rho_p$, mass per unit length $m_p$ and Young's modulus of elasticity $E_p$ is embedded in a homogeneous soil layer of thickness $H(=L)$ resting on a rigid base. Pile spacing is denoted with $s$. The pile group is loaded by either harmonic lateral loads $V(t) = V_0 e^{i\omega t}$ transmitted through rigid cap or vertically propagating shear waves expressed in the form of harmonic horizontal displacement $u_g(t) = u_{g0} e^{i\omega t}$ at rigid base level. This section employs the following main assumptions: (a) foundation remains elastic during either seismic ground shaking or lateral head loading; (b) soil restraining action can be modeled using a bed of linear or equivalent-linear Winkler springs and dashpots, uniformly distributed along the pile axis; (c) perfect contact (i.e., no gap and slippage) exist between pile and soil; (d) the flexural deformations of the pile group are dominant during oscillations; (e) the frequency of horizontal excitation is assumed to be equal to the fundamental frequency of the soil medium.

Makris and Gazetas [2.25] developed a simple three steps methodology to obtain the response of pile groups under either harmonic head loading or seismic excitation based on wave "interference model", by using this method, pile-soil-pile interaction can be decomposed in the following three steps which is explained in detail below.

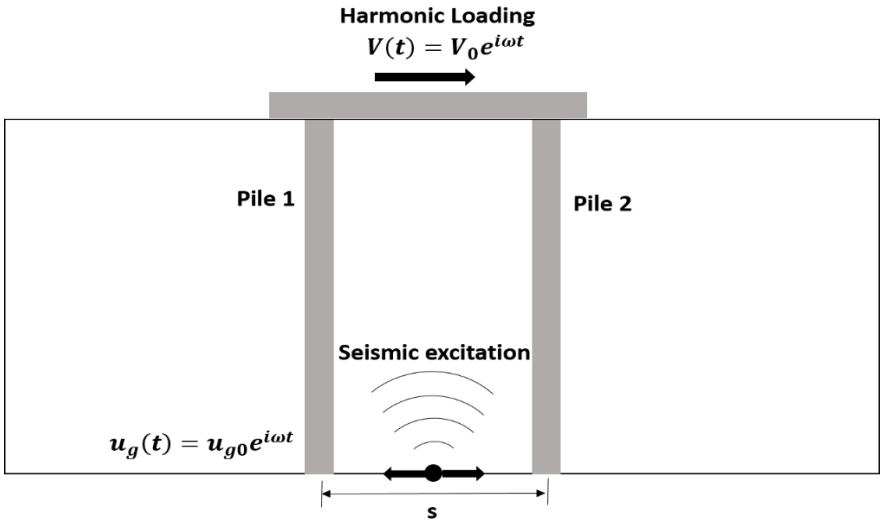


**Figure 2.1:** Problem considered for dynamic soil-pile interaction.

## 2.2 Step1: the response of a solitary "active" pile

The lateral deflection $u_{11}(z)$ of 'active' pile embedded in a homogeneous layer, subjected to either lateral inertial loads at its head or kinematic seismic deformations of the surrounding soil (Figure 2.2), is determined using a Beam-on-Dynamic-Winkler-Foundation method with relevant complex-valued dynamic springs and dashpots. Therefore by using a dynamic Winkler model soil-pile interaction is being to account. Soil is modelled as a linear elastic material with Poisson's ratio $\upsilon_s$, mass density $\rho_s$, and frequency-independent material damping $\beta_s$ which is expressed through a complex-valued shear modulus $G_s^* = G_s(1 + 2i\beta_s)$. The reaction of soil to the lateral pile motion is modeled by bed of continuously-distributed frequency-dependent springs $k_x$ and dashpots $c_x$ along the pile length which represent the stiffness and damping due to radiation and hysteretic energy dissipation.

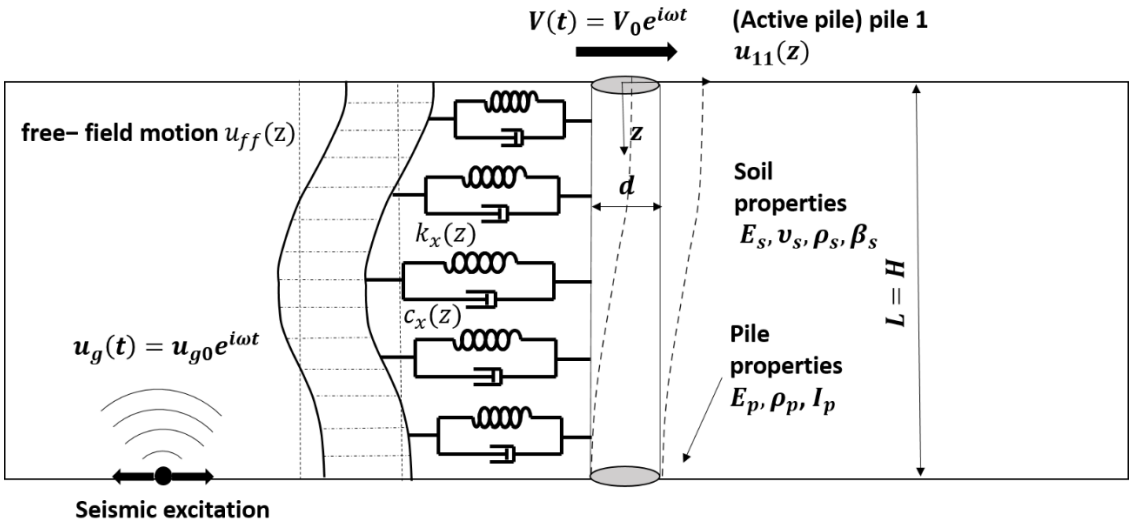


**Figure 2.2:** The response of a solitary "active" pile under either lateral inertial loads at its head or seismic waves.

### 2.2.1 The Dynamic Winkler modulus at the fundamental frequency of the soil layer

The basic problem in the implementation of Winkler models lies in the assessment of the moduli of the Winkler springs and dashpots. Current methods for determining these parameters can be classified into three main groups [2.26]: (a) experimental methods; (b) simplified theoretical models; and (c) calibration with rigorous numerical solutions. One of the simplest theoretical model is the one proposed by Novak [2.14]. In this model it is assumed that the soil is subjected to dynamic plane strain deformation and the lateral soil impedance according to this model is given by:

$$k_x^*(\omega) = \pi G_s^* s^2 \frac{4K_1(q)K_1(s) + sK_1(q)K_0(s) + qK_0(q)K_1(s)}{qK_0(q)K_1(s) + sK_1(q)K_0(s) + qsK_0(q)K_0(s)} \tag{2.1}$$

$$s = \frac{ia_0}{2\sqrt{1+2i\beta_s}}, q = \frac{s}{\eta_u}, \eta_u = \sqrt{\frac{2(1-\upsilon_s)}{1-2\upsilon_s}} \tag{2.2}$$

where $a_0 = \omega d/V_s$ denotes the dimensionless frequency factor, frequency-dependent springs and dashpots can be calculated by matching the pile dynamic pile response from Winkler and from rigorous numerical solutions (finite-element analysis), Dobry et al [2.27] derived the following expressions:

$$k_x = \delta E_s \tag{2.3}$$

$$\delta = 1.67\left(\frac{E_p}{E_s}\right)^{-0.053} \tag{2.4}$$

Makris and Gazetas [2.25] proposed the following approximate expressions for the distributed springs and dashpots:

$$k_x \approx 1.2E_s \tag{2.5}$$

$$c_x = (c_x)_{radiation} + (c_x)_{hysteresis} \approx 6a_0^{-\frac{1}{4}}\rho_s V_s d + 2\beta_s \frac{k_x}{\omega} \tag{2.6}$$

However the importance of above methods, each can be criticized for certain shortcomings that limit their applicability and make them unappealing to geotechnical engineers. For example, Winkler values which are obtained based on experimental approaches pertain mostly to large-amplitude static loads, and do not take account properly for law-strain soil stiffness, energy dissipation or frequency effects ([2.23]). On the other hand numerical complexities in certain parameters ranges may be encountered into calibrations with rigorous numerical solutions in group. Plane strain models have shortcomings that limit their applicability. Anoyatis et al [2.28] stated that these models are accurate only for infinitely-long piles embedded in a half space, as dynamic impedance function in Equations (2.1), (2.3) and (2.5) is independent of the conditions at the boundaries of the soil layer. Consequently, it lacks potential to capture the resonance effects in a soil stratum overlying a stiff base (which is of particular interest in this study). To overcome these shortcomings of the plane strain model, Mylonakis [2.19] proposed a technique within the framework of the plane strain model which follows the pioneering work of Nogami and Novak [2.29]. Another special feature of Mylonakis' model, is that the complex valued modulus $k_x^*$ is derived under consideration of normal stresses in the soil slice. In this model, sinusoidal and exponential shape functions were assumed for the variation of the displacement field in the soil along the vertical coordinate. Then, this vertical coordinate was eliminated by integrating the governing equations over the thickness of the soil profile, simplifying the

three-dimensional problem into a two-dimensional one similar to the plane strain model. In this study, these Winkler parameters developed by Mylonakis are utilized, given by the following expressions:

$$k_x^*(\omega) = \pi G_s^* s^2 \frac{4K_1(q)K_1(s) + sK_1(q)K_0(s) + qK_0(q)K_1(s)}{qK_0(q)K_1(s) + sK_1(q)K_0(s) + qsK_0(q)K_0(s)} \tag{2.7}$$

$$\mathrm{s} = \frac{1}{2}\sqrt{a_c^2 - \frac{a_0^2}{1+2i\beta_s}}\,, q = \frac{s}{\eta_u}\,, \eta_u = \sqrt{\frac{2-\upsilon_s}{1-\upsilon_s}} \tag{2.8}$$

$$a_c = b_u d, b_u^2 = \frac{\int_0^H (\frac{d\chi(z)}{dz})^2\, dz}{\int_0^H (\chi(z))^2\, dz} \tag{2.9}$$

where, $a_c$ stands for a dimensionless characteristic frequency (termed as "cutoff frequency") below which no waves can emanate from the pile-soil interface and as a result, radiation damping will not be produced. The real part of Equation (2.7) is the soil stiffness $k_x = Real(k_x^*)$ and the imaginary part presents soil damping $c_x\omega = Imag(k_x^*)$ , $\chi(z)$ is the shape function to describe the lateral vibrations along the pile length.

### 2.2.2 Selection of shape function

To calculate the impedance of the soil medium using the proposed method, pertinent shape function $\chi(z)$ which satisfies the boundary conditions of soil-pile deformations is needed. Mylonakis [2.19] proposed shape functions which are convincing for engineering estimates of lateral response. In the lateral mode, a sinusoidal shape function is employed:

$$\chi(z) = \cos\left(\frac{\pi z}{2H}\right) \tag{2.10}$$

The cutoff frequency can be calculated with this shape function:

$$a_c = \frac{\pi r}{H} \tag{2.11}$$

An alternative shape function can be employed by using Winkler theory ([2.30]) which coincides to the deformed shape of a fixed-head hinged-base cylinder.

$$\chi(z) = e^{-\mu z}\{-e^{2\mu z}(\cos(\mu L) - \sin(\mu L)) + e^{4\mu L}(\cos(\mu L) + \sin(\mu L)) - e^{2\mu L}[(-1 + e^{2\mu L})\cos(2\mu L - \mu z) + (1 + e^{2\mu z})\sin(2\mu L - \mu z)]\} \tag{2.12}$$

The corresponding cutoff frequency of the system can be obtained from the following expression

$$a_{cu} = \mu\sqrt{2\frac{-1 + E_8 - 2E_2[1 + 4\mu L + E_4(-1 + 4\mu L)C_2 + 2E_2(1 + E_4)S_2 + 2E_4(-8\mu L + S_4)}{3(-1 + E_8) + 2E_2[3(-1 + E_4)C_2 - (3 - 4\mu L + E_4(3 + 4\mu L) + 6E_2C_2)S_2}} \tag{2.13}$$

where $E_j, S_j$ and $C_j$ denote, respectively, the functions $\exp(j \times \mu L), \sin(j \times \mu L), \cos(j \times \mu L)$. $\mu$ in the above equations is a shape parameter that can be estimated by( [2.27],[2.30] and [2.31]).

$$\mu \approx (\frac{E_s}{4E_p I_p})^{1/4} \tag{2.14}$$

For simplicity, a sinusoidal shape function (Equation (2.10)) is selected in which the cutoff frequency coincides with the fundamental frequency of homogenous soil layer in shearing vibrations.

## 2.3 Step2: attenuation of soil displacement away from active pile (source pile)

Cylindrical waves are emitted from the periphery of the vibrating active pile with amplitude equal to the deflected pile shape $u_{11}(z)$ (Figure 2.3)., it is assumed the waves propagate in an essentially horizontal manner, the free-field soil displacement at a distance $s$ and angle $\theta$ from the direction of loading $u_s(s, z, \theta)$ is given by (Dobry and Gazetas [2.32]):

$$u_s(s, z, \theta) \approx \psi(s, \theta)\Delta u_{11} \tag{2.15}$$

In Equation (2.15) $\Delta u_{11}$ is the difference between single pile deflections and free-field soil displacements $u_{ff}$. For inertial loading, this difference is equal to the deflection of the active single pile: $\Delta u_{11} = u_{11}$, while for kinematic loading, it is identical to the response of the scattered free-field of the soil: $\Delta u_{11} = u_{11} - u_{ff}$. Indeed this difference perturbs the seismic wave field. $\psi(s, \theta)$ is the dimensionless attenuation function of the horizontal soil displacement with radial distance from the pile and direction of loading. Dobry and Gazetas [2.32] derived the simple asymptotic formulae (Equations (2.16) an (2.17)):

$$\psi_{21}(s, 0) = (\frac{2s}{d})^{-1/2} \exp[-\left(\frac{s}{d} - \frac{1}{2}\right)(\beta_s + i)\frac{V_s}{V_{La}} a_0] \tag{2.16}$$

$$\psi_{21}\left(s, \frac{\pi}{2}\right) = (\frac{2s}{d})^{-1/2} \exp[-\left(\frac{s}{d} - \frac{1}{2}\right)(\beta_s + i) a_0] \tag{2.17}$$

where $u_s(s, z, \theta) =$ horizontal soil displacement generated by active pile (source pile) ; $\psi_{21}(s, 0)$ and $\psi_{21}\left(s, \frac{\pi}{2}\right) =$ attenuation functions corresponding to wave travelling along and perpendicular to the direction of loading, respectively; $V_{La}$ is the so-called "Lysmer's analogue" wave velocity accounting for the compression-extension waves near the surface $V_{La} = 3.4V_s/[(1 - \upsilon_s)]$ ([1.33]); $\theta$= angle between the direction of loading and the line connecting the pile centers; s= axis-to-axis distance between the direction of loading and the line connecting the pile centers.

Several approximate models are available to idealize wave propagation in soil medium. One simplified approach is the two-dimensional plane strain model developed by Gazetas and Dobry [2.33]. The fundamental assumption in their model is that compression-extension waves propagate in the two quarter-planes along the direction of loading, and simultaneously shear waves propagate in the two quarter-planes perpendicular to the direction of loading. The exactness of the method has shortcomings when dealing with shallow layers of soil. Mylonakis [2.19] pointed out that the plane strain model in the presence of a rigid base cannot capture fundamental frequency effects. To overcome this discrepancy, he presented a new model for the attenuation functions in which beyond the fundamental frequency of soil layer, results are in

agreement with the plane strain model, but at smaller frequencies they diverge. In this study, the attenuation functions, presented in Equations (2.18) and (2.19), provided by Mylonakis [2.19] are employed.

$$\psi_{21}(s,0) = (\frac{2s}{d})^{-1/2}\exp[-\left(\frac{s}{d}-\frac{1}{2}\right)\sqrt{a_c^2-\frac{a_0^2}{1+2i\beta_s}}] \tag{2.18}$$

$$\psi_{21}\left(s,\frac{\pi}{2}\right) = (\frac{2s}{d})^{-1/2}\exp[-\left(\frac{s}{d}-\frac{1}{2}\right)\eta_u^{-1}\sqrt{a_c^2-\frac{a_0^2}{1+2i\beta_s}}] \tag{2.19}$$

$$\psi_{21}(s,\theta) = \psi_{21}(s,0)\cos^2(\theta) + \psi_{21}\left(s,\frac{\pi}{2}\right)\sin^2(\theta) \tag{2.20}$$

In this study, since the excitation frequency is assumed to be equal to the fundamental frequency of the soil layer Equations (2.18) and (2.19) can be rewritten as Equations (2.21) and (2.22).

$$\psi_{21}(s,0) = (\frac{2s}{d})^{-1/2}\exp[-\left(\frac{s}{d}-\frac{1}{2}\right)\frac{\pi r}{H}\sqrt{\frac{2i\beta_s}{1+2i\beta_s}}] \tag{2.21}$$

$$\psi_{21}\left(s,\frac{\pi}{2}\right) = (\frac{2s}{d})^{-1/2}\exp[-\left(\frac{s}{d}-\frac{1}{2}\right)\frac{\pi r}{H}\eta_u^{-1}\sqrt{\frac{2i\beta_s}{1+2i\beta_s}}] \tag{2.22}$$

According to the model proposed by Mylonakis, at a distance $s$ from the vibrating pile and angle $\theta$ from the direction of loading**,** the displacement field can be expressed as:

$$u_s(s,z,\theta) = \psi_{21}(s,\theta)\Delta u_{11} = \psi_{21}(s,\theta){u^I}_{11}(z) \qquad \text{for inertial loading} \tag{2.23}$$

$$u_s(s,z,\theta) = \psi_{21}(s,\theta)\Delta u_{11} = \psi_{21}(s,\theta)\left({u^K}_{11}(z) - u_{ff}\right) \qquad \text{for kinematic loading} \tag{2.24}$$

The effect of frequency on the attenuation function is illustrated in Figure 2.3, in which the amplitude of $\psi_{21}(s,\theta=0)$ is plotted as function of frequency for six pile spacings $s/d$. Corresponding results obtained from the plane strain model are also shown for comparison.

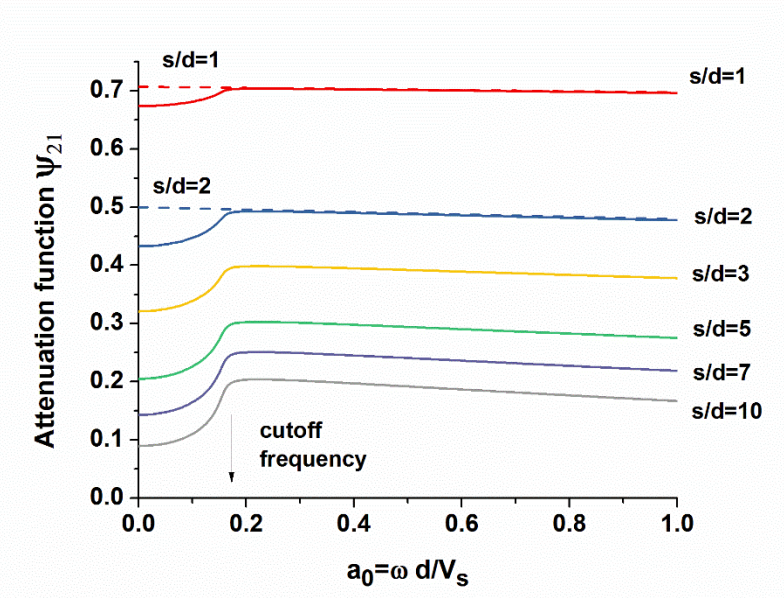


**Figure 2.3:** Attenuation of soil displacement around a pile: lateral mode, $\left(\frac{L}{d} = 20\,, v_s = 0.4\,, \beta_s = 0.05\right)$.

At the cutoff frequency a significant increase in $\psi$ is observed which may exceed 100% of the static value particularly at large distances from the pile. This implies that special care should be taken in calculating group effects if the predominant frequency of the excitation are close to the cutoff frequency of the system.

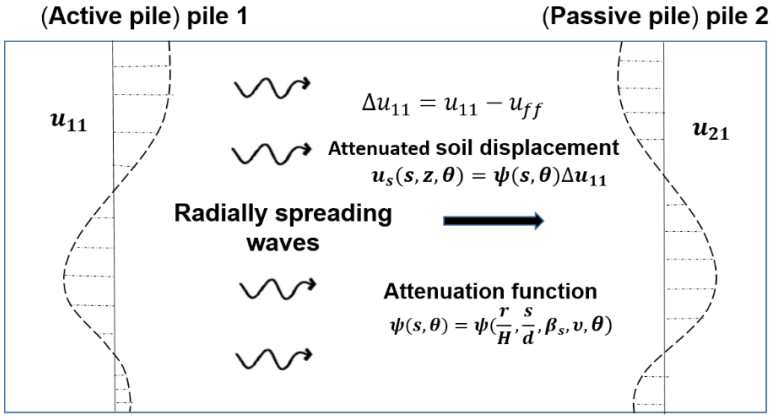


**Figure 2.4:** Schematic illustration for computing influence of active pile on adjacent passive pile.

## 2.4 Step3: the response of a solitary "passive" pile

As it is shown in Figure 2.4 the presence of passive pile will modify the arriving wave field $u_s$ and it tends to resist the free-field motion of step 2 with its inertial and relative flexural rigidity. This interaction between passive pile and surrounding soil leads to a diffraction of the incoming wave field. In result, passive pile displacement will be different from free-field displacement, based on the flexibility of the passive pile, its deflection will vary between two extremes. For long-flexible pile, it will experience $u_{21}(z) \approx u_s(z)$ and for rigid pile, it may remain approximately unchanged $u_{21}(z) \approx 0$. For soil-passive pile interaction, a Beam-on-Dynamic-Winkler-Foundation model is utilized in which the excitation takes the shape of a support motion, that is equal to the attenuated free-field displacement $u_s(z)$. The response of pile to this excitation will yield the desired passive pile response $u_{21}(z)$.

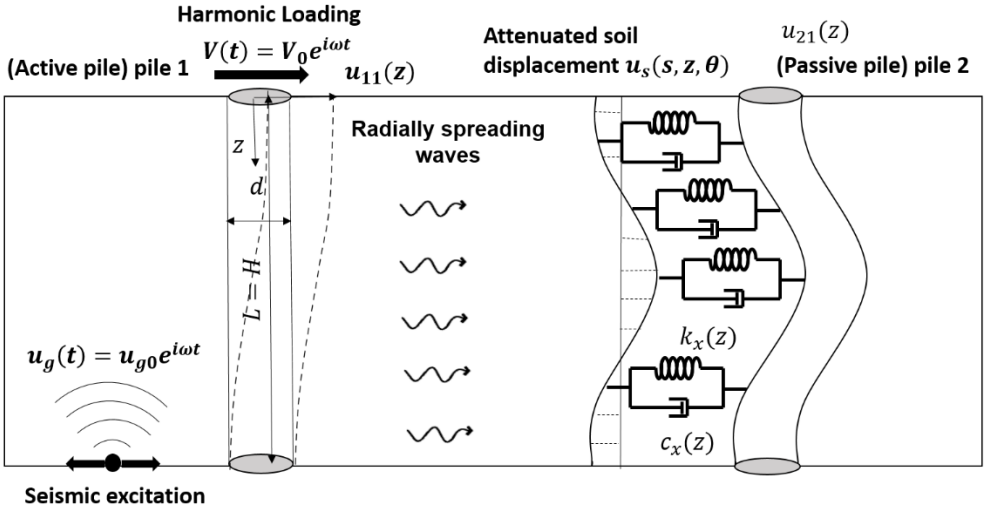


**Figure 2.5:** The response of a solitary "passive" pile under influence of the active pile.

Consequently a general methodology has been extended for analysis of dynamic pile-soil-pile interaction problems under both inertial and kinematic effects. This method is comprised of three independent steps, which can be used efficiently to solve and analyze the problem of inertial and kinematic interaction separately. Pile soil interaction which is simulated through a series of independent dynamic Winkler springs and dashpots and physically-motivated approximations are used to model diffraction and attenuation of seismic waves away from each pile. When a group of piles fixed to a cap is subjected to incident seismic

waves, the response of each individual pile can be studied as a combination of not only the kinematic part, but also the inertial part owing to the restriction imposed by the rigid cap. In this study, the soil-pile model is assumed to exhibit linear behavior and therefore for simplicity, both inertial and kinematic effects are treated in the context of two modular problems (active and passive pile response). Each sub-problem is addressed separately in the following chapters.

## References


[2.1] Roesset, J.M. (1980). Stiffness and damping coefficients of foundations. In dynamic response of structures: Experimentation, observation, prediction and control (ed. G. C. Hart), pp. 1-30. Reston, VA: ASCE.

[2.2] Syngros, K. (2004). Seismic response of piles and pile-supported bridge piers evaluated through case histories. PhD thesis, City University of New York.

[2.3] Balney, G. W., Kausel, E. and Roesset, J.M. (1976). Dynamic stiffness of piles. *Proc. 2nd Int. Conf. on Numerical Mehtods in Geomechanics, Blacksburg, VA* 1001-1012.

[2.4] Kaynia, AM., Kausel E. Dynamic stiffness and seismic response of pile groups. Research report no. R82-03. *Cambridge*, MA: Massachusetts Institute of Technology; 1982.

[2.5] Ji, F. and Pak, R. Y. S. (1996). Scattering of vertically-incident P waves by an embedded pile. *Soil Dynamics and Earthquake Engineering*, 15, No. 3, 211-222.

[2.6] Banerjee, P. K. and Sen, R. (1987). Dynamic behaviour of axially and laterally loaded piles and pile groups. In Dynamic behaviour of foundations and buried structures (Developments in Mechanics and Foundation Engineering, Vol. 3) (eds P.K. Banerjee and R. Butterfield), pp. 95-133. London: Elsevier Applied Science.

[2.7] Sanchez-Salinero, I. (1982). Static and dynamic stiffness of single piles, Geotechnical Engineering Report GR82-31. Austin, TX: University of Texas.

[2.8] Blaney, G. W., Muster, G. L. & O'Neil, M. W. (1987). Vertical vibration test of a full-scale pile group. In Dynamic response pile foundations: Experiment analysis and observation (ed. T. Nogami), ASCE GSP No. 11, pp. 149-165. Reston, VA: ASCE.

[2.9] Tazoh, T., Shimizu, K. and Wakahara, T. (1987). Seismic observations and analysis of grouped piles. In Dynamic response of pile foundations: Experiment, analysis and observation (ed. T. Nogami), GSP 11, pp.1-20. Reston, VA: ASCE.

[2.10] Bhattacharya, S., Madabhushi, S. P. G. and Bolton, M. D. (2004). An alternative mechanism of pile failure in liquefiable deposits during earthquakes. *Géotechnique* 54, No. 3, 203-213.

[2.11] Boulanger, R. W., Curras, C. J., Kuttar, B. L., Wilson, D. W. and Abghari, A. (1999). Seismic-pile-structure interaction experiments and analyses *Journal of Geotechnical and Geoenvironmental Engineering* ASCE. 125, No. 9, 750-759.

[2.12] Knappett, J. A. and Madabhushi, S. P. G. (2009). Influence of axial load on lateral pile response in liquefiable soils. Part 1: Physical modelling. *Gétechnique* 59, No. 7, 571-581.

[1.13] Baranov, V. A. (1967). On the calculation of an embedded foundation, Vorposy Dinamiki i Prognostic (Polytechnical Institute of Riga, Latvia), No. 14, 195-209 (in Russian).

[2.14] Novak, M. (1974). Dynamic stiffness and damping of piles. *Canadian Geotechnical Journal*, 11, No. 4, 574-598.

[2.15] Novak, M., Nogami, T. and Aboul-Ella, F. (1978). Dynamic soil reactions for plane strain case. *Journal of Engineering Mechanics*. Div. ASCE 104, No. 44, 953-959.

[2.16] Mylonakis, G. (1995). Contributions to static and seismic analysis of piles and pile-supported bridge piers. PhD thesis, State University of New York at Buffalo.

[2.17] Nogami, T. and Novak, M. (1976). Soil-pile interaction in vertical vibration. *Earthquake Engineering and Structural. Dynamics*. 4, No. 3, 277-293.

[2.18] Tajimi, H. (1969) Dynamic analysis of a structure embedded in an elastic stratum. In: *proceedings of the 4th world conference on earthquake engineering*, Santiago, Chile.

[2.19] Mylonakis, G. (2001) Elastodynamic model for large-diameter end-bearing shafts. *Soil and Foundations*,41(3);31-44.

[2.20] Saitoh, M. (2005) Fixed-head pile bending by kinematic interaction and criteria for its minimization at optimal pile radius. *Journal of Geotechnical and Geoenvironmental Engineering* ASCE,131 (10):1243-1251.

[2.21] Pender, M. J. (1993). A seismic pile foundation design analysis. Bull. NZ Nat. *Society of Earthquake Engineering* 26, No. 1, 49-160.

[2.22] Randolph, M. F. and Wroth, C. P. (1978). Analysis of deformation of vertically loaded piles. *Journal of Geotechnical and Geoenvironmental Engineering* ASCE 104, No. 12,1465-1488.

[2.23] Reese, L. C. & Van Impe, W. F. (2000). Single piles and pile groups under lateral loading. Rotterdam: Balkema.

[2.24] Mylonakis, G. & Gazetas, G. (1998). Settlement and additional internal forces of grouped piles in layered soil. *Gétechnique* 48, No. 1,55-72.

[2.25] Makris N, Gazetas G. Dynamic pile-soil-pile interaction. Part II: Lateral and seismic response. *Earthquake Engineering And Structural Dynamics*, 21(2):145-62.

[2.26] Anoyatis G, Mylonakis G. (2012) Dynamic Winkler modulus for axially loaded piles. *Geotechnique*, 62(6):521-36.

[2.27] Dobry, R., Vicente, E., O'Rourke, M.J., and Roesset, J.M. (1982). Horizontal stiffness and damping of single piles, *Journal of Geotechnical and Geoenvironmental Engineering* ASCE 108(3), 439-459.

[2.28] Anoyatis, G., Mylonakis, G., Lemnitzer, A. (2016) Soil reaction to lateral harmonic pile motion. *Soil Dynamics and Earthquake Engineering*, (87):164-179.

[2.29] Novak, M., Nogami, T. (1977) Soil-pile interaction in horizontal vibration. *Earthquake Engineering and Structural Dynamics*, 5(3):263-81.

[2.30] Scott R. F (1981): Foundation Analysis, *Prentice Hall*.

[2.31] Poulos, H. G. and Davis, E. H. (1980): Pile Foundation Analysis and Design, *John Wiley and Sons*.

[2.32] Dobry, R., Gazetas, G. (1988) Simple method for dynamic stiffness and damping of floating pile groups. *Geotéchnique*, London, 38(4): 557-74.

[2.33] Gazetas, G., Dobry, R. (1983) Horizontal response of piles in layered soils. *Journal of Geotechnical and Geoenvironmental Engineering* ASCE, 110:20-40.

# CHAPTER 3
# INERTIAL RESPONSE OF PILE GROUPS

The deformations of a structure during earthquake generate inertial forces atop the pile foundation systems. Investigation on lateral response of single piles and pile groups due to induced inertial forces has attracted a vast amount of researches. Various types of techniques have been proposed to investigate the behavior of pile-soil-structure under dynamic inertial loads in recent years, such as continuum approach (Novak [3.1]; Novak and Aboul-Ella [3.2]), boundary element method (Kaynia and Kausel [3.3]; Sen, Kausel and Banerjee [3.4]) finite element solutions, (Blaney , Kausel and Roesset [3.5] ;Wolf and VonArx [3.6]) . A simplified approach was also presented by (Makris and Gazetas [3.7]) for calculating the dynamic response and internal forces caused by harmonic loading atop the pile cap. That method is based on generalized Winkler model in conjunction with a three step wave interference solution for pile to pile effect. Although those studies had led to sufficient understanding in the behavior of inertial response of pile-soil-structure systems, the predictions of inertial bending remains questionable. For design purposes, it is necessary to determine pile radius because the size of the radius directly affects the bending stiffness of the pile $EI$. When inertial loading is significant, increasing the pile radius is a proper technique to decrease bending strains. Saitoh [3.8] proposed a closed form formula in order to obtain optimal radius of vertical, cylindrical fixed-head single pile embedded in a homogeneous elastic soil layer and supported by rotationally compliant bedrock. Particularly the frequency of horizontal excitation was assumed to be equal to the natural frequency of the soil medium. The variations in normalized inertial bending strains as a function of the slenderness ratio $r/H$ was investigated. Despite this effort, researches on the influence of the pile radius on bending strains in soil-pile group systems where inertial interaction is predominant, has not reported yet, therefore to establish criteria for optimal pile radius in pile group, variations of inertial bending strains with respect to pile radius should be quantified in a systematic way. This chapter attempts to offer comprehensive

relations between radius and the inertial bending strains at the head of vertical, cylindrical pile group embedded in a homogeneous soil layer, pile group is assumed to be under harmonic loading at the head, and different constraint conditions at the pile group tip (hinged and fixed) is considered. Analytical results will be assessed through Beam-on-Dynamic-Winkler-foundation (BDWF) model. Mylonakis and Nikolaou [3.9] implied that, in dominance of inertial responses in fundamental frequency of soil-pile system, the inertial bending would be significant, particularly at upper part of the piles. Therefore to get insight into the physics of the problem and basic characteristics, it would be beneficial to investigate inertial bending strains in the fundamental frequency of soil layer.

## 3.1 Analytical solution of inertial bending of pile groups

The soil-pile-structure system is shown in Figure 3.1: two vertical cylindrical piles of length *L*, diameter *d*, pile cross-sectional moment of inertia $I_p$ , mass density $\rho_p$ , mass per unit length of the piles $m_p$ and Young's modulus $E_p$ is embedded in a homogeneous soil layer of thickness $H(=L)$ resting on a rigid base. Pile spacing is denoted with $s$. Soil is modelled as a linear elastic material of Poisson's ratio $v_s$, mass density $\rho_s$, and frequency-independent material damping $\beta_s$ which is expressed through a complex-valued shear modulus $G_s^* = G_s(1 + 2i\beta_s)$ and as a Winkler foundation resisting the lateral pile motion by continuously-distributed frequency-dependent linear springs $k_x$ and dashpots $c_x$ along the pile length. The pile group is assumed to be excited by harmonic horizontal load at the head. This section employs the following main assumptions: (a) foundation remains elastic during either seismic ground shaking or lateral head loading; (b) soil restraining action can be modeled using a bed of linear or equivalent-linear Winkler springs and dashpots, uniformly distributed along the pile axis; (c) perfect contact (i.e., no gap and slippage) exist between pile and soil; (d) the flexural deformations of the pile group are dominant during oscillations; (e) the frequency of horizontal excitation is assumed to be equal to the fundamental frequency of the soil medium.

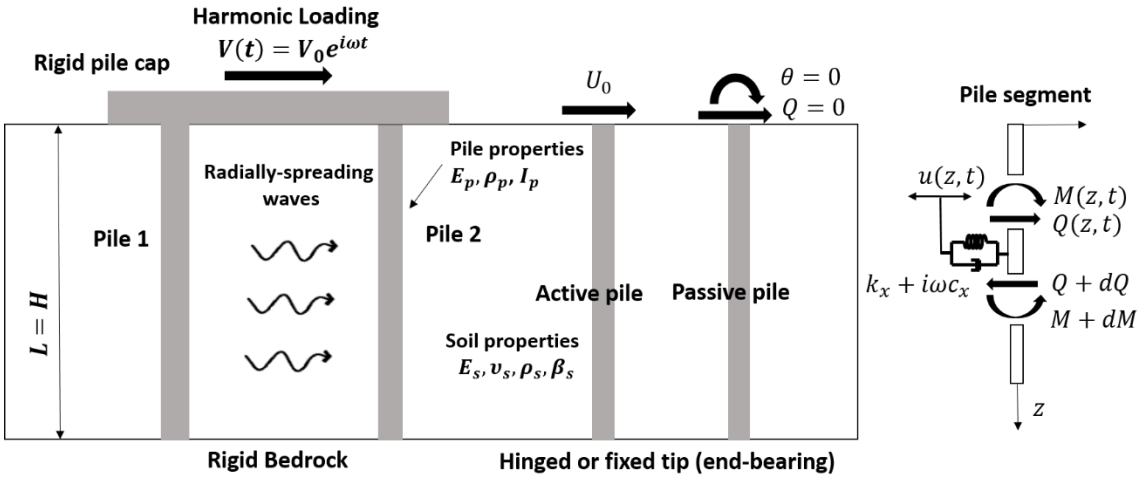


**Figure 3.1:** Problem considered for inertial interaction with different tip conditions.

## 3.2 Deflection of active pile (source pile)

Let $u_{11}(z,t) = u_{11}(z)e^{i\omega_g t}$ denote the harmonic pile deflection. With reference to Figure 3.1 dynamic equilibrium under harmonic steady-state conditions yields:

$$\frac{d^4 u_{11}(z)}{dz^4} + 4\lambda^4 u_{11}(z) = 0 \tag{3.1}$$

Where $\lambda = \lambda(\omega)$ is the characteristics wave number governing the attenuation functions of pile displacement with depth and $\omega_g$ is the fundamental frequency of the homogeneous soil layer**.** The solution will yield harmonic horizontal deflection of the active pile $u^I{}_{11}(z,t) = u^I{}_{11}(z)e^{i\omega_g t}$ in terms of inertial integration constants $A^I{}_{11}$, $B^I{}_{11}, C^I{}_{11}$, $D^I{}_{11}$ which are dependent on the boundary conditions. For both hinged and fixed tip conditions, constants can be obtained as following relations.

$$\lambda = \left(\frac{k_x + ic_x\omega_g - m_p{\omega_g}^2}{4E_p I_p}\right)^{1/4} \tag{3.2}$$

$$\omega_g = \omega_{cutoff} = \frac{\pi V_s}{2H} \tag{3.3}$$

### 3.2.1 Boundary conditions of active pile (hinged pile groups):

$$u^{I}_{11}(z=0)=u_0 \;,\; {\theta^{I}}_{11}(z=0)=0 \;,\; \frac{d^2u^{I}_{11}(z=H)}{dz^2}=0 \;,\; u^{I}_{11}(z=H)=0 \tag{3.4}$$

$$\begin{bmatrix} 1 & 0 & 1 & 0 \\ 1 & 1 & -1 & 1 \\ -e^{\lambda H}\sin(\lambda H) & e^{\lambda H}\cos(\lambda H) & e^{-\lambda H}\sin(\lambda H) & -e^{-\lambda H}\cos(\lambda H) \\ e^{\lambda H}\cos(\lambda H) & e^{\lambda H}\sin(\lambda H) & e^{-\lambda H}\cos(\lambda H) & e^{-\lambda H}\sin(\lambda H) \end{bmatrix} \begin{Bmatrix} A^{I}_{11} \\ B^{I}_{11} \\ C^{I}_{11} \\ D^{I}_{11} \end{Bmatrix} = \begin{Bmatrix} u_0 \\ 0 \\ 0 \\ 0 \end{Bmatrix} \tag{3.5}$$

### 3.2.2 Boundary conditions of active pile (fixed-tip pile groups)

$$u^{I}_{11}(z=0)=u_0 \;,\; {\theta^{I}}_{11}(z=0)=0 \;,\; \frac{du^{I}_{11}(z=H)}{dz}=0 \;,\; u^{I}_{11}(z=H)=0 \tag{3.6}$$

$$\begin{bmatrix} 1 & 0 & 1 & 0 \\ 1 & 1 & -1 & 1 \\ e^{\lambda H}(\cos(\lambda H)-\sin(\lambda H)) & e^{\lambda H}(\cos(\lambda H)+\sin(\lambda H)) & -e^{-\lambda H}(\cos(\lambda H)+\sin(\lambda H)) & e^{-\lambda H}(-\sin(\lambda H)+\cos(\lambda H)) \\ e^{\lambda L}\cos(\lambda H) & e^{\lambda H}\sin(\lambda H) & e^{-\lambda H}\cos(\lambda H) & e^{-\lambda H}\sin(\lambda H) \end{bmatrix} \begin{Bmatrix} A^{I}_{11} \\ B^{I}_{11} \\ C^{I}_{11} \\ D^{I}_{11} \end{Bmatrix} = \begin{Bmatrix} u_0 \\ 0 \\ 0 \\ 0 \end{Bmatrix} \tag{3.7}$$

## 3.3 Attenuation of soil displacement away from active pile (source pile)

This step starts by calculating the difference between single pile deflections and free-field soil displacements, $\Delta u_{11}$ (Figure 2.3). For inertial loading, this difference is equal to the deflection of the active single pile: $\Delta u_{11} = {u^{I}}_{11}(z)$, new cylindrical waves emanate from the periphery of the vibrating active pile while spreading outward in all directions. In this study attenuation functions of Mylonakis [3.10] is used. With reference to Equation (2.15), at a distance $s$ from the vibrating pile and angle $\theta$ from the direction of loading**,** the free-field soil displacement can be expressed as:

$$u_s(s,z,\theta) = \psi_{21}(s,\theta)\Delta u_{11} = \psi_{21}(s,\theta){u^{I}}_{11}(z) \tag{3.8}$$

## 3.4 Interaction of the passive pile (receiver) with arriving waves

Considering a passive pile (receiver pile) located at a distance $s$ from the active pile (source pile), the diffracted wave field generated by the active pile as represented by Equation (3.8) propagates to strike the passive pile. The passive pile does not exactly follow the diffracted wave field [3.11], [3.12] and its flexural rigidity tends to resist these induced displacements, resulting in a modified motion at the soil-passive pile interface. In order to determine the additional displacement, which is experienced by passive pile, the dynamic equilibrium of an infinitesimal pile segment is considered, yielding the following equation governing the deflection $u_{21}(z)$ of the passive pile.

$$\frac{d^4u_{21}(z)}{dz^4} + 4\lambda^4 u_{21}(z) = \frac{k_x + i\omega_g c_x}{E_p I_p}\psi_{21}(s,\theta)u^I{}_{11}(z) \tag{3.9}$$

When the active pile is excited by the lateral harmonic loading $u^I{}_{11}(z=0)e^{i\omega_g t} = u_0 e^{i\omega_g t}$ at the head, the solution of Equation (3.9) gives us the additional inertial displacement of the passive pile. This displacement consists of two parts; $(u^I{}_{21}(z))_1$ as homogeneous solution and $(u^I{}_{21}(z))_2$ as particular solution.

$$u^K{}_{21}(z) = (u^I{}_{21}(z))_1 + (u^I{}_{21}(z))_2 \tag{3.10}$$

$$(u^I{}_{21}(z))_1 = e^{\lambda z}\left(A_{21}{}^I\cos(\lambda z) + B_{21}{}^I\sin(\lambda z)\right) + e^{-\lambda z}\left(C_{21}{}^I\cos(\lambda z) + D_{21}{}^I\sin(\lambda z)\right) \tag{3.11}$$

$$(u^I{}_{21}(z))_2 = \frac{k_x + ic_x\omega_g}{16E_pI_p\lambda^3}\psi_{21}(s,\theta)[ze^{\lambda z}(A'\cos(\lambda z) + B'\sin(\lambda z)) + ze^{-\lambda z}(C'\cos(\lambda z) + D'\sin(\lambda z))] \tag{3.12}$$

$$A' = -(A_{11}^I + B_{11}^I)\ ,\ B' = (A_{11}^I - B_{11}^I)\ ,\ C' = (C_{11}{}^I - D_{11}{}^I)\ ,\ D' = (C_{11}{}^I + D_{11}{}^I) \tag{3.13}$$

In particular solution, (Equation. (3.12)), $A', B', C'$ and $D'$ are integration constants in which $A_{11}^I, B_{11}^I, C_{11}{}^I$ and $D_{11}{}^I$ are known inertial integration constants (i.e. they have already been determined from the boundary conditions of the active pile). In homogeneous solution $A_{21}^I, B_{21}^I, C_{21}{}^I$ and $D_{21}{}^I$ are inertial integration constants that should be determined from the boundary conditions of the passive pile.

### 3.4.1 Boundary conditions of passive pile (hinged pile groups)

$$\theta^{I}{}_{21}(z=0)=0 \quad , \quad \frac{d^3u^I_{21}(z=0)}{dz^3}=0 \quad , \frac{d^2u^I_{21}(z=H)}{dz^2} \quad , \quad u^I_{21}(z=H)=0 \tag{3.14}$$

$$\begin{bmatrix} 1 & 1 & -1 & 1 \\ -1 & 1 & 1 & 1 \\ -e^{\lambda H}\sin(\lambda H) & e^{\lambda H}\cos(\lambda H) & e^{-\lambda H}\sin(\lambda H) & -e^{-\lambda H}\cos(\lambda H) \\ e^{\lambda H}\cos(\lambda H) & e^{\lambda H}\sin(\lambda H) & e^{-\lambda H}\cos(\lambda H) & e^{-\lambda H}\sin(\lambda H) \end{bmatrix} \begin{Bmatrix} A^I_{21} \\ B^I_{21} \\ C^I_{21} \\ D^I_{21} \end{Bmatrix} = \begin{Bmatrix} H1 \\ H_2 \\ H_3 \\ H_4 \end{Bmatrix} \tag{3.15}$$

$$\begin{Bmatrix} H1 \\ H_2 \\ H_3 \\ H_4 \end{Bmatrix} = \begin{Bmatrix} 0 \\ 2\alpha_{21}u_0 \dfrac{cos(2\lambda H)+cosh(2\lambda H)}{sinh(2\lambda H)-sin(2\lambda H)} \\ \dfrac{4}{3}\alpha_{21}u_0 \dfrac{\lambda H\, cos(\lambda H)\, cosh(\lambda H)}{sinh(2\lambda H)-sin(2\lambda H)} \\ \dfrac{4}{3}\alpha_{21}u_0 \dfrac{\lambda H sin(\lambda H)\, sinh(\lambda H)}{sin(2\lambda H)-sinh(2\lambda H)} \end{Bmatrix} \tag{3.16}$$

### 3.4.2 Boundary conditions of passive pile (end-bearing pile groups)

$$\theta^{I}{}_{21}(z=0)=0 \quad , \quad \frac{d^3u^I_{21}(z=0)}{dz^3}=0 \quad , \frac{du^I_{21}(z=H)}{dz}=0 \quad , \quad u^I_{21}(z=H)=0 \tag{3.17}$$

$$\begin{bmatrix} 1 & 1 & -1 & 1 \\ -1 & 1 & 1 & 1 \\ \lambda e^{\lambda H}(\cos(\lambda H)-\sin(\lambda H)) & \lambda e^{\lambda H}(\cos(\lambda H)+\sin(\lambda H)) & -\lambda e^{-\lambda H}(\cos(\lambda H)+\sin(\lambda H)) & \lambda e^{-\lambda H}(-\sin(\lambda H)+\cos(\lambda H)) \\ e^{\lambda L}\cos(\lambda H) & e^{\lambda H}\sin(\lambda H) & e^{-\lambda H}\cos(\lambda H) & e^{-\lambda H}\sin(\lambda H) \end{bmatrix} \begin{Bmatrix} A^I_{21} \\ B^I_{21} \\ C^I_{21} \\ D^I_{21} \end{Bmatrix} = \begin{Bmatrix} H1 \\ H_2 \\ H_3 \\ H_4 \end{Bmatrix} \tag{3.18}$$

$$\begin{Bmatrix} H1 \\ H_2 \\ H_3 \\ H_4 \end{Bmatrix} = \begin{Bmatrix} 0 \\ 2\alpha_{21}u_0 \dfrac{sin(2\lambda H)+sinh(2\lambda H)}{cosh(2\lambda H)+cos(2\lambda H)-2} \\ \dfrac{8}{3}\alpha_{21}u_0 \dfrac{\lambda H\, sin(\lambda H)\, sinh(\lambda H)}{cosh(2\lambda H)+cos(2\lambda H)-2} \\ 0 \end{Bmatrix} \tag{3.19}$$

$$\alpha_{21}=\frac{3}{4}\psi_{21}(s,\theta)\frac{k_x+ic_x\omega}{k_x+ic_x\omega-m\omega^2} \tag{3.20}$$

## 3.5 Inertial interaction factors

According to the calculation of pile group response, an important difficulty will arise, for instance with the only two piles, the presence of the second pile changes the axial symmetry of the single pile problem, therefore, three dimensional analysis of the problem is necessary. Significantly for large pile groups,

substantial computational effort will be needed. Poulos [3.13] and Butterfield and Banerjee [3.14] implied that group effects can be estimated by superimposing the effects of only two piles. This type of analysis referred to as the "superposition method".

The above definition for the interaction factor is very important in study of pile groups. Once the interaction factors between individual piles have been determined, pile group response can be obtained through simple system of algebraic equations. A large amount of researches with resource to rigorous numerical solutions ([3.13]~[3.15]) or simple physical models have been conducted on obtaining the static interaction factors, also the interaction factor concept was extended to dynamic problems by (Kaynia and Kausel [3.3]; Dobry and Gazetas [3.16]). Their results for pile group systems showed good match in comparison with the results from rigorous numerical solutions.

The inertial interaction factor ${\alpha^I}_{21}(s,\theta)$ between two piles is defined as the response of a pile carrying no load at its head (passive pile), subjected to the ground displacement induced by an adjacent pile (active pile), which carries either horizontal force or moment atop its head. The inertial interaction factor then is defined as the response atop the passive pile, normalized by the response of the active pile which is caused by its own loading. This can be written as:

$$\alpha = \frac{\text{additional displacement atop the pile 2 due to the adjacent pile 1}}{\text{dispalcement atop the pile 1 due to its own head load}} = \frac{u_{21}(0)}{u_{11}(0)} \tag{3.21}$$

In flexural vibrations, the inertial interaction factor is expressed by a 2×2 complex matrix.

$$[\alpha^I] = [{\alpha^I}_{21}(s,\theta)] = \begin{bmatrix} {\alpha^I}_{uP} & {\alpha^I}_{uM} \\ {\alpha^I}_{\phi P} & {\alpha^I}_{\phi M} \end{bmatrix} \tag{3.22}$$

where $\alpha_{uP}$= swaying inertial interaction factor; $\alpha_{\phi M}$= rocking inertial interaction factor; $\alpha_{uM}$ and $\alpha_{\phi P}$= cross-swaying-rocking factors. Dobry and Gazetas [3.16] introduced a simplified model for calculating the

dynamic interaction factor between piles in homogeneous soil profiles. They assume that: (1) cylindrical waves are emitted from all points along active pile shaft. The waves propagate through the soil and strike simultaneously the shaft of the passive pile; (2) the passive pile follows exactly attenuated ground motion this infer that interaction between passive pile and encompassing soil is neglected; and (3) the rocking and cross-swaying-rocking interaction factors are small therefore they could be neglected. Based on these suppositions the interaction factors are written as:

$$\alpha^I{}_{uP} \approx \psi(s,\theta);\ \alpha^I{}_{uM} \approx \alpha^I{}_{\phi P} \approx\ \alpha^I{}_{\phi M} \approx 0 \tag{3.23}$$

Despite the simplicity of the method of Dobry and Gazetas, in the case of inhomogeneous soil or slender piles the accuracy of their proposed method gradually degenerates. A similar three-step model was introduced by Makris and Gazetas [3.11] who considered only infinitely-long fixed-head piles in homogeneous soil. To overcome the drawbacks of the Dobry and Gazetas [3.16] method, an improved model is developed by Mylonakis and Gazetas [3.12] who studied lateral vibrations of finite pile length and soil layering. In this study pile cap is assumed to be rotationally fixed. Therefore, $\alpha^I{}_{\phi M}$= rocking inertial interaction factor; $\alpha^I{}_{uM}$ and $\alpha^I{}_{\phi P}$= cross-swaying-rocking interaction factors will be equal to zero and inertial interaction factor between active pile (pile 1) and passive pile (pile 2) can be simplified as:

$$\alpha^I{}_{uP}(s,\theta) = \alpha^I{}_{21}(s,\theta) = \frac{u^I_{21}(0)}{u^I_{11}(0)} \tag{3.24}$$

$$\alpha^I{}_{21}(s,\theta) = \frac{A^I_{21} + B^I_{21}}{A^I_{11} + B^I_{11}} = \frac{k_x + ic_x\omega_g}{k_x + ic_x\omega_n - m_p{\omega_g}^2}\psi_{21}(s,\theta)\xi_{uP} \tag{3.25}$$

The dimensionless diffraction factor $\xi_{uP}$ and inertial interaction factors are related to the boundary conditions at the tip of the fixed-head pile groups and for both cases of hinged and end-bearing (fixed) tip have been obtained in the following sections.

### 3.5.1 Inertial interaction factor for hinged-tip pile groups

$$\alpha^I_{21}(s,\theta) = \frac{u^I_{21}(0)}{u^I_{11}(0)} = \frac{3}{4}\psi(s,\theta)\frac{k_x + ic_x\omega}{k_x + ic_x\omega - m\omega^2}\xi_{hg}(\lambda H) = \alpha_{21}\xi_{hg}(\lambda H) \tag{3.26}$$

$$\xi_{hg}(\lambda H) = \frac{m1}{m2} \tag{3.27}$$

$$m1 = -sinh(4\lambda H) - 2cos(2\lambda H)sinh(2\lambda H) + 2sin(2\lambda H)cosh(2\lambda H) + sin(4\lambda H) + \left(\frac{8\lambda H}{3}\right) sin(2\lambda H)sinh(2\lambda H) \tag{3.28}$$

$$\mathrm{m2} = -sinh(4\lambda H) - 2cos(2\lambda H)sinh(2\lambda H) + 2sin(2\lambda H)cosh(2\lambda H) + sin(4\lambda H) \tag{3.29}$$

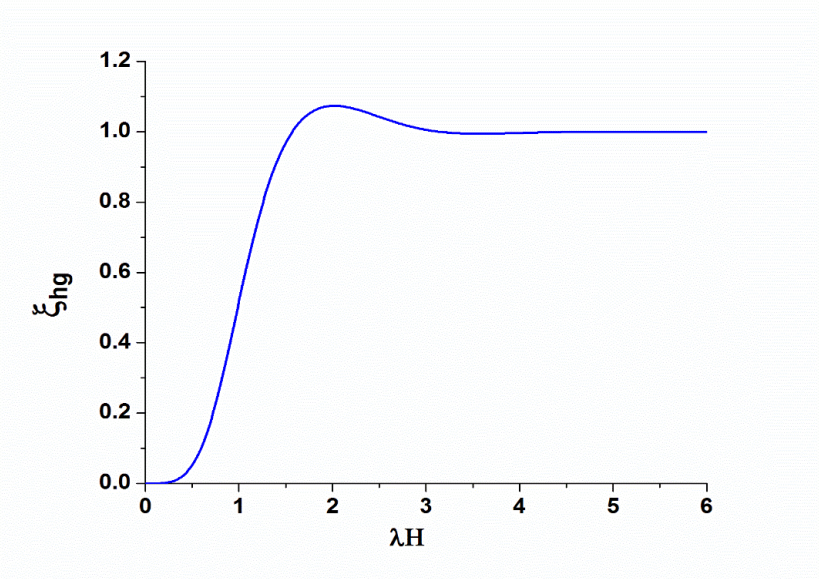


**Fig 3.2:** Dimensionless diffraction factor for hinged-tip pile groups.

### 3.5.2 Inertial interaction factor for fixed-tip pile groups

$$\alpha_{21}^{I}(s,\theta) = \frac{u_{21}^{I}(0)}{u_{11}^{I}(0)} = \frac{3}{4}\psi(s,\theta)\frac{k_x + ic_x\omega}{k_x + ic_x\omega - m\omega^2}\xi_{en}(\lambda H) = \alpha_{21}\xi_{en}(\lambda H) \tag{3.30}$$

$$\xi_{en}(\lambda H) = \frac{m1}{m2} \tag{3.31}$$

$$m1 = -4sin(2\lambda H) + sinh(4\lambda H) + 2cos(2\lambda H)sinh(2\lambda H) + 2sin(2\lambda H)cosh(2\lambda H) - 4sin(2\lambda H) + sin(4\lambda H) - \left(\frac{8\lambda H}{3}\right)cosh(2\lambda H) + \left(\frac{8\lambda H}{3}\right) + \left(\frac{8\lambda H}{3}\right)cos(2\lambda H)cosh(2\lambda H) - \left(\frac{8\lambda H}{3}\right)cos(2\lambda H) \tag{3.32}$$

$$m2 = -4\sin(2\lambda \mathrm{H}) + sinh(4\lambda H) + 2cos(2\lambda H)sinh(2\lambda H) + 2sin(2\lambda H)cosh(2\lambda H) - 4sin(2\lambda H) + sin(4\lambda H) \tag{3.33}$$

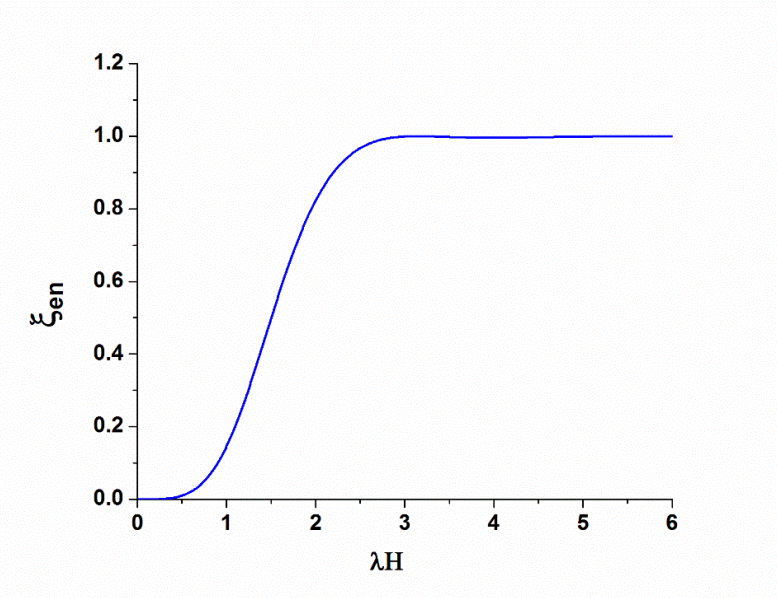


**Figure 3.3:** Dimensionless diffraction factor for fixed-tip pile groups.

## 3.6 Inertial curvature ratios

(1) Inertial curvature ratio of the active pile is defined as the ratio of the active pile head curvature as a single solitary pile due to its own inertial head loading to the active pile-top displacement [3.17]; (2) Inertial curvature ratio of the passive pile is defined as the ratio of the passive pile head curvature due to the additional inertial head displacement of the passive pile to the active pile-top displacement due to the inertial head loading [3.17];

$$\beta_{11}^{I} = \frac{u_{11}^{I}{}''(0)}{u_{11}^{I}(0)} = \frac{2\lambda^2(B_{11}{}^{I} - D_{11}{}^{I})}{A_{11}{}^{I} + C_{11}{}^{I}} \tag{3.34}$$

$$\beta_{21}^{I} = \frac{u_{21}^{I}{}''(0)}{u_{11}^{I}(0)} = \frac{\frac{2\lambda^2}{3}(3(B_{21}{}^{I} - D_{21}{}^{I}) - 2\alpha_{21}(B_{11}{}^{I} - D_{11}{}^{I}))}{A_{11}{}^{I} + C_{11}{}^{I}} \tag{3.35}$$

### 3.6.1 Inertial curvature ratios for hinged-tip pile groups

$$\beta_{11}^{I} = \frac{u_{11}^{I}{}''(0)}{u_{11}^{I}(0)} = -2\lambda^2 \frac{\sin(2\lambda H) + \sinh(2\lambda H)}{(\sinh(2\lambda H) - \sin(2\lambda H))} \tag{3.36}$$

$$\beta_{21}^{I} = \frac{u_{21}^{I}{}''(0)}{u_{11}^{I}(0)} = -2\lambda^2 \alpha_{21} H_{2hg}(\lambda H) \tag{3.37}$$

$$H_{2hg}(\lambda H) = \frac{m11}{m22} \tag{3.38}$$

$$\begin{aligned} \mathrm{m11} = \cosh(6\lambda \mathrm{H}) &- 3cosh(2\lambda H) + 2cos(2\lambda H)cosh(4\lambda H) - 3cos(2\lambda H) \\ &+ 2cos(4\lambda H)cosh(2\lambda H) + cos(6\lambda H) - 16\lambda H sinh(2\lambda H) \\ &- 8\lambda H cos(2\lambda H)sinh(4\lambda H) + 16\lambda H sin(2\lambda H) + 8\lambda H sin(4\lambda H)cosh(2\lambda H) \end{aligned} \tag{3.39}$$

$$\begin{aligned} \mathrm{m22} = 3(&cosh(2\lambda H) + cosh(6\lambda H) + 2cos(2\lambda H)cosh(4\lambda H) - cos(2\lambda H) \\ &- 2cos(4\lambda H)cosh(2\lambda H) - cos(6\lambda H) - 4sin(2\lambda H)sinh(4\lambda H) \\ &- 4sin(4\lambda H)sinh(2\lambda H) \end{aligned} \tag{3.40}$$

### 3.6.2 Inertial curvature ratios for fixed-tip pile groups

$$\beta_{11}^{I} = -2\lambda^2 \frac{\cosh(2\lambda H) - \cos(2\lambda H)}{(\cosh(2\lambda H) + \cos(2\lambda H) - 2)} = -2\lambda^2 H_{1en}(\lambda H) \tag{3.41}$$

$$\beta_{21}^{I} = \frac{u_{21}^{I}{}''(0)}{u_{11}^{I}(0)} = -2\lambda^2 \alpha_{21} H_{2en}(\lambda H) \tag{3.42}$$

$$H_{2en}(\lambda H) = \frac{m11}{m22} \tag{3.43}$$

$$\begin{aligned} m11 = &sinh(4\lambda H) - sin(4\lambda H) - 2sinh(2\lambda H)cos(2\lambda H) + 2sin(2\lambda H)cosh(2\lambda H) \\ &- 8\lambda H sin(2\lambda H)sinh(2\lambda H) \end{aligned} \tag{3.44}$$

$$\begin{aligned} m22 = 3(&sinh(4\lambda H) - 4sinh(2\lambda H) + 2cos(2\lambda H)sinh(2\lambda H) + 2sin(2\lambda H)cosh(2\lambda H) \\ &- 4sin(2\lambda H) + sin(4\lambda H)) \end{aligned} \tag{3.45}$$

## 3.7 Inertial response of pile-soil system

A pile group with identical *N* piles was considered to be connected by a rigid cap restricted against rotation and subjected to lateral loading $V(t) = V_0 e^{i\omega_g t}$ at the head of pile group. The total horizontal response of *N* pile at the head may be calculated as the sum of the following components: (1) The horizontal displacement at the head of single (solitary) pile due to its own head loading with the amplitudes $P_1$ , ... , $P_N$ ; (2) The additional horizontal displacement at the head of the pile transmitted from the other *N*-

*1* piles due to their head-loading with the amplitudes $P_1 \dots , P_N$.When the horizontal head displacement of the foundation is expressed by $U^{(G)}$, the compatibility condition can be described by:

$$\begin{cases} U^{(G)} = \sum_{j=1}^{N} {\alpha^I}_{ij} \frac{P_j}{{K_x}^{(1)}} \\ \sum_{j=1}^{N} P_j = V_0 \end{cases} \tag{3.46}$$

These system of equations can be set into a matrix form as:

$$\begin{bmatrix} 1 & -{\alpha^I}_{11} & -{\alpha^I}_{12} & \dots & -{\alpha^I}_{1N} \\ 1 & -{\alpha^I}_{11} & -{\alpha^I}_{11} & \dots & -{\alpha^I}_{2N} \\ \vdots & \vdots & \vdots & \vdots & \vdots \\ 1 & -{\alpha^I}_{N1} & -{\alpha^I}_{N2} & \cdots & -{\alpha^I}_{NN} \\ 0 & 1 & 1 & \cdots & 1 \end{bmatrix} \begin{Bmatrix} U^{(G)} \\ \frac{P_1}{{K_x}^{(1)}} \\ \frac{P_2}{{K_x}^{(1)}} \\ \vdots \\ \frac{P_N}{{K_x}^{(1)}} \end{Bmatrix} = \begin{Bmatrix} 0 \\ 0 \\ \vdots \\ 0 \\ \frac{V_0}{{K_x}^{(1)}} \end{Bmatrix} \tag{3.47}$$

where ${\alpha^I}_{ij}$ are the interaction factors for inertial loading in the case where $i = j \;\; {\alpha^I}_{ij} = 1$ and ${K_x}^{(1)}$ is the dynamic stiffness at the head of single pile (Equations (3.48) and (3.49)). Finally by using superposition method the total curvature can be expressed as:

$${K_x}^{(1)} = EI\lambda^3 F(\lambda H) \tag{3.48}$$

$$F(\lambda H) = \begin{cases} 4\dfrac{\cos(2\lambda H) + \cosh(2\lambda H)}{-\sin(2\lambda H) + \sinh(2\lambda H)} & \text{end} - \text{bearing} \\ 4\dfrac{\sin(2\lambda H) + \sinh(2\lambda H)}{\cos(2\lambda H) + \cosh(2\lambda H) - 2} & \text{hinged} \end{cases} \tag{3.49}$$

$$U_i''(0) = \sum_{j=1}^{N} \beta_{ij}^I \frac{P_j}{{K_x}^{(1)}} \tag{3.50}$$

Finally by using superposition method the total curvature can be expressed as:

$$\begin{Bmatrix} U_1''(0) \\ U_2''(0) \\ \vdots \\ U_N''(0) \end{Bmatrix} = \begin{bmatrix} \beta_{11}^I & \beta_{12}^I & \dots & \beta_{1N}^I \\ \beta_{21}^I & \beta_{22}^I & \dots & \beta_{2N}^I \\ \vdots & \vdots & \vdots & \vdots \\ \beta_{N1}^I & \beta_{N2}^I & \dots & \beta_{NN}^I \end{bmatrix} \begin{Bmatrix} \frac{P_1}{K_x{}^{(1)}} \\ \frac{P_2}{K_x{}^{(1)}} \\ \vdots \\ \frac{P_N}{K_x{}^{(1)}} \end{Bmatrix} \tag{3.51}$$

Further Inertial curvature ratio can be set to matrix form:

$$\begin{bmatrix} \beta_{11}^I & \beta_{12}^I & \dots & \beta_{1N}^I \\ \beta_{21}^I & \beta_{22}^I & \dots & \beta_{2N}^I \\ \vdots & \vdots & \vdots & \vdots \\ \beta_{N1}^I & \beta_{N2}^I & \dots & \beta_{NN}^I \end{bmatrix} = -2\lambda^2 \begin{bmatrix} H_1(\lambda H) & \alpha_{12}H_2(\lambda H) & \dots & \alpha_{1N}H_2(\lambda H) \\ \alpha_{21}H_2(\lambda H) & H_1(\lambda H) & \dots & \alpha_{2N}H_2(\lambda H) \\ \vdots & \vdots & \vdots & \vdots \\ \alpha_{N1}H_2(\lambda H) & \alpha_{N2}H_2(\lambda H) & \dots & H_1(\lambda H) \end{bmatrix} \tag{3.52}$$

$$\beta_{\mathrm{ij}}{}^I = -2\lambda^2 (H_1(\lambda H)[I] + H_2(\lambda H)[\alpha'_{ij}]) \tag{3.53}$$

$$[\alpha'_{ij}] = [\alpha_{ij}] - [I] \tag{3.54}$$

Based on (9) group displacement $U^G$ and vector of forces $\left\{\frac{P_i}{K_x{}^{(1)}}\right\}$ can be obtained as:

$$\left\{\frac{P_i}{K_x{}^{(1)}}\right\} = \{\gamma_j\}\frac{V_0}{K_x{}^{(1)}} \tag{3.55}$$

Vector $\{\gamma_j\}$ is displacement group factor which can be obtained after solving Equation (3.47). By replacing vector forces in Equation (3.50) bending strains at the head of each pile in pile groups in vector form can be calculated as following expression:

$$\{\varepsilon_{pi}^I(0)\} = \{-\frac{d}{2}\frac{d^2U_i(z=0)}{dz^2}\} \tag{3.56}$$

In reality pile foundations are subjected two simultaneous actions arising from kinematic and inertial soil-pile interaction. Therefore in this study, to assist in understanding the main characteristics of the inertial interaction, it would be beneficial to normalize the inertial bending strains $\varepsilon_{pi}^I$ at the head of each pile with

respect to soil deformations or mean shear strain of the homogeneous soil layer which is defined as $\gamma_s$ ([3.8]). Therefore the closed form formula of the normalized bending strains can be written as follows:

$$\left\{\frac{\varepsilon_{pi}^{I}(0)}{\gamma_s}\right\} = [\beta_{ij}^{I}]\{\gamma_j\}\frac{fr}{\frac{\pi}{8}(\frac{r}{H})^3(\lambda H)F(\lambda H)} \tag{3.56}$$

Factor $fr$ is a dimensionless factor which is related to the effect of the lateral load relative to the deformation of the soil layer. This factor is a complex value since there is a phase lag $\varphi_r$ between lateral load $V$ and the mean shear strain of the soil medium $\gamma_s$ therefore, this factor can be rewritten again by the following formula:

$$fr = Fre^{i\varphi_r} \tag{3.57}$$

where

$$Fr = \left|\frac{V_0}{E_p\gamma_s H^2}\right| \tag{3.58}$$

and

$$\varphi_r = \arg(\frac{V_0}{\gamma_s}) \tag{3.59}$$

The calculation of the factor $Fr$ is based on estimation of the maximum values of the lateral load $V_0$ and the mean shear strain $\gamma_s$. The estimation of phase lag $\varphi_r$ in Equation (3.59) is a complex task because there have been few researches into the estimation of phase lag between the lateral load $V_0$ and mean shear strain $\gamma_s$ (ground motion), particularly in soil-pile-structure systems where kinematic interaction is predominant. Murono and Nishimura [3.18] investigated fundamental characteristics of the phase lag between the lateral load and the ground motion. They indicated that three types of phase lag (Figure 3.4) can occur and they are associated with the ratio of the natural period of soil-pile-structure system $T_s$ and the fundamental natural period of a soil medium $T_g$ in a soil-pile-structure system where the kinematic interaction dominates, and are as follows: (1) in the case of $T_s/T_g \leq 1$, the phase lag of the lateral load with respect to the ground

motion tends to become zero; (2) in the case of $T_s/T_g \approx 1$, the phase lag tends to become $-\pi/2$; and (3) in the case of $T_s/T_g \geq 1$, the phase lag tends to become $-\pi$ ( in accordace with design coefficients in their study, $-3\pi/4$ would be practically appropriate).

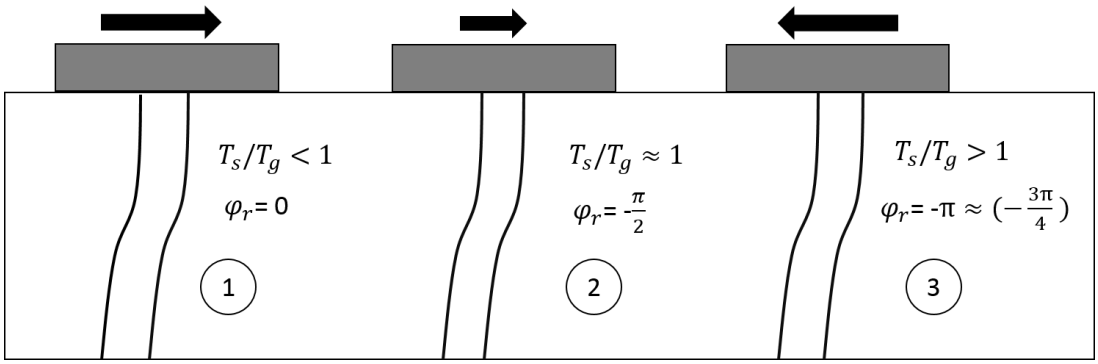


**Figure 3.4:** Different types of phase lag between amplitude of inertial lateral loads and soil deformations.

## 3.8 Verification of the method with numerical method

In order to verify the accuracy of the proposed method, two cases including single pile and 3×3 piles with tip condition (hinged) are considered. Piles are connected by a rotationally restricted rigid cap. Also, piles are subjected to harmonic head loading $V(t) = V_0 e^{i\omega_g t}$ as shown in Figure 3.5. The frequency of the horizontal excitation equals to the fundamental frequency of the soil medium. Results are compared against those of a three-dimensional time-harmonic continuum linear model based on a coupled finite elements-boundary elements (FE-BE) formulation [19,20]. In this formulation approach, the boundary element method (BE) is used to model the dynamic behavior of the homogeneous, viscoelastic, isotropic, linear soil medium; while finite elements are used for piles, the piles are represented by FE as beams according to the Bernoulli hypothesis. The piles are treated as load lines acting within the soil, so their presence does not affect the soil continuity. Welded boundary conditions are assumed at the pile-soil interface. From the boundary element point of view, the loads arising from the pile–soil interaction are modelled as distributions of interaction forces applied on an internal line defined by the pile axis, which can be named as ‘load-line’ (see Figure 3.5). Piles rigidity is provided by mono-dimensional finite elements, bonded to

the surrounding soil by equilibrium and compatibility conditions. In this section it is assumed that the phase lag is equal to zero.

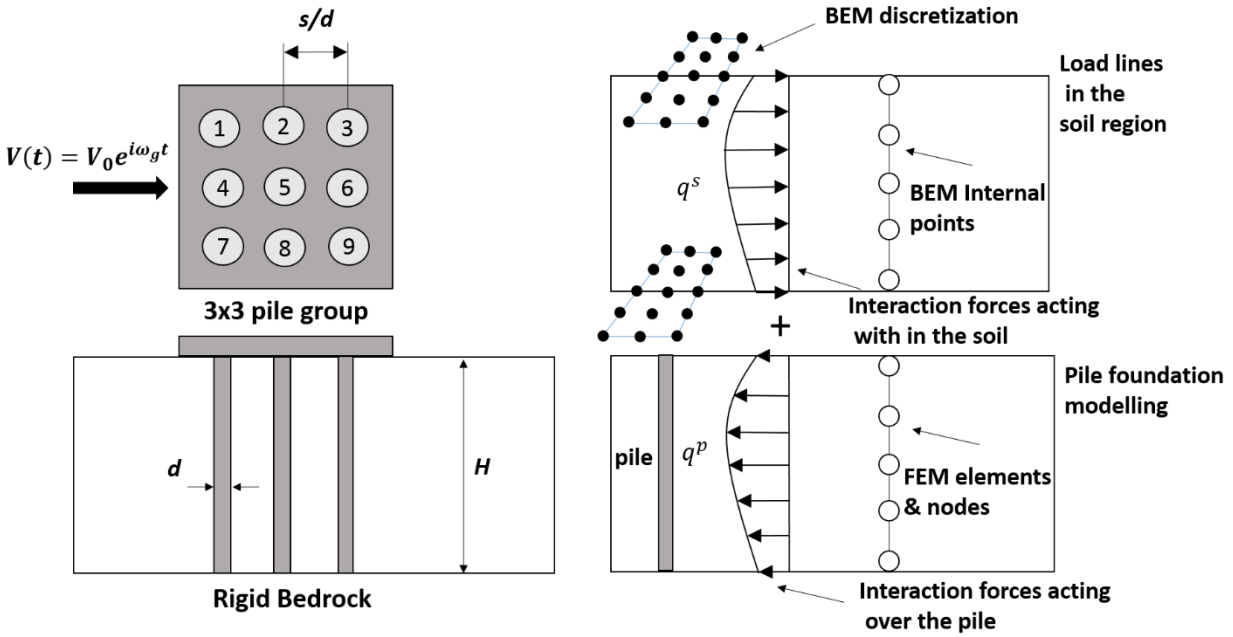


**Figure 3.5:** Pile foundation modelling through FEM-BEM coupling formulation.

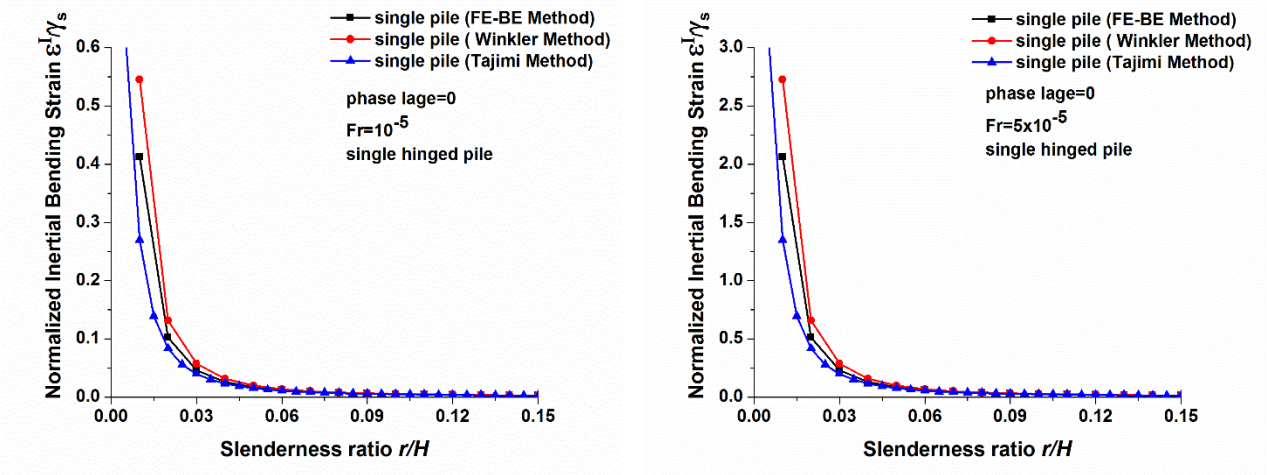


**Figure 3.6:** Normalized inertial bending strains of hinged single pile. Comparison of the present method with rigorous results by FE-BE and Tajimi method ($\frac{\rho_p}{\rho_s} = 1.43,\ \upsilon_s = 0.4\ , \beta_s = 0.05\ , \frac{E_p}{E_s} = 1000$ ).

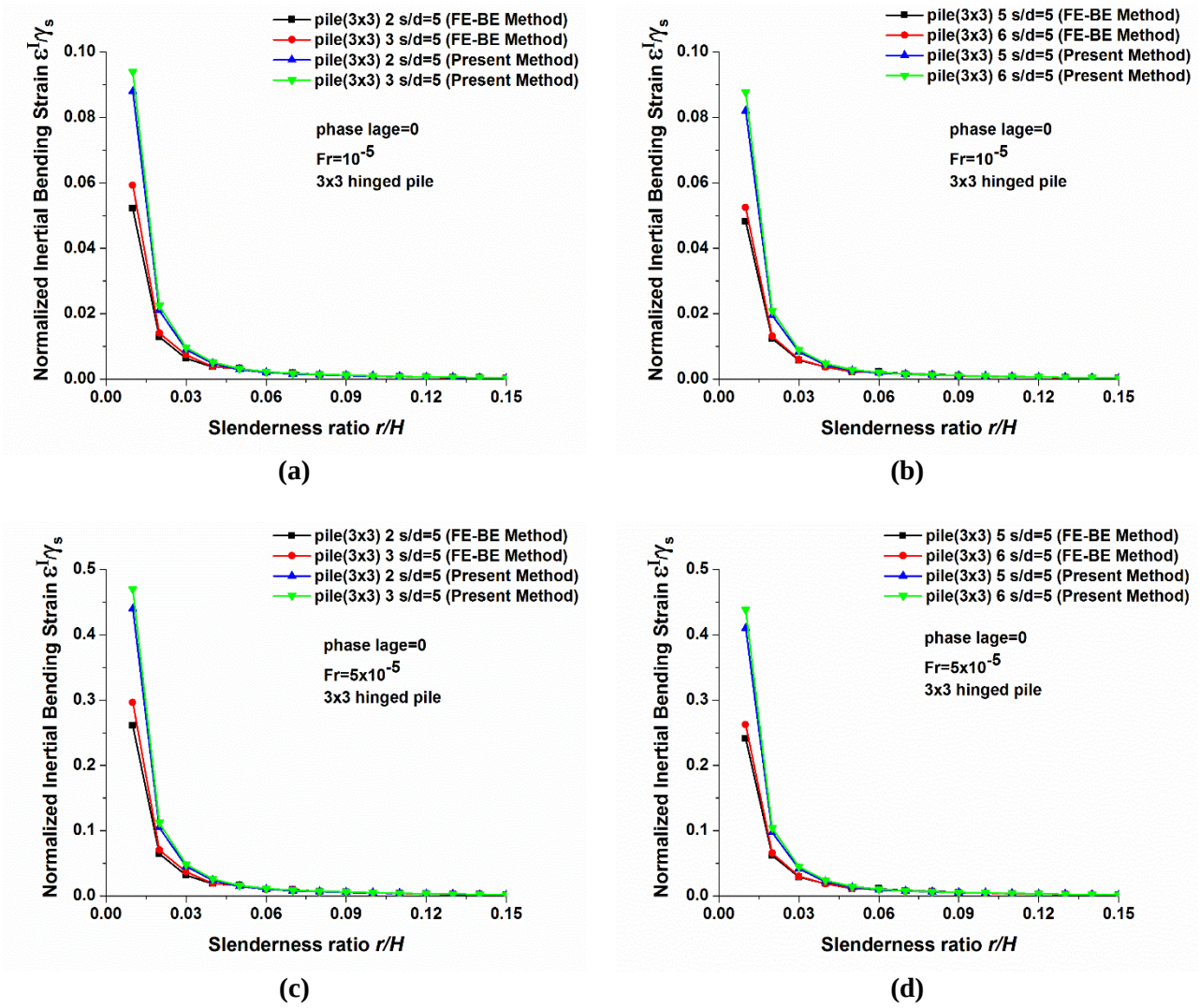


**Figure 3.7:** Normalized inertial bending strains of 3×3 hinged pile groups. Comparison of the present method with rigorous results by FE-BE method ($\frac{\rho_p}{\rho_s} = 1.43,\ \upsilon_s = 0.4\ , \beta_s = 0.05\ , \frac{E_p}{E_s} = 1000\ , \frac{s}{d} = 5$).

In Figures 3.6 and 3.7, normalized inertial bending strains in single hinged piles and 3× 3 hinged pile groups respectively presented with three different methods of FE-BE, Proposed method of this study and Tajimi method. Their variations as functions of the slenderness ratio $r/H$ with different values of the factor $Fr$ for the phase lag $\varphi_r = 0$ are depicted. With reference to Figure 3.6, it is observed that all of these methods are converged together at slenderness ratio $/H \approx 0.03$ . However before this slenderness ratio they differ a little in their values, the proposed method has the values larger than the others, the Tajimi method has the smaller values and the FE-BE method locate between the Tajimi method and the proposed method. In

Figure 3.7, the proposed method are compared with FE-BE method for 3×3 hinged pile groups. It is also observed that the proposed method overestimate inertial bending strains for small values of the slenderness ratios $r/H \approx 0.03$.

## 3.9 Behavior of inertial bending in pile groups

To have further insight into the characteristics and behavior of the normalized inertial bending strains against slenderness ratio $r/H$ by using the expression proposed in Equation (3.56), additional studies of the 3×3 fixed-head pile groups with different boundary conditions at the tip (fixed or hinged) are carried out. Piles are subjected to harmonic head loading $(t) = V_0 e^{i\omega_g t}$ . The frequency of excitation is assumed to be equal to the fundamental frequency of the soil layer. Special attention is paid to the effects of the parameters like pile spacing $/d$ , pile-soil stiffness ratio $E_p/E_s$, factor $Fr$ on the normalized inertial bending strains in the group.

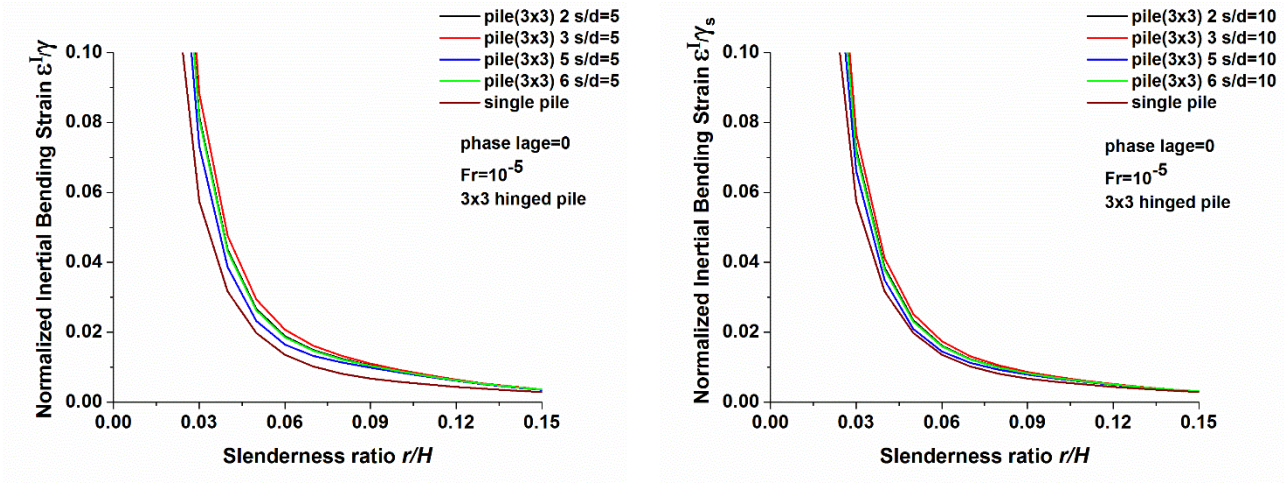


**Figure 3.8:** Normalized inertial bending strains of 3×3 hinged pile groups $(\frac{\rho_p}{\rho_s} = 1.43,\ \upsilon_s = 0.4\ , \beta_s = 0.05\ , \frac{E_p}{E_s} = 1000, Fr = 10^{-5})$.

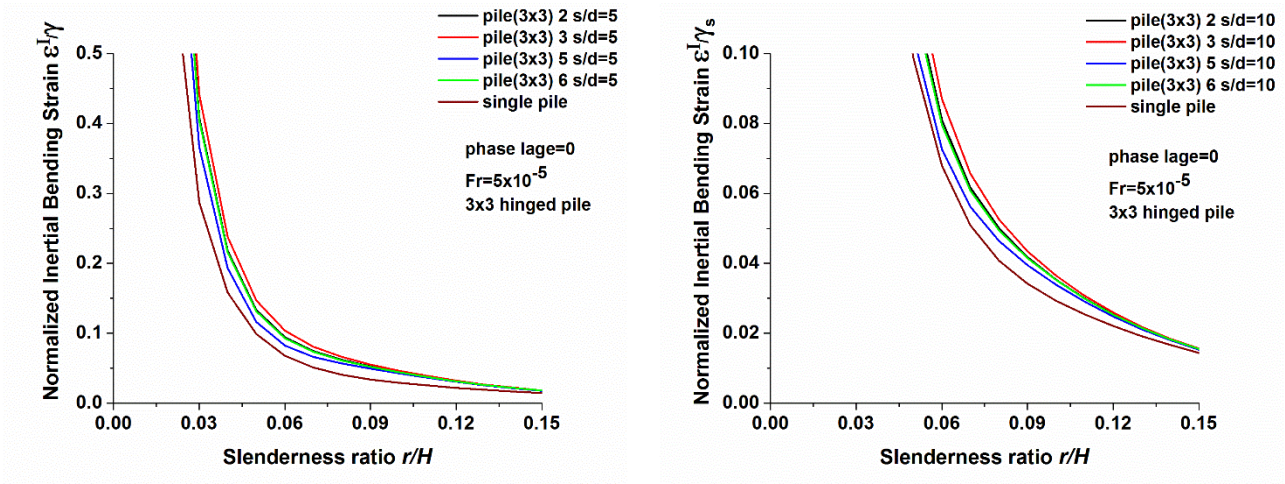


**(a)** **(b)**

**Figure 3.9:** Normalized inertial bending strains of 3×3 hinged pile groups ($\frac{\rho_p}{\rho_s} = 1.43,\ \upsilon_s = 0.4\ , \beta_s = 0.05\ , \frac{E_p}{E_s} = 1000, Fr = 5 \times 10^{-5}$).

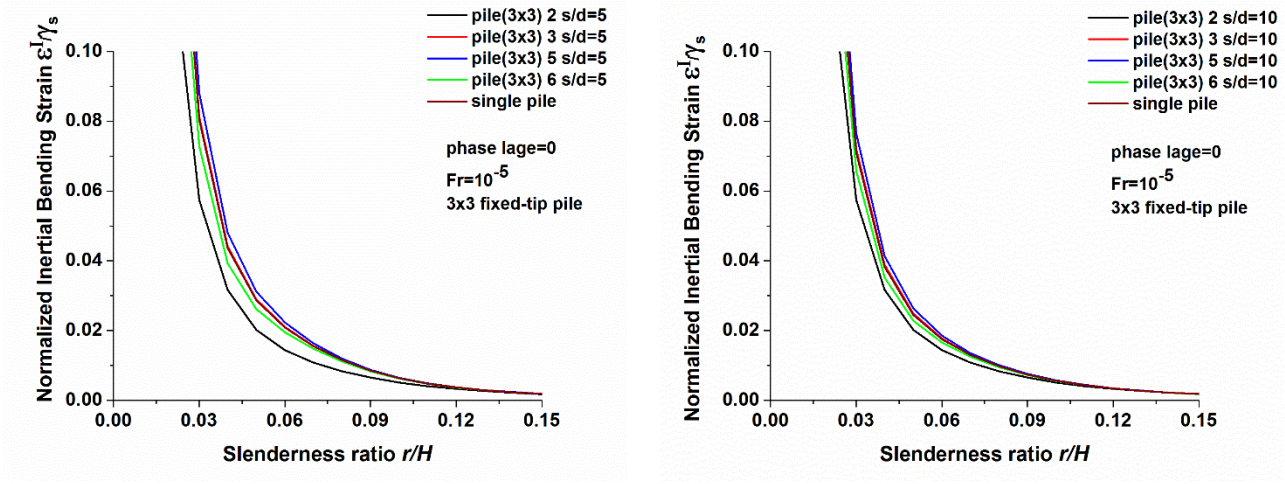


**(a)** **(b)**

**Figure 3.10:** Normalized inertial bending strains of 3×3 fixed-tip pile groups ($\frac{\rho_p}{\rho_s} = 1.43,\ \upsilon_s = 0.4\ , \beta_s = 0.05\ , \frac{E_p}{E_s} = 1000, Fr = 10^{-5}$ ).

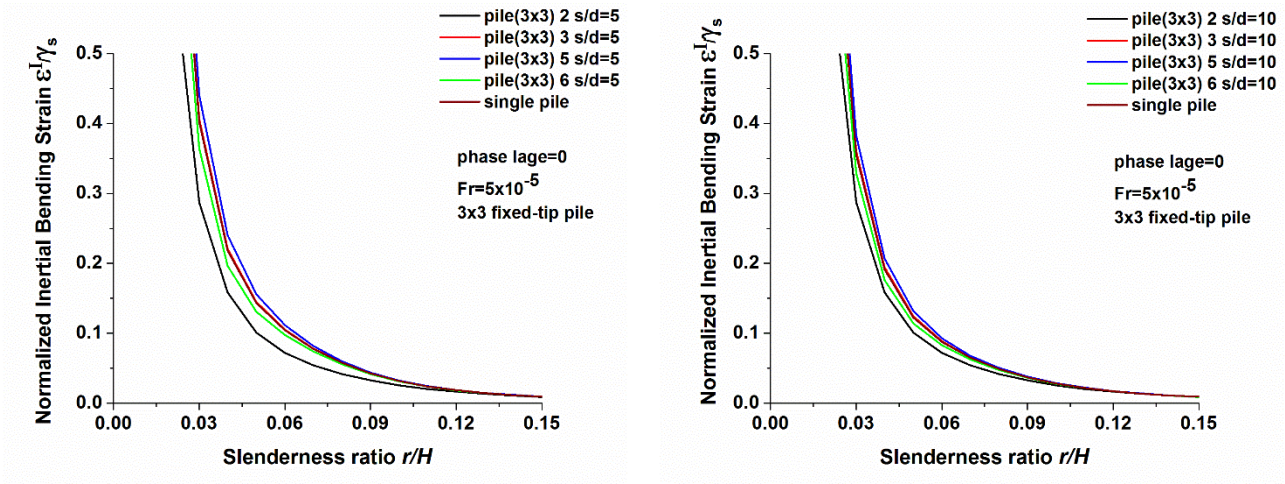


**(a)** **(b)**

**Figure 3.11:** Normalized inertial bending strains of 3×3 fixed-tip pile groups ($\frac{\rho_p}{\rho_s} = 1.43,\ \upsilon_s = 0.4\ , \beta_s = 0.05\ , \frac{E_p}{E_s} = 1000, Fr = 5 \times 10^{-5}$ ).

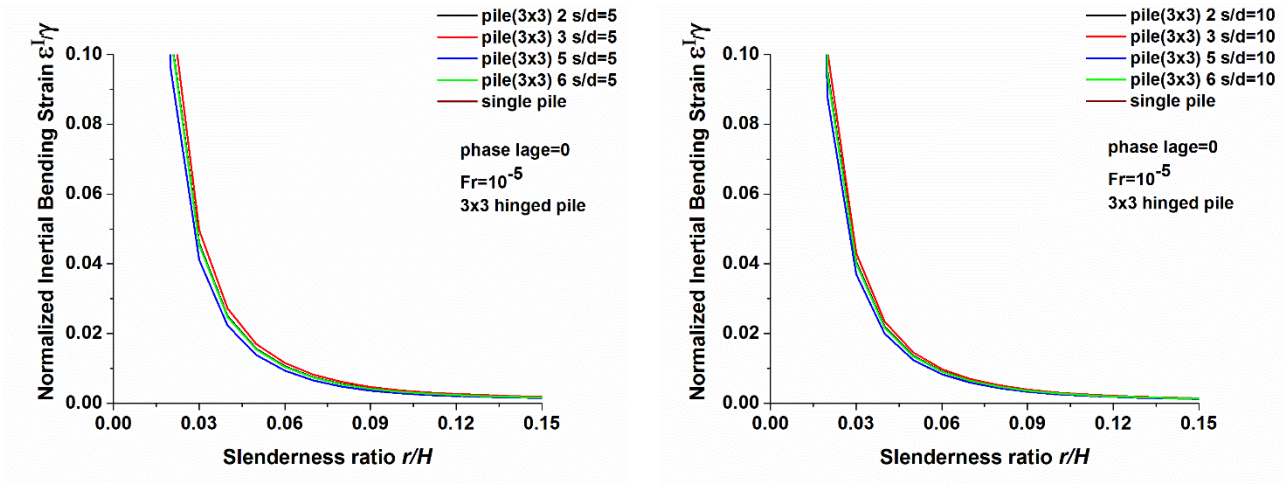


**(a)** **(b)**

**Figure 3.12:** Normalized inertial bending strains of 3×3 hinged-tip pile groups ($\frac{\rho_p}{\rho_s} = 1.43,\ \upsilon_s = 0.4\ , \beta_s = 0.05\ , \frac{E_p}{E_s} = 100,\ Fr = 10^{-5}$).

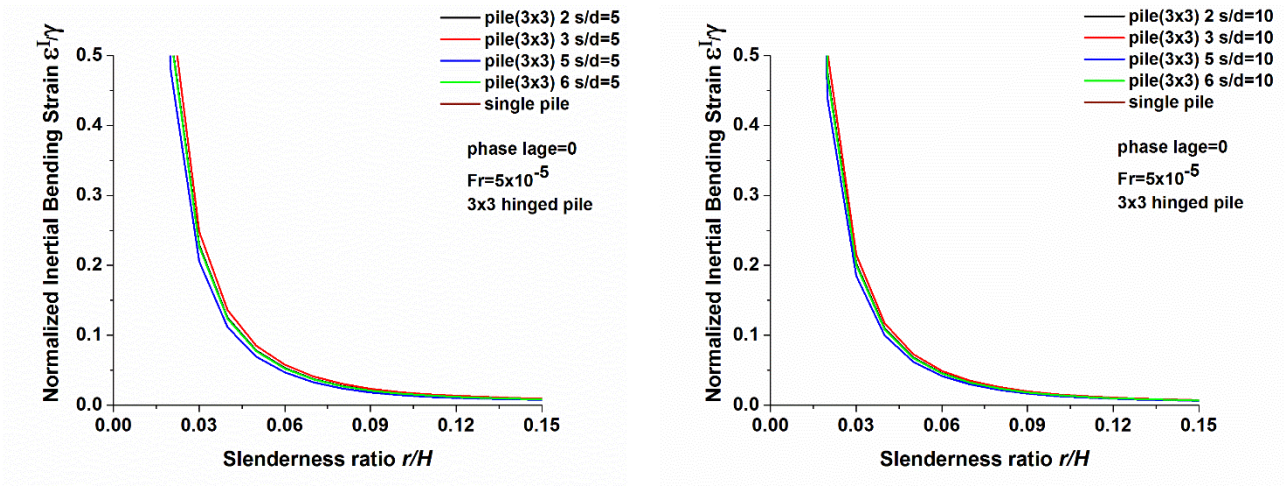


**(a)** **(b)**

**Figure 3.13:** Normalized inertial bending strains of 3×3 hinged-tip pile groups $(\frac{\rho_p}{\rho_s} = 1.43,\ \upsilon_s = 0.4\ , \beta_s = 0.05\ , \frac{E_p}{E_s} = 100, Fr = 5 \times 10^{-5}\ )$.

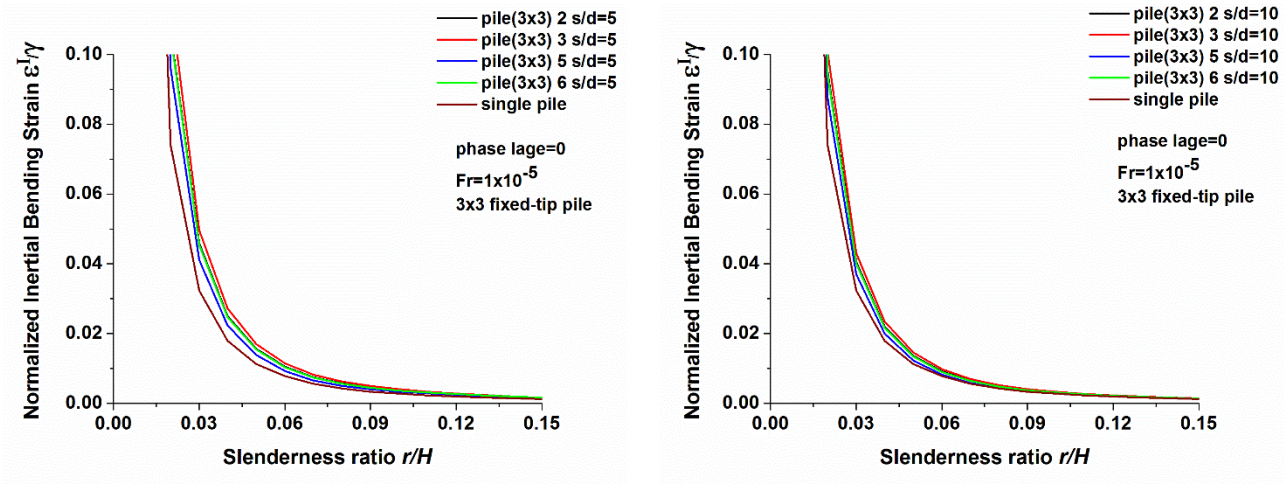


**(a)** **(b)**

**Figure 3.14:** Normalized inertial bending strains of 3×3 fixed-tip pile groups $(\frac{\rho_p}{\rho_s} = 1.43,\ \upsilon_s = 0.4\ , \beta_s = 0.05\ , \frac{E_p}{E_s} = 100, Fr = 10^{-5}\ )$.

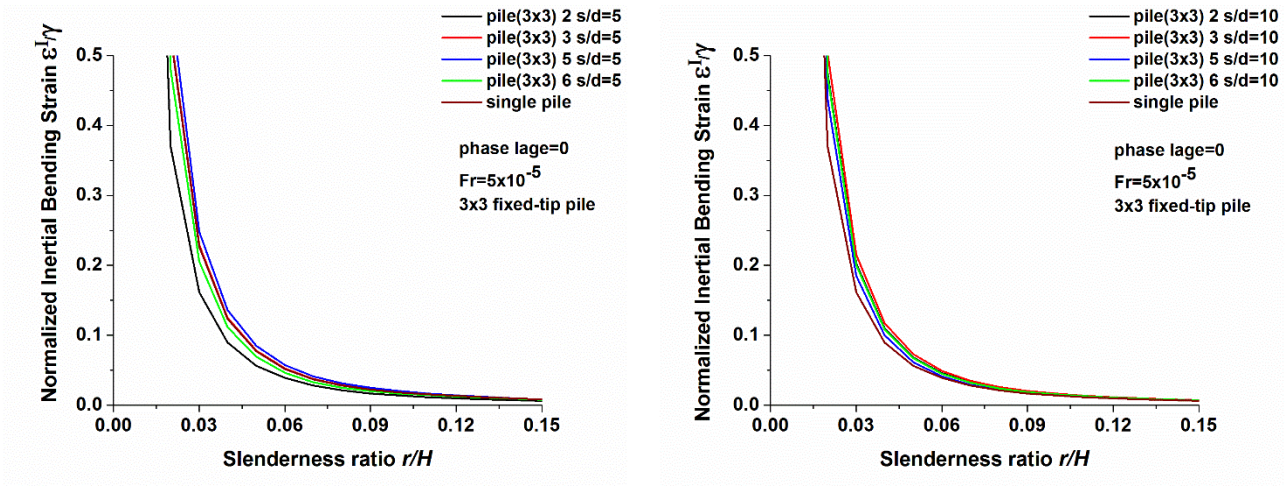


**(a)** **(b)**

**Figure 3.15:** Normalized inertial bending strains of 3×3 fixed-tip pile groups ($\frac{\rho_p}{\rho_s} = 1.43,\ \upsilon_s = 0.4\ , \beta_s = 0.05\ , \frac{E_p}{E_s} = 100\ , Fr = 5 \times 10^{-5}$).

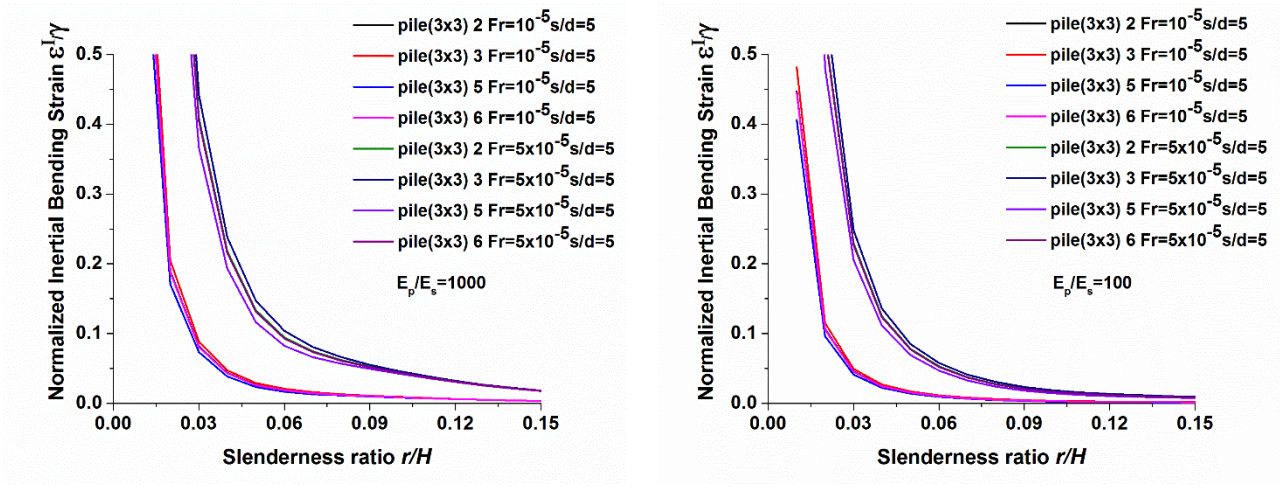


**(a)** **(b)**

**Figure 3.16:** Normalized inertial bending strains of 3×3 hinged-tip pile groups with different parameters ($\frac{E_p}{E_s} = 100,1000, Fr = 10^{-5}, 5 \times 10^{-5}\ \frac{\rho_p}{\rho_s} = 1.43,\ \upsilon_s = 0.4\ , \beta_s = 0.05, \varphi_r = 0, \frac{s}{d} = 5$).

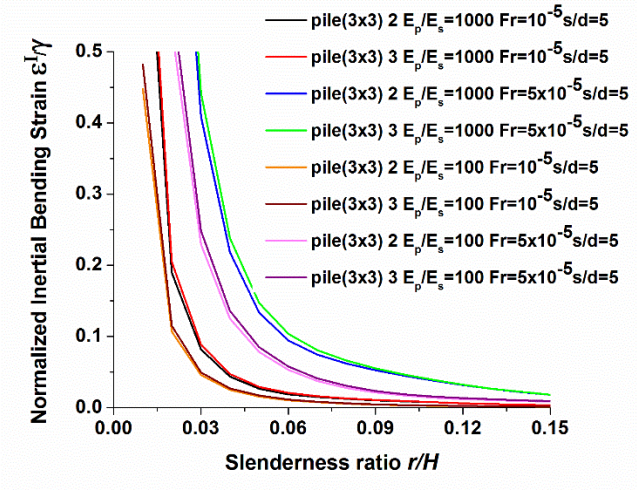


**Figure 3.17:** Normalized inertial bending strains of 3×3 hinged-tip pile groups (pile2, pile3) with different parameters ($\frac{E_p}{E_s} = 100,1000, Fr = 10^{-5}, 5 \times 10^{-5} \frac{\rho_p}{\rho_s} = 1.43,\ \upsilon_s = 0.4\ , \beta_s = 0.05, \varphi_r = 0\ , \frac{s}{d} = 5$).

Figures 3.8 through 3.17 show the values of normalized inertial bending strains in 3× 3 pile groups with different tip conditions (hinged and fixed). Their variations as functions of the slenderness ratio $r/H$ with different values of the factor $Fr = 10^{-5}, 5 \times 10^{-5}$and the pile-soil stiffness ratio $E_p/E_s = 100,1000$, pile spacing $s/d = 5,10$ for the phase lag $\varphi_r = 0$ are presented. These figures reveal that even in pile group configurations, each pile follows the general trend of the single pile. In addition, it is worth noting that in pile groups normalized inertial bending strains are very close to those of the single pile over the entire range of the slenderness ratio $r/H$. Therefore within the entire range of slenderness ratios $r/H$, the normalized inertial bending strains of piles in a group can be estimated by that of the single pile. Indeed this can be validated from Figures 3.8 through 3.17. Furthermore, as the pile spacing $s/d$ increases, normalized bending strains of pile groups converge to those of single piles. For small values of the slenderness ratio $r/H$, normalized inertial bending strains tend to increase. However, strains significantly decrease as $r/H$ increases. To assist in understanding of the behavior of the inertial bending strains in the pile groups. The detailed results and the influence of important parameters $(Fr, E_p/E_s)$ on behavior of inertial bending strains are explained in the following sections:

### 3.9.1 Effect of factor $Fr$

The results of Figures 3.8 through 3.13 for 3×3 pile groups and single pile with different tip conditions and different parameters, imply that the value of normalized inertial bending strains at the head of each pile in pile groups and single pile tend to shift to larger values, while the factor $Fr$ increases. This behavior can be more clearly seen in Figures 3.12 and 3.13. This reason is physically linked to the effect of lateral inertial loads associated with the factor $Fr$, this increase seems to be more significant for large values of the pile-soil stiffness ratios $E_p/E_s$.

### 3.9.2 Effect of pile-soil stiffness ratio $E_p/E_s$

The results of Figures 3.8 through 3.13 indicate that the values of the normalized inertial bending strains tend to shift to larger values as the pile-soil stiffness ratio $E_p/E_s$ increases. For $E_p/E_s \to \infty$ piles behave inflexibly and regardless of fixity conditions at the tip, all piles will experience higher values of the inertial bending strains. This reason can be validated from Figure 3.13.

## 3.10 Conclusions

An efficient method has been extended to compute the bending strains of fixed-head pile groups of finite length embedded in a homogeneous soil layer, where inertial interaction dominates. This method allows the inertial bending strains to be obtained in closed form formula while using dynamic Winkler model in conjunction with an extension to three dimensional of Novak's plain-strain model. This model is free of the drawbacks of the two dimensional plain-strain model reproducing cutoff frequency of the soil-pile system. Pile group effect is considered through interaction factors and the inertial bending strains are normalized with respect to a mean shear strain of a soil stratum $\gamma_s$ then variation of normalized inertial bending strains against slenderness ratio $r/H$ are investigated which gives valuable insight into the characteristics of the inertial bending strains in pile groups. Homogeneous solutions are considered in active and passive piles

deflections for appropriately considering various boundary conditions when estimating bending strains. Solutions for pile group response are performed in fundamental frequency of soil strata.

In pile groups when the slenderness ratios $r/H$ approach zero in all piles, inertial bending strains become infinite. The inertial bending strains decrease significantly as slenderness ratio $r/H$ increases. The inertial bending strains of the piles in a group are very close to those of a single pile. This conclusion allows to approximate the behaviour of pile groups under inertial loads in fundamental frequency of homogeneous soil layer with that of single of the single pile.

## References


[3.1] Novak, M. (1974) Dynamic Stiffness and Damping of piles. *Canadian Geotechnical Journal*, Vol.11, No.5, pp.574-598.

[3.2] Novak, M., and Aboul-Ella, F. (1978) Impedance Functions of Piles in Layered Media. *Journal of The Engineering Mechanics* Division,ASCE 1978 Vol. 104, No. 3,pp. 643-661.

[3.3] Kaynia, AM., Kausel, E. (1982) Dynamic stiffness and seismic response of pile groups. Research report no. R82-03. Cambridge, MA: Massachusetts Institute of Technology.

[3.4] Sen, R., Kausel, E. and Banerjee, P.K. (1985) Dynamic analysis of piles and pile groups embedded in nonhomogeneous soil. *International Journal for Numerical and Analytical Methods*, 9:507-524.

[3.5] Blaney, G.W., Kausel, E. and Roesset, J.M. (1976) Dynamic stiffness of piles, *proceeding.* $2^{nd}$ *International Conference On Numerical Methods in Geomechanics*. Blacksburg, Virginia, pp.1001-1012.

[3.6] Wolf, J.P., Von Arx, G.A. (1982) Horizontally Travelling Waves in Group of Piles Taking Pile-Soil-Pile Interaction into Account, *International Journal of Earthquake Engineering and Structural Dynamics*, Vol. 10.pp. 225-273.

[3.7] Makris, N., Gazetas, G. (1992) Dynamic pile-soil-pile interaction. Part II: Lateral and seismic response. *Earthquake Engineering And Structural Dynamics*, 21(2):145-62.

[3.8] Saitoh, M. (2005) Fixed-head pile bending by kinematic interaction and criteria for its minimization at optimal pile radius. *Journal of Geotechnical and Geoenvironmental Engineering* ASCE, 131 (10):1243-1251.

[3.9] Mylonakis, G., Nikolaou, A.S. (1997) Soil-pile-bridge seismic interaction: kinematic and inertial effects. Part I: soft soil. *Earthquake Engineering and Structural Dynamics*, 26:337-359.

[3.10] Mylonakis, G. (2001) Elastodynamic model for large-diameter end-bearing shafts. Journal Jpn Geotech Soc *: Soils and Foundations*,41(3);31-44.

[3.11] Makris, N., Gazetas, G. (1992) Dynamic pile-soil-pile interaction. Part II: Lateral and seismic response. *Earthquake Engineering And Structural Dynamics*, 21(2):145-62.

[3.12] Mylonakis, G., Gazetas, G. (1999) Lateral Vibration And Inertial Forces of Grouped Piles In Layered Soil. *Journal of Geotechnical and Geoenvironmental Engineering*, 125: 16-25.

[3.13] Poulos, H.G. (1968) Analysis of the settlement of pile groups, *Geotechnique*, Vol. 18,449-471.

[3.14] Batterfield, R. and Banerjee, P.K. (1971) The problem pile cap and pile group interaction, *Geotechnique*, Vol.21, 135-142.

[3.15] Poulos, H.G. and Davis, E.H. (1980) Pile foundation analysis and design:*John Wiley &Sons*.

[3.16] Dobry, R., Gazetas, G. (1988) Simple method for dynamic stiffness and damping of floating pile groups. *Geotéchnique*, London, 38(4): 557-74.

[3.17] Takewaki, I., Kishida, A. (2005) Efficient analysis of pile-group effect on seismic stiffness and strength design of buildings, *Soil Dynamics and Earthquake Engineering*, 25(5): 355-367.

[3.18] Murono, Y., and Nishimura, A. Evaluation of seismic force of pile foundation induced by inertial and kinematic interaction. Proc., 12$^{th}$ World Conference. On Earthquake Engineering, New Zealand 2000, No1496.

[3.19] Padrón LA, Aznárez JJ, Maeso O. (2007) BEM-FEM coupling model for the dynamic analysis of piles and pile groups. *Engineering Analysis with Boundary Elements*, 31(6):473-484.

[3.20] Padrón, LA., Aznárez, JJ., Maeso, O. (2008) Dynamic analysis of piled foundations in stratified soils by a BEM-FEM model. *Soil Dynamics and Earthquake Engineering*, 28(5):333-346.

# CHAPTER 4
# KINEMATIC RESPONSE OF PILE GROUPS

It is well understood that the transmission of seismic waves to the base of a pile-supported structure is different than the free-field motion, because of the dynamic interaction between the foundation and the surrounding soil will occur. This interaction develops regardless of the presence of a superstructure and is referred to as kinematic effect. This problem has received large attention in recent years ([4.1]~[4.15]), and several studies have devoted to investigation of the nature of seismic ground motion and the mechanism of soil-pile interaction to determine the seismic design loads for pile-supported structures. Modern seismic codes and provisions have acknowledged theses aspects and suggest accounting for soil-structure interaction effects in the foundation and superstructure design [4.16],[4.17].

For soil-pile group systems where kinematic interaction dominates, there has been no investigation into the effects of the pile radius on the bending strains. In order to establish criteria for optimal pile radius for kinematically excited pile groups, it is essential to quantify variations of kinematic bending strains with respect to pile radius in a systematic way. This chapter focuses on obtaining a comprehensive relation between the pile radius and the kinematic bending strains at the head of a cylindrical vertical pile group under kinematic loading. Piles are considered to be embedded in a homogeneous elastic stratum resting on a rigid bedrock, being the pile length identical to the thickness of the soil stratum. Two different constraint conditions are considered at the pile tip: (a) hinged tip, and (b) end-bearing (fixed) tip. With an understanding that the maximum value of kinematic bending strains at the head of a pile occurs at the fundamental frequency of the soil stratum for most of the soil profiles [4.5], such specific frequency is targeted in this chapter. Analytical formulations are obtained based on the beam-on-dynamic-Winkler-foundation method. After a brief presentation of the analytical model and its validation, a comprehensive parametric analysis is carried out by varying the main parameters governing the dynamic response of piles.

## 4.1 Analytical solution of kinematic bending of pile groups

The soil-pile system under consideration is shown in Figure 4.1: two vertical cylindrical piles each of length $L$, diameter $d$, cross-sectional moment of inertia $I_p$, mass density $\rho_p$, mass per unit length $m_p$ and Young's modulus of elasticity $E_p$ is embedded in a homogeneous soil layer of thickness $H(=L)$ resting on a rigid base. Pile spacing is denoted with $s$. Soil is modelled as a linear elastic material with Poisson's ratio $\upsilon_s$, mass density $\rho_s$, and frequency-independent material damping $\beta_s$ which is expressed through a complex-valued shear modulus $G_s^* = G_s(1 + 2i\beta_s)$. The reaction of soil to the lateral pile motion is modeled by continuously-distributed frequency-dependent springs $k_x$ and dashpots $c_x$ along the pile length. The pile group is loaded by vertically propagating shear waves expressed in the form of harmonic horizontal displacement $u_g(t) = u_{g0}e^{i\omega t}$ at rigid base level. This section employs the following main assumptions: (a) foundation remains elastic during either seismic ground shaking or lateral head loading; (b) soil restraining action can be modeled using a bed of linear or equivalent-linear Winkler springs and dashpots, uniformly distributed along the pile axis; (c) perfect contact (i.e., no gap and slippage) exist between pile and soil; (d) the flexural deformations of the pile group are dominant during oscillations; (e) the frequency of horizontal excitation is assumed to be equal to the fundamental frequency of the soil medium.

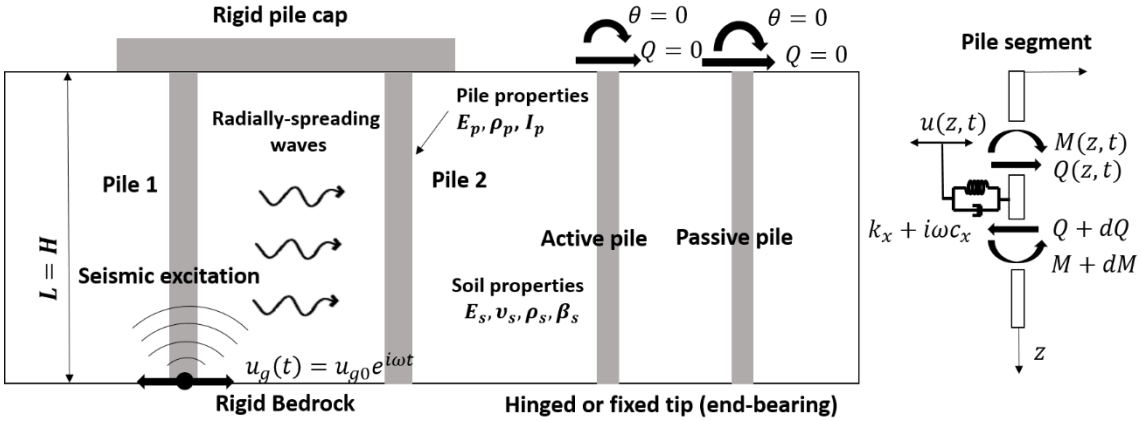


**Figure 4.1:** Problem considered for kinematic interaction with different tip conditions.

## 4.2 Free-field response

In one dimensional analysis based on linear stress-strain laws, stress at any depth $z$ can be obtained as:

$$\tau = -G_s^* \frac{\partial u_{ff}}{\partial z} \tag{4.4}$$

where $\tau$ is the shear stress and $u_{ff}$ is the displacement of the free-field soil which is dependent on time and depth. By considering forced harmonic oscillations of the free-field displacement $u_{ff}(z,t) = u_{ff}(z)e^{i\omega_g t}$ , the equilibrium of forces in the horizontal direction which is acting on a small soil element yields the following differential equation.

$$\frac{d^2 u_{ff}}{dz^2} + \delta^2 u_{ff} = 0 \tag{4.2}$$

In Equation (4.2) $\delta = \omega_g / V_s^*$ is the soil wavenumber, $V_s^* = V_s\sqrt{1 + 2i\beta_s}$ is the complex-valued shear wave velocity of the soil, and $\omega_g$ is the cyclic fundamental frequency of the soil layer. By solving Equation (4.2) and applying the boundary conditions, i.e., zero shear stresses at the free surface and the displacement at the base equals to the induced base displacement $u_{g0}$, the following relation can be obtained[4.18],[4.19].

$$u_{ff}(z,t) = u_{ff0}\cos(\delta z)e^{i\omega_g t} = u_{g0}\frac{\cos(\delta z)}{\cos(\delta H)}e^{i\omega_g t} \tag{4.3}$$

$$\omega_g = \omega_{cutoff} = \frac{\pi V_s}{2H} \tag{4.4}$$

Equation (4.3) describes a standing wave of amplitude $u_{ff0}$ at the soil surface ($z = 0$). By assuming the amplitude of the seismic excitation at the base ($u_{g0}$), the amplification function can be expressed [4.18], [4.19] as:

$$\frac{u_{ff0}}{u_{g0}} = \frac{1}{cos(\delta H)} \tag{4.5}$$

When a group of piles fixed to a cap is subjected to incident seismic waves, the response of each individual pile can be studied as a combination of not only the kinematic part, but also the inertial part owing to the restriction imposed by the rigid cap. In this study, the soil-pile model is assumed to exhibit linear behavior and therefore, both inertial and kinematic interaction effects (has been explained in detail in chapter three) can be studied separately in the context of two modular problems (active and passive pile response). Because inertial problem has been explained in detail in chapter three, only kinematic problem is addressed in the incoming sections.

## 4.3 Deflection of active pile (source pile)

Let $u_{11}(z,t) = u_{11}(z)e^{i\omega_g t}$ denote the harmonic pile deflection. With reference to Figure 5.1 dynamic equilibrium under harmonic steady-state conditions yields:

$$\frac{d^4u_{11}(z)}{dz^4} + 4\lambda^4 u_{11}(z) = \frac{k_x + i\omega_g c_x}{E_p I_p} u_{g0} \frac{\cos(\delta z)}{\cos(\delta H)} \tag{4.6}$$

where $\lambda = \lambda(\omega)$ is the characteristic wavenumber governing the attenuation of pile displacement with depth.

$$\lambda = \left(\frac{k_x + ic_x\omega_g - m_p{\omega_g}^2}{4E_p I_p}\right)^{1/4} \tag{4.7}$$

### 4.3.1 Kinematic response of the active pile (source pile)

It is supposed here that the active pile is excited by kinematic loading $u_g(t) = u_{g0}e^{i\omega_g t}$ at the bedrock. Because of the flexural rigidity, pile will resist the induced lateral vibration of the free-field $u_{ff}(z,t) = u_{ff}(z)e^{i\omega_g t}$ (Equation (4.3)). With such excitation, the pile would undergo deflections (Equation (4.8)) over its entire length, which consist of homogeneous and particular solutions. Homogeneous solution is given in terms of kinematic integration constants ${A^K}_{11}$, ${B^K}_{11}$, ${C^K}_{11}$, ${D^K}_{11}$ which are dependent on the boundary

conditions. $\Gamma$ is a dimensionless response coefficient given by Equation (4.9). Makris and Gazetas [4.20] who investigated the lateral and seismic response of piles, noted that the contribution of the homogeneous solution in most practical cases is not as important as that of the particular solution and can be neglected. In this work, however, since different boundary conditions at the pile tip are considered, homogeneous solution for both cases of active and passive pile is taken into account.

$$u^K{}_{11}(z) = e^{\lambda z}\left(A^K{}_{11}cos(\lambda z) + B^K{}_{11}sin(\lambda z)\right) + e^{-\lambda z}\left(C^K{}_{11}cos(\lambda z) + D^K{}_{11}sin(\lambda z)\right) + \Gamma u_{g0}\frac{\cos(\delta z)}{\cos(\delta H)} \tag{4.8}$$

$$\Gamma = \frac{k_x + ic_x\omega_g}{E_pI_p\delta^4 + k_x + ic_x\omega_g - m_p{\omega_g}^2} \tag{4.9}$$

#### 4.3.1.1 Boundary conditions of active pile (hinged-tip pile groups)

$$\theta^K{}_{11}(z=0) = 0 \quad , \quad \frac{d^3u^K_{11}(z=0)}{dz^3} = 0 \quad , \frac{d^2u^K_{11}(z=H)}{dz^2} = 0 \quad , \quad u^K_{11}(z=H) = u_{g0} \tag{4.10}$$

$$\begin{bmatrix} 1 & 1 & -1 & 1 \\ -1 & 1 & 1 & 1 \\ -2e^{\lambda H}\sin(\lambda H) & 2e^{\lambda H}\cos(\lambda H) & 2e^{-\lambda H}\sin(\lambda H) & -2e^{-\lambda H}\cos(\lambda H) \\ e^{\lambda L}\cos(\lambda H) & e^{\lambda H}\sin(\lambda H) & e^{-\lambda H}\cos(\lambda H) & e^{-\lambda H}\sin(\lambda H) \end{bmatrix} \begin{Bmatrix} A^K_{11} \\ B^K_{11} \\ C^K_{11} \\ D^K_{11} \end{Bmatrix} = \begin{Bmatrix} 0 \\ 0 \\ \frac{\delta^2}{\lambda^2}\Gamma u_{g0} \\ u_{g0}(1-\Gamma) \end{Bmatrix} \tag{4.11}$$

By normalizing the both sides with respect to $\frac{\Gamma u_{g0}}{\cos(\delta H)}$ the matrix form could be simplified into the following from:

$$\begin{bmatrix} 1 & 1 & -1 & 1 \\ -1 & 1 & 1 & 1 \\ -2e^{\lambda H}\sin(\lambda H) & 2e^{\lambda H}\cos(\lambda H) & 2e^{-\lambda H}\sin(\lambda H) & -2e^{-\lambda H}\cos(\lambda H) \\ e^{\lambda L}\cos(\lambda H) & e^{\lambda H}\sin(\lambda H) & e^{-\lambda H}\cos(\lambda H) & e^{-\lambda H}\sin(\lambda H) \end{bmatrix} \begin{Bmatrix} \bar{A}^K_{11} \\ \bar{B}^K_{11} \\ \bar{C}^K_{11} \\ \bar{D}^K_{11} \end{Bmatrix} = \begin{Bmatrix} 0 \\ 0 \\ \frac{\delta^2}{\lambda^2}\cos(\delta H) \\ \frac{(1-\Gamma)}{\Gamma}\cos(\delta H) \end{Bmatrix} \tag{4.12}$$

#### 4.3.1.2 Boundary conditions of active pile (fixed-tip pile groups)

$$\theta^K{}_{11}(z=0) = 0 \quad , \quad \frac{d^3u^K_{11}(z=0)}{dz^3} = 0 \quad , \frac{du^K_{11}(z=H)}{dz} = 0 \quad , u^K_{11}(z=H) = u_g \tag{4.13}$$

$$\begin{bmatrix} 1 & 1 & -1 & 1 \\ -1 & 1 & 1 & 1 \\ \lambda e^{\lambda H}(\cos(\lambda H)-\sin(\lambda H)) & \lambda e^{\lambda H}(\cos(\lambda H)+\sin(\lambda H)) & -\lambda e^{-\lambda H}(\cos(\lambda H)+\sin(\lambda H)) & \lambda e^{-\lambda H}(-\sin(\lambda H)+\cos(\lambda H)) \\ e^{\lambda L}\cos(\lambda H) & e^{\lambda H}\sin(\lambda H) & e^{-\lambda H}\cos(\lambda H) & e^{-\lambda H}\sin(\lambda H) \end{bmatrix} \begin{Bmatrix} A_{11}^K \\ B_{11}^K \\ C_{11}^K \\ D_{11}^K \end{Bmatrix} = \begin{Bmatrix} 0 \\ 0 \\ u_{g0}\frac{\delta}{\lambda}\Gamma\frac{\sin(\delta H)}{\cos(\delta H)} \\ u_{g0}(1-\Gamma) \end{Bmatrix} \tag{4.14}$$

By normalizing both sides with respect to $\frac{\Gamma u_{g0}}{\cos(\delta H)}$ the matrix form could be simplified into the following form:

$$\begin{bmatrix} 1 & 1 & -1 & 1 \\ -1 & 1 & 1 & 1 \\ \lambda e^{\lambda H}(\cos(\lambda H)-\sin(\lambda H)) & \lambda e^{\lambda H}(\cos(\lambda H)+\sin(\lambda H)) & -\lambda e^{-\lambda H}(\cos(\lambda H)+\sin(\lambda H)) & \lambda e^{-\lambda H}(-\sin(\lambda H)+\cos(\lambda H)) \\ e^{\lambda L}\cos(\lambda H) & e^{\lambda H}\sin(\lambda H) & e^{-\lambda H}\cos(\lambda H) & e^{-\lambda H}\sin(\lambda H) \end{bmatrix} \begin{Bmatrix} \bar{A}_{11}^K \\ \bar{B}_{11}^K \\ \bar{C}_{11}^K \\ \bar{D}_{11}^K \end{Bmatrix} = \begin{Bmatrix} 0 \\ 0 \\ \frac{\delta}{\lambda}\sin(\delta H) \\ \frac{(1-\Gamma)}{\Gamma}\cos(\delta H) \end{Bmatrix} \tag{4.15}$$

## 4.4 Attenuation of soil displacement away from active pile (source pile)

This step starts by calculating the difference between single pile deflections and free-field soil displacements, $\Delta u_{11}$ (Figure 2.3). for kinematic loading, this difference is identical to the response of the scattered free-field of the soil: $\Delta u_{11} = u^K{}_{11}(z) - u_{ff}$, new cylindrical waves emanate from the periphery of the vibrating active pile while spreading outward in all directions. In this study attenuation functions of Mylonakis [3.10] is used. With reference to Equation (2.15), at a distance $s$ from the vibrating pile and angle $\theta$ from the direction of loading**,** the free-field soil displacement can be expressed as:

$$u_s(s,z,\theta) = \psi_{21}(s,\theta)\Delta u_{11} = \psi_{21}(s,\theta)(u^K{}_{11}(z) - u_{ff}) \tag{4.16}$$

## 4.5. Interaction of the passive pile (receiver pile) with arriving waves

Considering a passive pile (receiver pile) located at a distance $s$ from the active pile (source pile), the diffracted wave field generated by the active pile as represented by Equation (2.24) propagates to strike the passive pile. The passive pile does not exactly follow the diffracted wave field [4.20],[4. 21] and its flexural rigidity tends to resist these induced displacements, resulting in a modified motion at the soil-passive pile interface. In order to determine the additional displacement, which is experienced by passive pile, the dynamic equilibrium of an infinitesimal pile segment is considered, yielding the following equation governing the deflection $u_{21}(z)$ of the passive pile.

$$\frac{d^4u_{21}(z)}{dz^4} + 4\lambda^4 u_{21}(z) = \frac{k_x + i\omega_g c_x}{E_p I_p}\psi_{21}(s,\theta)\left(u^K{}_{11}(z) - u_{ff}\right) \tag{4.17}$$

## 4.6 Kinematic response of the passive pile (receiver pile)

When the active pile is excited by kinematic loading $u_g(t) = u_{g0}e^{i\omega_g t}$ at the bedrock, the additional displacement at the soil-passive pile interface can be obtained through solution of Equation (4.16). Additional kinematic displacement of the passive pile consists of three part; $(u^K{}_{21}(z))_1$ as homogeneous solution, $(u^K{}_{21}(z))_2$ and $(u^K{}_{21}(z))_3$ as particular solutions.

$$u^K{}_{21}(z) = (u^K{}_{21}(z))_1 + (u^K{}_{21}(z))_2 + (u^K{}_{21}(z))_3 \tag{4.18}$$

$$(u^K{}_{21}(z))_1 = e^{\lambda z}(A^K{}_{21}\cos(\lambda z) + B^K{}_{21}\sin(\lambda z)) + e^{-\lambda z}(C^K{}_{21}\cos(\lambda z) + D^K{}_{21}\sin(\lambda z)) \tag{4.19}$$

$$(u^K{}_{21}(z))_2 = \frac{k_x + ic_x\omega_n}{16E_p I_p\lambda^3}\psi_{21}(s,\theta)[ze^{\lambda z}(A'\cos(\lambda z) + B'\sin(\lambda z)) + ze^{-\lambda z}(C'\cos(\lambda z) + D'\sin(\lambda z))] \tag{4.20}$$

$$A' = -(A^K_{11} + B^K_{11})\ ,\ B' = (A^K_{11} - B^K_{11})\ ,\ C' = (C_{11}{}^K - D_{11}{}^K)\ ,\ D' = (C_{11}{}^K + D_{11}{}^K) \tag{4.21}$$

$$({u^K}_{21}(z))_3 = \psi_{21}(s,\theta)u_{g0}\Gamma(\Gamma-1)\frac{\cos(\delta z)}{\cos(\delta H)} \tag{4.22}$$

In the particular solution (Equation (4.20)), $A', B', C'$ and $D'$ are integration constants in which $A_{11}^K, B_{11}^K, , C_{11}^K$ and , $D_{11}^K$ are known kinematic integration constants (i.e. they have already been determined from the boundary conditions of the active pile). In the homogeneous solution $A_{21}^K, B_{21}^K, {C_{21}}^K$ and ${D_{21}}^K$ are integration constants that should be determined from the boundary conditions of the passive pile.

### 4.6.1 Boundary conditions of passive pile (hinged-tip pile groups)

$${\theta^K}_{21}(z=0)=0 \quad , \quad \frac{d^3u_{21}^K(z=0)}{dz^3}=0 \quad , \frac{d^2u_{21}^K(z=H)}{dz^2}=0 \quad , u_{21}^K(z=H)=0 \tag{4.23}$$

By normalizing both sides of the system of equations with respect to $\frac{\Gamma u_{g0}}{\cos(\delta H)}$ the matrix form could be simplified into the following form:

$$\begin{bmatrix} 1 & 1 & -1 & 1 \\ -1 & 1 & 1 & 1 \\ -2e^{\lambda H}\sin(\lambda H) & 2e^{\lambda H}\cos(\lambda H) & 2e^{-\lambda H}\sin(\lambda H) & -2e^{-\lambda H}\cos(\lambda H) \\ e^{\lambda L}\cos(\lambda H) & e^{\lambda H}\sin(\lambda H) & e^{-\lambda H}\cos(\lambda H) & e^{-\lambda H}\sin(\lambda H) \end{bmatrix} \begin{Bmatrix} \bar{A}_{21}^K \\ \bar{B}_{21}^K \\ \bar{C}_{21}^K \\ \bar{D}_{21}^K \end{Bmatrix} = \begin{Bmatrix} 0 \\ 0 \\ \bar{\alpha}_{21}\frac{\delta^2}{\lambda^2}\cos(\delta H)+H_3 \\ -\bar{\alpha}_{21}\cos(\delta H)+H_4 \end{Bmatrix} \tag{4.24}$$

$$A = \frac{\delta^2}{\lambda^2}\cos(\delta H)\,, \quad B = \frac{(1-\Gamma)}{\Gamma}\cos(\delta H) \tag{4.25}$$

$$H_3 = \alpha_{21}[AG_1(\lambda H) + BG_2(\lambda H)] = \alpha_{21}G' \tag{4.26}$$

$$H_4 = \alpha_{21}\lambda H[AG_1{}'(\lambda H) + BG_2{}'(\lambda H)] = \alpha_{21}\lambda H G'' \tag{4.27}$$

$$G_1(\lambda H) = \frac{2cosh(2\lambda H) + \lambda H sinh(2\lambda H) + 2cos(2\lambda H) - \lambda H sin(2\lambda H)}{3(cos(2\lambda H) + cosh(2\lambda H))} \tag{4.28}$$

$$G_2(\lambda H) = \frac{-2\lambda H(sin(2\lambda H) + sinh(2\lambda H))}{3(cos(2\lambda H) + cosh(2\lambda H))} \tag{4.29}$$

$$G_1'(\lambda H) = \frac{sinh(2\lambda H) + sin(2\lambda H)}{6(cos(2\lambda H) + cosh(2\lambda H))} \tag{4.30}$$

$$G_2'(\lambda H) = \frac{2sinh(2\lambda H) - 2sin(2\lambda H)}{6(cos(2\lambda H) + cosh(2\lambda H))} \tag{4.31}$$

### 4.6.2 Boundary conditions of passive pile (fixed-tip pile groups)

$$\theta^K{}_{21}(z=0) = 0 \ , \quad \frac{d^3u_{21}^K(z=0)}{dz^3} = 0 \quad , \frac{du_{21}^K(z=H)}{dz} = 0 \ , \ u_{21}^K(z=H) = 0 \tag{4.32}$$

By normalizing both sides of the system of equations with respect to $\frac{\Gamma u_{go}}{\cos(\delta H)}$ the matrix form could be simplified into the following form:

$$\begin{bmatrix} 1 & 1 & -1 & 1 \\ -1 & 1 & 1 & 1 \\ \lambda e^{\lambda H}(\cos(\lambda H) - \sin(\lambda H)) & \lambda e^{\lambda H}(\cos(\lambda H) + \sin(\lambda H)) & -\lambda e^{-\lambda H}(\cos(\lambda H) + \sin(\lambda H)) & \lambda e^{-\lambda H}(-\sin(\lambda H) + \cos(\lambda H)) \\ e^{\lambda L}\cos(\lambda H) & e^{\lambda H}\sin(\lambda H) & e^{-\lambda H}\cos(\lambda H) & e^{-\lambda H}\sin(\lambda H) \end{bmatrix} \begin{Bmatrix} \bar{A}_{21}^K \\ \bar{B}_{21}^K \\ \bar{C}_{21}^K \\ \bar{D}_{21}^K \end{Bmatrix} = \begin{Bmatrix} 0 \\ 0 \\ \bar{\alpha}_{21}\frac{\delta}{\lambda}\sin(\delta H) + H_3 \\ -\bar{\alpha}_{21}\cos(\delta H) + \alpha_{21}\frac{A\lambda H}{3} \end{Bmatrix} \tag{4.33}$$

$$A = \frac{\delta}{\lambda}\sin(\delta H) \ , \ B = \frac{(1-\Gamma)}{\Gamma}\cos(\delta H) \tag{4.34}$$

$$H_3 = \alpha_{21}[AG_1(\lambda H) + BG_2(\lambda H)] = \alpha_{21}G' \tag{4.35}$$

$$G_1(\lambda H) = \frac{sinh(2\lambda H) + sin(2\lambda H) + 2\lambda H cosh(2\lambda H) + 2\lambda H cos(2\lambda H)}{3(sin(2\lambda H) + sinh(2\lambda H))} \tag{4.36}$$

$$G_2(\lambda H) = \frac{2\lambda H(sin(2\lambda H) - sinh(2\lambda H))}{3(sin(2\lambda H) + sinh(2\lambda H))} \tag{4.37}$$

## 4.7 Kinematic interaction factor

The kinematic interaction factor $\alpha^{K}{}_{21}(s,\theta)$ between active pile (pile 1) and passive pile (pile 2) is defined as the ratio of the kinematic additional top horizontal displacement of the passive pile resulting from the kinematic loading of active pile to the pile-top kinematic horizontal displacement of the active pile. Makris and Gazetas [4.20] derived a simplified equation (Equation. (4.39)) for estimating kinematic interaction factors for infinitely-long fixed-head piles in homogeneous soil. The kinematic interaction factors in the case of fixed-head piles with finite length are calculated in this study (Equation (4.40)).

$$\alpha_{21} = \frac{3}{4}\psi_{21}(s,\theta)\frac{k_x + ic_x\omega}{k_x + ic_x\omega - m\omega^2} \tag{4.38}$$

$$\bar{\alpha}_{21} = \psi_{21}(s,\theta)(\Gamma - 1) \tag{4.39}$$

$$\alpha^{K}{}_{21}(s,\theta) = \frac{u^{K}{}_{21}(0)}{u^{K}{}_{11}(0)} = \frac{A^{K}{}_{21} + C^{K}{}_{21} + \dfrac{\psi_{21}(s,\theta)(\Gamma-1)\Gamma u_{g0}}{cos(\delta H)}}{A^{K}{}_{11} + C^{K}{}_{11} + \dfrac{\Gamma u_{g0}}{cos(\delta H)}} \tag{4.40}$$

### 4.7.1 Kinematic interaction factor for fixed-tip pile groups:

$$\alpha^{K}_{21}(s,\theta) = \frac{u^{K}{}_{21}(0)}{u^{K}{}_{11}(0)} = \frac{\bar{A}^{K}_{21} + \bar{C}^{K}_{21} + 1}{\bar{A}^{K}_{11} + \bar{C}^{K}_{11} + 1} = \frac{(AF_{11} - F_{22}\cos(\delta H) + 1)}{(AF_{11} + BF_{22} + 1)}\bar{\alpha}_{21} + \frac{(G'F_{11} + \lambda HG''F_{22})}{(AF_{11} + BF_{22} + 1)}\alpha_{21} \tag{4.41}$$

$$F_{11} = \frac{-sin(\lambda H)sinh(\lambda H)}{(cos(2\lambda H) + cosh(2\lambda H))} \qquad F_{22} = \frac{2cosh(\lambda H)cos(\lambda H)}{(cos(2\lambda H) + cosh(2\lambda H))} \tag{4.42}$$

### 4.7.2 Kinematic interaction factor for fixed-tip pile groups:

$$\alpha^{K}_{21}(s,\theta) = \frac{u^{K}{}_{21}(0)}{u^{K}{}_{11}(0)} = \frac{\bar{A}^{K}_{21} + \bar{C}^{K}_{21} + 1}{\bar{A}^{K}_{11} + \bar{C}^{K}_{11} + 1} = \frac{(AF_{11} - F_{22}\cos(\delta H) + 1)}{(AF_{11} + BF_{22} + 1)}\bar{\alpha}_{21} + \frac{\left(G'F_{11} + \dfrac{A\lambda H}{3}F_{22}\right)}{(AF_{11} + BF_{22} + 1)}\alpha_{21} \tag{4.43}$$

$$F_{11}(\lambda H) = \frac{-2sin(\lambda H)sinh(\lambda H)}{\left(sin(2\lambda H) + sinh(2\lambda H)\right)} \quad , \quad F_{22}(\lambda H) = \frac{(2cosh(\lambda H)sin(\lambda H) + 2cos(\lambda H)sinh(\lambda H))}{(sin(2\lambda H) + sinh(2\lambda H))} \tag{4.44}$$

Further kinematic interaction can be set to matrix form:

$$\begin{bmatrix} \alpha_{11}^K & \alpha_{12}^K & \dots & \alpha_{1N}^K \\ \alpha_{21}^K & \alpha_{22}^K & \dots & \alpha_{2N}^K \\ \vdots & \vdots & \vdots & \vdots \\ \alpha_{N1}^K & \alpha_{N2}^K & \dots & \alpha_{NN}^K \end{bmatrix} = \begin{bmatrix} 1 & 0 & \dots & 0 \\ 0 & 1 & \dots & 0 \\ \vdots & \vdots & \vdots & \vdots \\ 0 & 0 & \dots & 1 \end{bmatrix} + \frac{Q_{11}}{D} \begin{bmatrix} 0 & \bar{\alpha}_{12} & \dots & \bar{\alpha}_{1N} \\ \bar{\alpha}_{21} & 0 & \dots & \bar{\alpha}_{2N} \\ \vdots & \vdots & \vdots & \vdots \\ \bar{\alpha}_{N1} & \bar{\alpha}_{N2} & \dots & 0 \end{bmatrix} + \frac{Q_{22}}{D} \begin{bmatrix} 0 & \alpha_{12} & \dots & \alpha_{1N} \\ \alpha_{21} & 0 & \dots & \alpha_{2N} \\ \vdots & \vdots & \vdots & \vdots \\ \alpha_{N2} & \alpha_{N2} & \dots & 0 \end{bmatrix} \tag{4.45}$$

Kinematic interaction factor can be set into a compact form:

$$\alpha_{\mathrm{ij}}{}^K = [\mathrm{I}] + \frac{Q_{11}}{D}\left[\bar{\alpha}_{ij}{}'\right] + \frac{Q_{22}}{D}\left[\alpha'_{ij}\right] \tag{4.46}$$

$$\left[\bar{\alpha}_{ij}{}'\right] = \left[\alpha_{ij}\right] - [I], \qquad \left[\bar{\alpha}_{\mathrm{ij}}\right] = \left[\alpha_{ij}\right] - [I] \tag{4.47}$$

For hinged-tip pile groups:

$$Q_1 = (AF_1 - F_2\cos(\delta H))\ , Q_2 = \left(G'F_1 + \lambda H G'' F_2 - \frac{2}{3}AF_1 - \frac{2}{3}BF_2\right) \tag{4.48}$$

$$F_1(\lambda H) = \frac{-cosh(\lambda H)cos(\lambda H)}{cos(2\lambda H) + cosh(2\lambda H)}, F_2(\lambda H) = \frac{-2sin(\lambda H)sinh(\lambda H)}{cos(2\lambda H) + cosh(2\lambda H)} \tag{4.49}$$

For fixed-tip pile groups:

$$\mathrm{Q}_1 = (\mathrm{AF}_1 - F_2\cos(\delta H))\ , Q_2 = \left(G'F_1 + \frac{A\lambda H}{3}F_2 - \frac{2}{3}AF_1 - \frac{2}{3}BF_2\right) \tag{4.50}$$

$$F_1(\lambda H) = \frac{-2cosh(\lambda H)cos(\lambda H)}{sin(2\lambda H) + sinh(2\lambda H)}\ , F_2(\lambda H) = \frac{2\big(cos(\lambda H)sinh(\lambda H) - sin(\lambda H)cosh(\lambda H)\big)}{sin(2\lambda H) + sinh(2\lambda H)} \tag{4.51}$$

## 4.8 Kinematic response of the pile-soil system

Consider a pile group with *N* identical piles connected by a rigid cap restricted against rotation and subjected to seismic excitation $u_g(t) = u_{g0}e^{i\omega_g t}$ at the bedrock surface, and let $U^K{}_{11} = \cdots = U^K{}_{\mathrm{NN}}$ denote the horizontal pile-top displacements of the *N* piles without any interaction among them when subjected to the seismic excitation at the bedrock surface [4.22].

The total horizontal response at the head of each pile may be calculated as the sum of the following components:

(1) The horizontal pile-top displacement as a single (solitary) pile when subjected to seismic excitation at the bedrock surface;

(2) The additional horizontal pile-top displacement resulting from the motions transmitted by the other *N-1* piles due to seismic excitation at the bedrock surface;

(3) The horizontal displacement at the head of a single (solitary) pile due to its own head loading with the amplitudes $P_1, \dots, P_N$;

(4) The additional horizontal displacement at the head of the pile transmitted from the other *N-1* piles due to their head-loading with the amplitudes $P_1 \dots, P_N$;

(1) and (2) are 'kinematic' effects, while (3) and (4) are 'inertial' effects. The total horizontal head displacement of pile *i* may be expressed as:

$$U_i = \sum_{j=1}^{N} (\alpha^K{}_{ij} U^K{}_{\mathrm{jj}} + \alpha^I{}_{ij} \frac{P_j}{K_x{}^{(1)}}) \tag{4.52}$$

When the horizontal head displacement of the foundation is expressed by $U^{(G)}$, the compatibility condition can be described by:

$$U_i = U^{(G)} = \sum_{j=1}^{N} (\alpha^K{}_{ij} U^K{}_{\mathrm{jj}} + \alpha^I{}_{ij} \frac{P_j}{K_x{}^{(1)}}) \tag{4.53}$$

Dividing both sides of Equation (4.53) by the common displacement $U^K{}_{11} = \cdots = U^K{}_{\mathrm{NN}}$ leads to:

$$\frac{U^{(G)}}{U^K{}_{11}} - \sum_{j=1}^{N} \alpha^I{}_{ij} \frac{P_j}{K_x{}^{(1)} U^K{}_{\mathrm{jj}}} = \sum_{j=1}^{N} \alpha^K{}_{ij} \tag{4.54}$$

Since the pile cap is considered massless and no external force is applied to the cap, equilibrium of the cap requires

$$\sum_{j=1}^{N} P_j = 0 \tag{4.55}$$

These systems of equations can be set into matrix form as:

$$\begin{bmatrix} 1 & -\alpha^I{}_{11} & -\alpha^I{}_{12} & \dots & -\alpha^I{}_{1N} \\ 1 & -\alpha^I{}_{11} & -\alpha^I{}_{11} & \dots & -\alpha^I{}_{2N} \\ \vdots & \vdots & \vdots & \vdots & \vdots \\ 1 & -\alpha^I{}_{N1} & -\alpha^I{}_{N2} & \cdots & -\alpha^I{}_{NN} \\ 0 & 1 & 1 & \cdots & 1 \end{bmatrix} \begin{Bmatrix} \dfrac{U^{(G)}}{U^K{}_{11}} \\ \dfrac{P_1}{K_x{}^{(1)} U^K{}_{11}} \\ \dfrac{P_2}{K_x{}^{(1)} U^K{}_{22}} \\ \vdots \\ \dfrac{P_N}{K_x{}^{(1)} U^K{}_{\mathrm{NN}}} \end{Bmatrix} = \begin{Bmatrix} \sum_{j=1}^{N} \alpha^K{}_{1j} \\ \sum_{j=1}^{N} \alpha^K{}_{2j} \\ \vdots \\ \sum_{j=1}^{N} \alpha^K{}_{Nj} \\ 0 \end{Bmatrix} \tag{4.56}$$

where $\alpha^I{}_{ij}$ are the interaction factors for inertial loading and $\alpha^K{}_{ij}$ are the interaction factors for kinematic loading, being $\alpha^I{}_{ii} = \alpha^K{}_{ii} = 1$, and $K_x{}^{(1)}$ the dynamic stiffness of the single pile. The bending moment at the head of pile *i* may be derived from the total curvature $U_i''(0)$ as:

$$M_i = E_p I_p U_i''(0) \tag{4.57}$$

## 4.9 Kinematic curvature ratios

The kinematic curvature ratio of the active pile is defined as the ratio of the active pile head curvature as a single solitary pile due to the kinematic loading of active pile when subjected to seismic excitation at the bedrock surface to the active pile-top displacement [4.22];

$$\beta_{11}^K = \frac{u_{11}^K{}''(0)}{u^K{}_{11}(0)} = \frac{2\lambda^2 \left(B_{11}{}^K - D_{11}{}^K\right) - \dfrac{\Gamma \delta^2 u_{g0}}{\cos(\delta H)}}{A_{11}{}^K + C_{11}{}^K + \dfrac{\Gamma u_{g0}}{\cos(\delta H)}} \tag{4.58}$$

$$\beta_{11}^{K} = \frac{u_{11}^{K}{}''(0)}{u_{11}^{K}(0)} = \frac{-2\lambda^2}{D}(AF_1 + BF_2) - \frac{\delta^2}{D} \tag{4.59}$$

The kinematic curvature ratio of the passive pile is defined as the ratio of the passive pile head curvature due to the additional kinematic head displacement of the passive pile to the active pile-top displacement due to the kinematic loading when subjected to seismic excitation at the bedrock surface [4.22];

$$\beta_{21}^{K} = \frac{u_{21}^{K}{}''(0)}{u^{K}{}_{11}(0)} = \frac{\frac{2\lambda^2}{3}\left(3\left(B_{21}{}^{K} - D_{21}{}^{K}\right) - 2\alpha_{21}(B_{11}{}^{K} - D_{11}{}^{K})\right) - \frac{\bar{\alpha}_{21}\Gamma\delta^2 u_{g0}}{\cos(\delta H)}}{A_{11}{}^{K} + C_{11}{}^{K} + \frac{\Gamma u_{g0}}{\cos(\delta H)}} \tag{4.60}$$

$$\beta_{21}^{K} = \frac{u_{21}^{K}{}''(0)}{u_{11}^{K}(0)} = \frac{-2\lambda^2}{D}(\bar{\alpha}_{21}Q_1 + \alpha_{21}Q_2) - \frac{\delta^2}{D}\bar{\alpha}_{21} \tag{4.61}$$

further kinematic curvature ratio can be set to matrix form:

$$\begin{bmatrix} \beta_{11}^{K} & \beta_{12}^{K} & \dots & \beta_{1N}^{K} \\ \beta_{21}^{I} & \beta_{22}^{I} & \dots & \beta_{2N}^{K} \\ \vdots & \vdots & \vdots & \vdots \\ \beta_{N1}^{K} & \beta_{N2}^{K} & \dots & \beta_{NN}^{K} \end{bmatrix} = -\delta^2\left[\bar{\alpha}_{ij}\right] - 2\lambda^2(Q_0\begin{bmatrix} 1 & 0 & \dots & 0 \\ 0 & 1 & \dots & 0 \\ \vdots & \vdots & \vdots & \vdots \\ 0 & 0 & \dots & 1 \end{bmatrix} + Q_1\begin{bmatrix} 0 & \bar{\alpha}_{12} & \dots & \bar{\alpha}_{1N} \\ \bar{\alpha}_{21} & 0 & \dots & \bar{\alpha}_{2N} \\ \vdots & \vdots & \vdots & \vdots \\ \bar{\alpha}_{N1} & \bar{\alpha}_{N2} & \dots & 0 \end{bmatrix} + Q_2\begin{bmatrix} 0 & \alpha_{12} & \dots & \alpha_{1N} \\ \alpha_{21} & 0 & \dots & \alpha_{2N} \\ \vdots & \vdots & \vdots & \vdots \\ \alpha_{N2} & \alpha_{N2} & \dots & 0 \end{bmatrix}) \tag{4.62}$$

kinematic curvature ratio can be set into a compact form:

$$\beta_{ij}{}^{K} = -\delta^2\left[\bar{\alpha}_{ij}\right] - 2\lambda^2(Q_0[I] + Q_1[\bar{\alpha}_{ij}{}'] + Q_2[\alpha'_{ij}]) \tag{4.63}$$

$$Q_0 = AF_1 + BF_2 \tag{4.64}$$

For hinged-tip pile groups:

$$A = \frac{\delta^2}{\lambda^2}\cos(\delta H)\,,\quad B = \frac{(1-\Gamma)}{\Gamma}\cos(\delta H) \tag{4.65}$$

For fixed-tip pile groups:

$$A = \frac{\delta}{\lambda}\sin(\delta H)\,,\quad B = \frac{(1-\Gamma)}{\Gamma}\cos(\delta H) \tag{4.66}$$

## 4.10 Total curvature ratios

Finally, by using the superposition method to add the kinematic and inertial effects together, the total curvature can be expressed as:

$$U_i''(0) = \sum_{j=1}^{N} (\beta_{ij}^K U^K{}_{\text{jj}} + \beta_{ij}^I \frac{P_j}{K_x{}^{(1)}}) \tag{4.67}$$

For simplicity of the expression, the following form can be reached.

$$\frac{U_i''(0)}{U^K{}_{\text{jj}}} = \sum_{j=1}^{N} (\beta_{ij}^K + \beta_{ij}^I \frac{P_j}{K_x{}^{(1)} U^K{}_{\text{jj}}}) \tag{4.68}$$

These systems of equations can be set into a matrix form as:

$$\begin{Bmatrix} \frac{U_1''(0)}{U^K{}_{11}} \\ \frac{U_2''(0)}{U^K{}_{22}} \\ \vdots \\ \frac{U_N''(0)}{U^K{}_{\text{NN}}} \end{Bmatrix} = \begin{bmatrix} \beta_{11}^K & \beta_{12}^K & \dots & \beta_{1N}^K \\ \beta_{21}^K & \beta_{22}^K & \dots & \beta_{2N}^K \\ \vdots & \vdots & \vdots & \vdots \\ \beta_{N1}^K & \beta_{N2}^K & \dots & \beta_{NN}^K \end{bmatrix} \begin{Bmatrix} 1 \\ 1 \\ \vdots \\ 1 \end{Bmatrix} + \begin{bmatrix} \beta_{11}^I & \beta_{12}^I & \dots & \beta_{1N}^I \\ \beta_{21}^I & \beta_{22}^I & \dots & \beta_{2N}^I \\ \vdots & \vdots & \vdots & \vdots \\ \beta_{N1}^I & \beta_{N2}^I & \dots & \beta_{NN}^I \end{bmatrix} \begin{Bmatrix} \frac{P_1}{K_x{}^{(1)} U^K{}_{11}} \\ \frac{P_2}{K_x{}^{(1)} U^K{}_{22}} \\ \vdots \\ \frac{P_N}{K_x{}^{(1)} U^K{}_{\text{NN}}} \end{Bmatrix} \tag{4.69}$$

$$\left\{\frac{U_i''(0)}{U^K{}_{11}}\right\} = [\beta_{ij}^K]\{I\} + \left[\beta_{ij}^I\right]\{\bar{P}_j\} \tag{4.70}$$

where the vector forces $\{\bar{P}_j\} = \left\{\frac{P_j}{K_x{}^{(1)} U^K{}_{\text{jj}}}\right\}$ is obtained by solving Equation (4.55). Bending strains can be calculated after obtaining bending moments at the head of each pile in the group in vector form:

$$\varepsilon_p(z) = -\frac{d}{2}\frac{d^2 U_i(z)}{dz^2} \tag{4.71}$$

$$\{\varepsilon_{pi}^K(0)\} = \{-\frac{d}{2} U_i''(0)\} \tag{4.72}$$

After calculating the simplified form of the bending strain vector, it can be expressed as:

$$\{\varepsilon_{pi}^K(0)\} = ([\beta_{ij}^K]\{I\} + [\beta_{ij}^I]\{\bar{P}_j\}) \frac{d\Gamma u_{g0}}{2\cos(\delta H)} \tag{4.73}$$

Afterwards, the kinematic bending strain $\varepsilon_{pi}^{K}$ at the head of the pile is normalized with respect to a mean shear strain of the soil medium $\gamma_s$ .The mean shear strain is defined as the absolute value of the maximum harmonic response displacement of the ground surface with respect to the bedrock divided by the height of the soil medium *H* as shown in Equation (4.74).

$$\gamma_s = \frac{u_{ff}(z=0) - u_{ff}(z=H)}{H} = \frac{\frac{u_{g0}}{\cos(\delta H)} - u_{g0}}{H} = \frac{u_{g0}}{H\cos(\delta H)}(1 - cos(\delta H)) \tag{4.74}$$

Therefore the closed form formula of the normalized bending strains can be written as follows

$$\left\{\frac{\varepsilon_{pi}^{K}(0)}{\gamma_s}\right\} = ([\beta_{ij}^{K}]\{I\} + [\beta_{ij}^{I}]\{\overline{P}_j\})\frac{(\frac{r}{H})\Gamma}{(1-\cos(\delta H))} \tag{4.75}$$

The normalized parameters are: (1) the slenderness ratio (the radius to height ratio of the piles, $r/H$); (2) the pile-soil stiffness ratio (i.e., ratio of Young's modulus of Elasticity) ($E_p/\,E_s$); (3) the ratio of the mass density of the pile $\rho_p$ and the soil $\rho_s$ ($\rho_p/\rho_s$).

## 4.11 Verification of the method and comparison in different boundary conditions

In order to verify the accuracy of the proposed method, three cases including single pile, 1×2, and 2×1 piles with different tip condition (hinged or fixed) are considered. Piles in the group are placed in a row and are connected by a rotationally restricted rigid cap. Also, piles are subjected to seismic excitation $u_g(t) = u_{g0}e^{i\omega_g t}$ at the bedrock in parallel and orthogonal directions with respect to the line connecting all piles centers as shown in Figure 4.2. The frequency of the horizontal excitation equals to the fundamental frequency of the soil medium. Results are compared against those of a three-dimensional time-harmonic continuum linear model based on a coupled finite elements-boundary elements (FE-BE) formulation [4.23],[4.24]. In this approach, the soil is modeled by BE as a homogeneous, viscoelastic, isotropic, linear medium; while the piles are represented by FE as Bernoulli's beams. The piles are treated as load lines

acting within the soil, so their presence does not affect the soil continuity. Welded boundary conditions are assumed at the pile-soil interface.

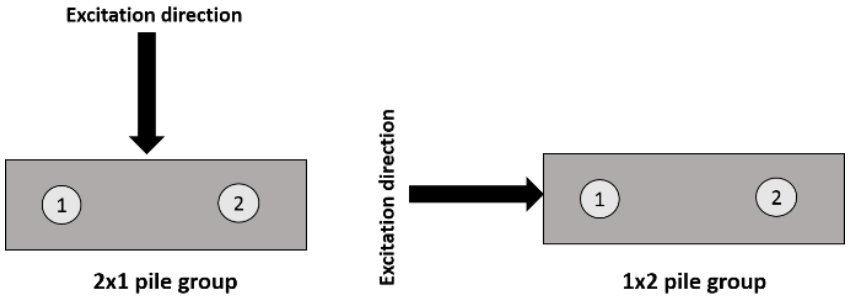


**Figure 4.2:** Two piles in line orthogonal (2×1) and parallel (1×2) to the excitation.

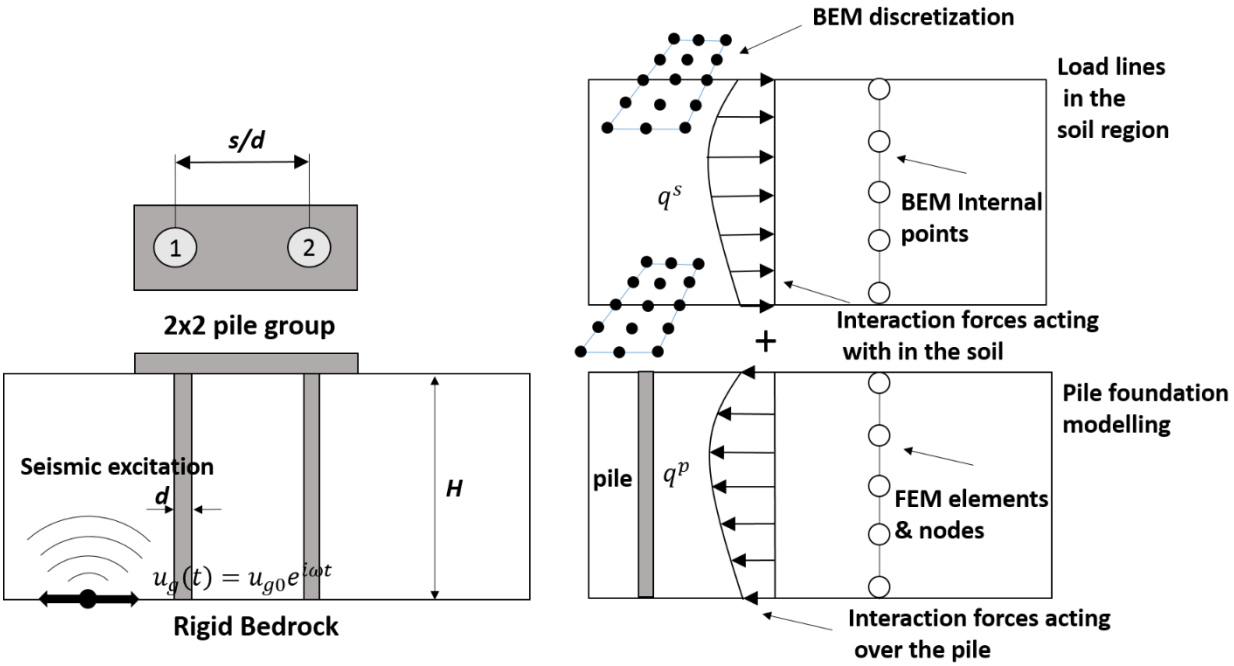


**Figure 4.3**: Pile foundation modelling through FEM-BEM coupling formulation.

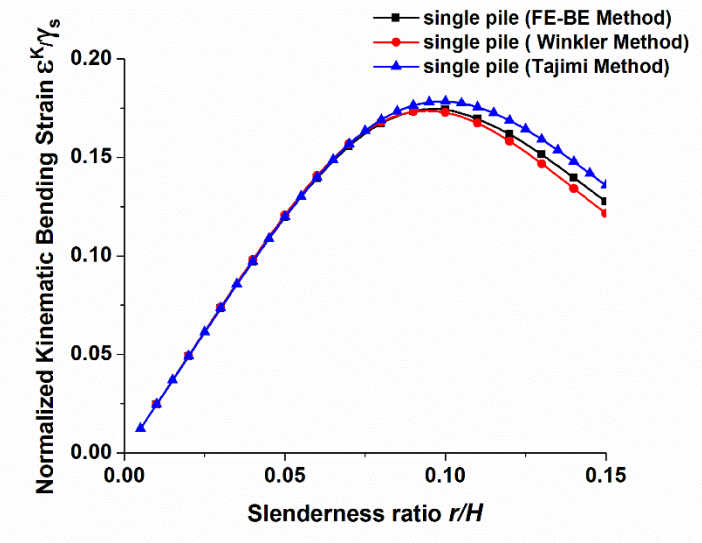


**Figure 4.4:** Normalized kinematic bending strains of single hinged pile. Comparison of the present method with rigorous results by FE-BE and Tajimi method ($\frac{\rho_p}{\rho_s} = 1.43,\ \upsilon_s = 0.4\ , \beta_s = 0.05\ , \frac{E_p}{E_s} = 1000\ , \frac{s}{d} = 5$).

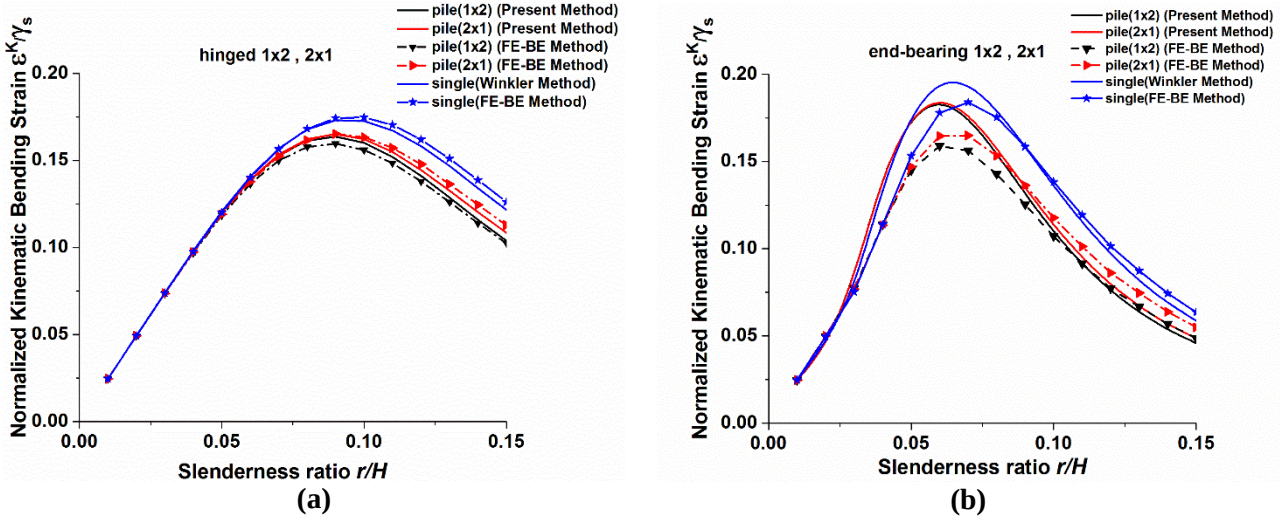


**Figure 4.5:** Normalized kinematic bending strains of hinged and fixed-tip1×2 and 2×1 pile group.Comparison of the present method with rigorous results by FE-BE method($\frac{\rho_p}{\rho_s} = 1.43,\ \upsilon_s = 0.4\ , \beta_s = 0.05\ , \frac{E_p}{E_s} = 1000\ , \frac{s}{d} = 5$).

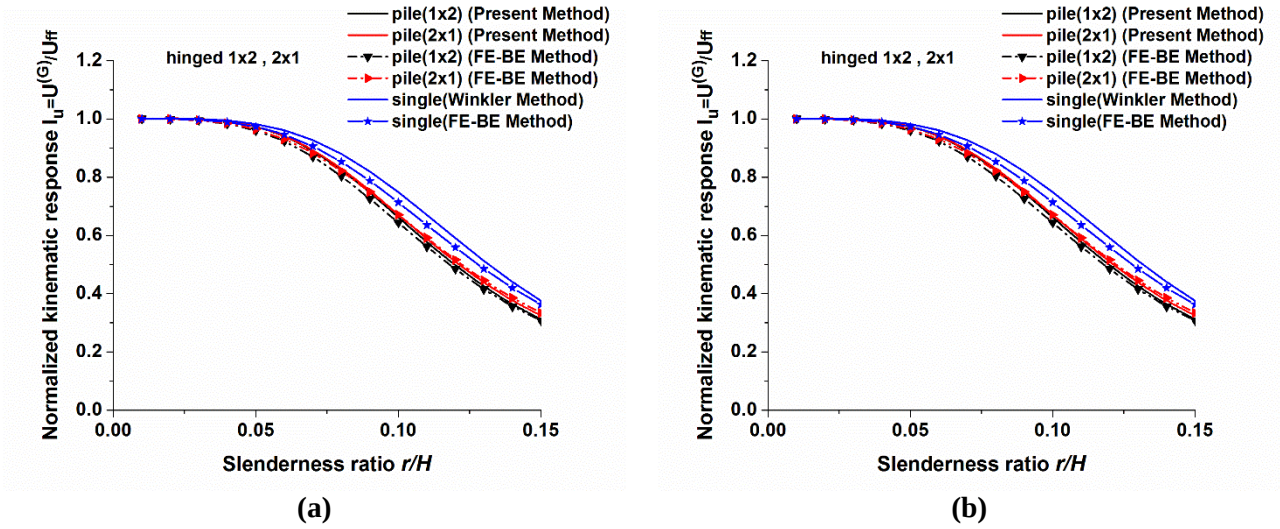


**Figure 4.6:** Normalized kinematic response of hinged and fixed-tip 1×2 and 2×1 pile groups. Comparison of the present method with rigorous results by FE-BE method ($\frac{\rho_p}{\rho_s} = 1.43,\ \upsilon_s = 0.4\ , \beta_s = 0.05\ , \frac{E_p}{E_s} = 1000\ , \frac{s}{d} = 5$).

Figures 5.4 and 5.5 shows the normalized kinematic bending strains at the head of single pile and each pile in 1x2 and 2x1 pile groups. Additional comparison is presented in Figure 4.6 in terms of normalized kinematic response factor $I_u = U^{(G)}/U_{ff0}$ . In all figures, results are plotted against slenderness ratio. For end-bearing piles, the maximum bending strains are higher than those of hinged piles, appearing for lower $r/H$ ratios. This observation may be due to the restriction effect of the pile tip that makes the rotation along the pile length difficult. As a result, pile cap will bear larger moments. With such consideration, the proposed method in this study has the benefit of simulating tip conditions for pile groups. It should be noted that the predictions of the proposed method convincingly match with the numerical results of the rigorous method. However, there are mismatches between amplitudes in the case of end-bearing pile group which may be related to the selection of proper shape functions in lateral motion. In this study, the basic shape function is selected as a sinusoidal function which reproduces the fundamental mode shape of the soil profile and hinged piles. The fundamental mode shape of the end-bearing pile due to lateral motion, however, cannot be reproduced by this simple harmonic shape function and its selection is dependent on the pile tip and head condition. It should be noted that the shape function in Equation (2.9) affects the frequency-dependent parameters in Equation (2.8), and those parameters play important roles in calculation

of the complex valued modulus $k_x^*$ (Equation (2.7)) and the attenuation function $\psi_{21}(s,\theta)$ (Equations (2.21) and (2.22)).

## 4.12 Behavior of kinematic bending in pile group

To have further insight into the characteristics and behavior of the normalized kinematic bending strains against slenderness ratio $r/H$ by using the expression proposed in Equation (4.75), additional studies of the fixed-head pile groups 2×2, 3×3 with different boundary conditions at the tip (fixed or hinged) are carried out. Piles are subjected to the seismic excitation $u_g(t) = u_{g0}e^{i\omega_g t}$ at the bedrock as shown in Figure 4.7. The frequency of excitation is assumed to be equal to the fundamental frequency of the soil layer. Special attention is paid to the effects of the parameters like pile spacing $s/d$ , pile-soil stiffness ratio $E_p/E_s$ and the number of piles *N* on the kinematic normalized bending strains in the group. Despite assumptions of Euler-Bernoulli beam being valid only for slenderness ratios below 0.2, a wider range ($r/H = 0 - 0.4$) is presented in this study in order to have a clear picture of the behavior of pile groups beyond the local maximum.

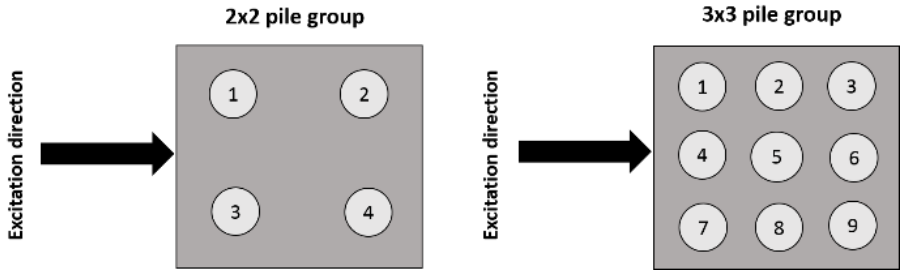


**Figure 4.7:** Depiction of pile groups under study.

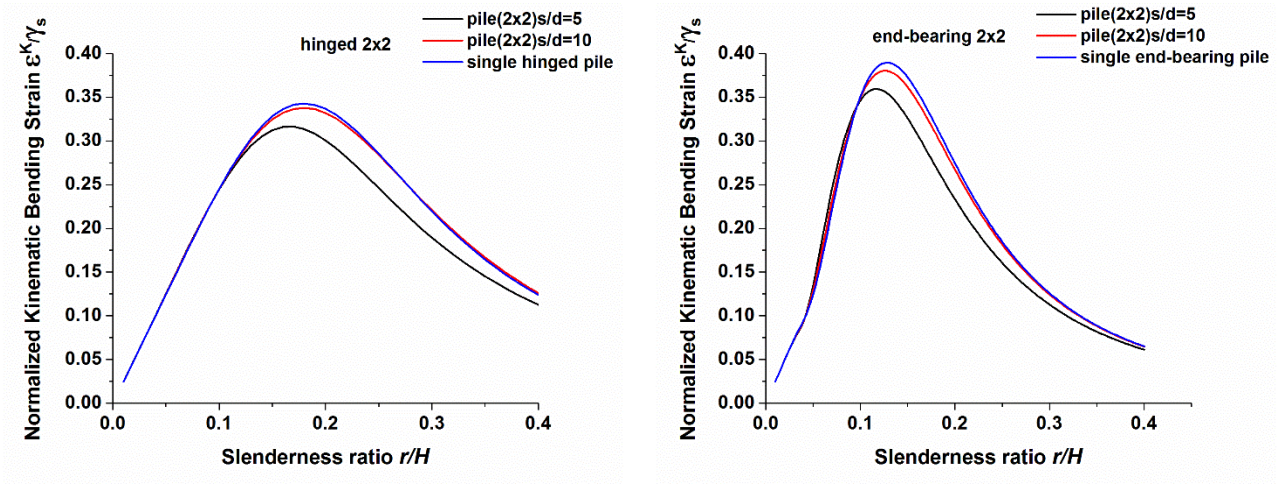


**(a)** **(b)**

**Figure 4.8:** Normalized kinematic bending strains of 2×2 hinged and end-bearing pile groups with respect to single pile ($\frac{\rho_p}{\rho_s} = 1.43,\ \upsilon_s = 0.4\ ,\ \beta_s = 0.05\ ,\frac{E_p}{E_s} = 100$).

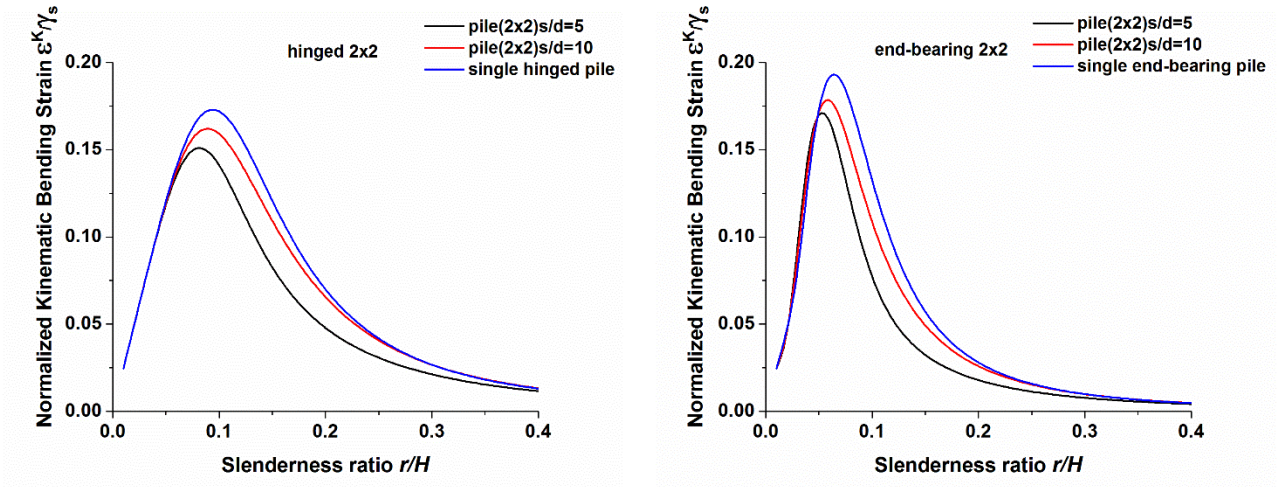


**(a)** **(b)**

**Figure 4.9:** Normalized kinematic bending strains of 2×2 hinged and end-bearing pile groups with respect to single pile ($\frac{\rho_p}{\rho_s} = 1.43,\ \upsilon_s = 0.4\ ,\ \beta_s = 0.05\ ,\frac{E_p}{E_s} = 1000$).

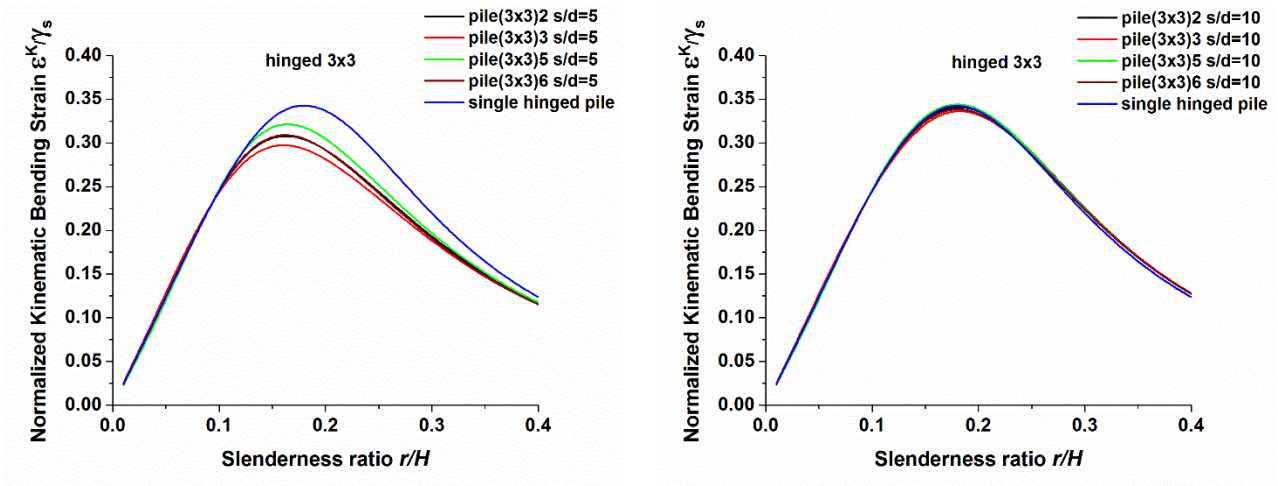


**Figure 4.10:** Normalized kinematic bending strains of 3×3 hinged pile groups with respect to single pile ($\frac{\rho_p}{\rho_s} = 1.43,\ \upsilon_s = 0.4\ ,\ \beta_s = 0.05\ ,\frac{E_p}{E_s} = 100$).

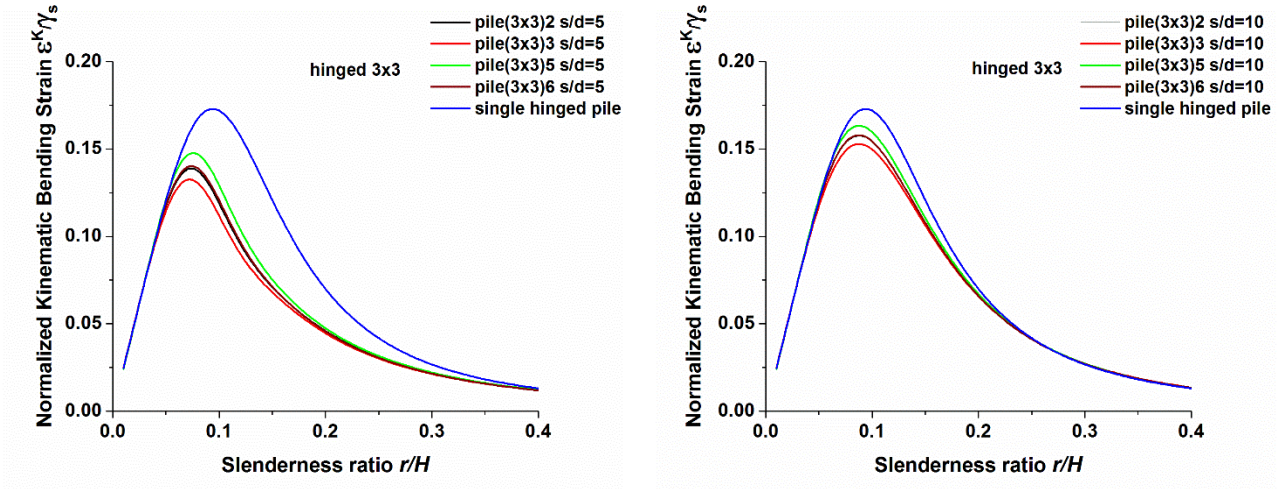


**Figure 4.11:** Normalized kinematic bending strains of 3×3 hinged pile groups with respect to single pile ($\frac{\rho_p}{\rho_s} = 1.43,\ \upsilon_s = 0.4\ ,\ \beta_s = 0.05\ ,\frac{E_p}{E_s} = 1000$).

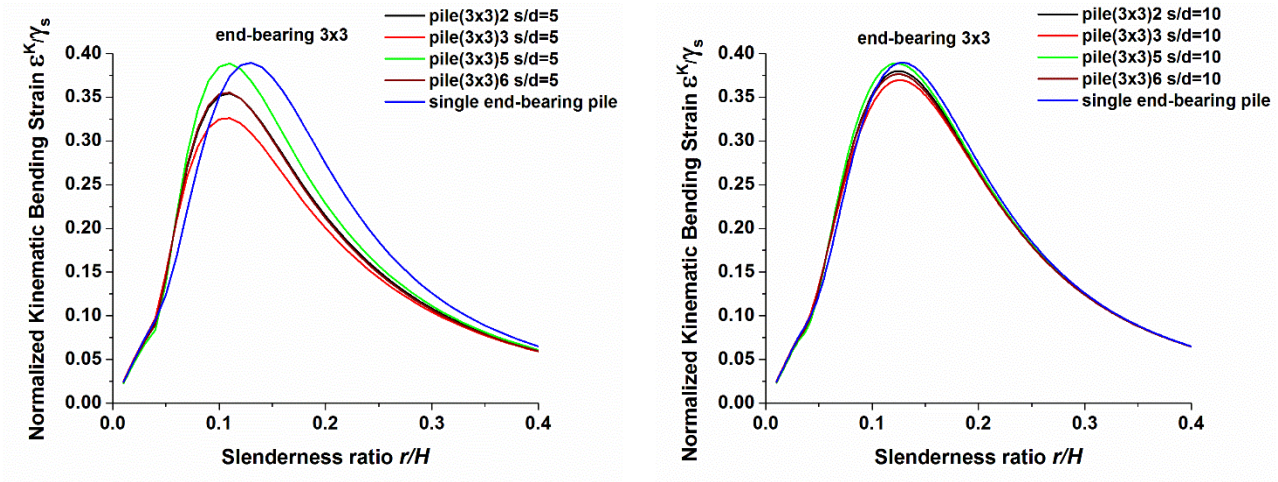


**Figure 4.12:** Normalized kinematic bending strains of 3×3 end-bearing pile groups with respect to single pile ($\frac{\rho_p}{\rho_s} = 1.43,\ \upsilon_s = 0.4\ ,\ \beta_s = 0.05\ ,\frac{E_p}{E_s} = 100$).

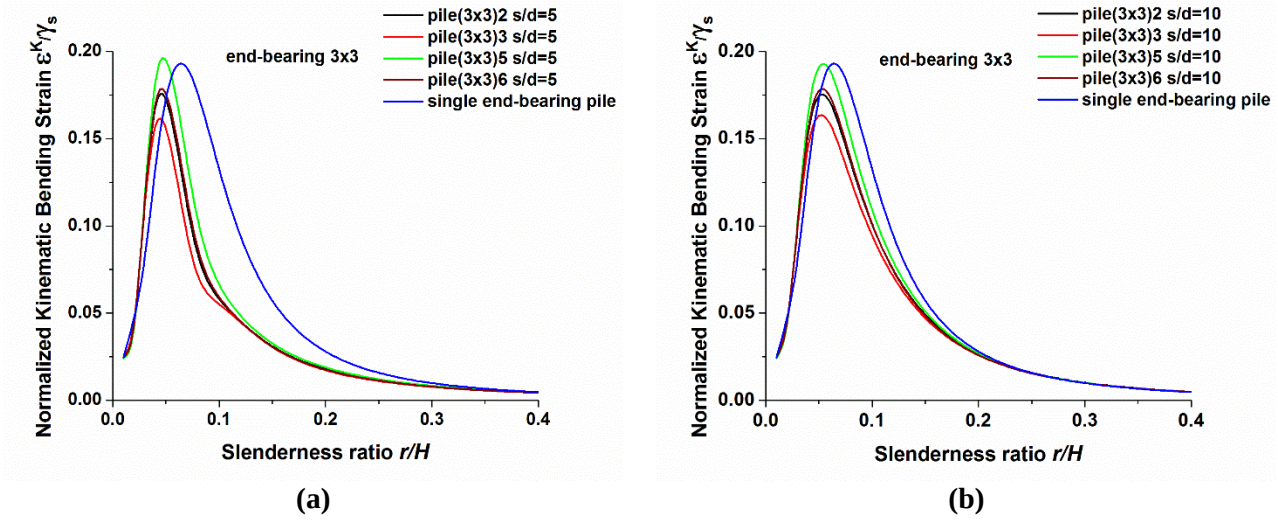


**Figure 4.13:** Normalized kinematic bending strains of 3×3 end-bearing pile groups with respect to single pile ($\frac{\rho_p}{\rho_s} = 1.43,\ \upsilon_s = 0.4\ ,\ \beta_s = 0.05\ ,\frac{E_p}{E_s} = 1000$).

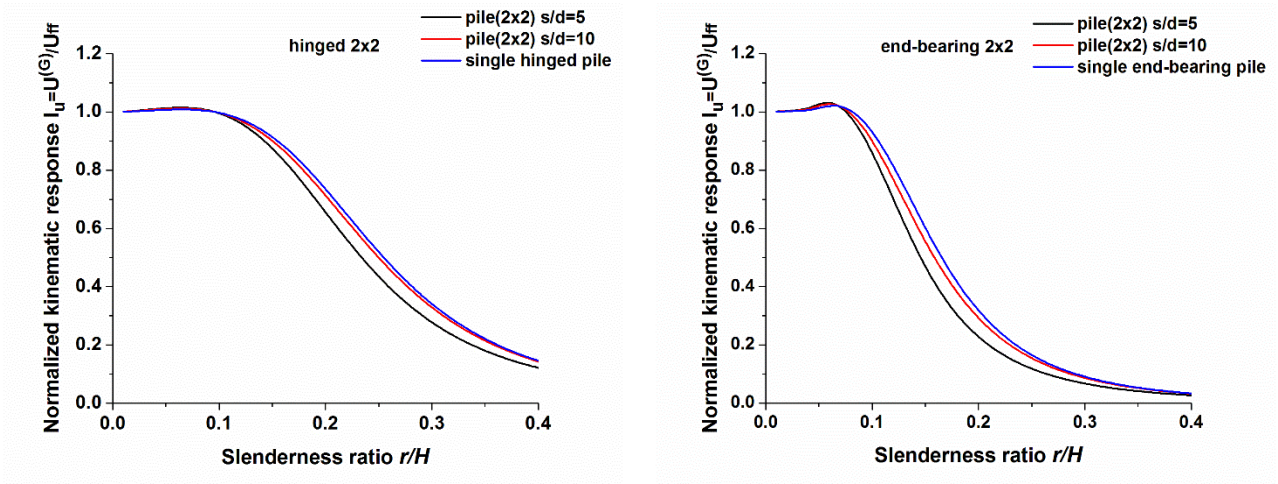


**Figure 4.14:** Normalized kinematic response of 2×2 hinged and end-bearing pile groups with respect to single pile ($\frac{\rho_p}{\rho_s} = 1.43,\ \upsilon_s = 0.4\ , \beta_s = 0.05\ , \frac{E_p}{E_s} = 100$ ).

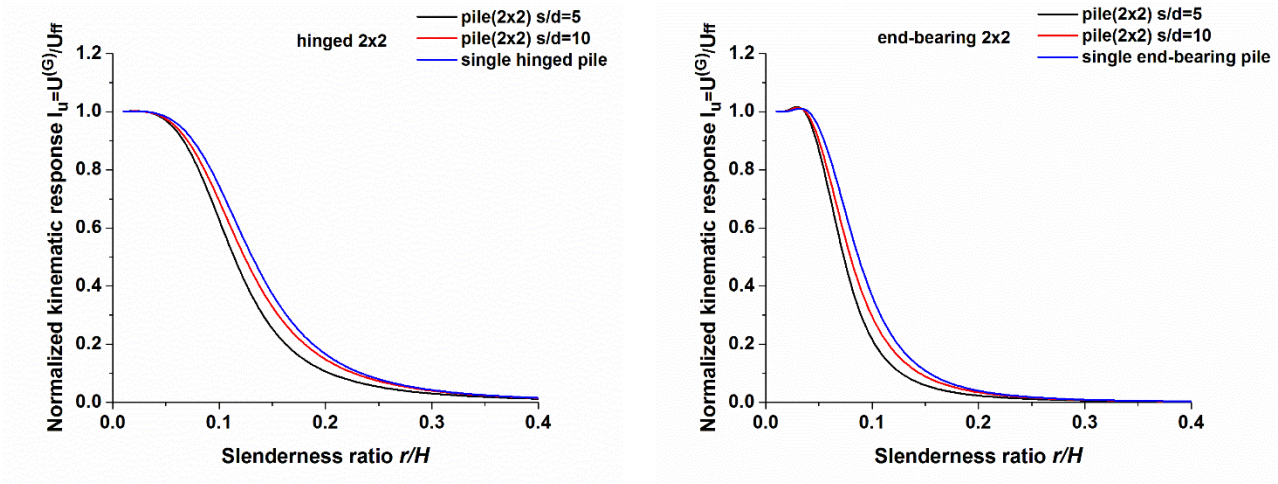


**Figure 4.15:** Normalized kinematic response of 2×2 hinged and end-bearing pile groups with respect to single pile ($\frac{\rho_p}{\rho_s} = 1.43,\ \upsilon_s = 0.4\ , \beta_s = 0.05\ , \frac{E_p}{E_s} = 1000$ ).

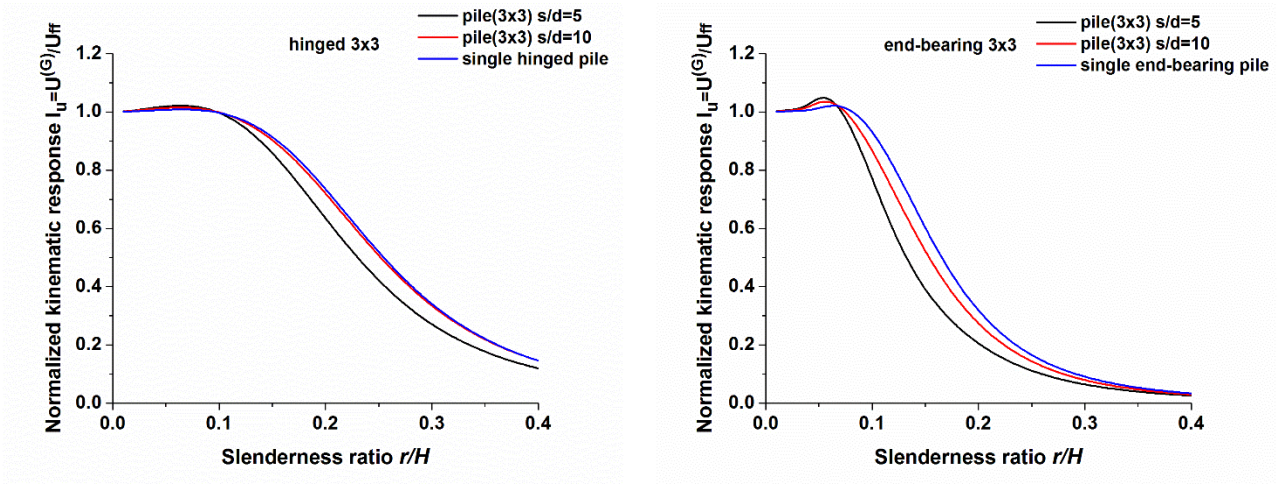


**Figure 4.16:** Normalized kinematic response of 3×3 hinged and fixed-tip pile groups with respect to single pile ($\frac{\rho_p}{\rho_s} = 1.43,\ \upsilon_s = 0.4\ , \beta_s = 0.05\ , \frac{E_p}{E_s} = 100$ ).

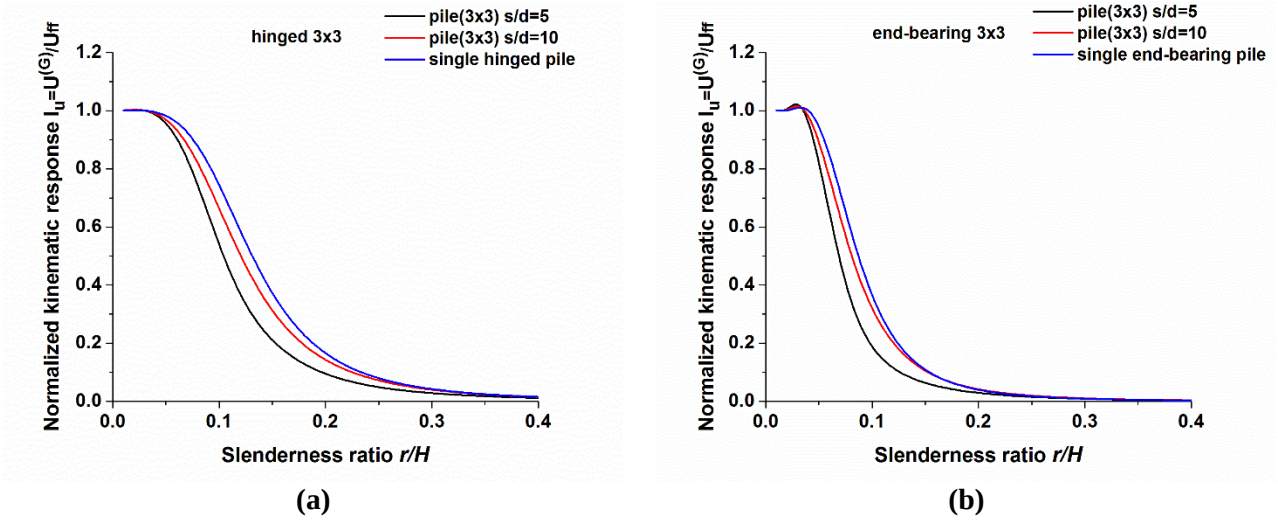


**Figure 4.17:** Normalized kinematic response of 3×3 hinged and fixed-tip pile groups with respect to single pile ($\frac{\rho_p}{\rho_s} = 1.43,\ \upsilon_s = 0.4\ , \beta_s = 0.05\ , \frac{E_p}{E_s} = 1000$ ).

Figures 4.8 through 4.13 show the variation of the normalized kinematic bending strains in both cases of hinged and end-bearing piles as a function of the slenderness ratio $r/H$ with different values of the pile spacing $s/d$ and pile-soil stiffness ratio $E_p/E_s$ . These figures reveal that even in pile group configurations, each pile interestingly follows the general trend of the single pile. Moreover, it is worth noting that in pile

groups normalized kinematic bending strains are generally slightly smaller than those of the single pile over the entire range of $r/H$. Furthermore, as the pile spacing $s/d$ increases, normalized kinematic bending strains of pile groups converge to those of single piles. The kinematic bending strains start from zero when slenderness ratios approach zero, increasing almost linearly up to a maximum located at values of $r/H$ between 0.05 and 0.18, corresponding to pile aspect ratios $L/d$ of 10 and 2.8, respectively. In end-bearing configurations, the maximum normalized kinematic bending strain always takes place at smaller slenderness ratio $r/H$ than in hinged configurations. For $r/H \to \infty$ piles behave as a rigid disk and regardless of fixity condition at the tip, all piles will experience zero bending strains. To assist in the understanding of the behaviour of the kinematic bending strains in the pile groups, the normalized kinematic seismic responses of both cases of 2×2 and 3×3 pile groups are shown in Figures 4.14 through 4.17. The existence of filtering effects in soil-pile systems has been proved in the published researches [4.3], [4.14], [4.20]. These effects are the outcome of pile resistance to adapting to the wavy movements of the free field. Based on Figures 4.14 through 4.17, it implies that filtering effects are clearly dependent on the number of piles in the group, pile-soil stiffness ratio $E_p/E_s$ , pile spacing $s/d$, and pile tip fixity conditions. The decline in amplitude of kinematic bending strains in pile groups can be physically linked to filtering effect which is more pronounced for close spacing piles and high pile-soil stiffness ratios.

As shown in Figures 4.8 through 4.13, interestingly a definite pattern of change in kinematic bending strains can be found. The local maximum of kinematic bending strain shifts to lower slenderness ratio when pile-soil stiffness ratio increases and this is compatible with single pile. The normalized kinematic bending strains of the piles in a group are smaller than those of the single pile in all cases except for the 3×3 end-bearing configuration at slenderness ratios $r/H$ below the location of the maximum. In this sense, it is worth noting that the maximum values for the case of pile groups appear at slenderness ratios slightly smaller than for single piles. In 3×3 pile groups, the pile in the center (i.e., pile 5) exhibits the highest value of bending strain (being closest to the single pile), while corner piles (i.e., piles 1, 3, 7 and 9) exhibit the smallest value

of bending strain. This means that although the boundary conditions change, distribution pattern of bending strains in pile groups remains unchanged.

For slenderness ratios $r/H$ below the location of the maximum, the kinematic bending strains of the piles in a group can always be approximated by that of the single pile. Indeed this can be validated using Figures 4.14 through 4.17 which show that the displacement of the head of the piles in a group are almost the same as that of a single pile. This implies that the effect of pile-to-pile interaction is relatively not as significant as it is when the slenderness ratio is large, justifying that kinematic bending strains of the piles in a group show a behavior almost identical to that of a single pile for small slenderness ratios $r/H$.

## 4.13 Conclusions

An efficient method has been developed to compute the bending strains of fixed-head pile groups of finite length embedded in a homogeneous soil layer where kinematic interaction dominates. The proposed method allows the kinematic bending strains to be obtained in a closed form formula while using a dynamic Winkler approach in conjunction with an extension to three-dimensions of Novak's plane strain expressions by Mylonakis. The enhanced model is free of the drawbacks of the two- dimensional plane strain model, as it is able to reproduce the cutoff frequency of the soil-pile system. Pile group effect is considered through interaction factors and the kinematic bending strains are normalized with respect to the mean shear strain of the soil stratum $\gamma_s$. The variation of normalized kinematic bending strains against slenderness ratio $r/H$ is investigated, revealing valuable insight into the characteristics of the kinematic bending strains in pile groups. Homogeneous solutions are considered in active and passive piles deflections for appropriately considering various boundary conditions when estimating kinematic bending strains. Solutions for pile groups' responses are obtained at the fundamental frequency of the soil stratum.

In pile groups when the slenderness ratios $r/H$ approach zero in all piles, kinematic bending strains become zero. The kinematic bending strains increase almost linearly up to a local maximum, gradually decreasing

afterwards. The presence of that local maximum implies the existence of a particular slenderness ratio $r/H$ that maximizes the kinematic bending strains in pile groups and should, therefore, be avoided. Below the local maximum, the kinematic bending strains of the piles in a group are very close to those of a single pile. This conclusion allows to use the "optimal pile radius" previously computed for single piles in pile groups. From the viewpoint of engineering practice, the range of typical slenderness ratio $r/H$ might be from nearly 0.01 to 0.1. Accordingly, it is conceived that due to the kinematic bending, when the slenderness ratio increases within that range, the normalized kinematic bending strain may increase almost linearly.

## References


[4.1] Dobry, R., O'Rourke, MJ. (1983) Discussion on " Seismic response of end-bearing piles" by Flores-Berrons R & Whitman RV". *Journal of the Geotechnical Engineering* Division ASCE ,109(5):778-81

[4.2] Mylonakis, G. (2001) Simplified model for seismic pile bending at soil layer inter-faces. *Soils and Foundations*, 41(4), 47-58.

[4.3] Flores-Berrones, R., Whitman, RV. (1982) Seismic response of end-bearing piles. *Journal of Geotechnical Engineering* Division ASCE 108(4):554-69.

[4.4] Margason, E. (1975) Pile bending during earthquake. Lecture ASCE/UC-Berkeley seminar on design construction & performance of deep foundation.

[4.5] Nikolaou, S., Mylonakis, G., Gazetas, G., Tazoh, T. (2001) Kinematic pile bending during earthquakes: analysis and field measurements. *Géotechnique*, 51(5):425-40.

[4.6] Maiorano, RMS., de Sanctis, L., Aversa, S., Mandolini, A. (2009) Kinematic response analysis of piled foundations under seismic excitations. *Canadian Geotechnical Journal*, 46(5):571-84.

[4.7] Sica, S., Mylonakis, G., Simonelli, AL. (2011) Transient kinematic pile bending in two-layer soil. *Soil Dynamics and Earthquake Engineering*, 31(7):891-905.

[4.8] Di Laora, R., Mandolini, A. and Mylonakis, G. (2012) insight on kinematic bending of flexible piles in layered soil. *Soil Dynamics and Earhquake Engineering*, 43: 309-322.

[4.9] Ohira, A., Tazoh, T., Nakahi S. and Shimizu, K. (1985) Observation and analysis of earthquake response behaviour of foundation piles in soft soil deposit. *Journal of Structural Mechanics and Earthquake Engineering*, 362/I-4,417-426 (in Japanese).

[4.10] Saitoh, M. (2005) Fixed-head pile bending by kinematic interaction and criteria for its minimization at optimal pile radius. *Journal of Geotechnical and Geoenvironmental Engineering* ASCE, 131 (10):1243-1251.

[4.11] Tajimi, H. (1969) Dynamic analysis of a structure embedded in an elastic stratum. In: *proceedings of the 4th world conference on earthquake engineering*, Santiago, Chile.

[4.12] Dezi, F., Carbonari , S., Leoni, G. (2009) Kinematic bending moments in pile foundations. *Soil Dynamics and Earthquake Engineering*, 30(3): 119-132.

[4.13] Kaynia, AM., Kausel, E. (1982) Dynamic stiffness and seismic response of pile groups. Research report no. R82-03. *Cambridge*, MA: Massachusetts Institute of Technology.

[4.14] K, Fan., Gazetas, G., Kaynia, AM., Kausel, E., Ahmad, S. (1991) Kinematic seismic response of single piles and pile groups. *Journal of Geotechnical Engineering*, 117 (12):1860-1879.

[4.15] Gazetas, G., K, Fan. (1993) Dynamic response of pile groups with different configurations. *Soil Dynamics and Earthquake Engineering*, (12):239-57.

[4.16] CENT/TC 250. Eurocode 8 Design of structures for earthquake resistance Part 5: Foundations, retaining structures and geotechnical aspects. European Committee for Standardization Technical Committee 250, Brussels, Belgium, Standard EN 1998-5,2003.

[4.17] Ministero delle Infrastructure. Nuov Norme Tecniche per le Costruzioni. DM 14.01.08. Gazzetta Ufficiale della Repubblica Italiana, No. 29, 4 Febbraio 2008 [in Italian].

[4.18] Anoyatis, G., Mylonakis, G., Lemnitzer, A. (2016) Soil reaction to lateral harmonic pile motion. *Soil Dynamics and Earthquake Engineering*, (87):164-179.

[4.19] Kramer, SL. (1996) Geotechnical earthquake engineering. *Prentice-Hall*, New York.

[1.20] Makris, N., Gazetas, G. (1992) Dynamic pile-soil-pile interaction. Part II: Lateral and seismic response. *Earthquake Engineering And Structural Dynamics*, 21(2):145-62.

[1.21] Mylonakis, G., Gazetas, G. (1999) Lateral Vibration And Inertial Forces of Grouped Piles In Layered Soil. *Journal of Geotechnical and Geoenvironmental Engineering*, 125: 16-25.

[4.22] Takewaki, I., Kishida, A. (2005) Efficient analysis of pile-group effect on seismic stiffness and strength design of buildings, *Soil Dynamics and Earthquake Engineering*, 25(5): 355-367.

[4.23] Padrón, LA., Aznárez, JJ., Maeso, O. (2007) BEM-FEM coupling model for the dynamic analysis of piles and pile groups. *Engineering Analysis with Boundary Elements*, 31(6):473-484.

[4.24] Padrón, LA., Aznárez, JJ., Maeso, O. (2008) Dynamic analysis of piled foundations in stratified soils by a BEM-FEM model. *Soil Dynamics and Earthquake Engineering*, 28(5):333-346.

# CHAPTER 5

# Total response of pile groups

In previous chapters, inertial and kinematic interaction were considered individually, however in reality those actions interact with each other detrimentally. Therefore, pile foundations in earthquake prone areas should be designed to withstand the presence of kinematic and inertial effects simultaneously, kinematic loads develop as a result of soil deformations in the vicinity of the pile and inertial loads imposed at the pile head. Mylonakis et al [5.1] demonstrated that for all piles in seismic areas with a wide range of geotechnical and geometrical parameters, always an optimal diameter (radius) exists which maximize safety against bending failure. Due to distinct importance of optimal pile radius in design issues and reducing seismic forces in soil-pile systems, this chapter aims at exploring these objectives: (i) to investigate the behaviour of soil-pile group systems under the simultaneous effect of kinematic and inertial forces; (ii) to quantify variation of the pile radius against bending of piles in pile groups; (iii) to assess the significance of the optimal pile radius in pile groups through pertinent numerical studies which encompass a wide range of parameters.

## 5.1 Analytical solution of total bending of pile groups

The soil-pile system under consideration is shown in Figure 5.1: a group of vertical cylindrical piles each of length $L$, diameter $d$, cross-sectional moment of inertia $I_p$, mass density $\rho_p$, mass per unit length $m_p$ and Young's modulus of elasticity $E_p$ is embedded in a homogeneous soil layer of thickness $H(=L)$ resting on a rigid base. Pile spacing is denoted with $s$. The pile group is loaded by harmonic lateral loads $V(t) = V_0 e^{i\omega t}$ transmitted through rigid cap and vertically propagating shear waves expressed in the form of harmonic horizontal displacement $u_g(t) = u_{g0} e^{i\omega t}$ at rigid base level. Main assumptions are given by: (a) foundation remains elastic during either seismic ground shaking or lateral head loading; (b) soil restraining action can be modeled using a bed of linear or equivalent-linear Winkler springs and dashpots, uniformly

distributed along the pile axis; (c) perfect contact (i.e., no gap and slippage) exist between pile and soil; (d) the flexural deformations of the pile group are dominant during oscillations; (e) the frequency of horizontal excitation is assumed to be equal to the fundamental frequency of the soil medium.

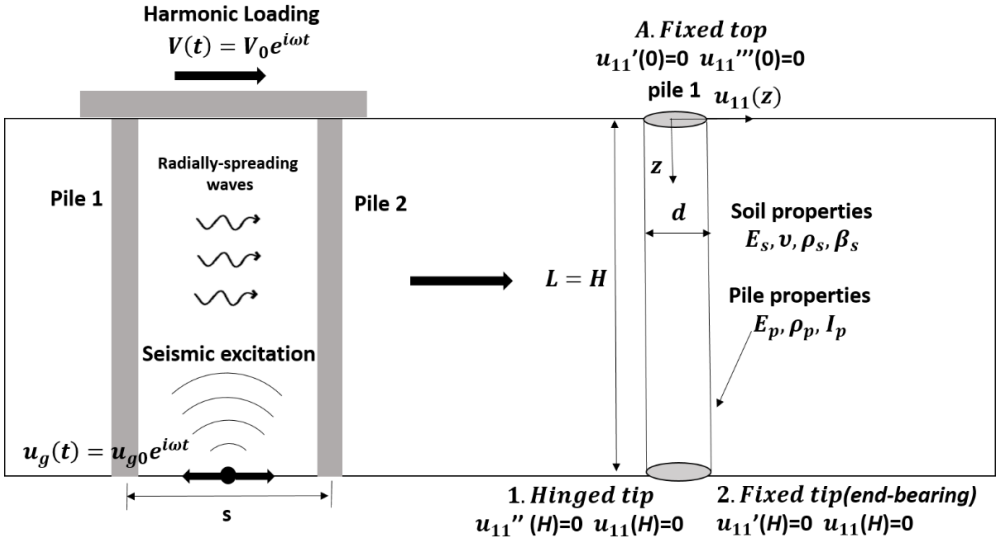


**Figure 5.1:** Problem considered for combined effect of inertial and kinematic interaction with different tip conditions.

## 5.2 Total response of the pile-soil system

Consider a pile group with identical *N* piles connected by a rigid cap restricted against rotation and subjected to seismic excitation $u_g(t) = u_{g0} e^{i\omega_g t}$ at the bedrock surface and lateral loading $V(t) = V_0 e^{i\omega_g t}$ at the head of pile group, and let $U^K{}_{11} = \cdots = U^K{}_{NN}$ denote the horizontal pile-top displacements of the *N* piles without any interaction among them when only subjected to the seismic excitation at the bedrock surface [4.22].

The total horizontal response at the head of each pile may be calculated as the sum of the following components:

(1) The horizontal pile-top displacement as a single (solitary) pile when subjected to seismic excitation at the bedrock surface.

(2) The horizontal displacement at the head of single (solitary) pile due to its own head loading (outcome of seismic excitation) with the amplitudes $P_1^K, \dots, P_N^K$.

(3) The additional horizontal pile-top displacement resulting from the motions transmitted by the other *N-1* piles due to seismic excitation at the bedrock surface.

(4) The additional horizontal pile-top displacement transmitted from the other *N-1* piles due to their head-loading (outcome of seismic excitation) with the amplitudes $P_1^K, \dots, P_N^K$.

(5) The horizontal pile-top displacement as a single (solitary) pile due to its own head loading (outcome of inertial forces atop the pile group) with the amplitudes $P_1^I, \dots, P_N^I$.

(6) The additional horizontal pile-top displacement transmitted from the other *N-1* piles due to their head-loading (outcome of inertial forces atop the pile group) with the amplitudes $P_1^I, \dots, P_N^I$.

(1) and (3) are 'kinematic' effects, while (2),(4),(5) and (6) are 'inertial' effects. When the horizontal head displacement of the foundation is expressed by $U^{(G)}$, the compatibility condition and equilibrium of forces at head of pile group can be described by:

$$U^{(G)} = U^{(G)I} + U^{(G)K} \tag{5.1}$$

$$U^{(G)} = U_i = \sum_{j=1}^{N} (\alpha^K{}_{ij} U^K{}_{\mathrm{jj}} + \alpha^I{}_{ij} \frac{P_j^K}{K_x{}^{(1)}} + \alpha^I{}_{ij} \frac{P_j^I}{K_x{}^{(1)}}) \tag{5.2}$$

$$\sum_{j=1}^{N} P_j = V_0 \tag{5.3}$$

where $U^{(G)I}$, $U^{(G)K}$ are respectively displacement groups when only inertial forces acting at the pile head and kinematic forces subjecting at the bedrock surface, Dividing both sides of Equation. (5.2) by the common displacement $U^K{}_{11} = \cdots = U^K{}_{\mathrm{NN}}$ leads to:

$$\frac{U^{(G)}}{U^K{}_{11}} - \sum_{j=1}^{N} \left(\alpha^I{}_{ij} \frac{P_j^K}{K_x{}^{(1)} U^K{}_{\mathrm{jj}}} + \alpha^I{}_{ij} \frac{P_j^I}{K_x{}^{(1)} U^K{}_{\mathrm{jj}}}\right) = \sum_{j=1}^{N} \alpha^K{}_{ij} \tag{5.4}$$

These systems of equations (Equation (5.4)) can be rewritten into matrix form as:

$$\begin{bmatrix} 1 & -\alpha^I{}_{11} & -\alpha^I{}_{12} & \dots & -\alpha^I{}_{1N} \\ 1 & -\alpha^I{}_{11} & -\alpha^I{}_{11} & \dots & -\alpha^I{}_{2N} \\ \vdots & \vdots & \vdots & \vdots & \vdots \\ 1 & -\alpha^I{}_{N1} & -\alpha^I{}_{N2} & \cdots & -\alpha^I{}_{NN} \\ 0 & 1 & 1 & \cdots & 1 \end{bmatrix} \begin{Bmatrix} \frac{U^{(G)}}{U^K{}_{11}} \\ \frac{P_1^K + P_1^I}{K_x{}^{(1)} U^K{}_{11}} \\ \frac{P_2^K + P_2^I}{K_x{}^{(1)} U^K{}_{22}} \\ \vdots \\ \frac{P_N^K + P_N^I}{K_x{}^{(1)} U^K{}_{\mathrm{NN}}} \end{Bmatrix} = \begin{Bmatrix} \sum_{j=1}^{N} \alpha^K{}_{1j} \\ \sum_{j=1}^{N} \alpha^K{}_{2j} \\ \vdots \\ \sum_{j=1}^{N} \alpha^K{}_{Nj} \\ \frac{\mathrm{V}_0}{K_x{}^{(1)} U^K{}_{\mathrm{NN}}} \end{Bmatrix} \tag{5.5}$$

$$\begin{bmatrix} 1 & -\alpha^I{}_{11} & -\alpha^I{}_{12} & \dots & -\alpha^I{}_{1N} \\ 1 & -\alpha^I{}_{11} & -\alpha^I{}_{11} & \dots & -\alpha^I{}_{2N} \\ \vdots & \vdots & \vdots & \vdots & \vdots \\ 1 & -\alpha^I{}_{N1} & -\alpha^I{}_{N2} & \cdots & -\alpha^I{}_{NN} \\ 0 & 1 & 1 & \cdots & 1 \end{bmatrix} \begin{Bmatrix} \frac{U^{(G)I}}{U^K{}_{11}} \\ \frac{P_1^I}{K_x{}^{(1)} U^K{}_{11}} \\ \frac{P_2^I}{K_x{}^{(1)} U^K{}_{22}} \\ \vdots \\ \frac{P_N^I}{K_x{}^{(1)} U^K{}_{\mathrm{NN}}} \end{Bmatrix} + \begin{bmatrix} 1 & -\alpha^I{}_{11} & -\alpha^I{}_{12} & \dots & -\alpha^I{}_{1N} \\ 1 & -\alpha^I{}_{11} & -\alpha^I{}_{11} & \dots & -\alpha^I{}_{2N} \\ \vdots & \vdots & \vdots & \vdots & \vdots \\ 1 & -\alpha^I{}_{N1} & -\alpha^I{}_{N2} & \cdots & -\alpha^I{}_{NN} \\ 0 & 1 & 1 & \cdots & 1 \end{bmatrix} \begin{Bmatrix} \frac{U^{(G)K}}{U^K{}_{11}} \\ \frac{P_1^K}{K_x{}^{(1)} U^K{}_{11}} \\ \frac{P_2^K}{K_x{}^{(1)} U^K{}_{22}} \\ \vdots \\ \frac{P_N^K}{K_x{}^{(1)} U^K{}_{\mathrm{NN}}} \end{Bmatrix} \tag{5.6}$$

$$= \begin{Bmatrix} 0 \\ 0 \\ \vdots \\ 0 \\ \frac{\mathrm{V}_0}{K_x{}^{(1)} U^K{}_{\mathrm{NN}}} \end{Bmatrix} + \begin{Bmatrix} \sum_{j=1}^{N} \alpha^K{}_{1j} \\ \sum_{j=1}^{N} \alpha^K{}_{2j} \\ \vdots \\ \sum_{j=1}^{N} \alpha^K{}_{Nj} \\ 0 \end{Bmatrix}$$

By separating kinematic and inertial effects, above matrix form can be expressed as:

$$\begin{bmatrix} 1 & -\alpha^{I}{}_{11} & -\alpha^{I}{}_{12} & \dots & -\alpha^{I}{}_{1N} \\ 1 & -\alpha^{I}{}_{11} & -\alpha^{I}{}_{11} & \dots & -\alpha^{I}{}_{2N} \\ \vdots & \vdots & \vdots & \vdots & \vdots \\ 1 & -\alpha^{I}{}_{N1} & -\alpha^{I}{}_{N2} & \cdots & -\alpha^{I}{}_{NN} \\ 0 & 1 & 1 & \cdots & 1 \end{bmatrix} \begin{Bmatrix} \frac{U^{(G)I}}{U^{K}{}_{11}} \\ \frac{P_1^I}{K^{(1)}U^{K}{}_{11}} \\ \frac{P_2^I}{K_x{}^{(1)}U^{K}{}_{22}} \\ \vdots \\ \frac{P_N^I}{K_x{}^{(1)}U^{K}{}_{\mathrm{NN}}} \end{Bmatrix} = \begin{Bmatrix} 0 \\ 0 \\ \vdots \\ 0 \\ \frac{\mathrm{V}_0}{K_x{}^{(1)}U^{K}{}_{\mathrm{NN}}} \end{Bmatrix} \tag{5.7}$$

$$\begin{bmatrix} 1 & -\alpha^{I}{}_{11} & -\alpha^{I}{}_{12} & \dots & -\alpha^{I}{}_{1N} \\ 1 & -\alpha^{I}{}_{11} & -\alpha^{I}{}_{11} & \dots & -\alpha^{I}{}_{2N} \\ \vdots & \vdots & \vdots & \vdots & \vdots \\ 1 & -\alpha^{I}{}_{N1} & -\alpha^{I}{}_{N2} & \cdots & -\alpha^{I}{}_{NN} \\ 0 & 1 & 1 & \cdots & 1 \end{bmatrix} \begin{Bmatrix} \frac{U^{(G)K}}{U^{K}{}_{11}} \\ \frac{P_1^K}{K_x{}^{(1)}U^{K}{}_{11}} \\ \frac{P_2^K}{K_x{}^{(1)}U^{K}{}_{22}} \\ \vdots \\ \frac{P_N^K}{K_x{}^{(1)}U^{K}{}_{\mathrm{NN}}} \end{Bmatrix} = \begin{Bmatrix} \sum_{j=1}^{N} \alpha^{K}{}_{1j} \\ \sum_{j=1}^{N} \alpha^{K}{}_{2j} \\ \vdots \\ \sum_{j=1}^{N} \alpha^{K}{}_{Nj} \\ 0 \end{Bmatrix} \tag{5.8}$$

where $\alpha^{I}{}_{ij}$ are the interaction factors for inertial loading and $\alpha^{K}{}_{ij}$ are the interaction factors for kinematic loading, being $\alpha^{I}{}_{ii} = \alpha^{K}{}_{ii} = 1$, and $K_x{}^{(1)}$ the dynamic stiffness of the single pile. The bending moment at the head of pile *i* may be derived from the total curvature $U_i''(0)$ as:

$$M_i = E_p I_p U_i''(0) \tag{5.9}$$

## 5.3 Total curvature ratios

Finally, by using the superposition method to add the kinematic and inertial effects together, the total curvature can be expressed as:

$$U_i^{T\,\prime\prime}(0) = U_i^{K\,\prime\prime}(0) + U_i^{I\,\prime\prime}(0) = \sum_{j=1}^{N} (\beta_{ij}^{K} U^{K}{}_{\mathrm{jj}} + \beta_{ij}^{I} \frac{P_j^K}{K_x{}^{(1)}} + \beta_{ij}^{I} \frac{P_j^I}{K_x{}^{(1)}}) \tag{5.10}$$

For simplicity of the expression, the following form can be reached:

$$\frac{U_i^{T\prime\prime}(0)}{U^K{}_{\text{jj}}} = \sum_{j=1}^{N} (\beta_{ij}^K + \beta_{ij}^I \frac{P_j^I}{K_x{}^{(1)} U^K{}_{\text{jj}}} + \beta_{ij}^I \frac{P_j^K}{K_x{}^{(1)} U^K{}_{\text{jj}}}) \tag{5.11}$$

These systems of equations can be set into a matrix form as:

$$\begin{Bmatrix} \frac{U_1^{T\prime\prime}(0)}{U^K{}_{11}} \\ \frac{U_2^{T\prime\prime}(0)}{U^K{}_{22}} \\ \vdots \\ \frac{U_N^{T\prime\prime}(0)}{U^K{}_{\text{NN}}} \end{Bmatrix} = \begin{bmatrix} \beta_{11}^K & \beta_{12}^K & \dots & \beta_{1N}^K \\ \beta_{21}^K & \beta_{22}^K & \dots & \beta_{2N}^K \\ \vdots & \vdots & \vdots & \vdots \\ \beta_{N1}^K & \beta_{N2}^K & \dots & \beta_{NN}^K \end{bmatrix} \begin{Bmatrix} 1 \\ 1 \\ \vdots \\ 1 \end{Bmatrix} + \begin{bmatrix} \beta_{11}^I & \beta_{12}^I & \dots & \beta_{1N}^I \\ \beta_{21}^I & \beta_{22}^I & \dots & \beta_{2N}^I \\ \vdots & \vdots & \vdots & \vdots \\ \beta_{N1}^I & \beta_{N2}^I & \dots & \beta_{NN}^I \end{bmatrix} \begin{Bmatrix} \frac{P_1^I}{K_x{}^{(1)} U^K{}_{11}} \\ \frac{P_2^I}{K_x{}^{(1)} U^K{}_{22}} \\ \vdots \\ \frac{P_N^I}{K_x{}^{(1)} U^K{}_{\text{NN}}} \end{Bmatrix} + \begin{bmatrix} \beta_{11}^I & \beta_{12}^I & \dots & \beta_{1N}^I \\ \beta_{21}^I & \beta_{22}^I & \dots & \beta_{2N}^I \\ \vdots & \vdots & \vdots & \vdots \\ \beta_{N1}^I & \beta_{N2}^I & \dots & \beta_{NN}^I \end{bmatrix} \begin{Bmatrix} \frac{P_1^K}{K_x{}^{(1)} U^K{}_{11}} \\ \frac{P_2^K}{K_x{}^{(1)} U^K{}_{22}} \\ \vdots \\ \frac{P_N^K}{K_x{}^{(1)} U^K{}_{\text{NN}}} \end{Bmatrix} \tag{5.12}$$

$$\begin{Bmatrix} \frac{U_i^{T\prime\prime}(0)}{U^K{}_{11}} \end{Bmatrix} = [\beta_{ij}^K]\{I\} + \left[\beta_{ij}^I\right]\{\bar{P}_j{}^I\} + \left[\beta_{ij}^I\right]\{\bar{P}_j{}^K\} \tag{5.13}$$

where the vector of forces for inertial and kinematic effects $\{\bar{P}_j{}^I\} = \left\{\frac{P_1^I}{K_x{}^{(1)} U^K{}_{\text{jj}}}\right\}$, $\{\bar{P}_j{}^K\} = \left\{\frac{P_1^K}{K_x{}^{(1)} U^K{}_{\text{jj}}}\right\}$ are obtained separately after solving Equations (5.7) and (5.8).

## 5.4 Total bending strain as fundamental measure of pile bending

It is beneficial to use total bending strain as a deformation-related quantity to quantify pile bending. The maximum total bending strain at the outer fibre of the pile cross-section, $\varepsilon_{pi}$, is related to bending moments as:

$$\varepsilon_{pi}^T(z) = \frac{M_i}{E_p I_p} r = \{-\frac{d}{2} \frac{d^2 U_i(z)}{dz^2}\} \tag{5.14}$$

where r is the distance from the neutral axis to the farthest fibre in the cross-section. Bending strain has several advantages over bending moment in assessing the seismic performance of a pile because: (i) it is dimensionless; (ii) it is directly measurable experimentally; (iii) it can be used to quantify damage (iv) ultimate ('failure') bending strains do not vary significantly among common structural materials. For instance, strains of the order of 0.1% is enough to inflict damage in conventionally-design concrete or steel beams. After obtaining kinematic and inertial bending moments at the head of each pile in the group in vector form, the total bending strains can be calculated by superimposing these to effects together which gives:

$$\{\varepsilon_{pi}^{T}(z=0)\} = \{-\frac{d}{2}\frac{d^2U_i(z=0)}{dz^2}\} \tag{5.15}$$

$$\{\varepsilon_{pi}^{T}(z=0)\} = \{\varepsilon_{pi}^{K}(0)\} + \{\varepsilon_{pi}^{I}(0)\} \tag{5.16}$$

Afterwards the total bending strain $\varepsilon_{pi}(0)$ at the head of each pile is normalized with respect to a mean shear strain of the soil medium $\gamma_s$ .The mean shear strain is defined as the absolute value of the maximum harmonic response displacement of the ground surface with respect to the bedrock divided by the height of the soil medium *H* as shown in Equation (5.17).

$$\gamma_s = \frac{u_{ff}(z=0) - u_{ff}(z=H)}{H} = \frac{\frac{u_{g0}}{\cos(\delta H)} - u_{g0}}{H} = \frac{u_{g0}}{Hcos(\delta H)}(1 - cos(\delta H)) \tag{5.17}$$

Therefore the closed form formula of the normalized total bending strains can be written as follows:

$$\left\{\frac{\varepsilon_{pi}^{T}(0)}{\gamma_s}\right\} = \left\{\frac{\varepsilon_{pi}^{K}(0)}{\gamma_s}\right\} + \left\{\frac{\varepsilon_{pi}^{I}(0)}{\gamma_s}\right\} \tag{5.18}$$

The first and the second terms in Equation (5.18) are associated with normalized kinematic and inertial bending, respectively, which have been quantified in closed form equations previously in chapters three and four. By using them, normalized total bending strains can be expressed by:

$$\left\{\frac{\varepsilon_{pi}^{T}(0)}{\gamma_s}\right\} = \left([\beta_{ij}^{K}]\{I\} + [\beta_{ij}^{I}]\{\overline{P}_j^{\,K}\}\right)\frac{(\frac{r}{H})\Gamma}{(1-\cos(\delta H))} + \frac{[\beta_{ij}^{I}]\{\gamma_j\}}{\frac{\pi}{8}(\frac{r}{H})^3(\lambda H)F(\lambda H)}N\left|\frac{V_0}{E_p\gamma_s H^2}\right|e^{i\varphi_r} \tag{5.19}$$

or

$$\left\{\frac{\varepsilon_{pi}^{T}(0)}{\gamma_s}\right\} = \left([\beta_{ij}^{K}]\{I\} + [\beta_{ij}^{I}]\{\overline{P}_j^{\,K}\}\right)\frac{\left(\frac{r}{H}\right)\Gamma}{(1-\cos(\delta H))} + \frac{[\beta_{ij}^{I}]\{\gamma_j\}}{\frac{\pi}{8}(\frac{r}{H})^3(\lambda H)F(\lambda H)}N.Fre^{i\varphi_r} \tag{5.20}$$

Factor $Fr$ is a dimensionless factor which is related to the effect of the lateral inertial load relative to the free-field deformation of the soil layer. $\varphi_r$ is the phase lag between lateral inertial load $V_0$ and mean shear strain $\gamma_s$ (ground motion). Both parameters have been obtained and discussed in detail in chapter three. $N$ is the number of piles in pile groups.

## 5.5 Behavior of total bending in pile groups

To have further insight into the characteristics and behavior of the normalized total bending strains against slenderness ratio $r/H$ by using the expression proposed in Equations (5.19) and (5.20), additional studies of the fixed-head pile groups 1×2, 2×2, 3×3 and 4×4 with different boundary conditions at the tip (fixed or hinged) are carried out. Piles are simultaneously subjected to the seismic excitation $u_g(t) = u_{g0}e^{i\omega_g t}$ at the bedrock and harmonic head loading $(t) = V_0 e^{i\omega_g t}$ . The frequency of excitation is assumed to be equal to the fundamental frequency of the soil layer. Special attention is paid to the effects of the parameters like pile spacing $/d$ , pile-soil stiffness ratio $E_p/E_s$, factor $Fr$, phase lag $\varphi_r$ and the number of piles $N$ on the normalized total bending strains in the group. Despite assumptions of Euler-Bernoulli beam being valid only for slenderness ratios below 0.2, a wider range ($r/H = 0 - 0.4$) is presented in this study in order to have a clear picture of the behavior of pile groups beyond the local maximum.

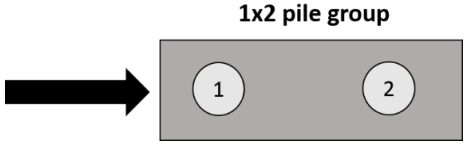


**Figure 5.2:** Depiction of 1×2 pile group.

### 5.5.1 Hinged-tip 1×2 pile groups:

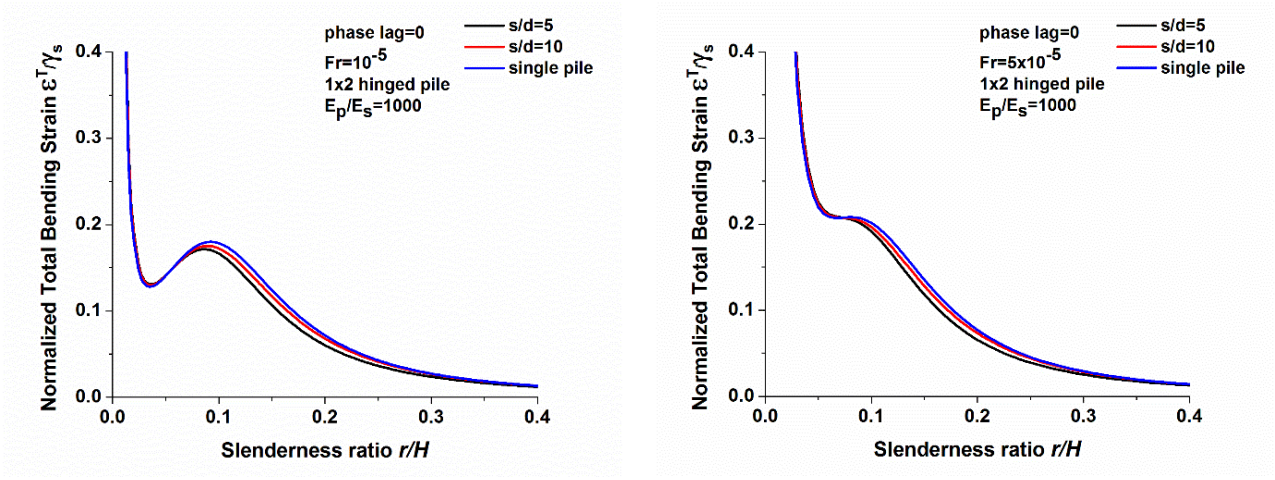


**Figure 5.3:** Normalized total bending strains of 1×2 hinged pile groups with respect to single pile ($\frac{\rho_p}{\rho_s} = 1.43,\ \upsilon_s = 0.4\ ,\ \beta_s = 0.05\ ,\frac{E_p}{E_s} = 1000,\ \varphi_r = 0$).

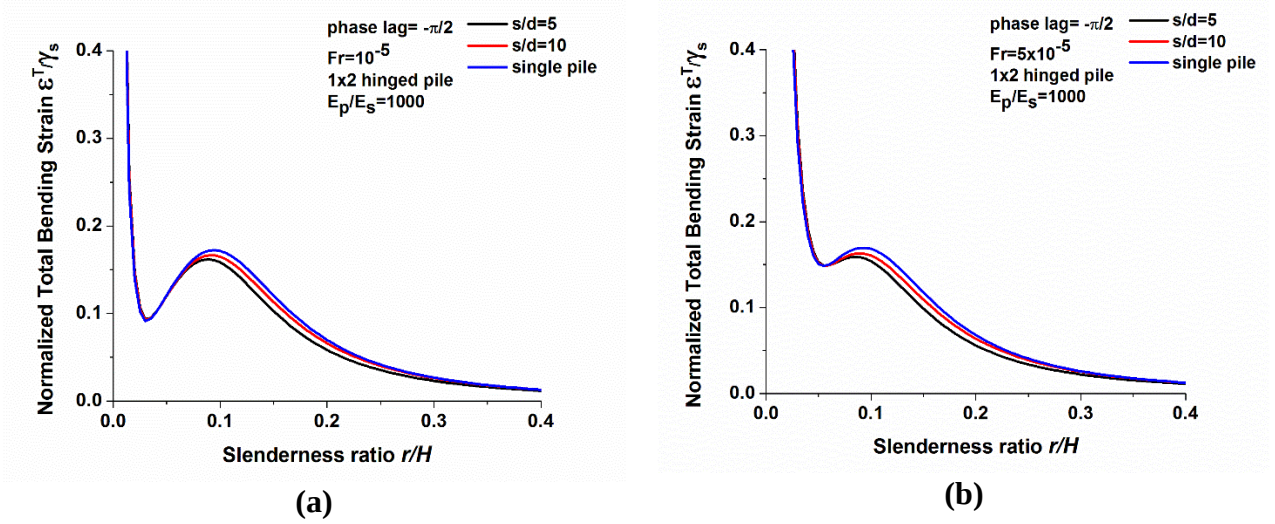


**Figure 5.4:** Normalized total bending strains of 1×2 hinged pile groups with respect to single pile ($\frac{\rho_p}{\rho_s} = 1.43,\ \upsilon_s = 0.4\ ,\ \beta_s = 0.05\ ,\frac{E_p}{E_s} = 1000,\ \varphi_r = -\frac{\pi}{2}$).

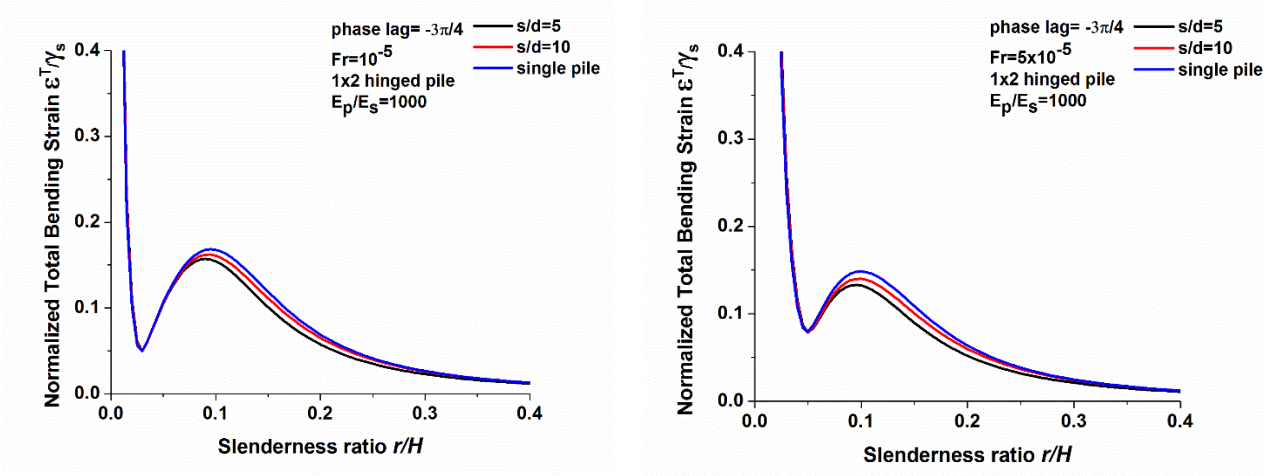


**Figure 5.5:** Normalized total bending strains of 1×2 hinged pile groups with respect to single pile ($\frac{\rho_p}{\rho_s} = 1.43,\ \upsilon_s = 0.4\ ,\ \beta_s = 0.05\ ,\frac{E_p}{E_s} = 1000,\ \varphi_r = -\frac{3\pi}{4}$).

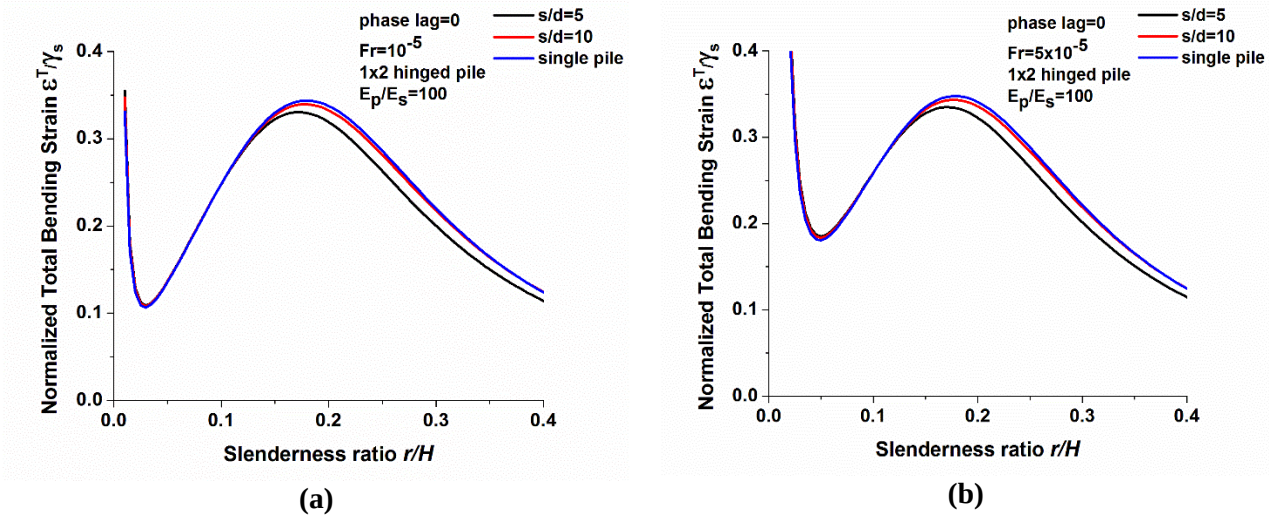


**Figure 5.6:** Normalized total bending strains of 1×2 hinged pile groups with respect to single pile ($\frac{\rho_p}{\rho_s} = 1.43,\ \upsilon_s = 0.4\ ,\ \beta_s = 0.05\ ,\frac{E_p}{E_s} = 100,\ \varphi_r = 0$).

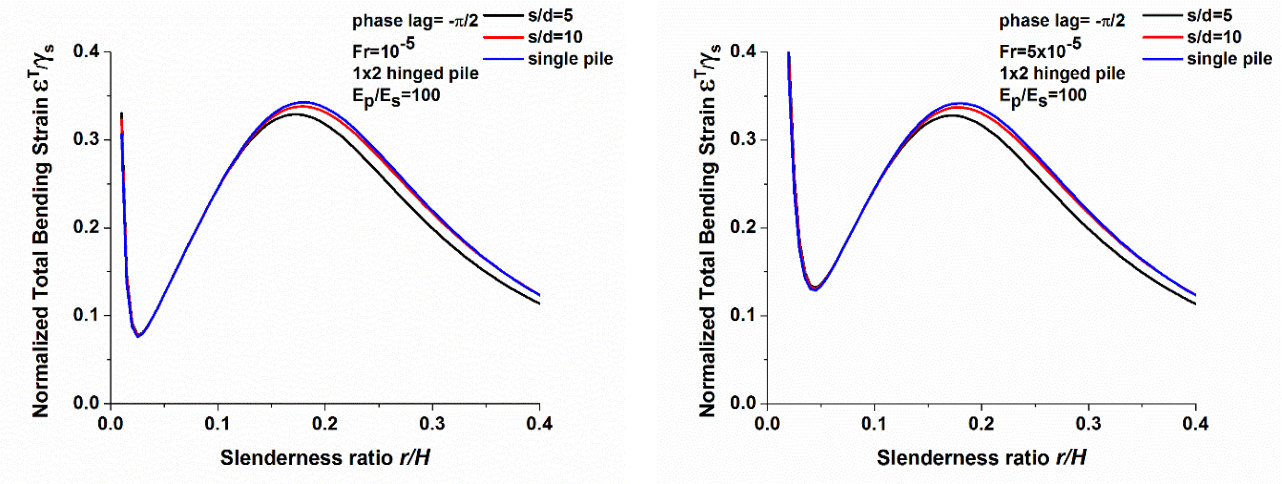


**Figure 5.7:** Normalized total bending strains of 1×2 hinged pile groups with respect to single pile ($\frac{\rho_p}{\rho_s} = 1.43,\ \upsilon_s = 0.4\ ,\ \beta_s = 0.05\ ,\frac{E_p}{E_s} = 100,\ \varphi_r = -\frac{\pi}{2}$).

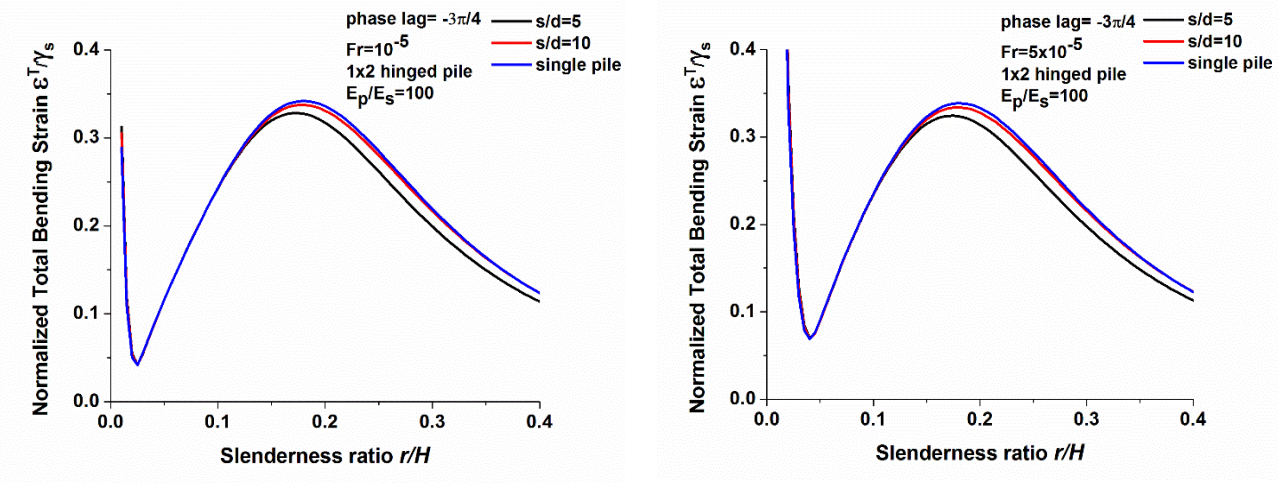


**Figure 5.8:** Normalized total bending strains of 1×2 hinged pile groups with respect to single pile ($\frac{\rho_p}{\rho_s} = 1.43,\ \upsilon_s = 0.4\ ,\ \beta_s = 0.05\ ,\frac{E_p}{E_s} = 100,\ \varphi_r = -\frac{3\pi}{4}$).

### 5.5.2 Fixed-tip 1×2 pile groups:

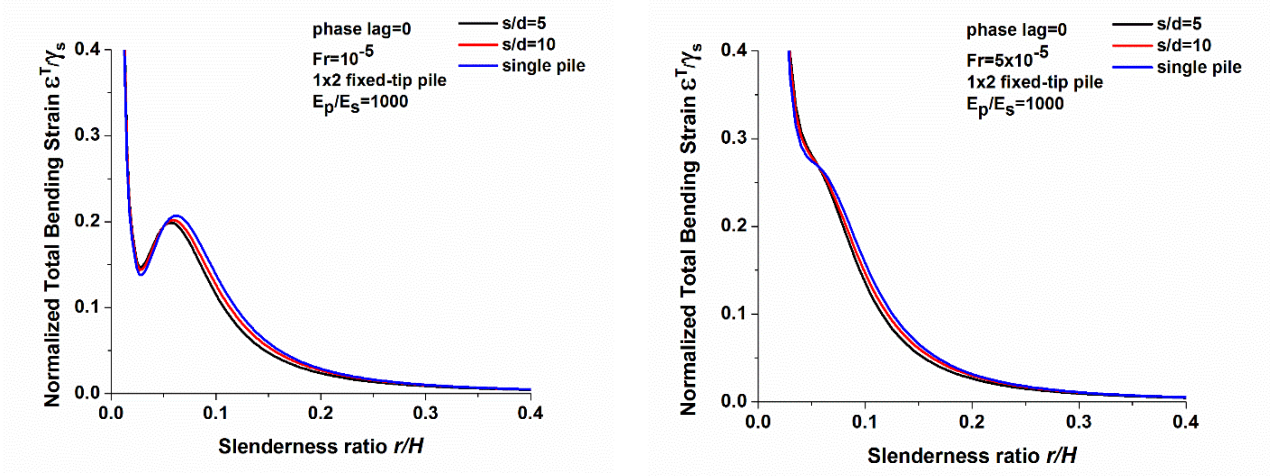


**Figure 5.9:** Normalized total bending strains of 1×2 fixed-tip pile groups with respect to single pile ($\frac{\rho_p}{\rho_s} = 1.43,\ \upsilon_s = 0.4\ ,\ \beta_s = 0.05\ ,\frac{E_p}{E_s} = 1000, \varphi_r = 0$).

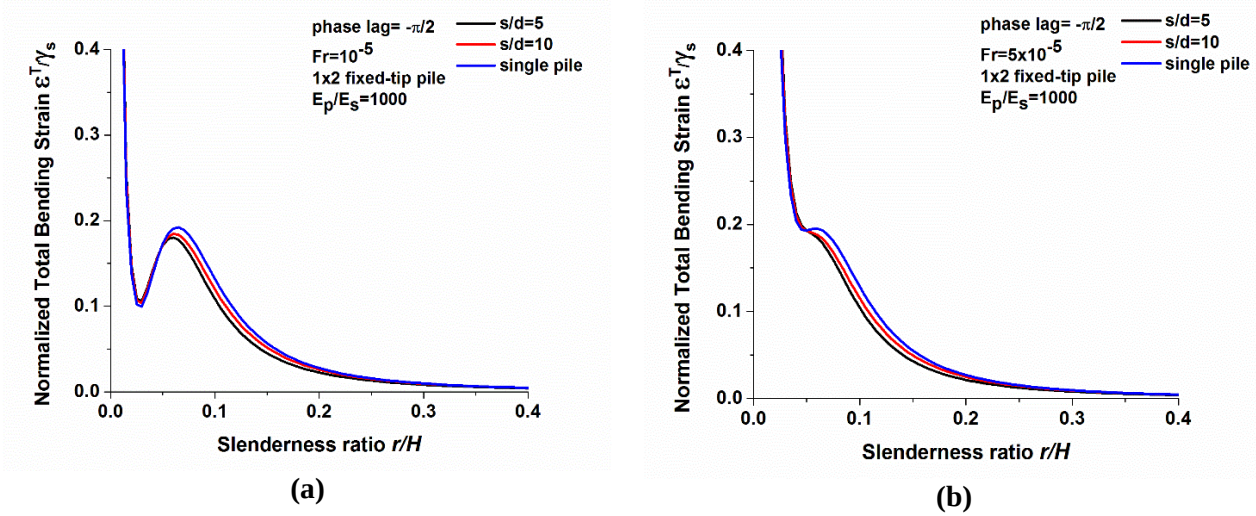


**Figure 5.10:** Normalized total bending strains of 1×2 fixed-tip pile groups with respect to single pile ($\frac{\rho_p}{\rho_s} = 1.43,\ \upsilon_s = 0.4\ ,\ \beta_s = 0.05\ ,\frac{E_p}{E_s} = 1000, \varphi_r = -\frac{\pi}{2}$).

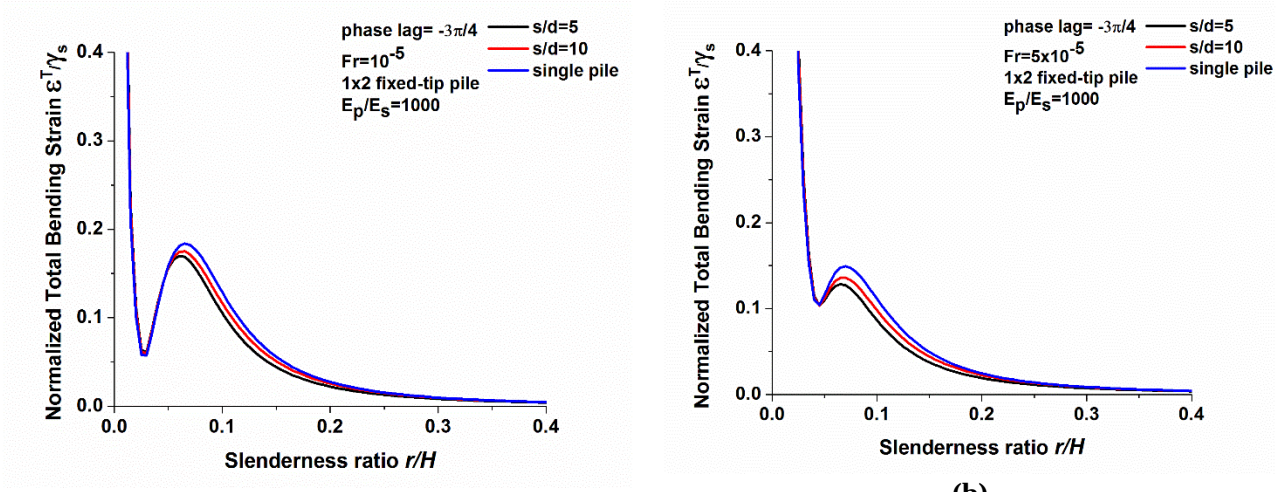


**Figure 5.11:** Normalized total bending strains of 1×2 fixed-tip pile groups with respect to single pile ($\frac{\rho_p}{\rho_s} = 1.43,\ \upsilon_s = 0.4\ ,\ \beta_s = 0.05\ ,\frac{E_p}{E_s} = 1000, \varphi_r = -\frac{3\pi}{4}$).

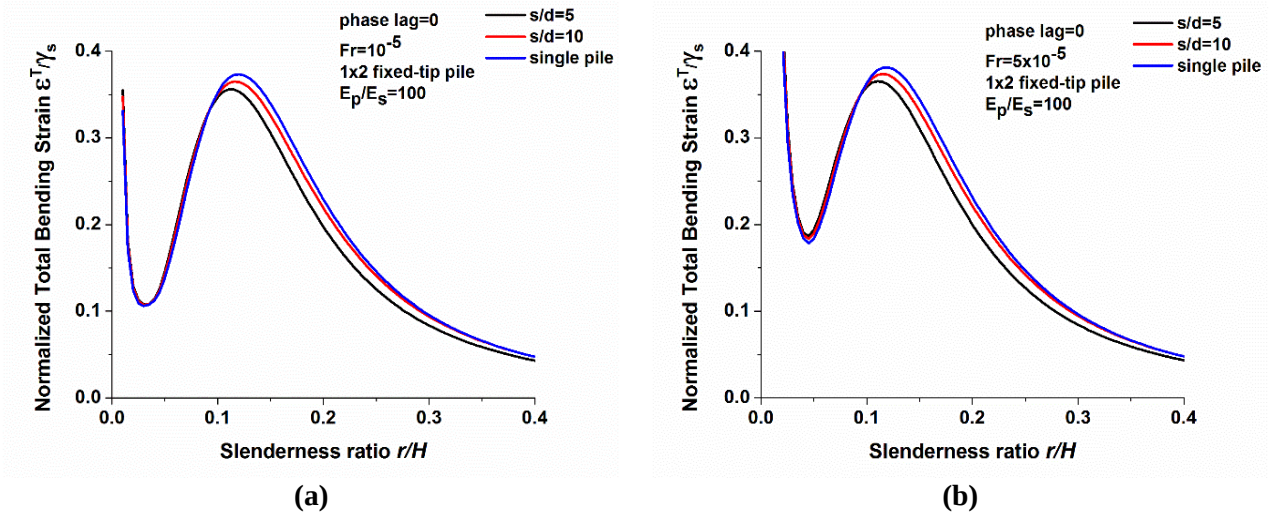


**Figure 5.12:** Normalized total bending strains of 1×2 fixed-tip pile groups with respect to single pile ($\frac{\rho_p}{\rho_s} = 1.43,\ \upsilon_s = 0.4\ ,\ \beta_s = 0.05\ ,\frac{E_p}{E_s} = 100, \varphi_r = 0$).

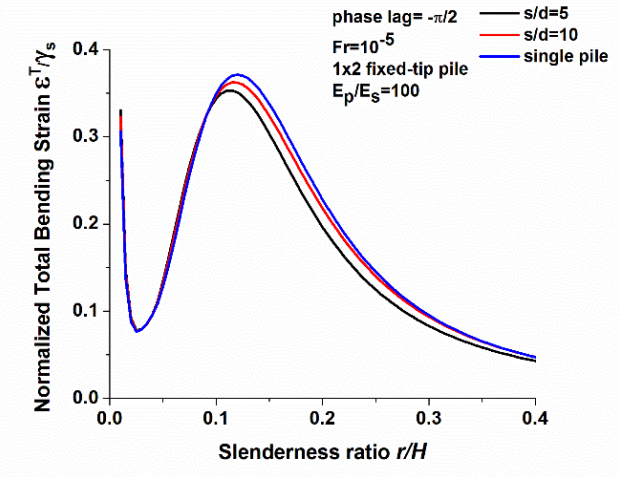


**(a)**

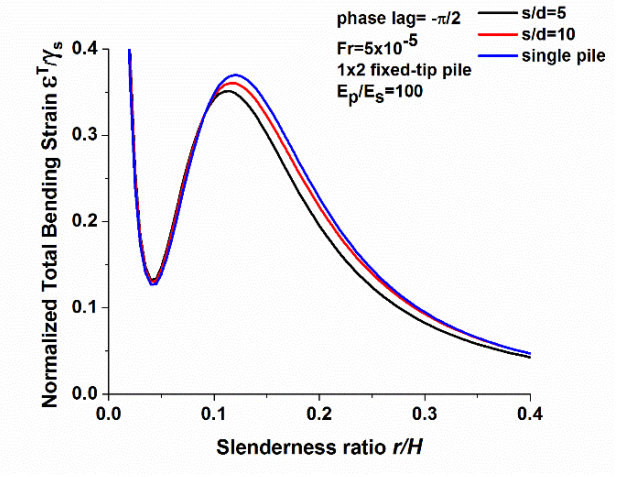


**(b)**

**Figure 5.13:** Normalized total bending strains of 1×2 fixed-tip pile groups with respect to single pile ($\frac{\rho_p}{\rho_s} = 1.43,\ \upsilon_s = 0.4\ ,\ \beta_s = 0.05\ ,\frac{E_p}{E_s} = 100, \varphi_r = -\frac{\pi}{2}$).

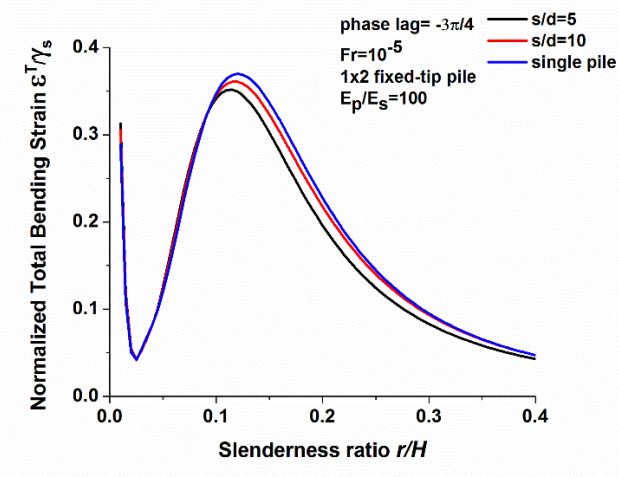


**(a)**

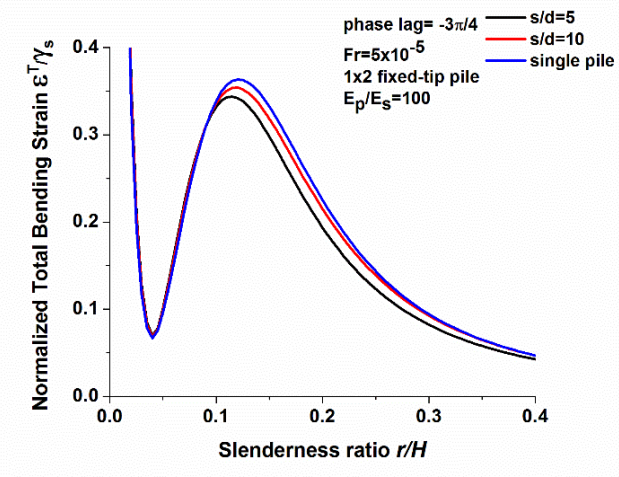


**(b)**

**Figure 5.14:** Normalized total bending strains of 1×2 fixed-tip pile groups with respect to single pile ($\frac{\rho_p}{\rho_s} = 1.43,\ \upsilon_s = 0.4\ ,\ \beta_s = 0.05\ ,\frac{E_p}{E_s} = 100, \varphi_r = -\frac{3\pi}{4}$).

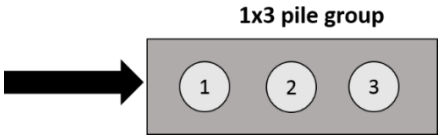


**Figure 5.15:** Depiction of 1x3 pile groups.

### 5.5.3 Hinged-tip 1×3 pile groups:

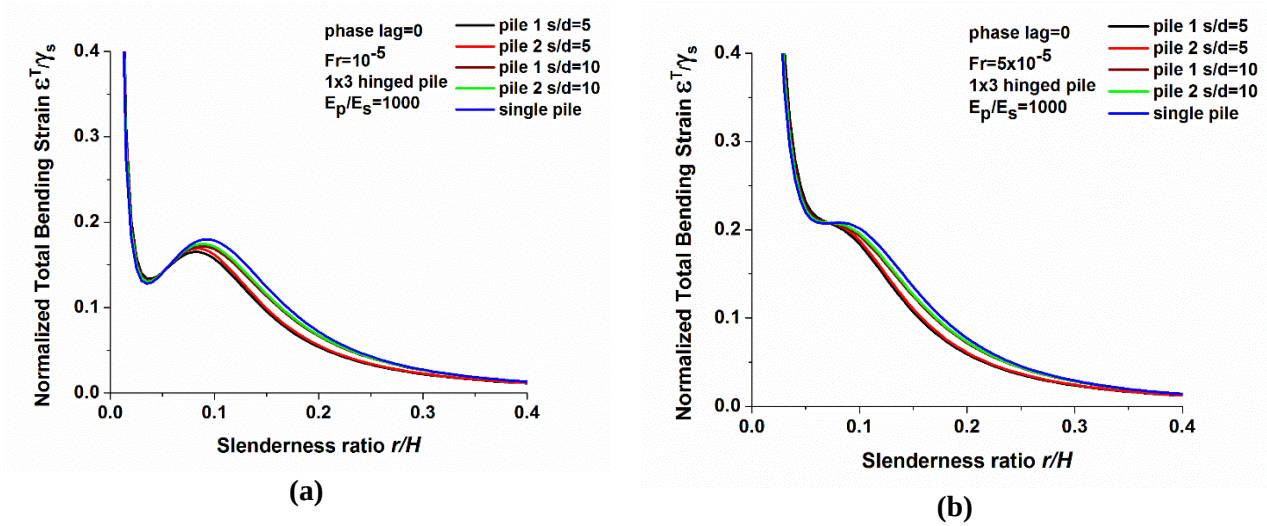


**Figure 5.16:** Normalized total bending strains of 1×3 hinged pile groups with respect to single pile ($\frac{\rho_p}{\rho_s} = 1.43,\ \upsilon_s = 0.4\ ,\ \beta_s = 0.05\ ,\frac{E_p}{E_s} = 1000, \varphi_r = 0$).

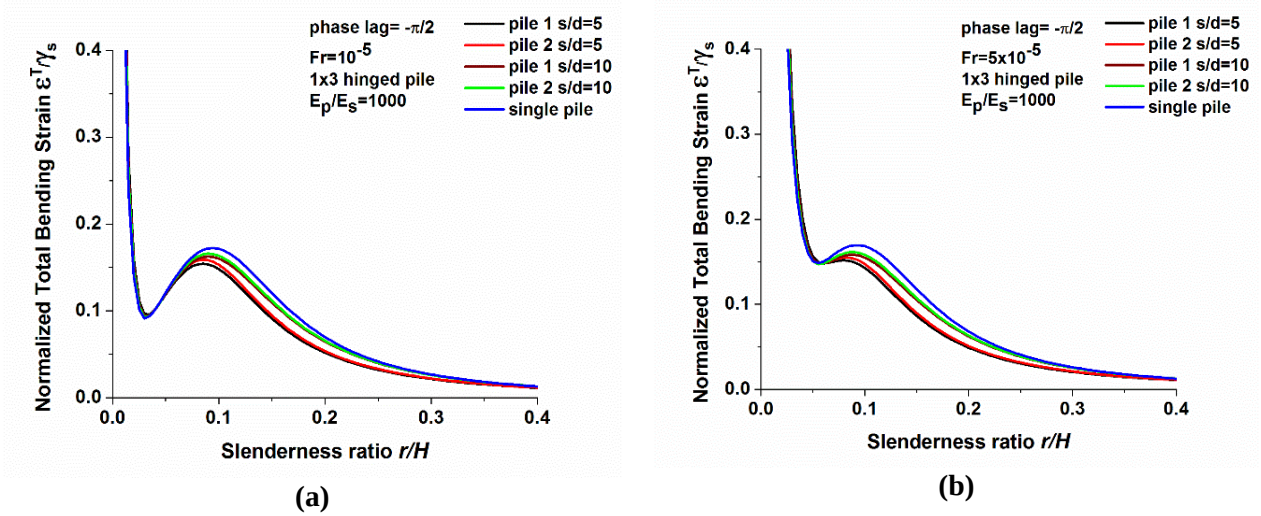


**Figure 5.17:** Normalized total bending strains of 1×3 hinged pile groups with respect to single pile ($\frac{\rho_p}{\rho_s} = 1.43,\ \upsilon_s = 0.4\ ,\ \beta_s = 0.05\ ,\frac{E_p}{E_s} = 1000, \varphi_r = -\frac{\pi}{2}$).

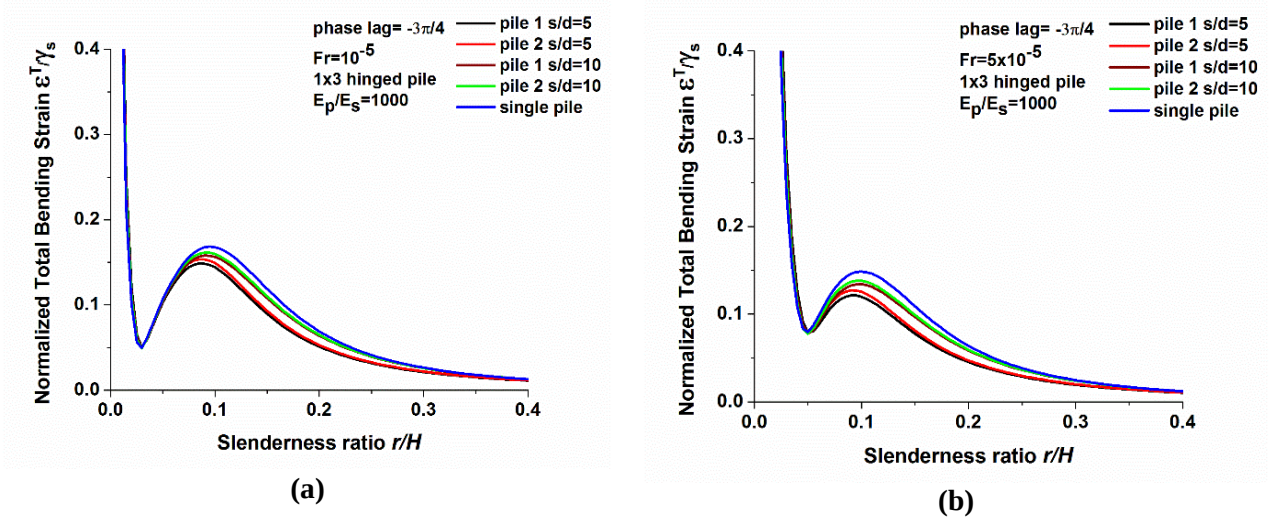


**Figure 5.18:** Normalized total bending strains of 1×3 hinged pile groups with respect to single pile ($\frac{\rho_p}{\rho_s} = 1.43,\ \upsilon_s = 0.4\ ,\ \beta_s = 0.05\ ,\frac{E_p}{E_s} = 1000, \varphi_r = -\frac{3\pi}{4}$).

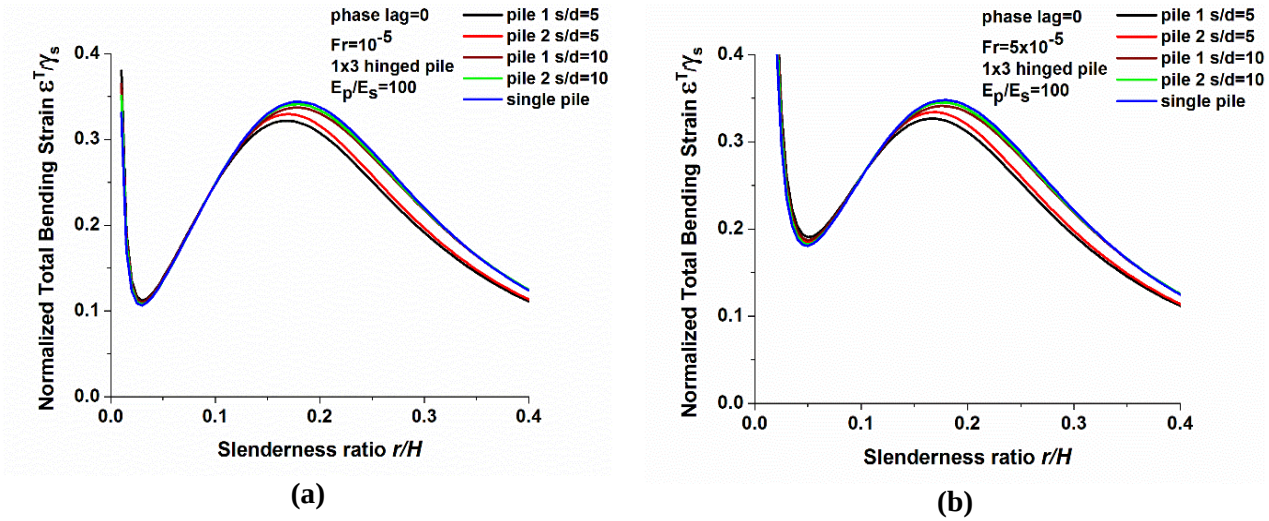


**Figure 5.19:** Normalized total bending strains of 1×3 hinged pile groups with respect to single pile ($\frac{\rho_p}{\rho_s} = 1.43,\ \upsilon_s = 0.4\ ,\ \beta_s = 0.05\ ,\frac{E_p}{E_s} = 100, \varphi_r = 0$).

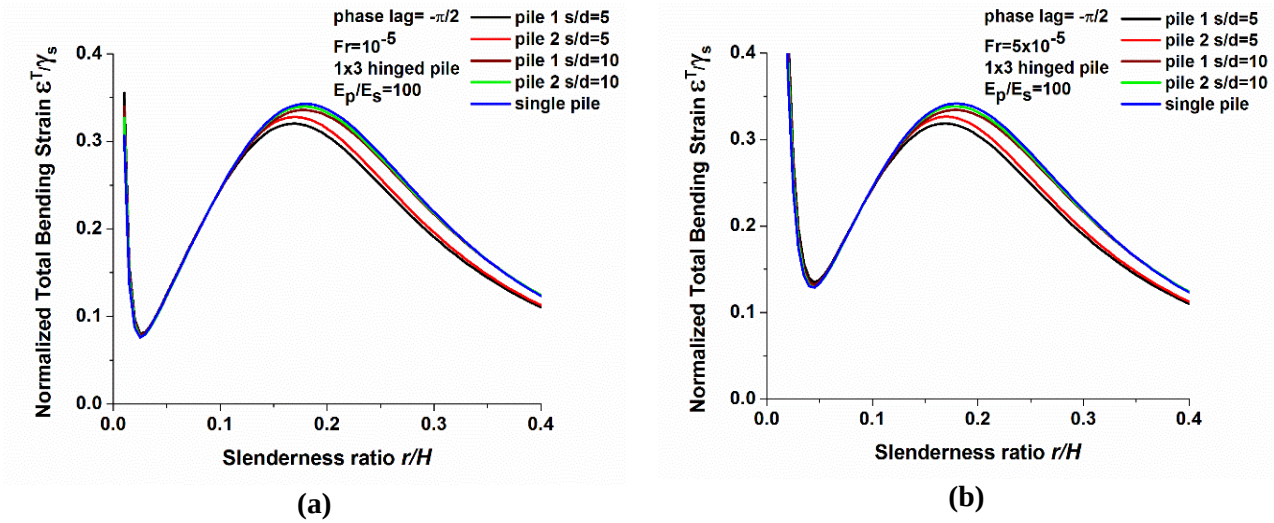


**Figure 5.20:** Normalized total bending strains of 1×3 hinged pile groups with respect to single pile ($\frac{\rho_p}{\rho_s} = 1.43,\ \upsilon_s = 0.4\ ,\ \beta_s = 0.05\ ,\frac{E_p}{E_s} = 100, \varphi_r = -\frac{\pi}{2}$).

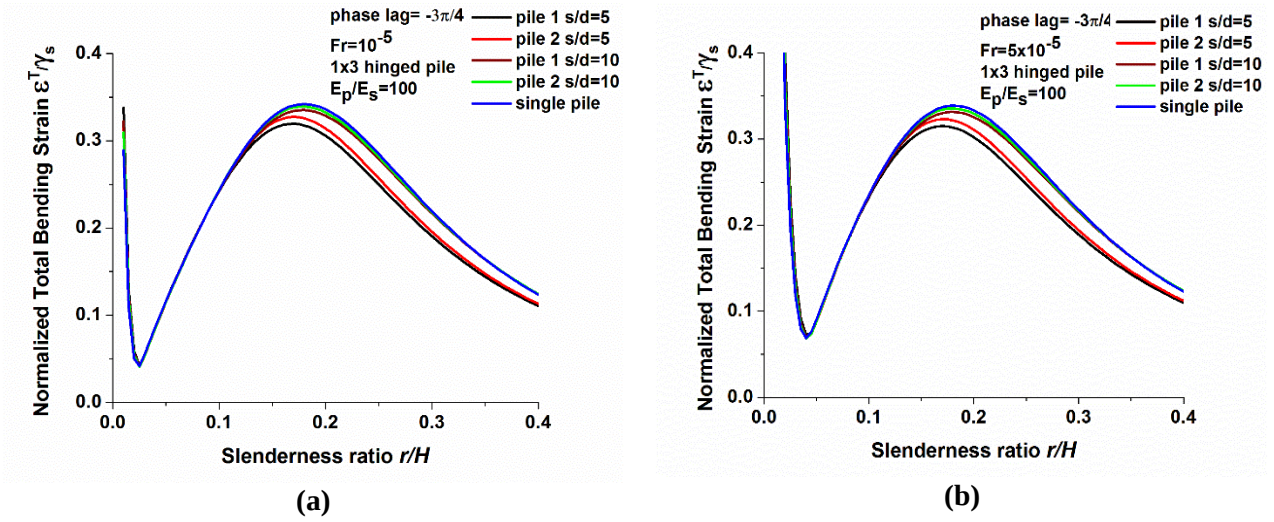


**Figure 5.21:** Normalized total bending strains of 1×3 hinged pile groups with respect to single pile ($\frac{\rho_p}{\rho_s} = 1.43,\ \upsilon_s = 0.4\ ,\ \beta_s = 0.05\ ,\frac{E_p}{E_s} = 100, \varphi_r = -\frac{3\pi}{4}$).

### 5.5.4 Fixed-tip 1×3 pile groups:

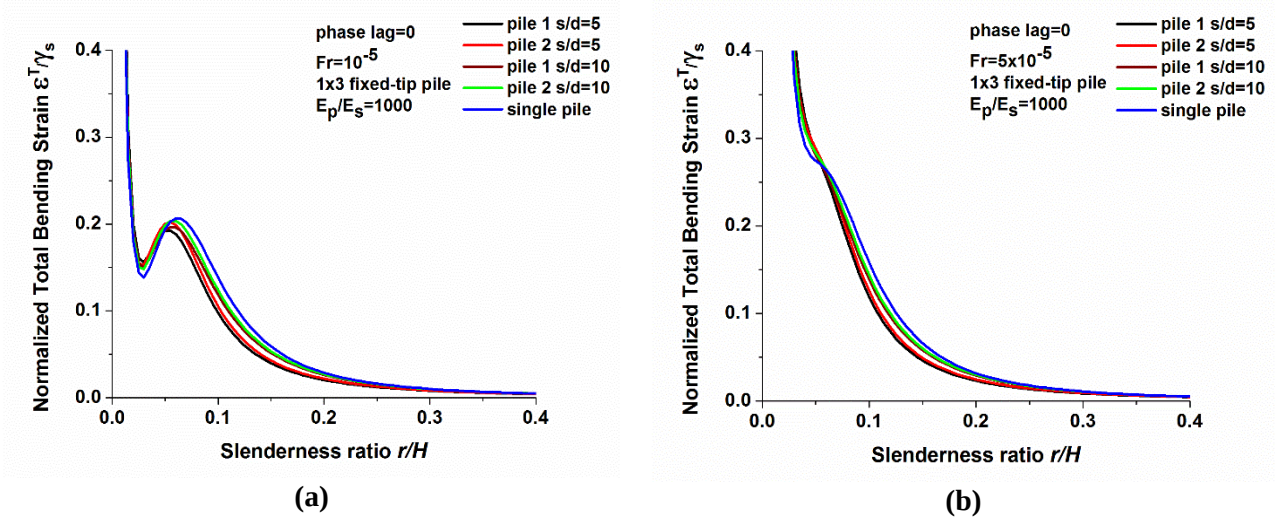


**Figure 5.22:** Normalized total bending strains of 1×3 fixed-tip pile groups with respect to single pile ($\frac{\rho_p}{\rho_s} = 1.43,\ \upsilon_s = 0.4\ ,\ \beta_s = 0.05\ ,\frac{E_p}{E_s} = 100, \varphi_r = 0$).

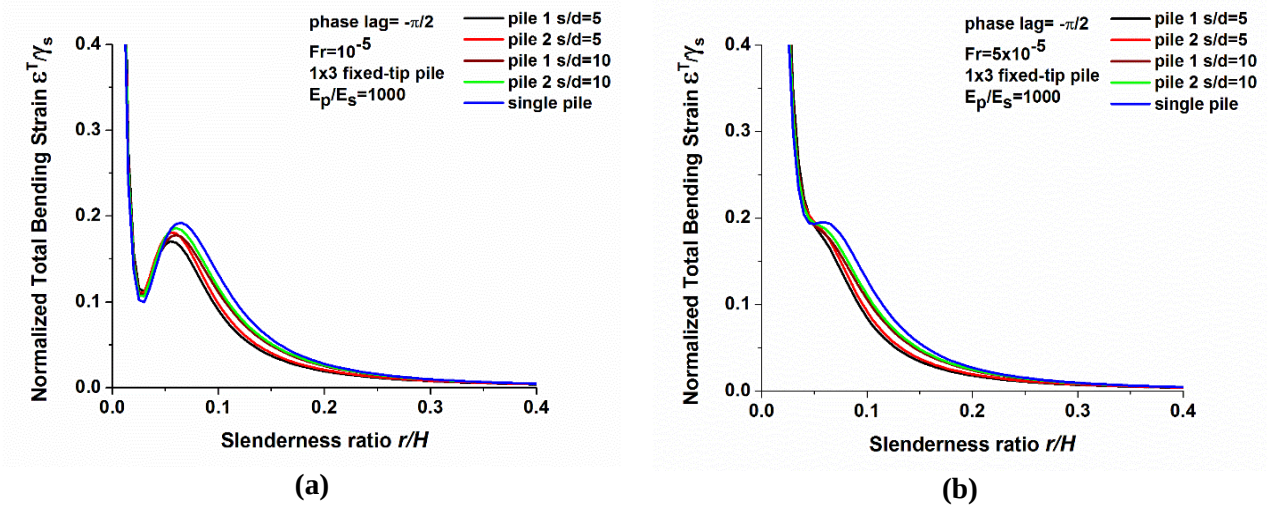


**Figure 5.23:** Normalized total bending strains of 1×3 fixed-tip pile groups with respect to single pile ($\frac{\rho_p}{\rho_s} = 1.43,\ \upsilon_s = 0.4\ ,\ \beta_s = 0.05\ ,\frac{E_p}{E_s} = 100, \varphi_r = -\frac{\pi}{2}$).

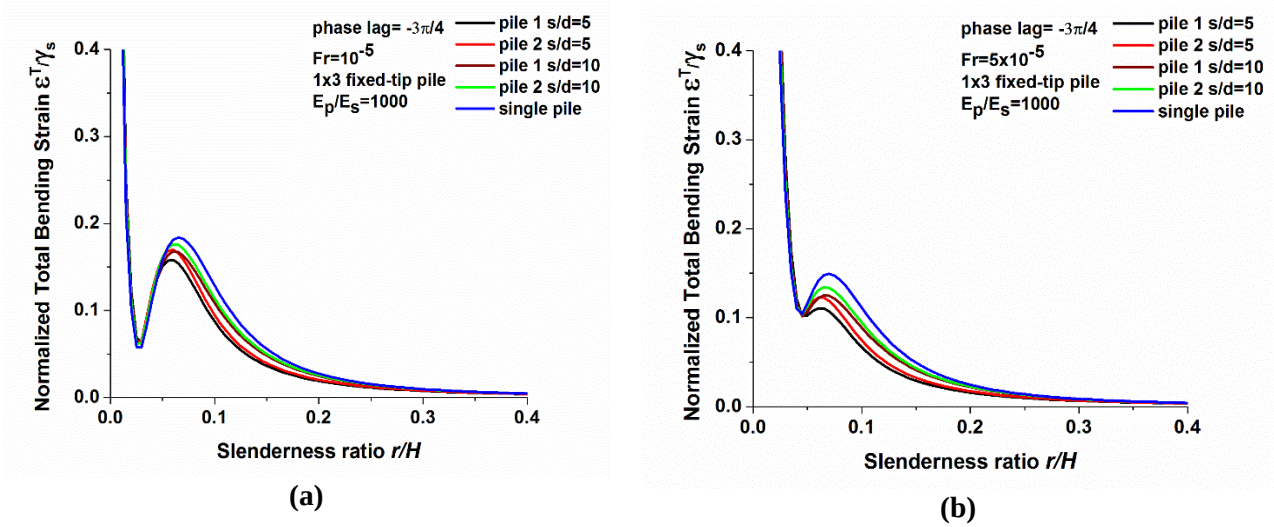


**Figure 5.24:** Normalized total bending strains of 1×3 hinged pile groups with respect to single pile ($\frac{\rho_p}{\rho_s} = 1.43,\ \upsilon_s = 0.4\ ,\ \beta_s = 0.05\ ,\frac{E_p}{E_s} = 100, \varphi_r = -\frac{3\pi}{4}$).

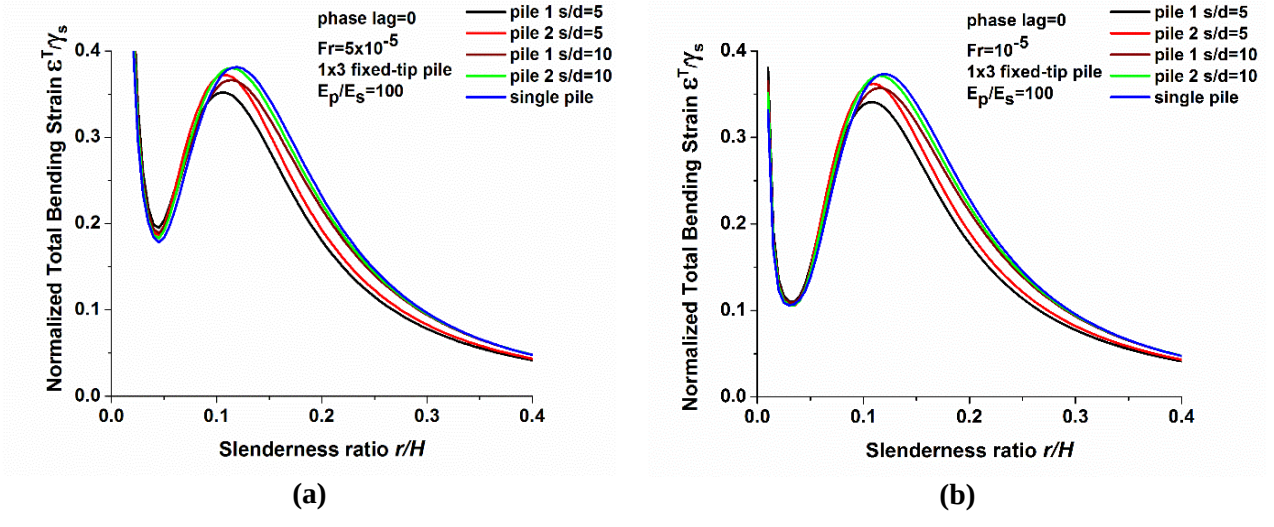


**Figure 5.25:** Normalized total bending strains of 1×3 fixed-tip pile groups with respect to single pile ($\frac{\rho_p}{\rho_s} = 1.43,\ \upsilon_s = 0.4\ ,\ \beta_s = 0.05\ ,\frac{E_p}{E_s} = 100, \varphi_r = 0$).

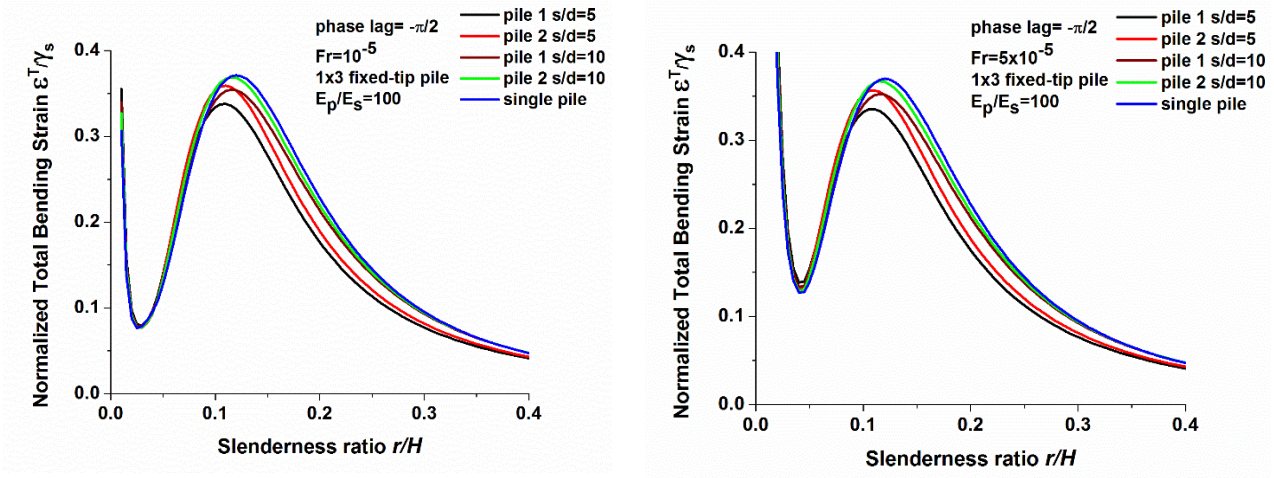


**Figure 5.26:** Normalized total bending strains of 1×3 fixed-tip pile groups with respect to single pile ($\frac{\rho_p}{\rho_s} = 1.43,\ \upsilon_s = 0.4\ ,\ \beta_s = 0.05\ ,\frac{E_p}{E_s} = 100, \varphi_r = -\frac{\pi}{2}$).

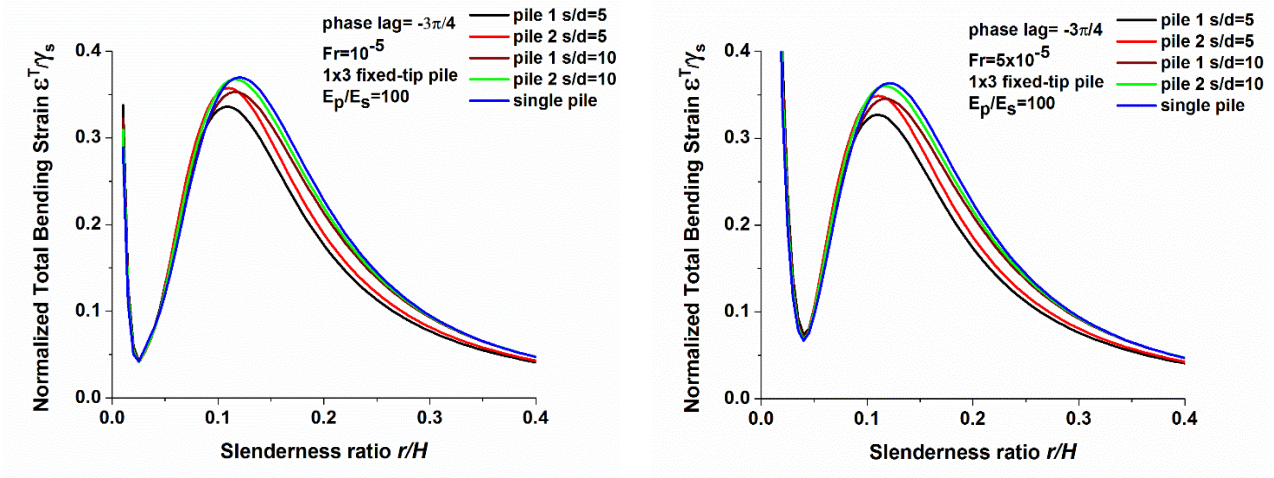


**Figure 5.27:** Normalized total bending strains of 1×3 fixed-tip pile groups with respect to single pile ($\frac{\rho_p}{\rho_s} = 1.43,\ \upsilon_s = 0.4\ ,\ \beta_s = 0.05\ ,\frac{E_p}{E_s} = 100, \varphi_r = -\frac{3\pi}{4}$).

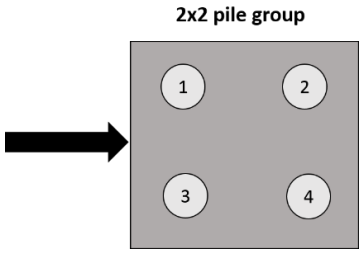


**Figure 5.28:** Depiction of 2x2 pile groups.

### 5.5.5 Hinged-tip 2×2 pile groups:

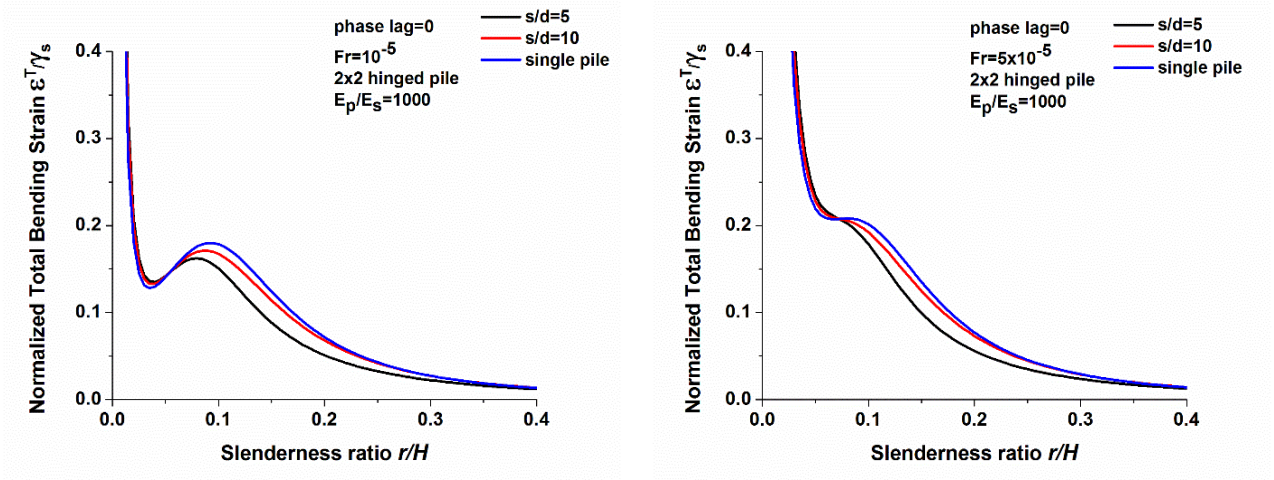


**Figure 5.29:** Normalized total bending strains of 2×2 hinged pile groups with respect to single pile ($\frac{\rho_p}{\rho_s} = 1.43,\ \upsilon_s = 0.4\ ,\ \beta_s = 0.05\ , \frac{E_p}{E_s} = 1000, \varphi_r = 0$).

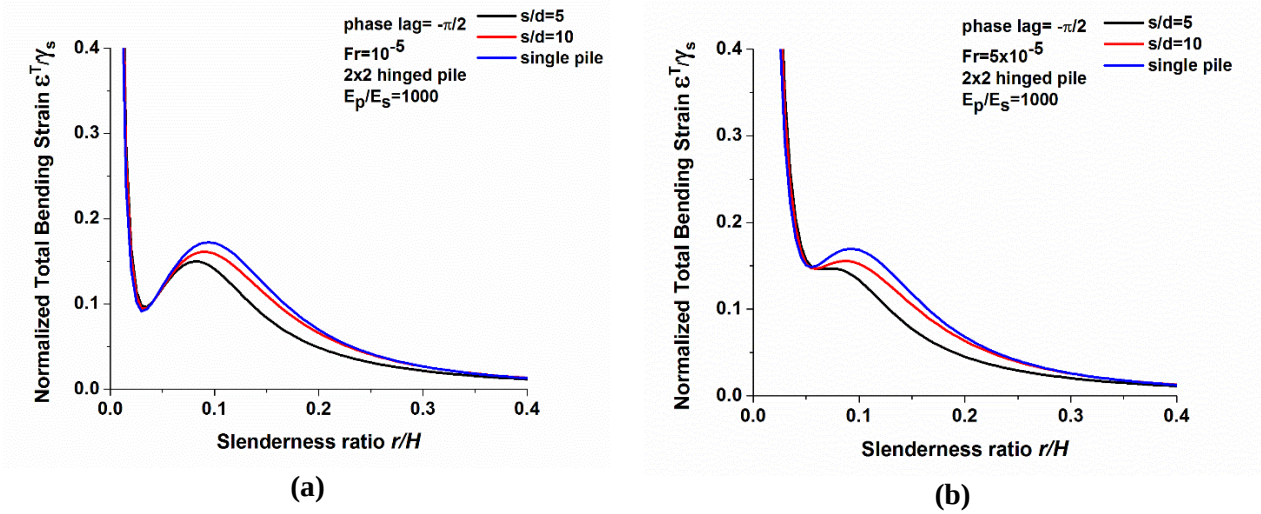


**Figure 5.30:** Normalized total bending strains of 2×2 hinged pile groups with respect to single pile ($\frac{\rho_p}{\rho_s} = 1.43,\ \upsilon_s = 0.4\ ,\ \beta_s = 0.05\ , \frac{E_p}{E_s} = 1000, \varphi_r = -\frac{\pi}{2}$).

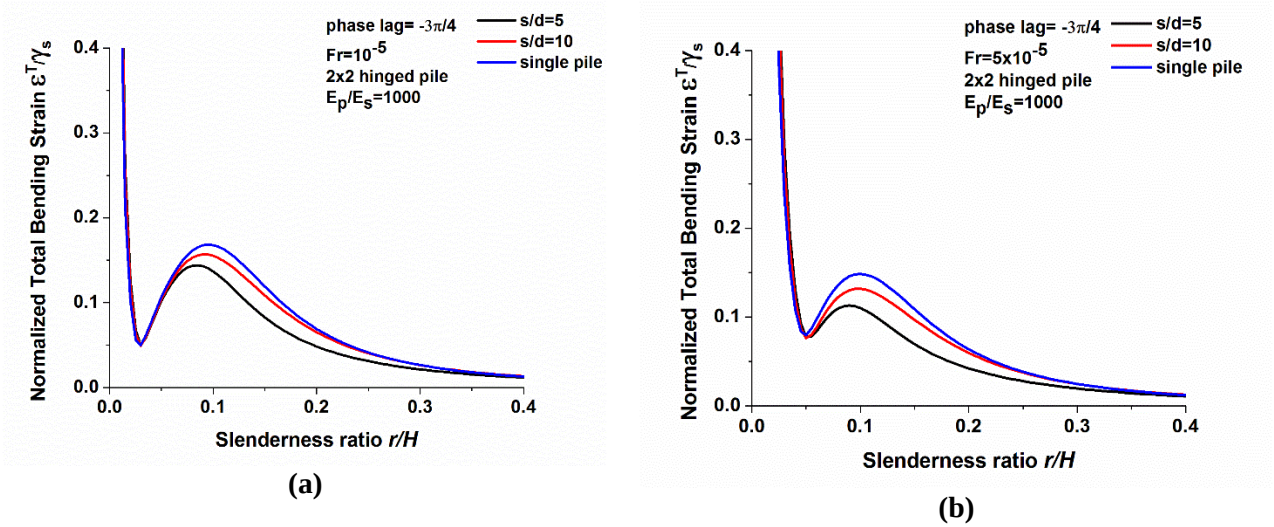


**Figure 5.31:** Normalized total bending strains of 2×2 hinged pile groups with respect to single pile ($\frac{\rho_p}{\rho_s} = 1.43,\ \upsilon_s = 0.4\ ,\ \beta_s = 0.05\ ,\frac{E_p}{E_s} = 1000, \varphi_r = -\frac{3\pi}{4}$).

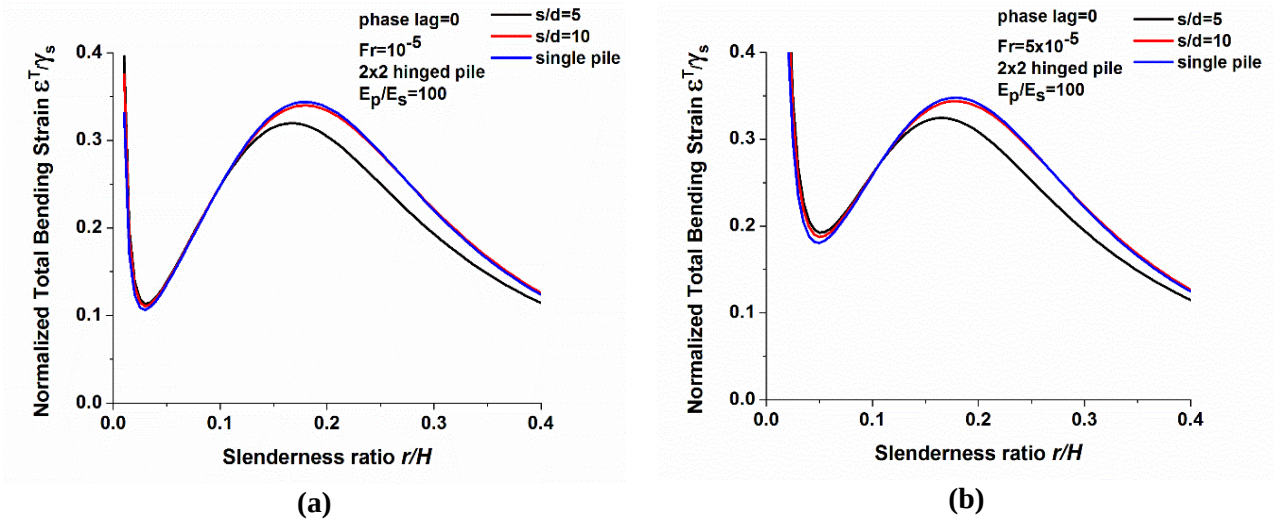


**Figure 5.32:** Normalized total bending strains of 2×2 hinged pile groups with respect to single pile ($\frac{\rho_p}{\rho_s} = 1.43,\ \upsilon_s = 0.4\ ,\ \beta_s = 0.05\ ,\frac{E_p}{E_s} = 100, \varphi_r = 0$).

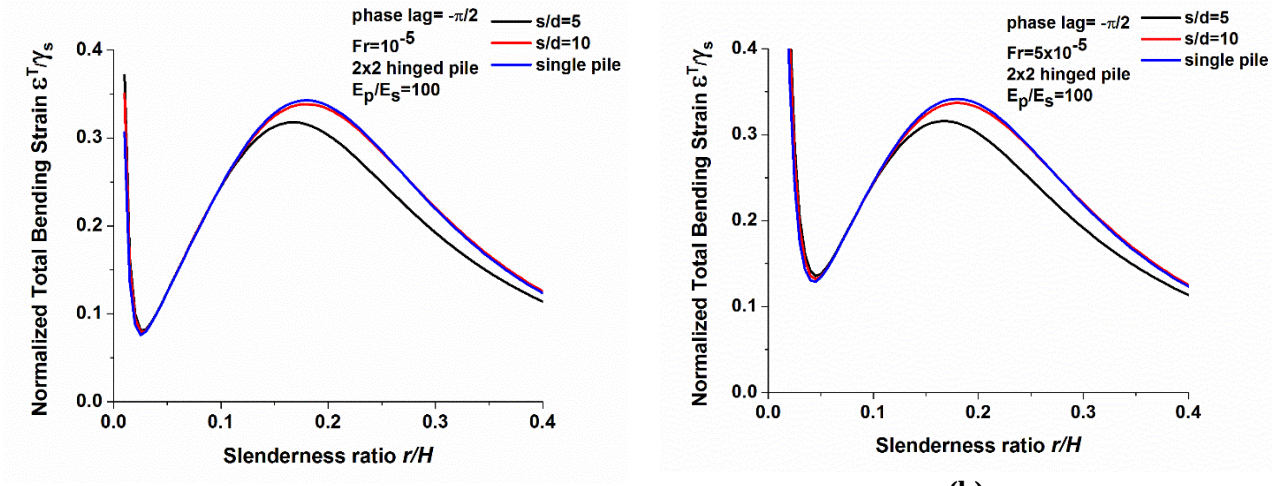


**Figure 5.33:** Normalized total bending strains of 2×2 hinged pile groups with respect to single pile ($\frac{\rho_p}{\rho_s} = 1.43,\ \upsilon_s = 0.4\ ,\ \beta_s = 0.05\ , \frac{E_p}{E_s} = 100, \varphi_r = -\frac{\pi}{2}$).

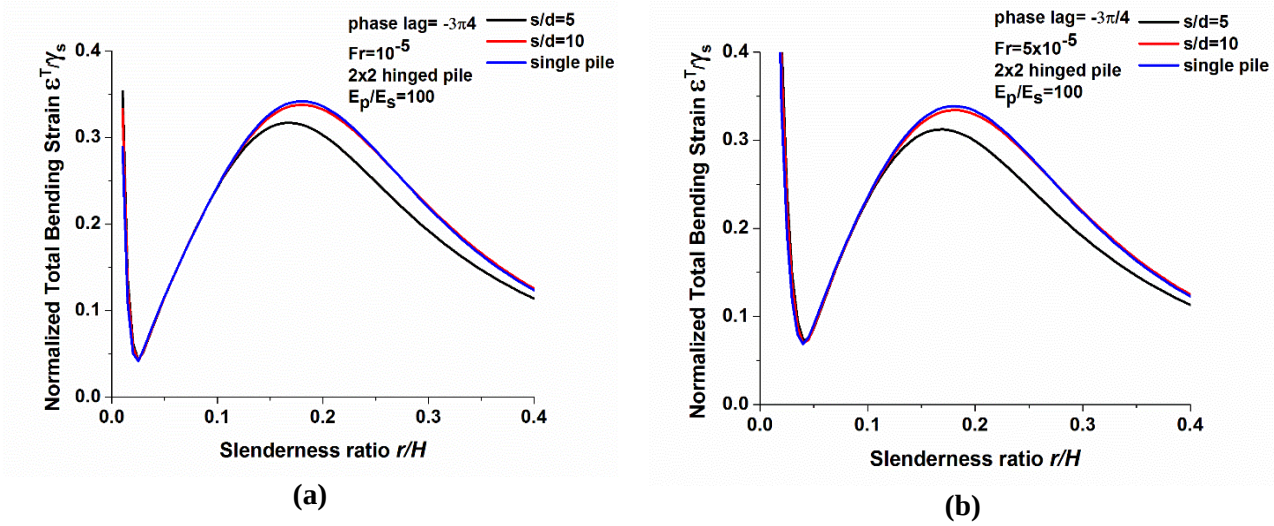


**Figure 5.34:** Normalized total bending strains of 2×2 hinged pile groups with respect to single pile ($\frac{\rho_p}{\rho_s} = 1.43,\ \upsilon_s = 0.4\ ,\ \beta_s = 0.05\ , \frac{E_p}{E_s} = 100, \varphi_r = -\frac{3\pi}{4}$).

### 5.5.6 Fixed-tip 2×2 pile groups:

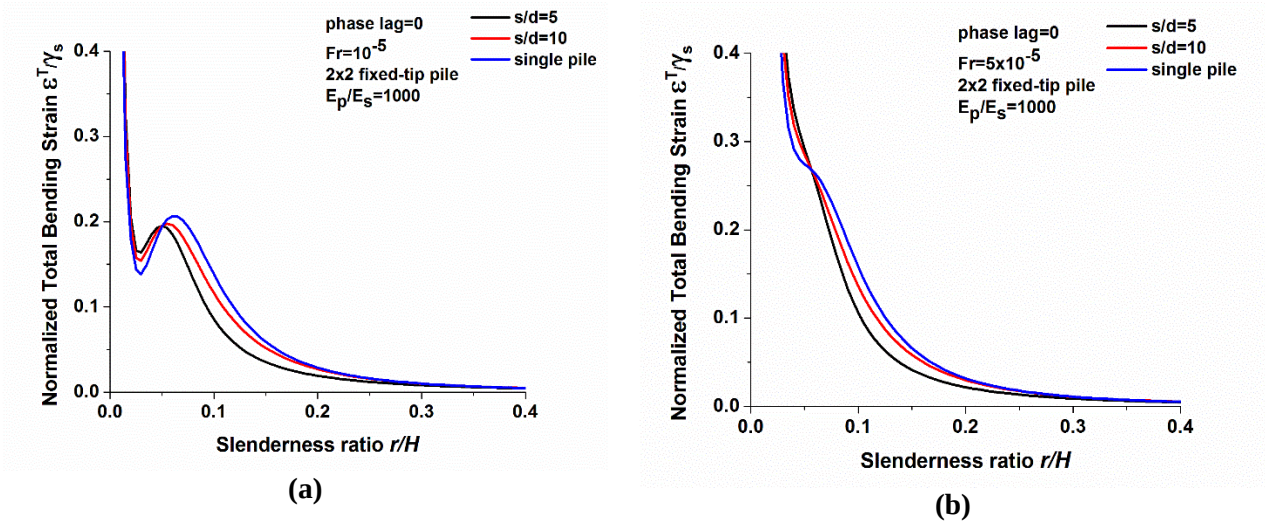


**Figure 5.35:** Normalized total bending strains of 2×2 fixed-tip pile groups with respect to single pile $(\frac{\rho_p}{\rho_s} = 1.43,\ \upsilon_s = 0.4\ ,\ \beta_s = 0.05\ , \frac{E_p}{E_s} = 1000, \varphi_r = 0)$.

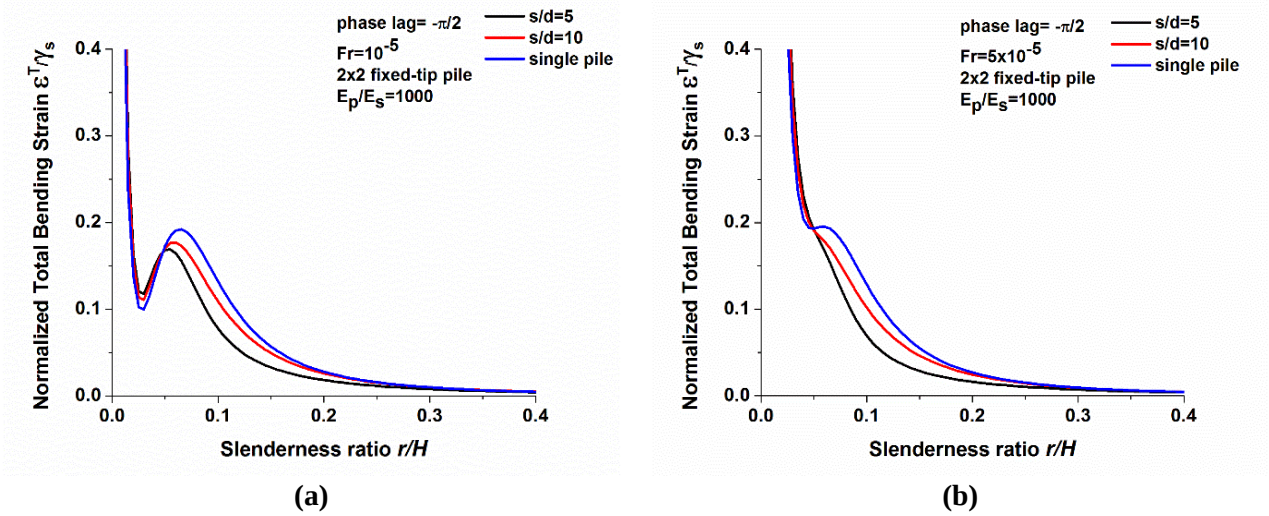


**Figure 5.36:** Normalized total bending strains of 2×2 fixed-tip pile groups with respect to single pile $(\frac{\rho_p}{\rho_s} = 1.43,\ \upsilon_s = 0.4\ ,\ \beta_s = 0.05\ , \frac{E_p}{E_s} = 1000, \varphi_r = -\frac{\pi}{2})$.

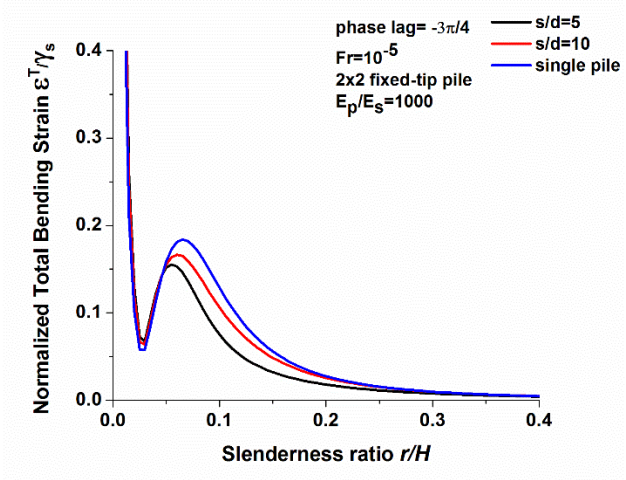


**(a)**

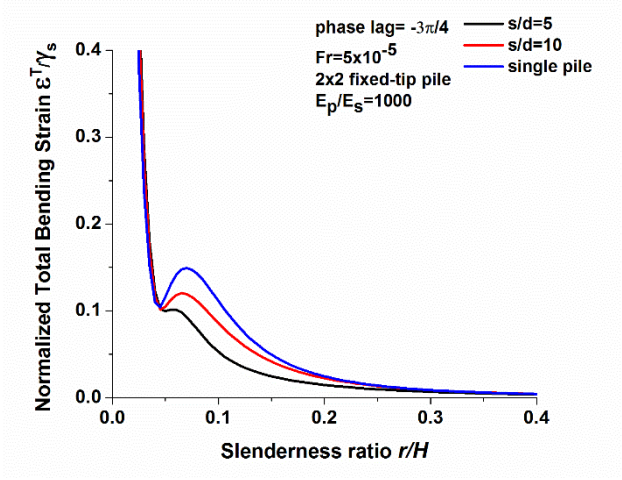


**(b)**

**Figure 5.37:** Normalized total bending strains of 2×2 fixed-tip pile groups with respect to single pile $(\frac{\rho_p}{\rho_s} = 1.43,\ \upsilon_s = 0.4\ ,\ \beta_s = 0.05\ ,\frac{E_p}{E_s} = 1000, \varphi_r = -\frac{3\pi}{4})$.

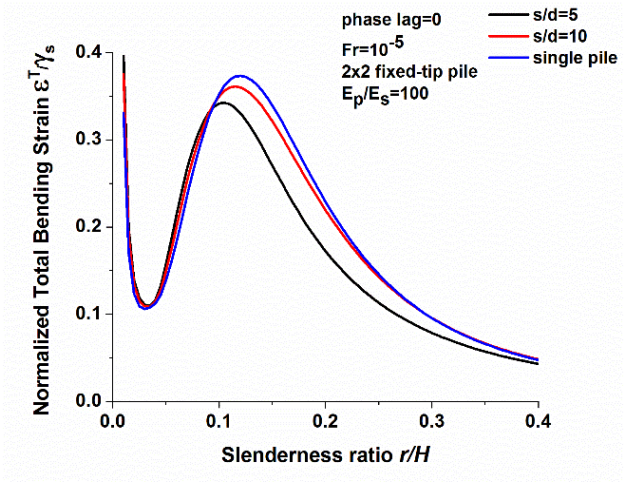


**(a)**

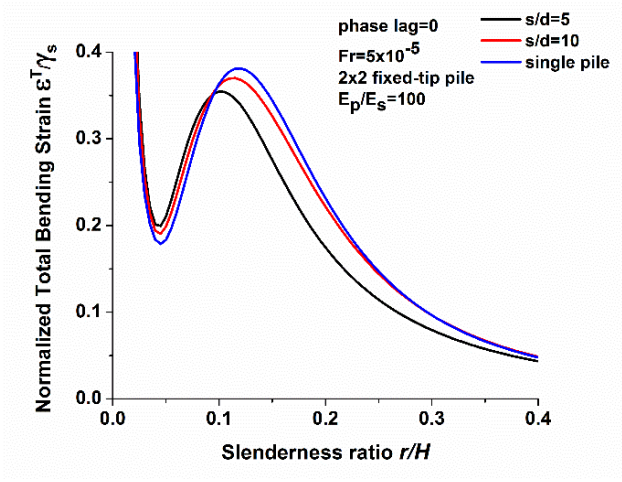


**(b)**

**Figure 5.38:** Normalized total bending strains of 2×2 fixed-tip pile groups with respect to single pile $(\frac{\rho_p}{\rho_s} = 1.43,\ \upsilon_s = 0.4\ ,\ \beta_s = 0.05\ ,\frac{E_p}{E_s} = 100, \varphi_r = 0)$.

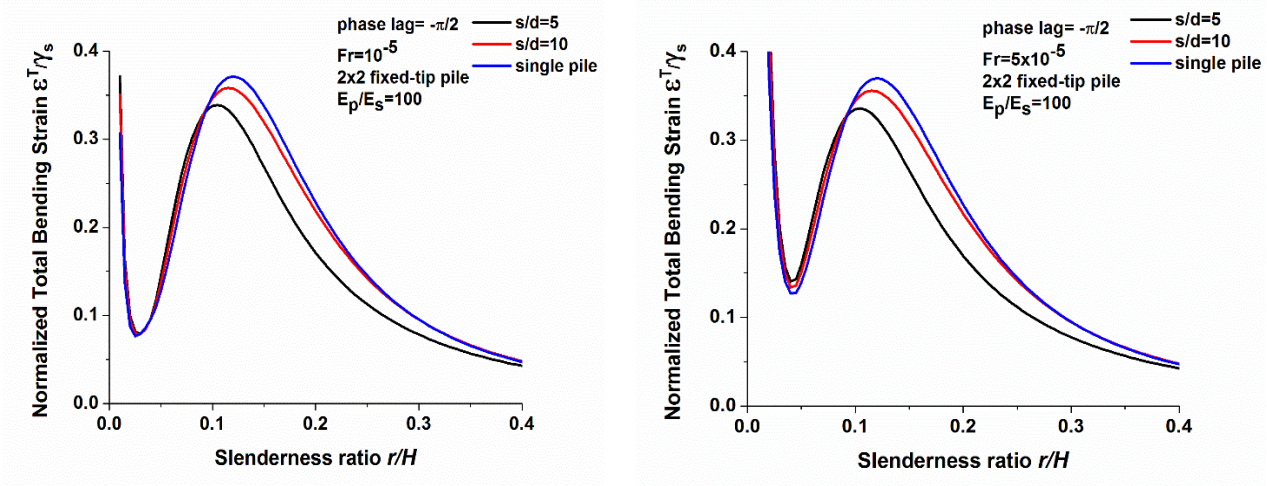


**Figure 5.39:** Normalized total bending strains of 2×2 fixed-tip pile groups with respect to single pile ($\frac{\rho_p}{\rho_s} = 1.43,\ \upsilon_s = 0.4\ ,\ \beta_s = 0.05\ , \frac{E_p}{E_s} = 100, \varphi_r = -\frac{\pi}{2}$).

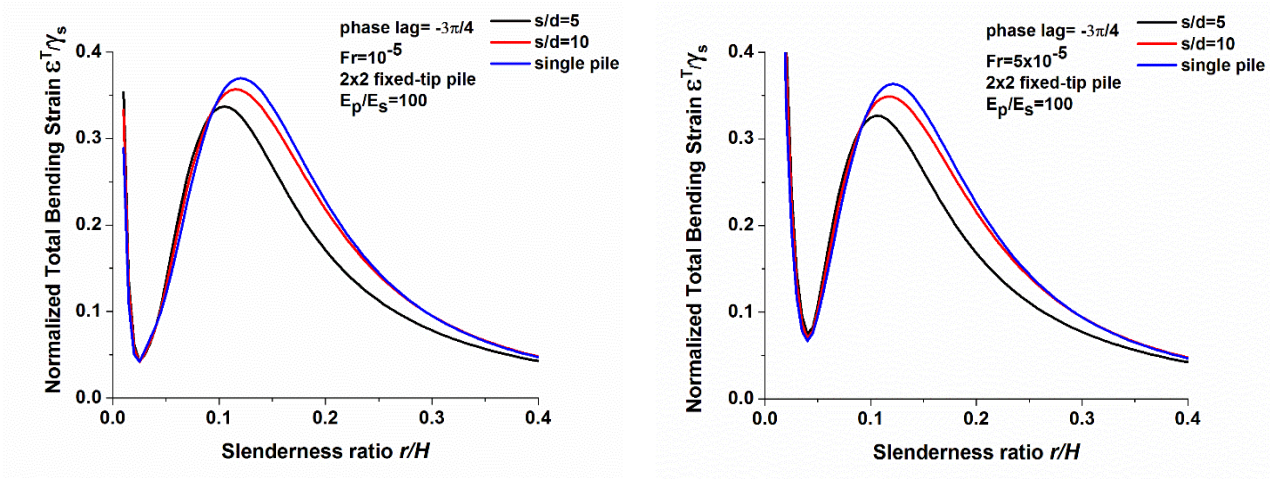


**Figure 5.40:** Normalized total bending strains of 2×2 fixed-tip pile groups with respect to single pile ($\frac{\rho_p}{\rho_s} = 1.43,\ \upsilon_s = 0.4\ ,\ \beta_s = 0.05\ , \frac{E_p}{E_s} = 100, \varphi_r = -\frac{3\pi}{4}$).

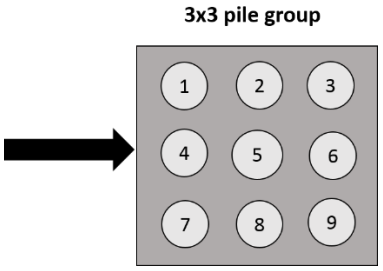


**Figure 5.41:** Depiction of 3x3 pile groups.

### 5.5.7 Hinged-tip 3×3 pile groups:

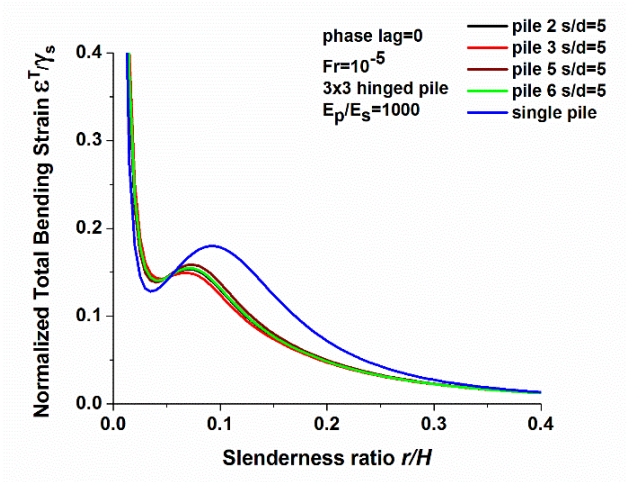


(a)

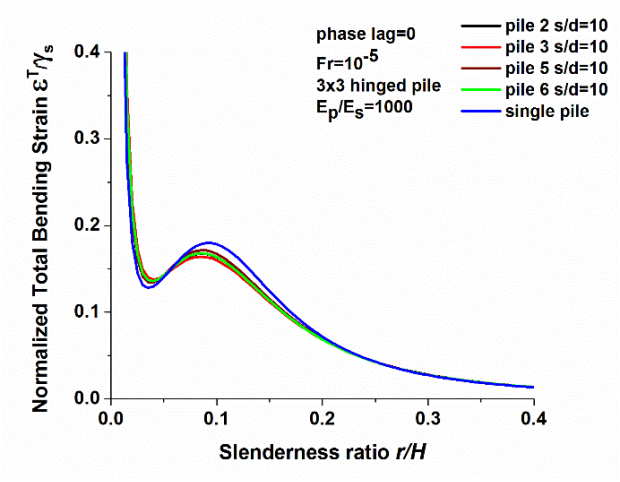


(b)

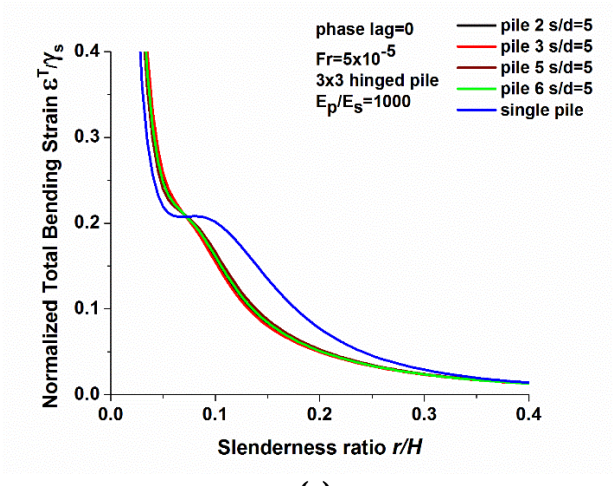


(c)

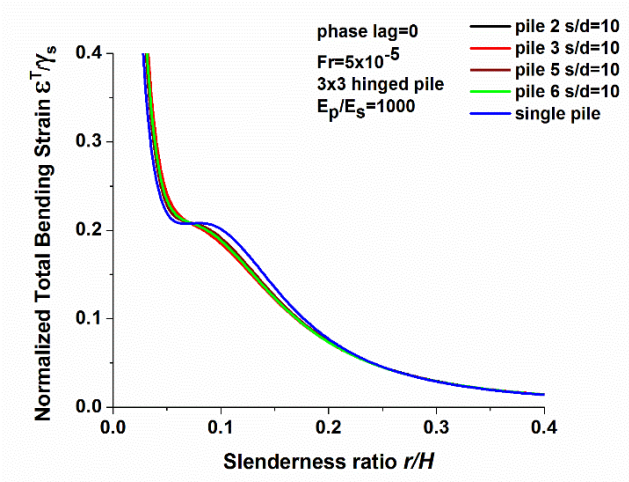


(d)

**Figure 5.42:** Normalized total bending strains of 3×3 hinged pile groups with respect to single pile ($\frac{\rho_p}{\rho_s} = 1.43,\ \upsilon_s = 0.4\ ,\ \beta_s = 0.05\ ,\frac{E_p}{E_s} = 1000, \varphi_r = 0$).

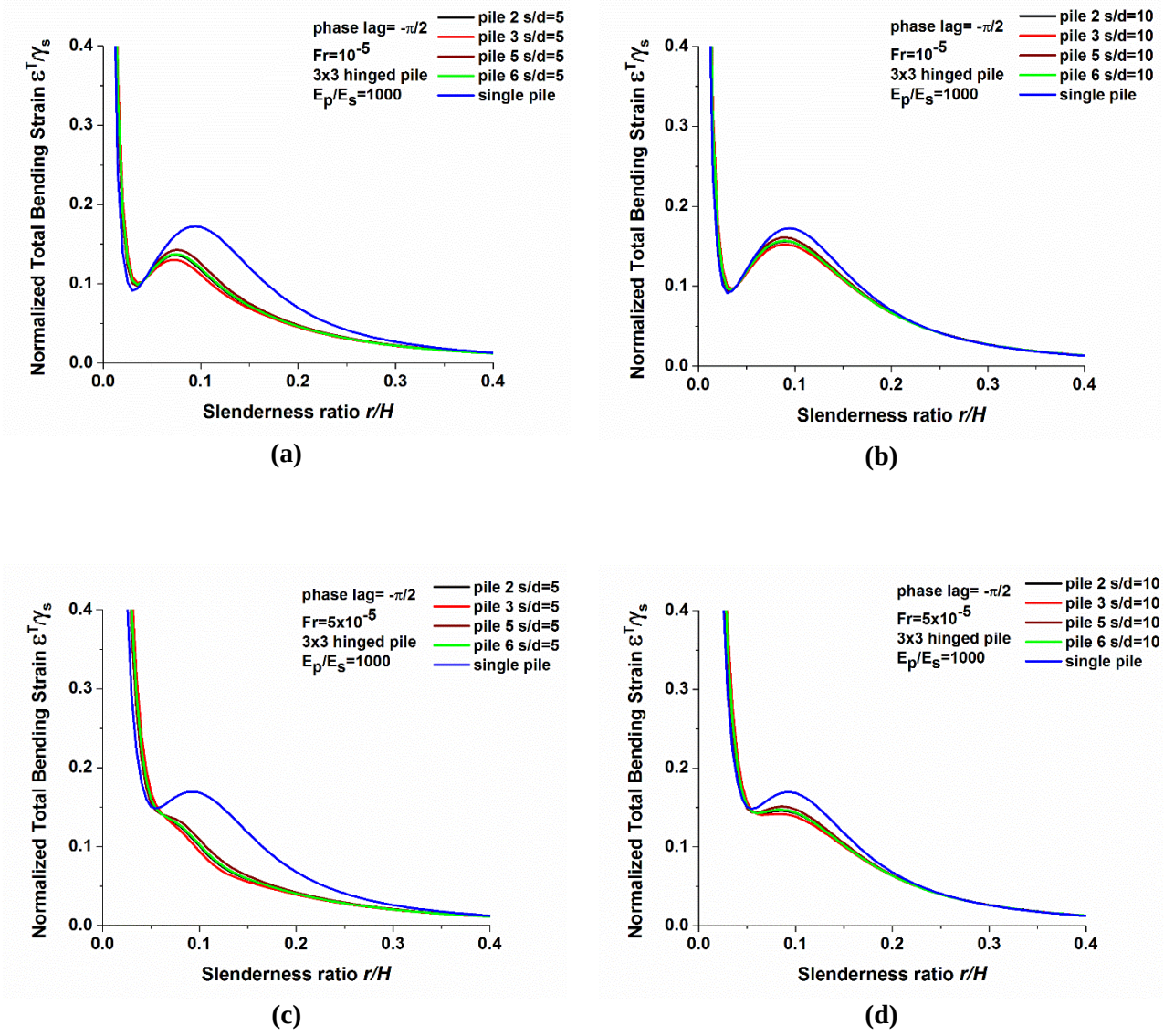


**Figure 5.43:** Normalized total bending strains of 3×3 hinged pile groups with respect to single pile ($\frac{\rho_p}{\rho_s} = 1.43,\ \upsilon_s = 0.4\ ,\ \beta_s = 0.05\ ,\frac{E_p}{E_s} = 1000, \varphi_r = -\frac{\pi}{2}$).

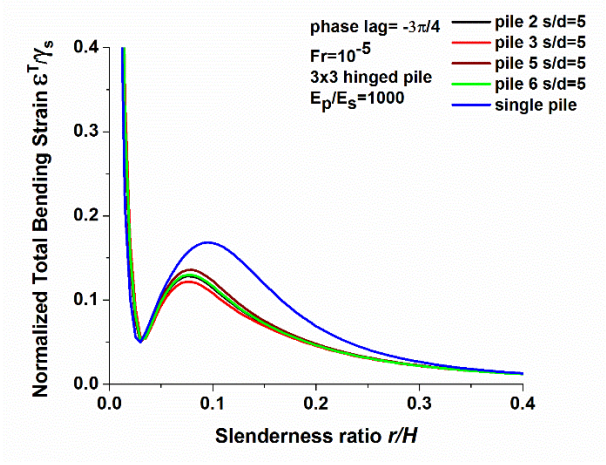


**(a)**

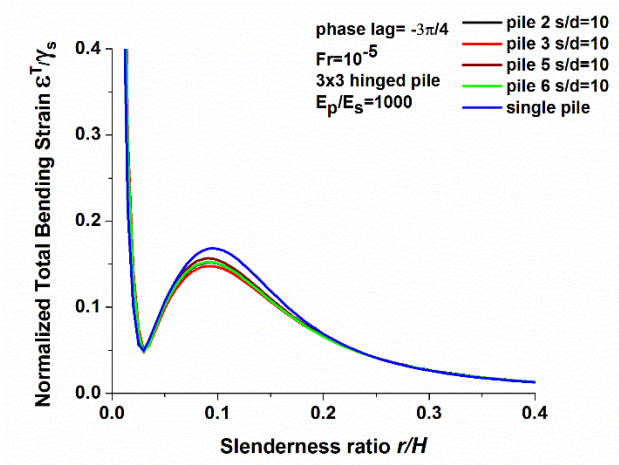


**(b)**

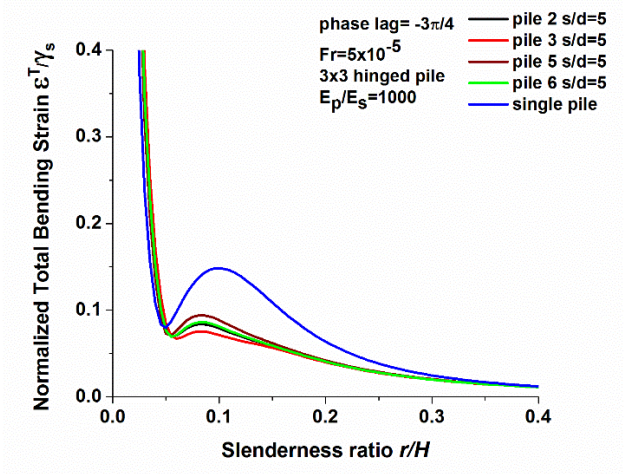


**(c)**

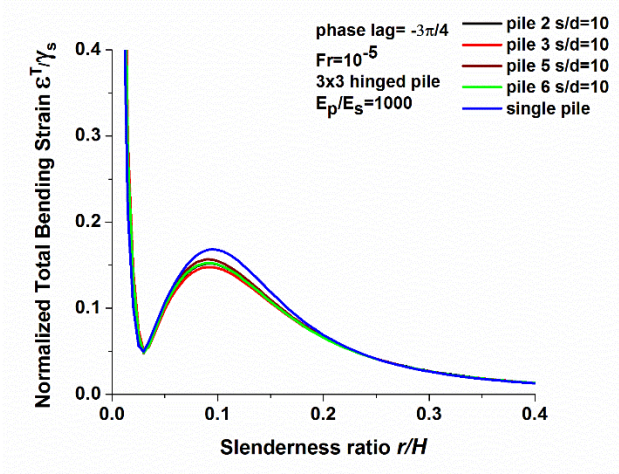


**(d)**

**Figure 5.44:** Normalized total bending strains of 3×3 hinged pile groups with respect to single pile ($\frac{\rho_p}{\rho_s} = 1.43,\ \upsilon_s = 0.4\ ,\ \beta_s = 0.05\ ,\frac{E_p}{E_s} = 1000, \varphi_r = -\frac{3\pi}{4}$).

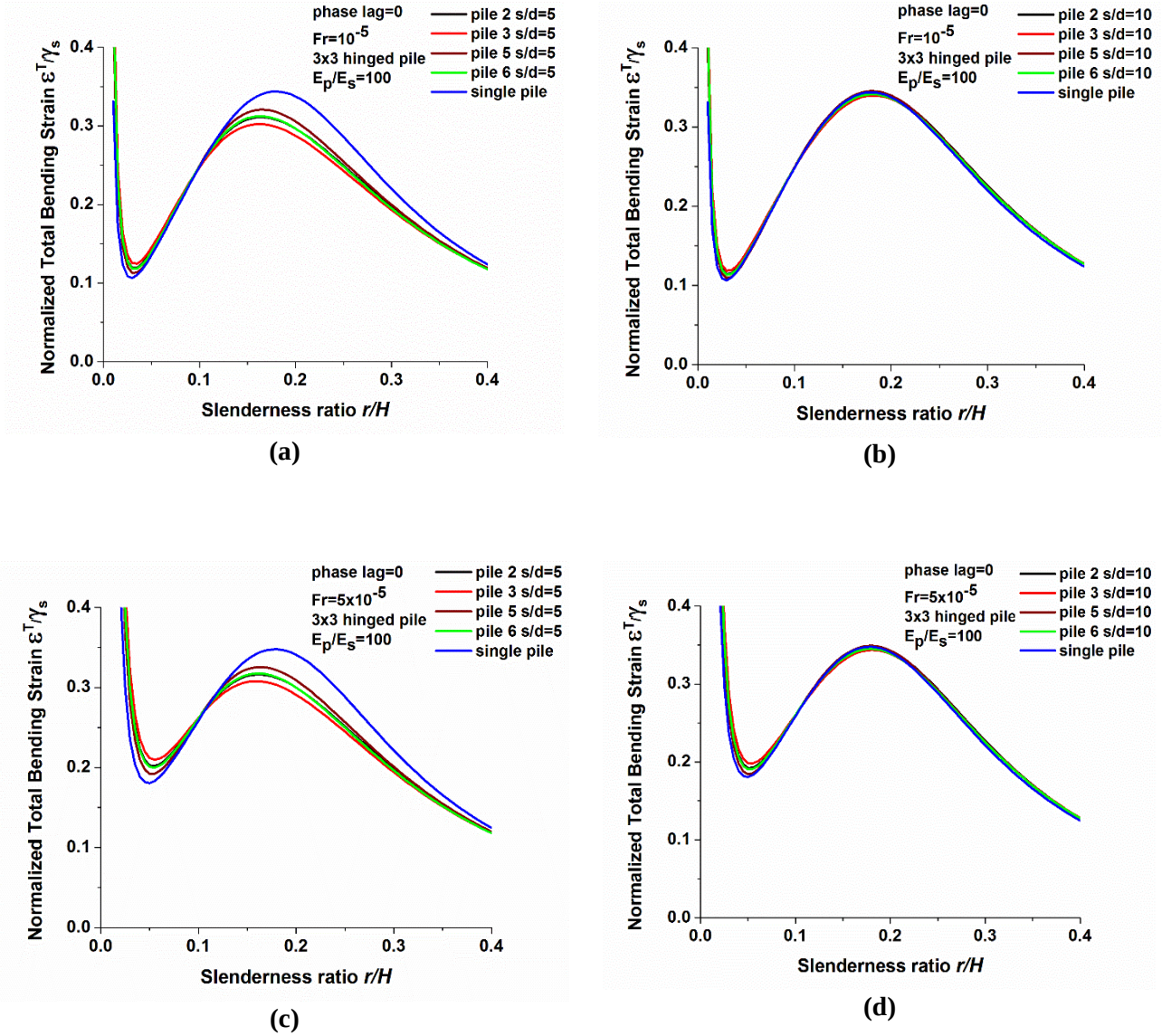


**Figure 5.45:** Normalized total bending strains of 3×3 hinged pile groups with respect to single pile ($\frac{\rho_p}{\rho_s} = 1.43,\ \upsilon_s = 0.4\ ,\ \beta_s = 0.05\ ,\frac{E_p}{E_s} = 100, \varphi_r = 0$).

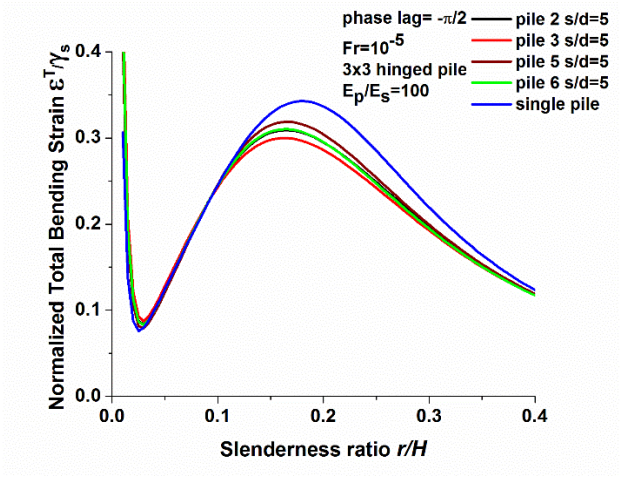


**(a)**

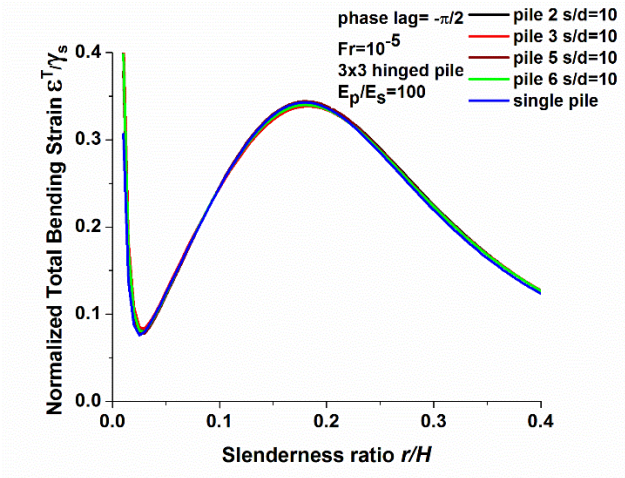


**(b)**

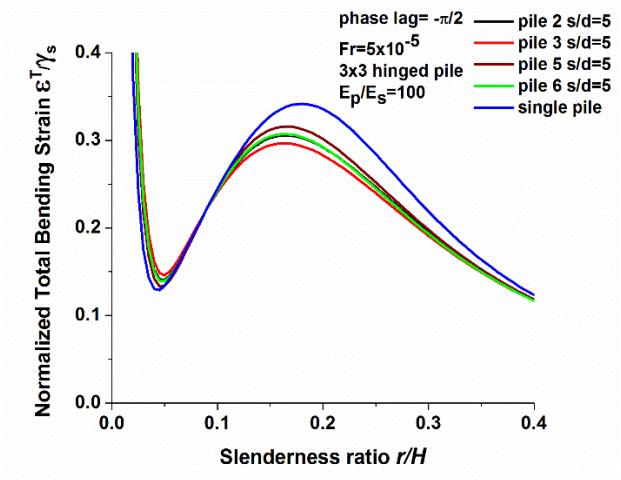


**(c)**

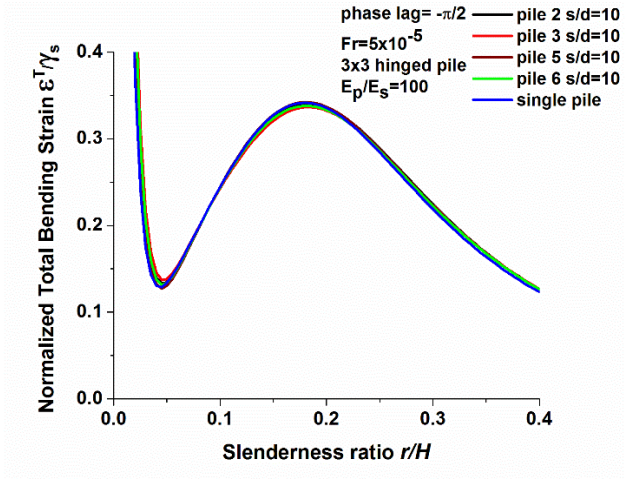


**(d)**

**Figure 5.46:** Normalized total bending strains of 3×3 hinged pile groups with respect to single pile ($\frac{\rho_p}{\rho_s} = 1.43,\ \upsilon_s = 0.4\ ,\ \beta_s = 0.05\ ,\frac{E_p}{E_s} = 100, \varphi_r = -\frac{\pi}{2}$).

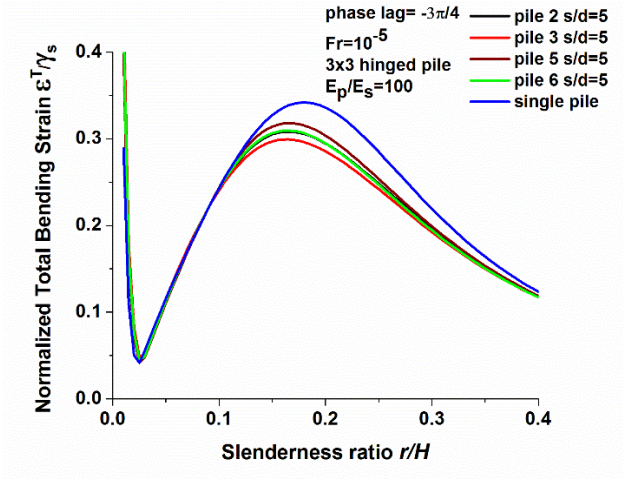


**(a)**

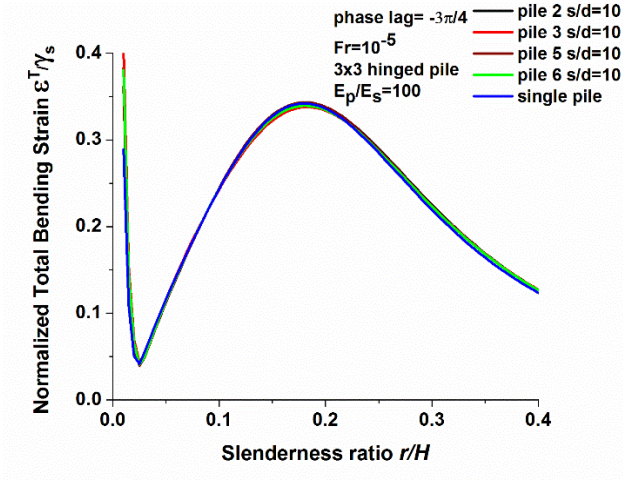


**(b)**

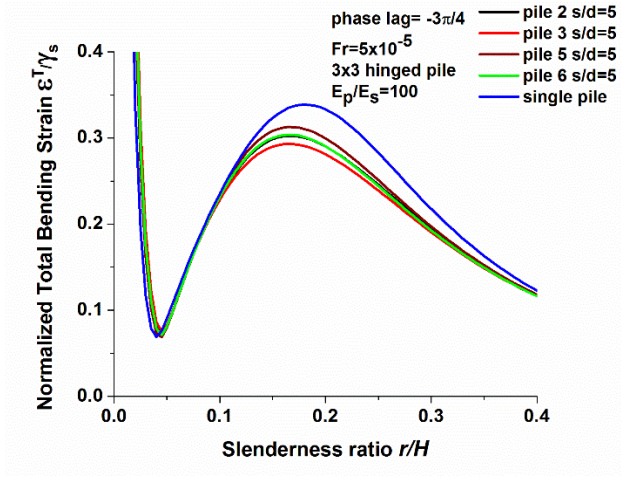


**(c)**

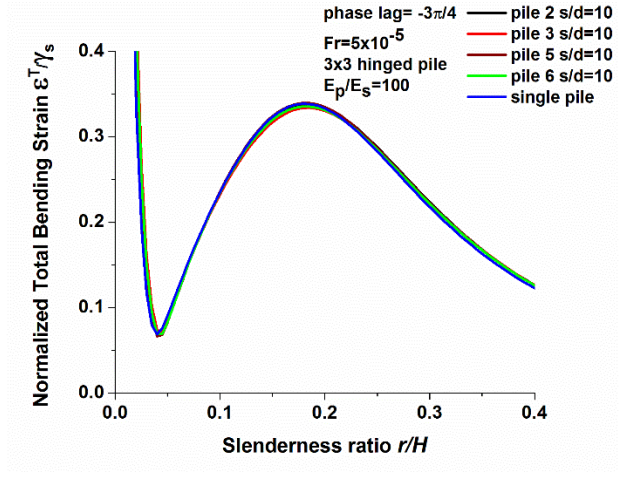


**(d)**

**Figure 5.47:** Normalized total bending strains of 3×3 hinged pile groups with respect to single pile ($\frac{\rho_p}{\rho_s} = 1.43,\ \upsilon_s = 0.4\ ,\ \beta_s = 0.05\ ,\frac{E_p}{E_s} = 100, \varphi_r = -\frac{3\pi}{4}$).

### 5.5.8 Fixed-tip 3×3 pile groups:

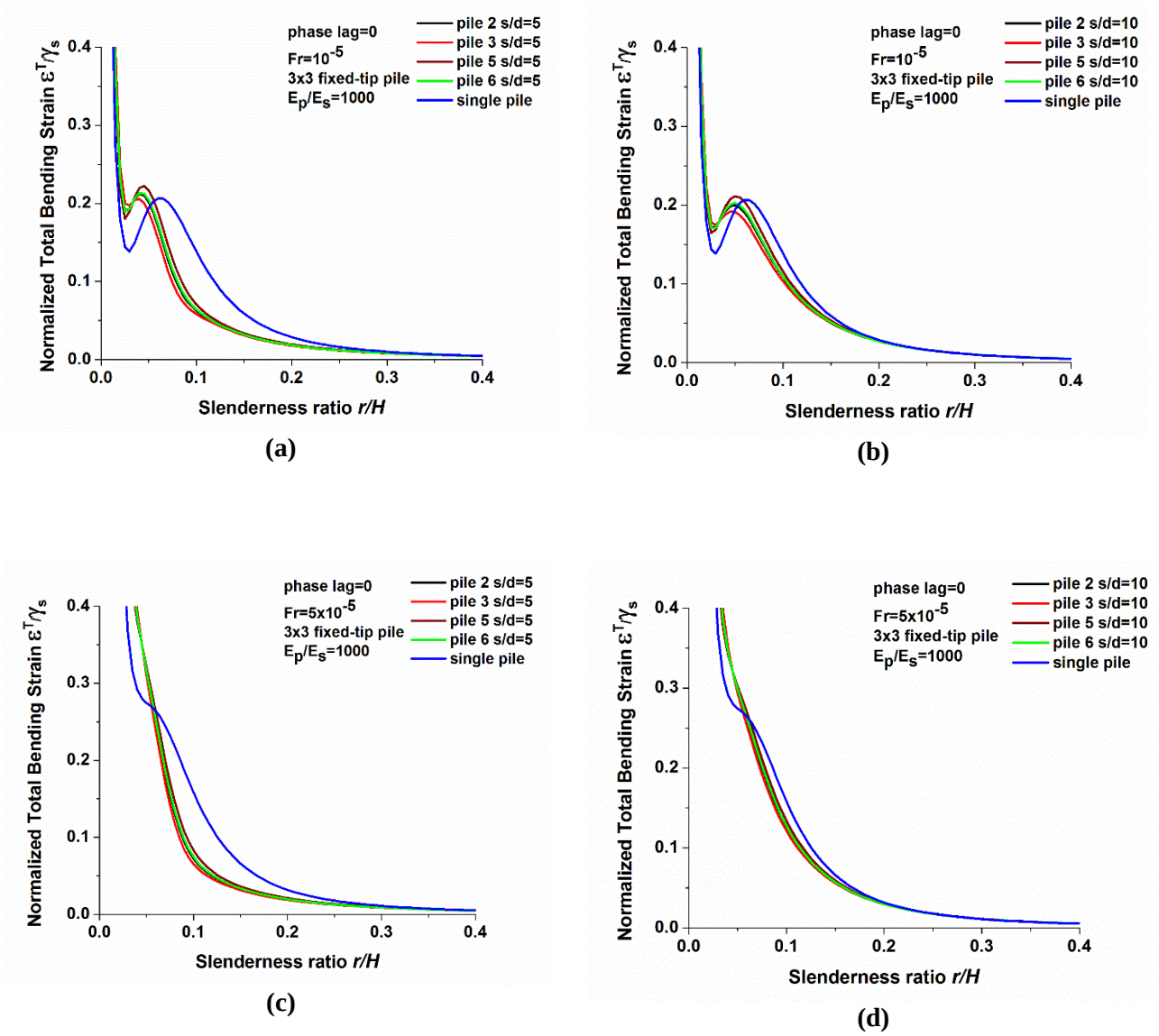


**Figure 5.48:** Normalized total bending strains of 3×3 fixed-tip pile groups with respect to single pile ($\frac{\rho_p}{\rho_s} = 1.43,\ \upsilon_s = 0.4\ ,\ \beta_s = 0.05\ ,\frac{E_p}{E_s} = 1000, \varphi_r = 0$).

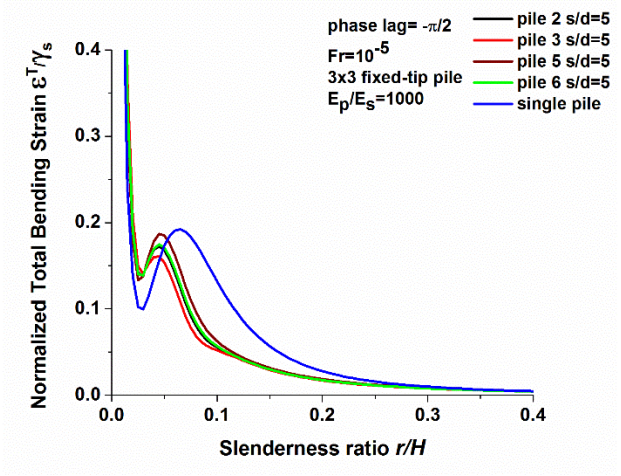


**(a)**

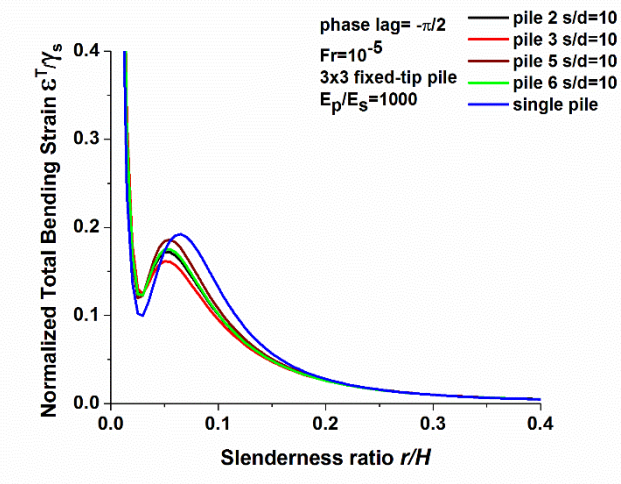


**(b)**

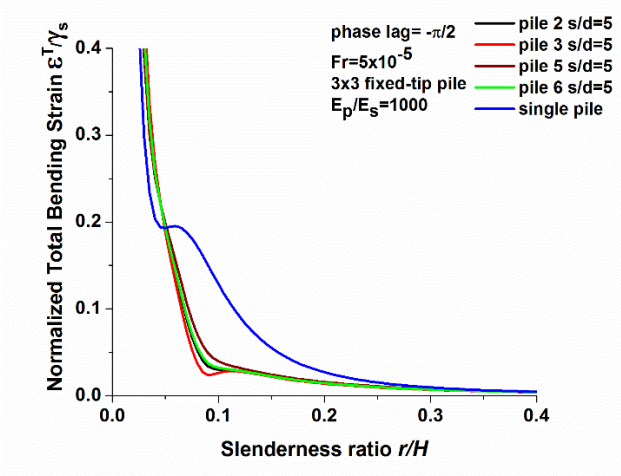


**(c)**

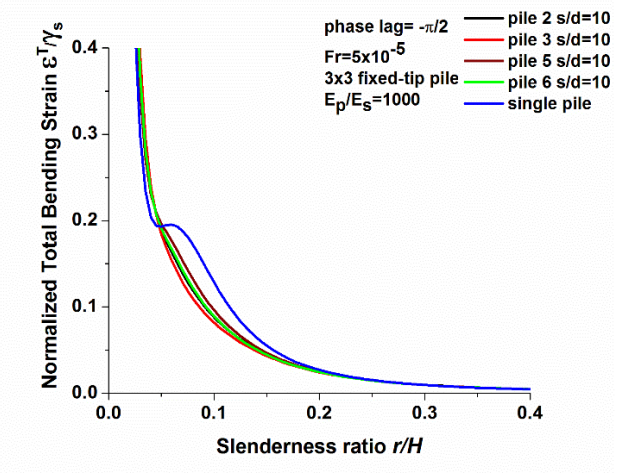


**(d)**

**Figure 5.49:** Normalized total bending strains of 3×3 fixed-tip pile groups with respect to single pile ($\frac{\rho_p}{\rho_s} = 1.43,\ \upsilon_s = 0.4\ ,\ \beta_s = 0.05\ ,\frac{E_p}{E_s} = 1000, \varphi_r = -\frac{\pi}{2}$).

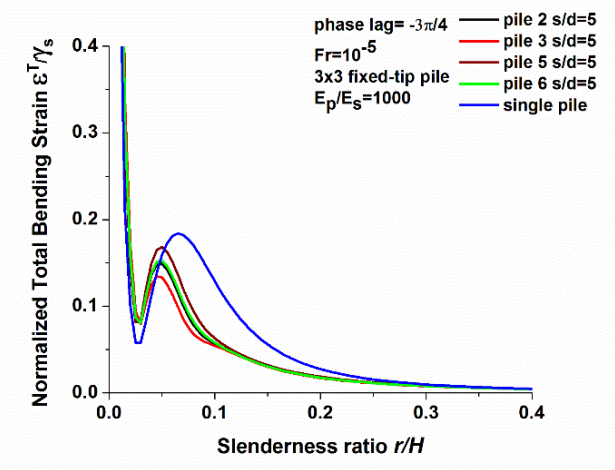


**(a)**

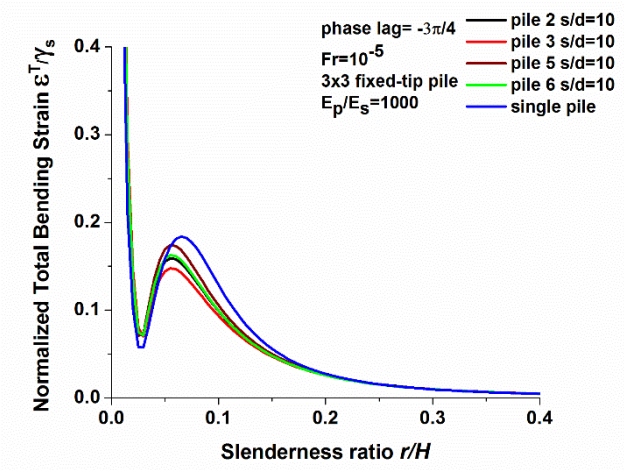


**(b)**

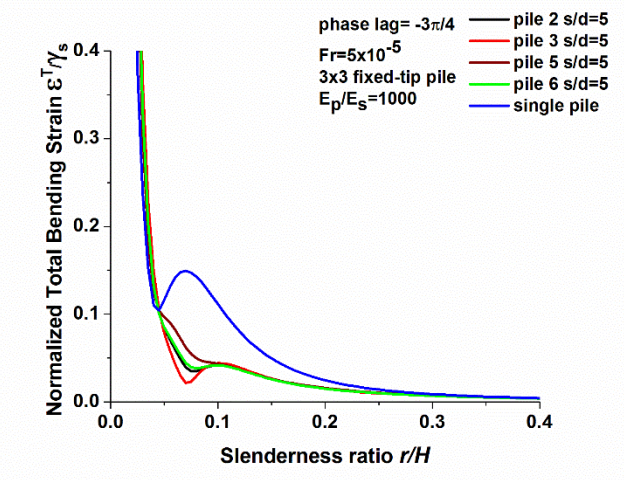


**(c)**

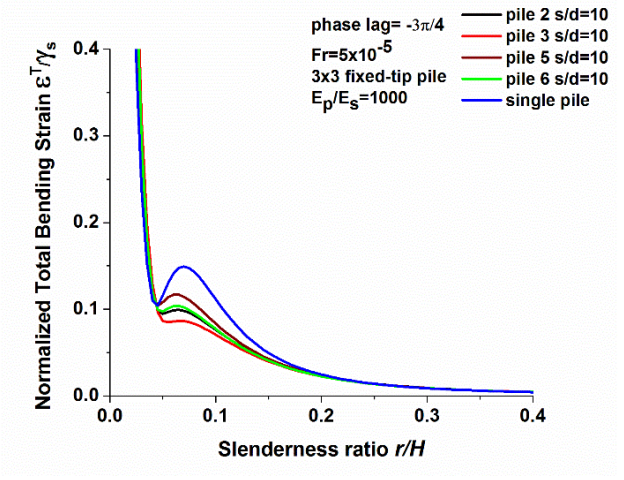


**(d)**

**Figure 5.50:** Normalized total bending strains of 3×3 fixed-tip pile groups with respect to single pile ($\frac{\rho_p}{\rho_s} = 1.43,\ \upsilon_s = 0.4\ ,\ \beta_s = 0.05\ ,\frac{E_p}{E_s} = 1000, \varphi_r = -\frac{3\pi}{4}$).

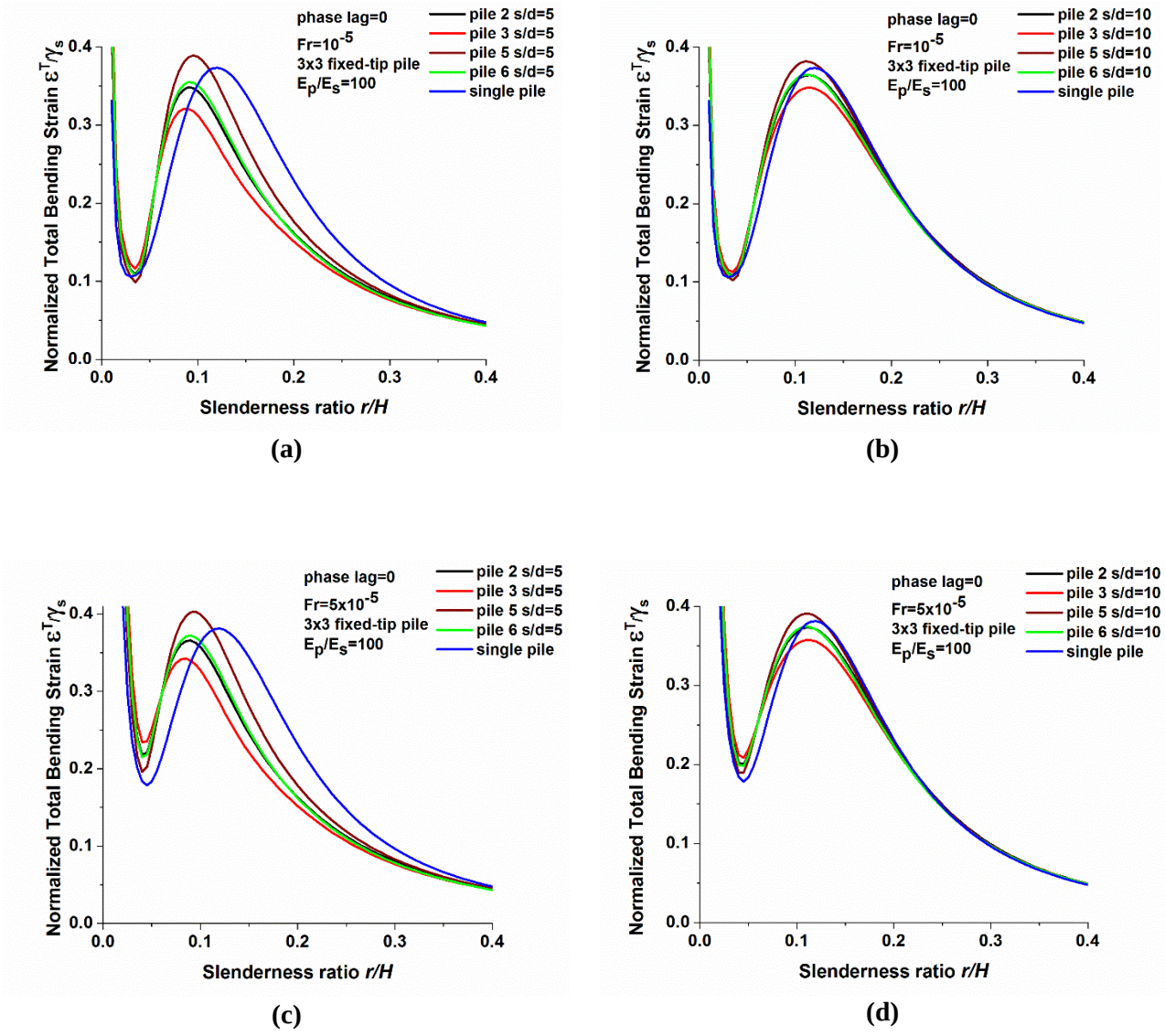


**Figure 5.51:** Normalized total bending strains of 3×3 fixed-tip pile groups with respect to single pile ($\frac{\rho_p}{\rho_s} = 1.43,\ \upsilon_s = 0.4\ ,\ \beta_s = 0.05\ ,\frac{E_p}{E_s} = 100, \varphi_r = 0$).

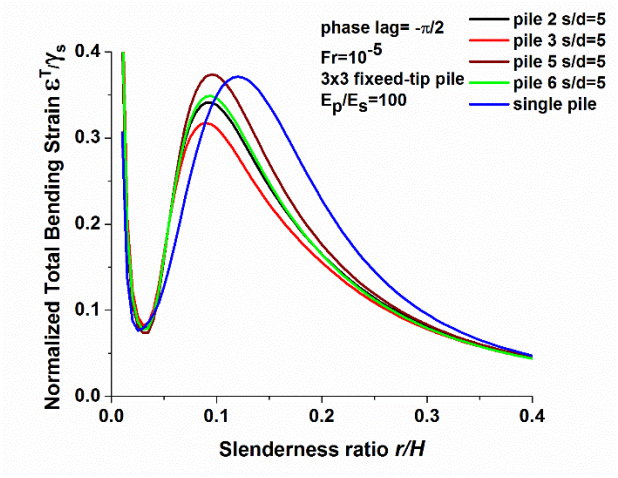


**(a)**

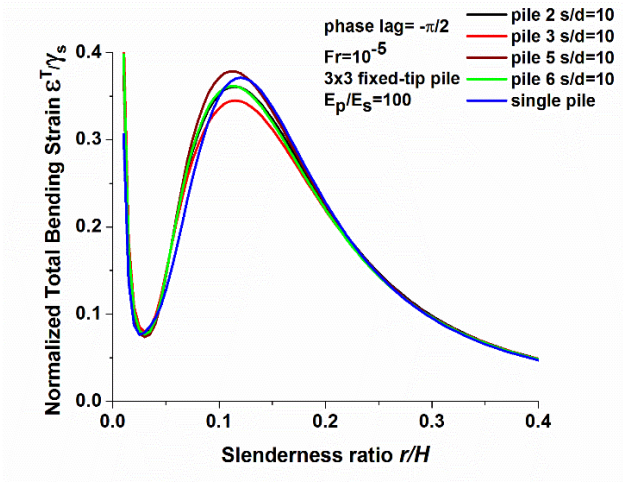


**(b)**

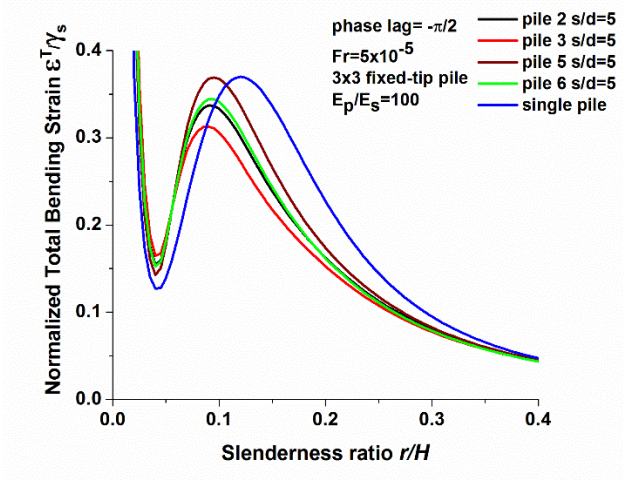


**(c)**

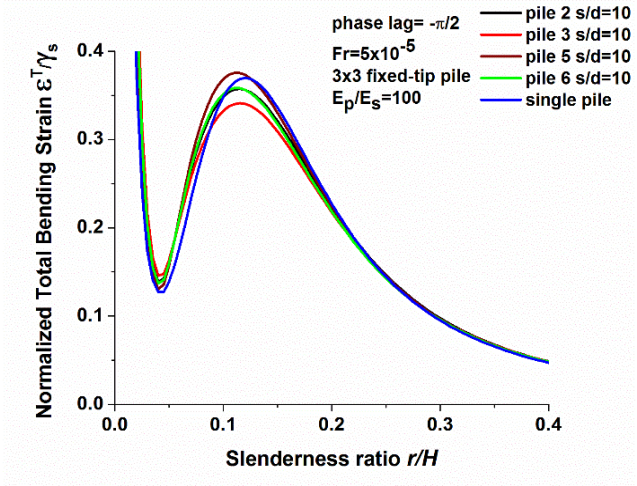


**(d)**

**Figure 5.52:** Normalized total bending strains of 3×3 fixed-tip pile groups with respect to single pile ($\frac{\rho_p}{\rho_s} = 1.43,\ \upsilon_s = 0.4\ ,\ \beta_s = 0.05\ , \frac{E_p}{E_s} = 100, \varphi_r = -\frac{\pi}{2}$).

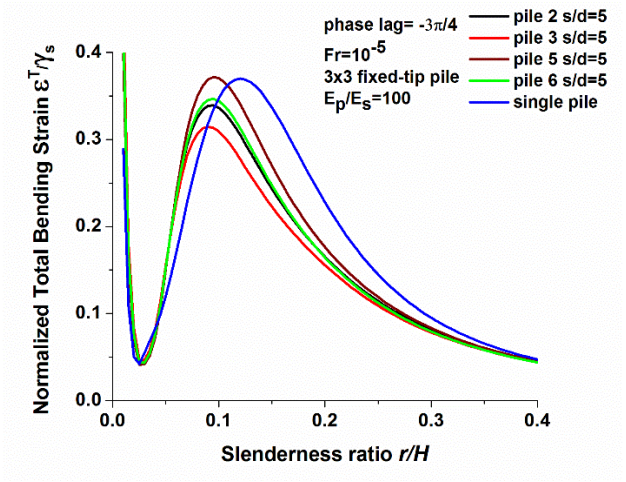


**(a)**

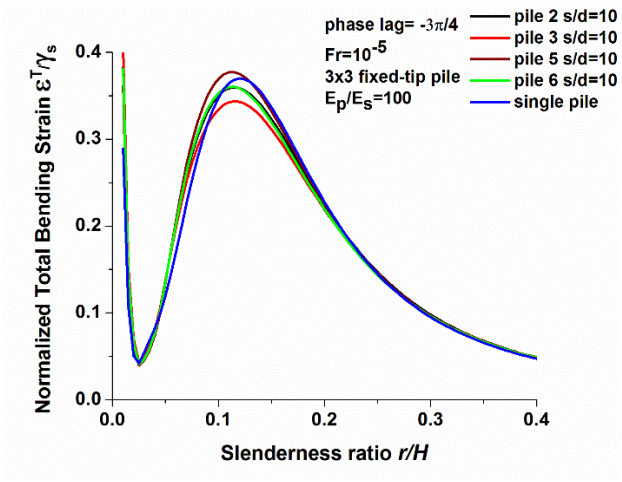


**(b)**

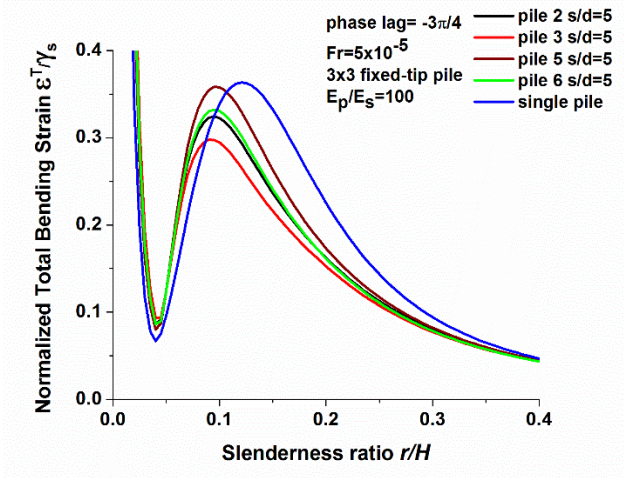


**(c)**

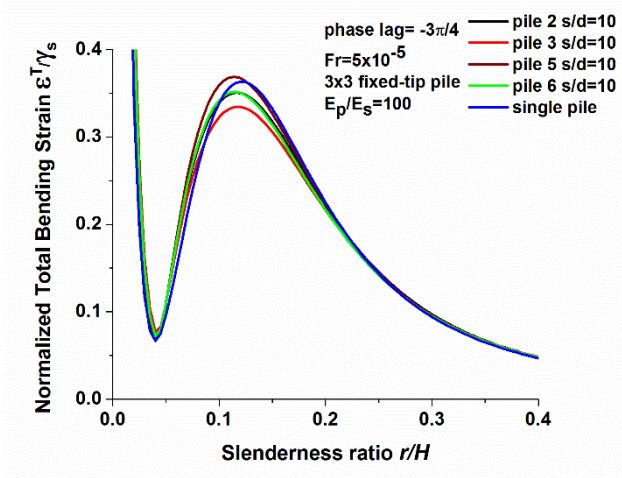


**(d)**

**Figure 5.53:** Normalized total bending strains of 3×3 fixed-tip pile groups with respect to single pile ($\frac{\rho_p}{\rho_s} = 1.43,\ \upsilon_s = 0.4\ ,\ \beta_s = 0.05\ ,\frac{E_p}{E_s} = 100, \varphi_r = -\frac{3\pi}{4}$).

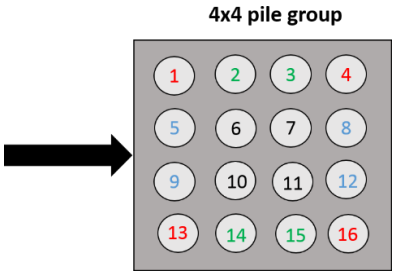


**Figure 5.54:** Depiction of 4x4 pile groups.

### 5.5.9 Hinged-tip 4×4 pile groups:

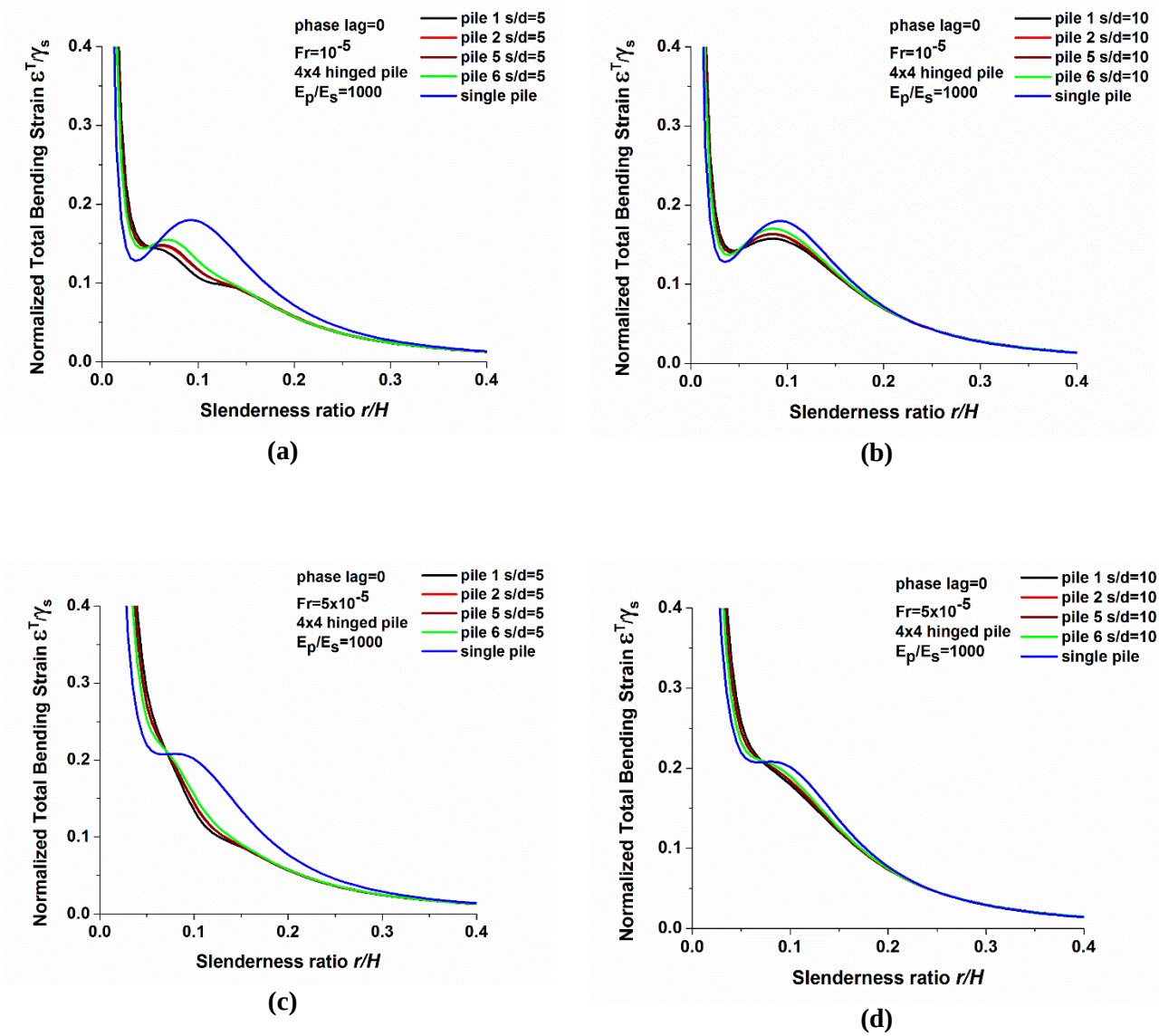


**Figure 5.55:** Normalized total bending strains of 4×4 hinged pile groups with respect to single pile ($\frac{\rho_p}{\rho_s} = 1.43,\ \upsilon_s = 0.4\ ,\ \beta_s = 0.05\ , \frac{E_p}{E_s} = 1000, \varphi_r = 0$).

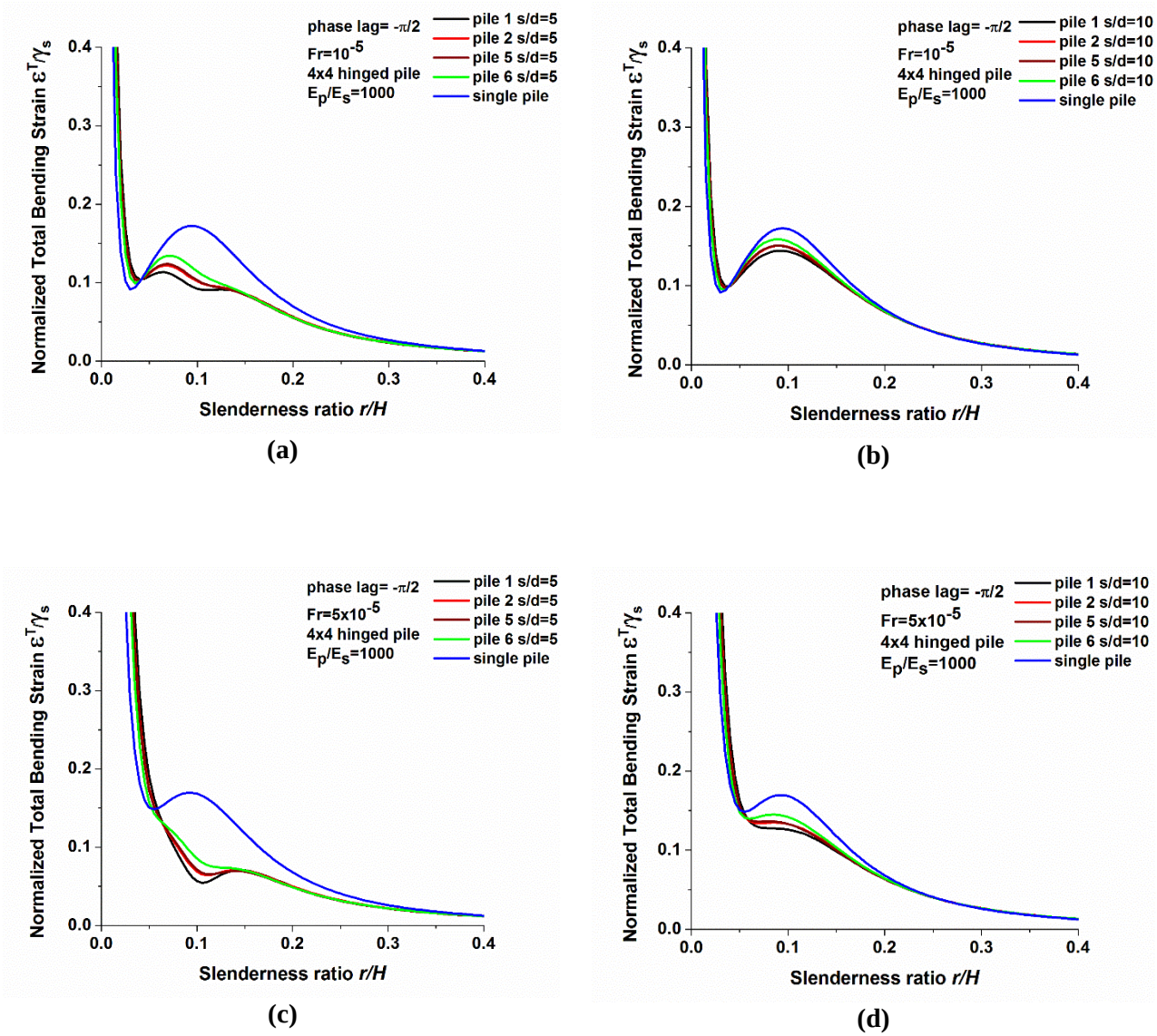


**Figure 5.56:** Normalized total bending strains of 4×4 hinged pile groups with respect to single pile ($\frac{\rho_p}{\rho_s} = 1.43,\ \upsilon_s = 0.4\ ,\ \beta_s = 0.05\ ,\frac{E_p}{E_s} = 1000, \varphi_r = -\frac{\pi}{2}$).

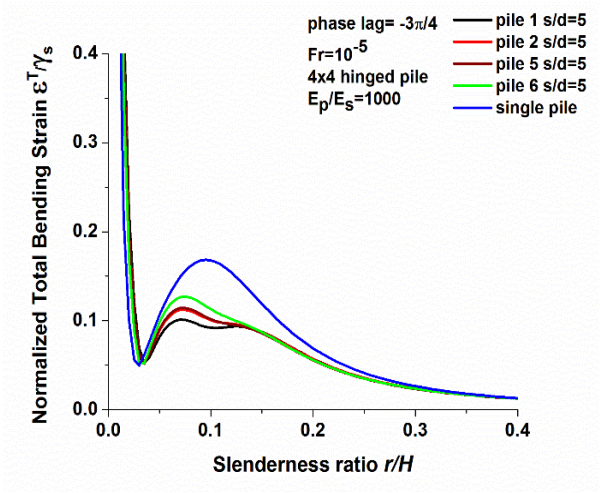


**(a)**

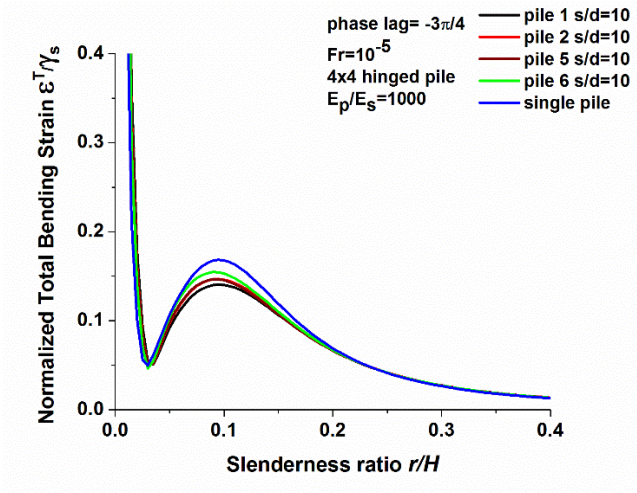


**(b)**

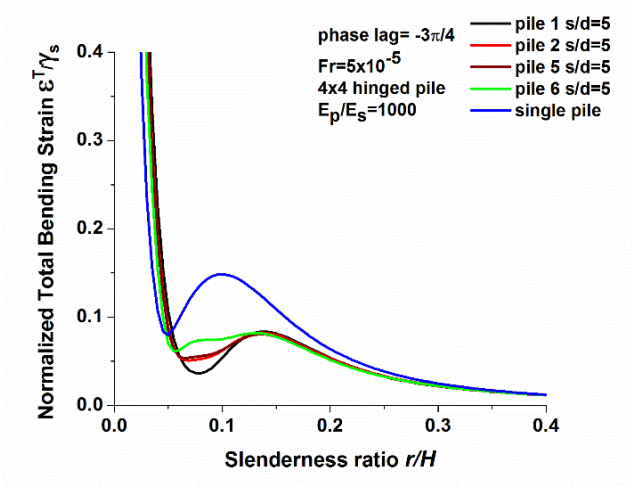


**(c)**

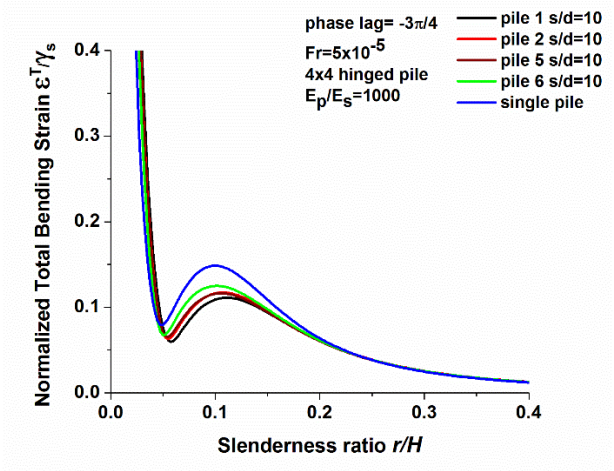


**(d)**

**Figure 5.57:** Normalized total bending strains of 4×4 hinged pile groups with respect to single pile ($\frac{\rho_p}{\rho_s} = 1.43,\ \upsilon_s = 0.4\ ,\ \beta_s = 0.05\ ,\frac{E_p}{E_s} = 1000, \varphi_r = -\frac{3\pi}{4}$).

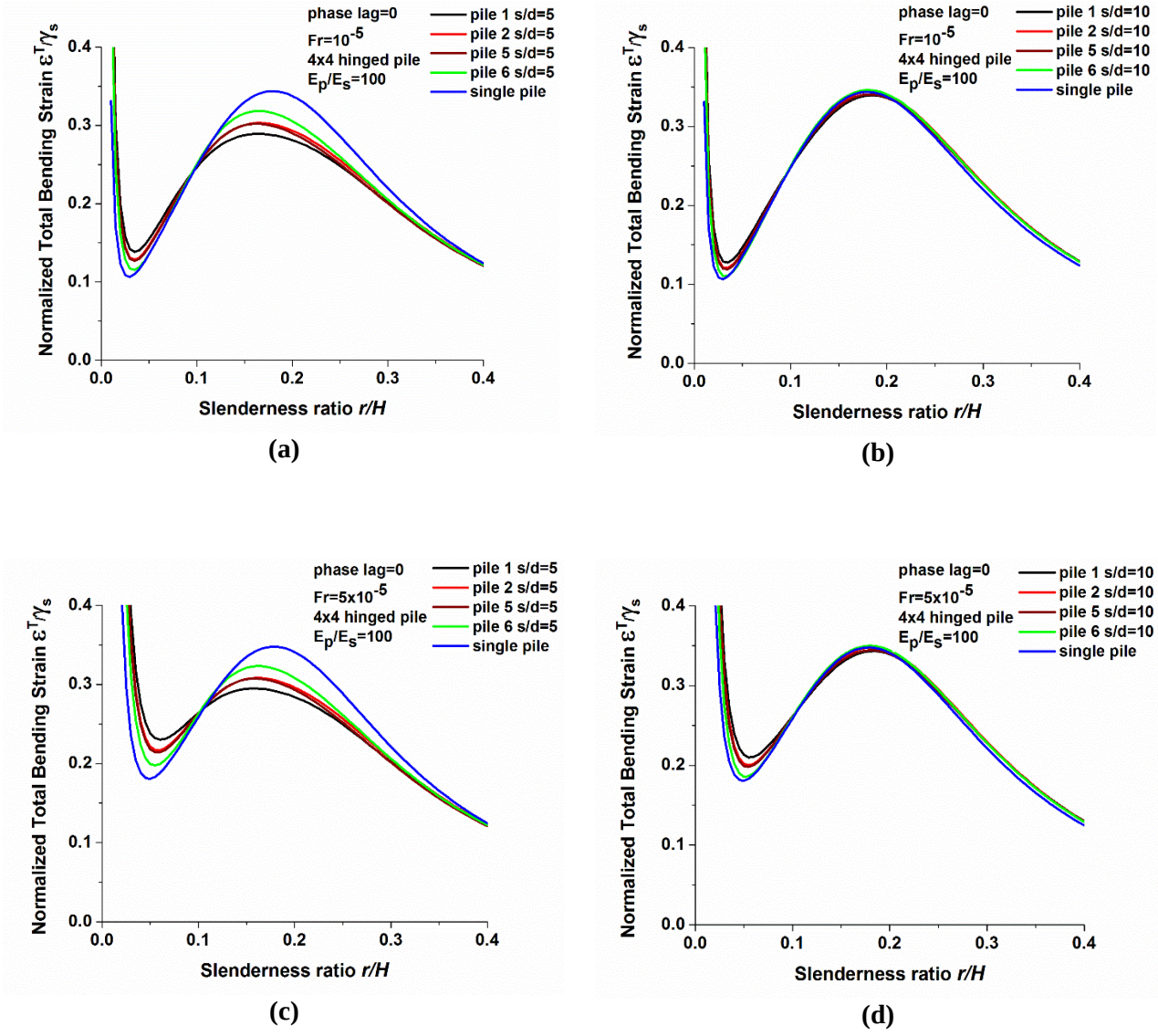


**Figure 5.58:** Normalized total bending strains of 4×4 hinged pile groups with respect to single pile ($\frac{\rho_p}{\rho_s} = 1.43,\ \upsilon_s = 0.4\ ,\ \beta_s = 0.05\ ,\frac{E_p}{E_s} = 100, \varphi_r = 0$).

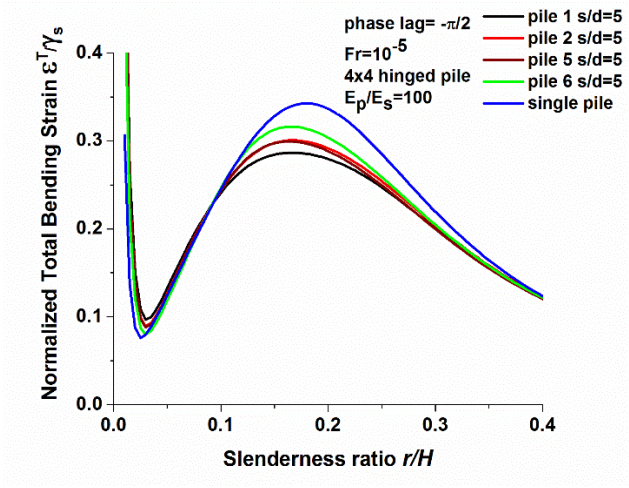


**(a)**

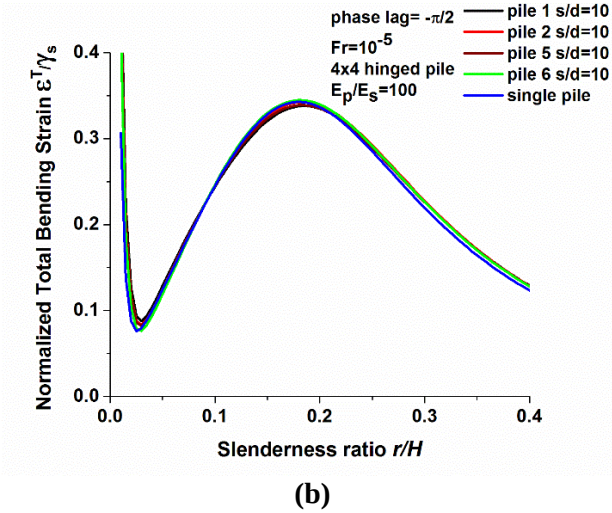


**(b)**

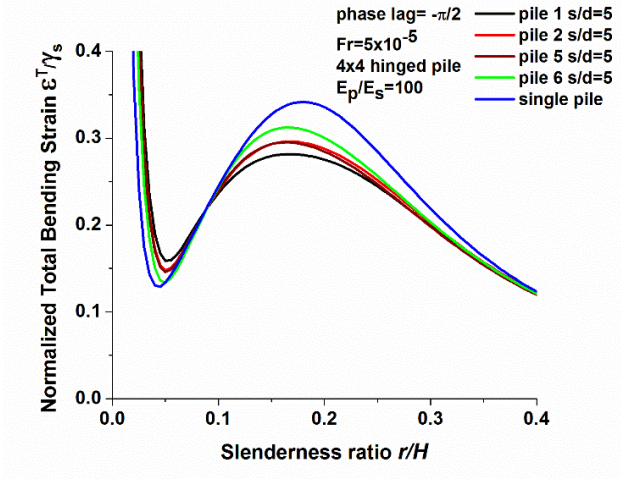


**(c)**

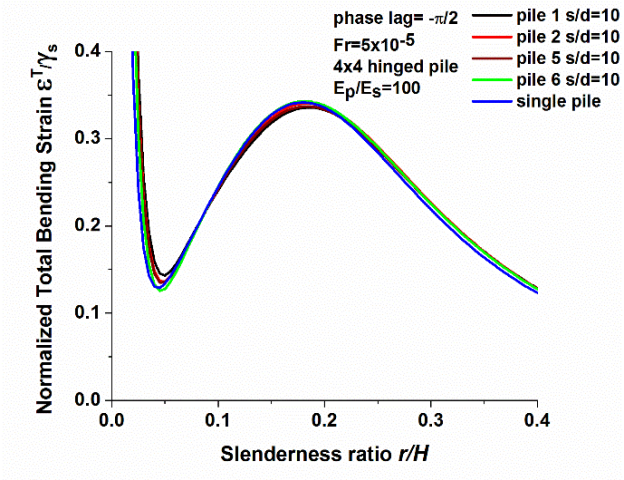


**(d)**

**Figure 5.59:** Normalized total bending strains of 4×4 hinged pile groups with respect to single pile ($\frac{\rho_p}{\rho_s} = 1.43,\ \upsilon_s = 0.4\ ,\ \beta_s = 0.05\ , \frac{E_p}{E_s} = 100, \varphi_r = -\frac{\pi}{2}$).

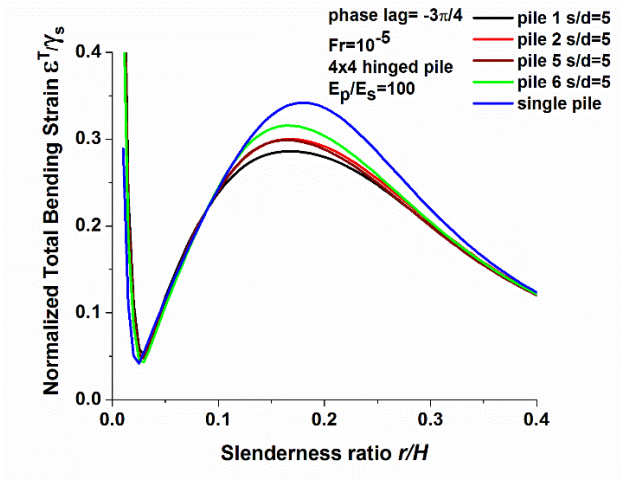


**(a)**

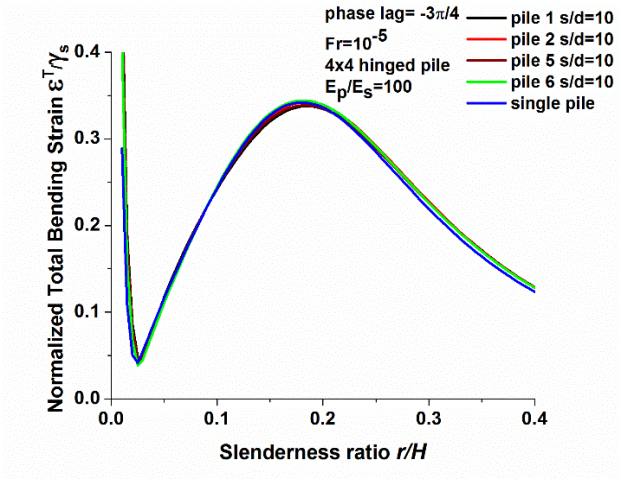


**(b)**

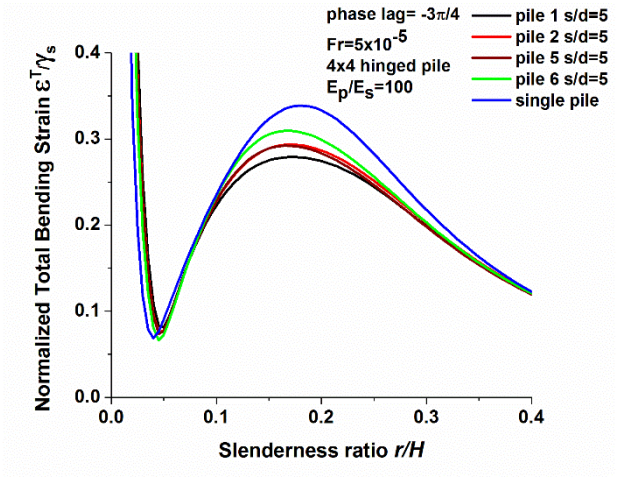


**(c)**

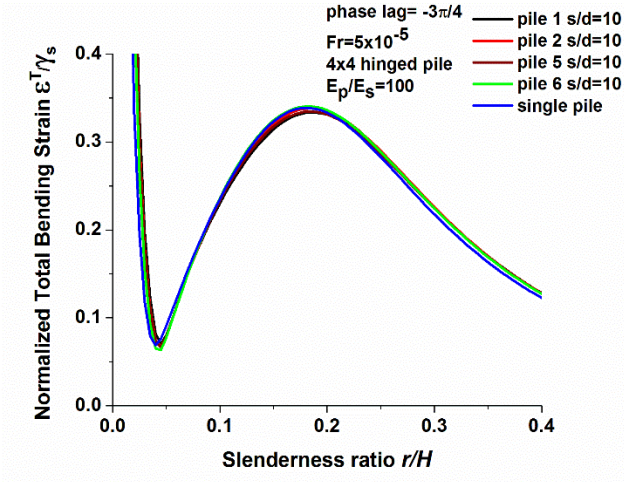


**(d)**

**Figure 5.60:** Normalized total bending strains of 4×4 hinged pile groups with respect to single pile ($\frac{\rho_p}{\rho_s} = 1.43,\ \upsilon_s = 0.4\ ,\ \beta_s = 0.05\ ,\frac{E_p}{E_s} = 100, \varphi_r = -\frac{3\pi}{4}$).

### 5.5.10 Fixed-tip 4×4 pile groups:

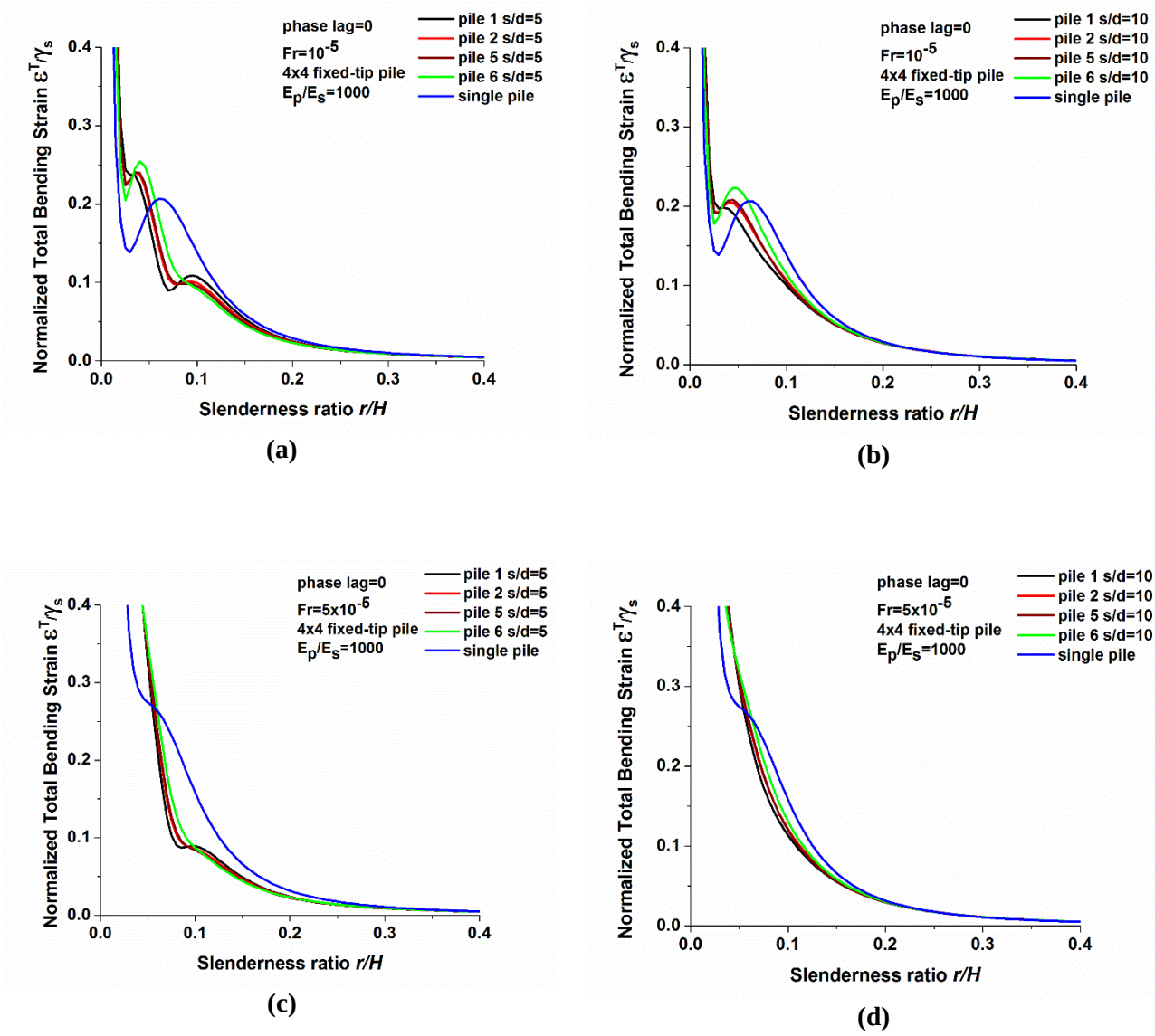


**Figure 5.61:** Normalized total bending strains of 4×4 fixed-tip pile groups with respect to single pile ($\frac{\rho_p}{\rho_s} = 1.43,\ \upsilon_s = 0.4\ ,\ \beta_s = 0.05\ , \frac{E_p}{E_s} = 1000, \varphi_r = 0$).

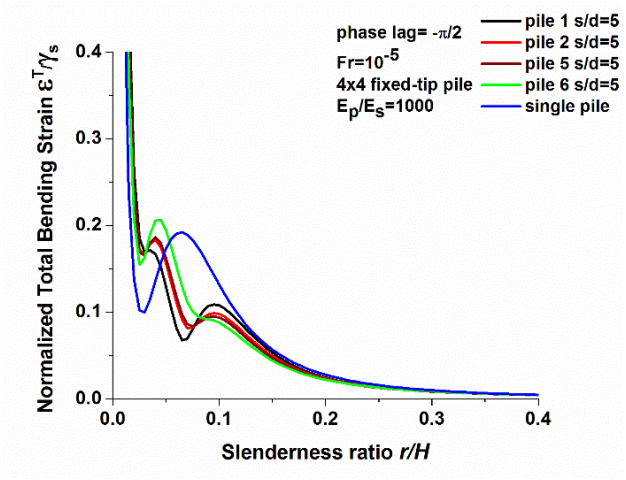


**(a)**

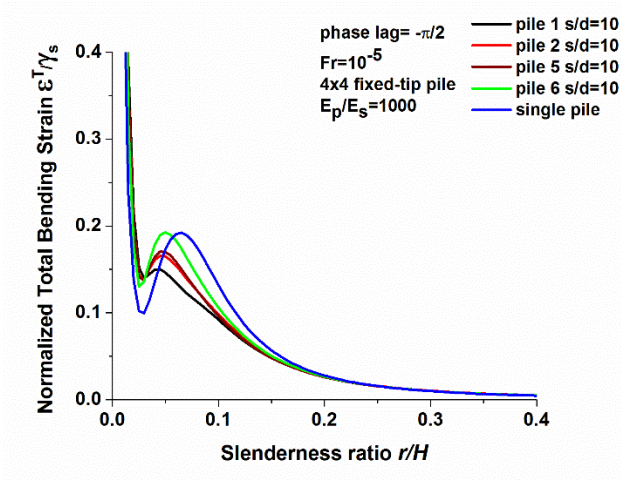


**(b)**

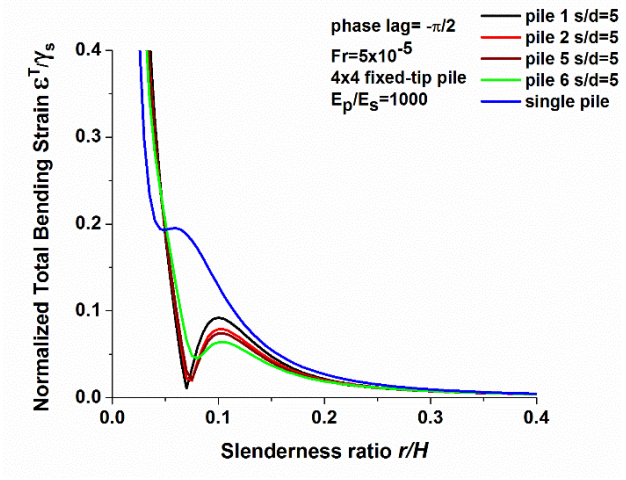


**(c)**

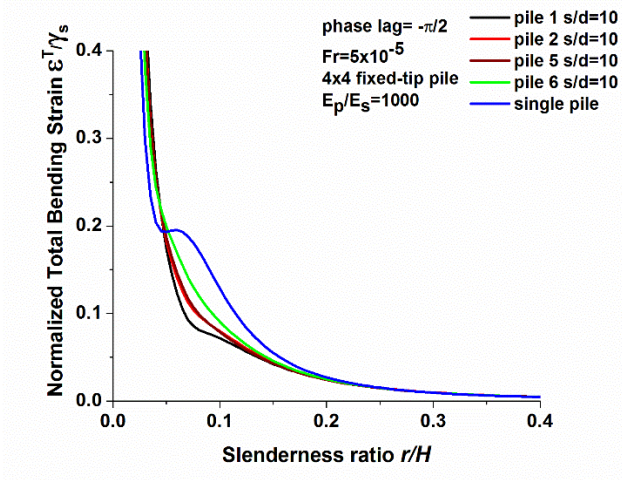


**(d)**

**Figure 5.62:** Normalized total bending strains of 4×4 fixed-tip pile groups with respect to single pile ($\frac{\rho_p}{\rho_s} = 1.43,\ \upsilon_s = 0.4\ ,\ \beta_s = 0.05\ ,\frac{E_p}{E_s} = 1000, \varphi_r = -\frac{\pi}{2}$).

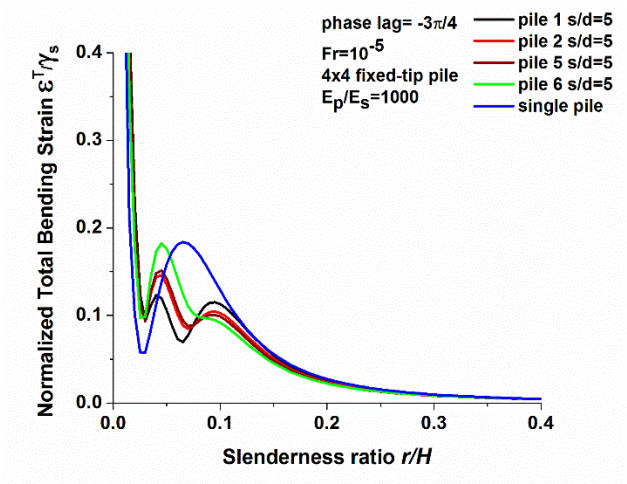


**(a)**

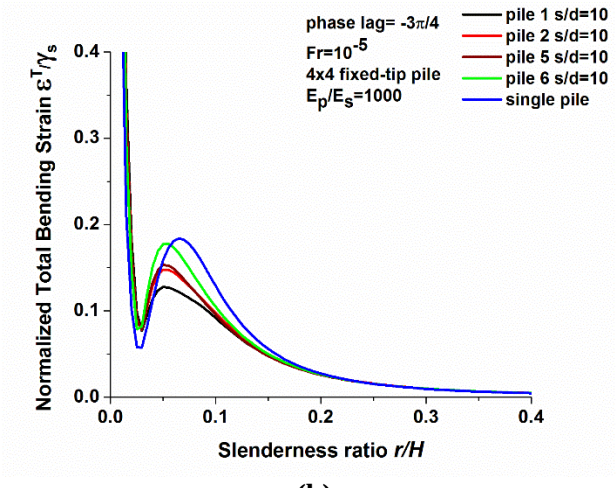


**(b)**

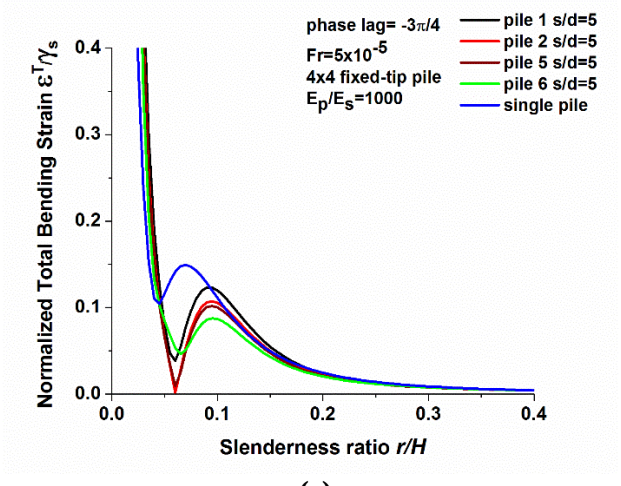


**(c)**

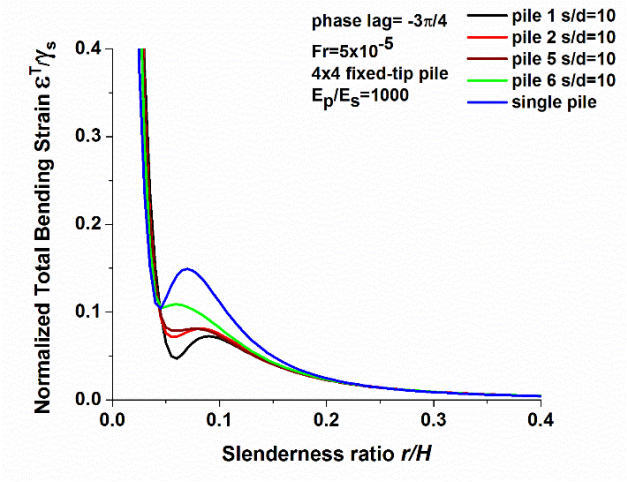


**(d)**

**Figure 5.63:** Normalized total bending strains of 4×4 fixed-tip pile groups with respect to single pile ($\frac{\rho_p}{\rho_s} = 1.43,\ \upsilon_s = 0.4\ ,\ \beta_s = 0.05\ ,\frac{E_p}{E_s} = 1000, \varphi_r = -\frac{3\pi}{4}$).

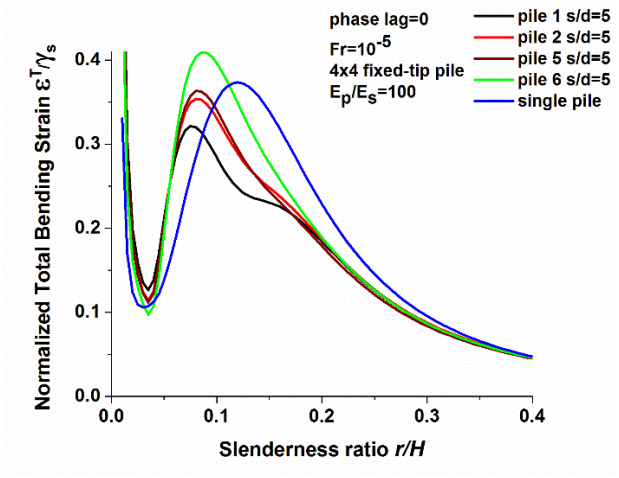


**(a)**

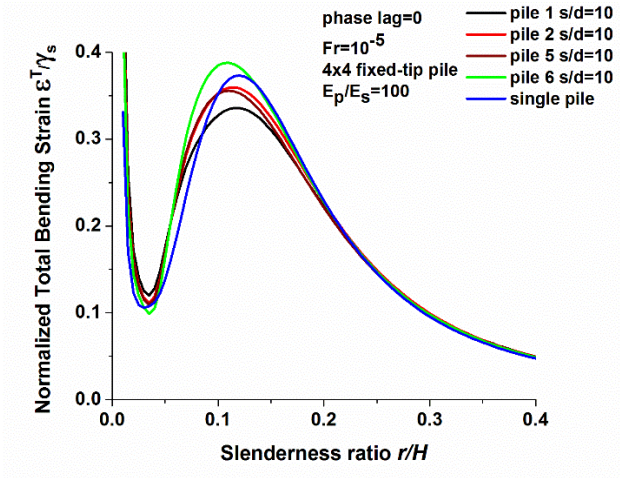


**(b)**

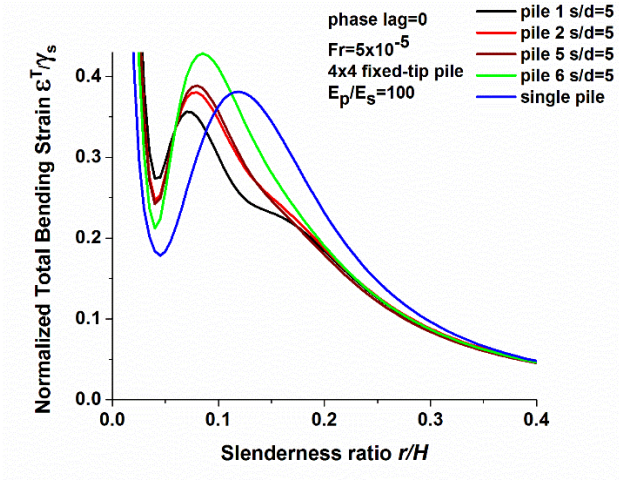


**(c)**

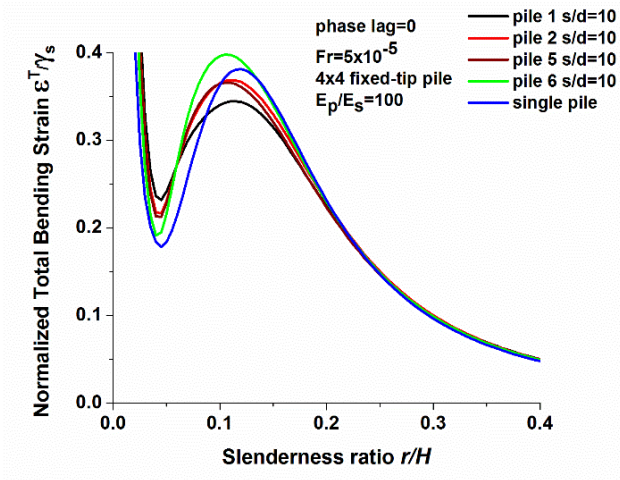


**(d)**

**Figure 5.64:** Normalized total bending strains of 4×4 fixed-tip pile groups with respect to single pile ($\frac{\rho_p}{\rho_s} = 1.43,\ \upsilon_s = 0.4\ ,\ \beta_s = 0.05\ ,\frac{E_p}{E_s} = 100, \varphi_r = 0$).

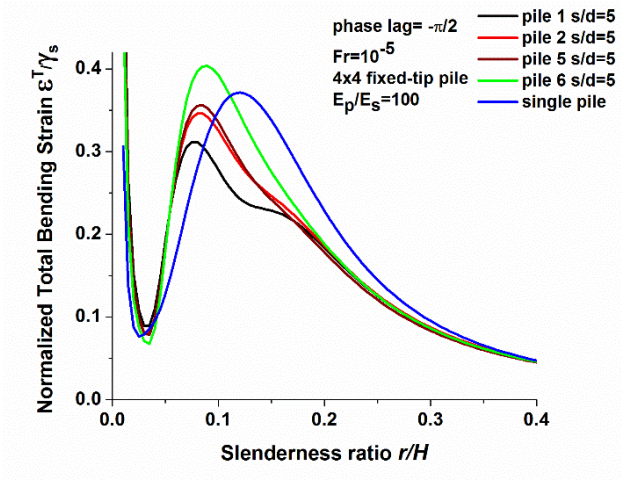


**(a)**

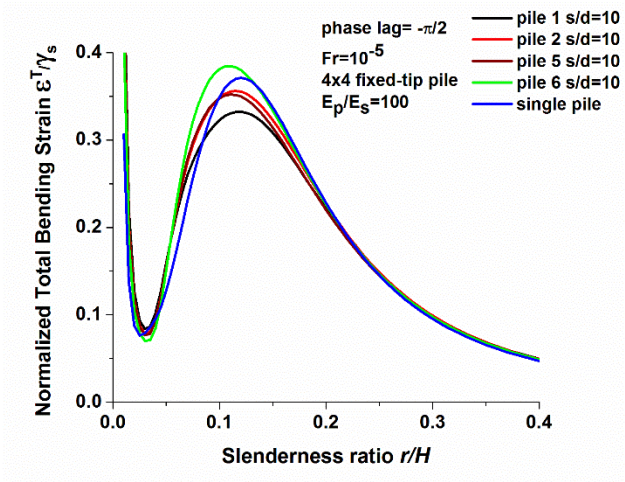


**(b)**

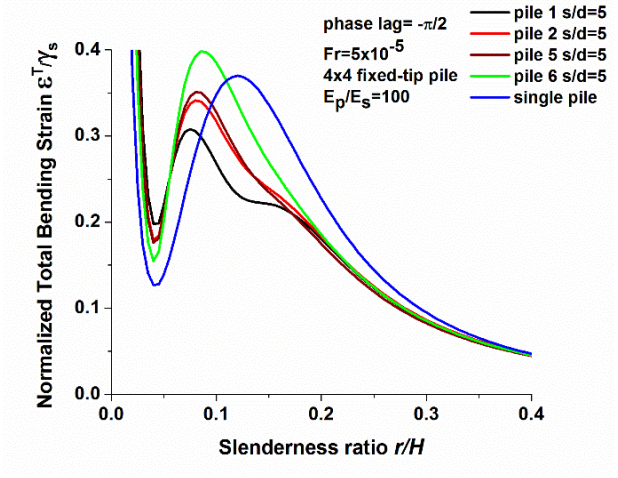


**(c)**

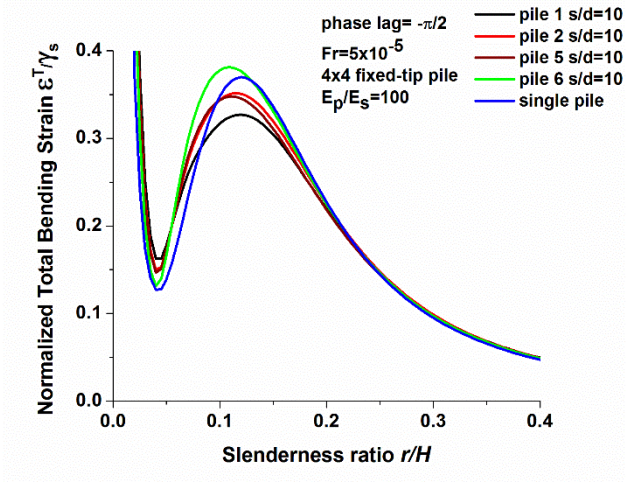


**(d)**

**Figure 5.65:** Normalized total bending strains of 4×4 fixed-tip pile groups with respect to single pile ($\frac{\rho_p}{\rho_s} = 1.43,\ \upsilon_s = 0.4\ ,\ \beta_s = 0.05\ , \frac{E_p}{E_s} = 100, \varphi_r = -\frac{\pi}{2}$).

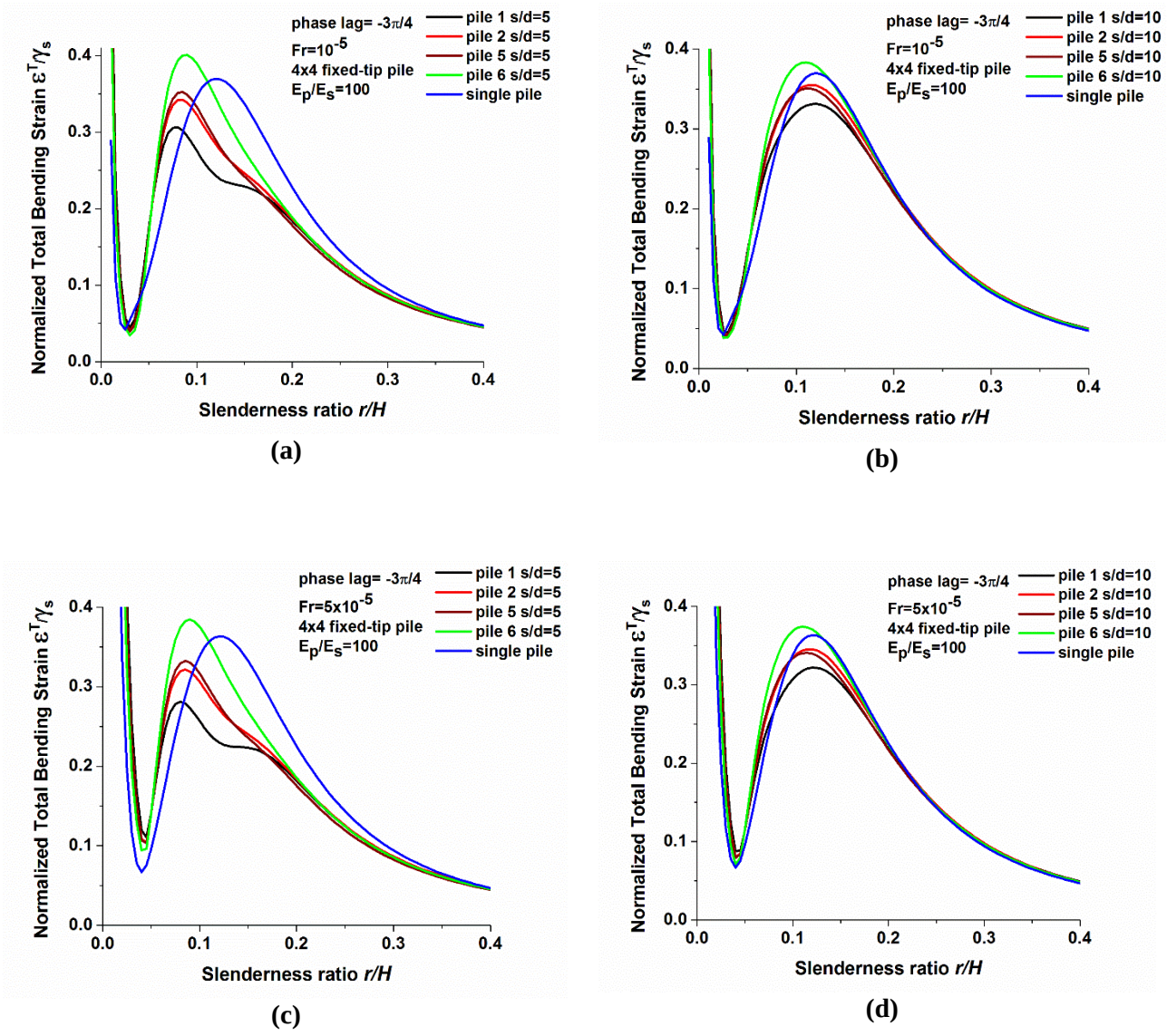


**Figure 5.66:** Normalized total bending strains of 4×4 fixed-tip pile groups with respect to single pile ($\frac{\rho_p}{\rho_s} = 1.43,\ \upsilon_s = 0.4\ ,\ \beta_s = 0.05\ ,\frac{E_p}{E_s} = 100, \varphi_r = -\frac{3\pi}{4}$).

Figures 5.3 through 5.66 show the variations in normalized total bending strains in both fixed-tip and hinged piles as a functions of the slenderness ratio $r/H$ with different values of the factor $Fr = 10^{-5}, 5 \times 10^{-5}$ phase lag $\varphi_r = 0, -\pi/2, -3\pi/4$ and pile-soil stiffness ratio $E_p/E_s = 100\ , 1000$. It is assumed that the mass density ratio $\rho_p/\rho_s = 1.43$ ; the material damping $\beta_s = 0.05$; and the Poissons's ratio $\upsilon_s = 0.4$. In order to illustrate the behavior of total bending strains in pile groups in detail, the results of normalized total

bending strains for $3 \times 3$ hinged pile groups in figures 5.42 through 5.44 ($E_p/E_s = 1000, \varphi_r = 0, -\pi/2, -3\pi/4$) are compared with those of Figures 5.45 through 5.47 ($E_p/E_s = 100, \varphi_r = 0, -\pi/2, -3\pi/4$). These figures indicate that even in pile group configurations, each pile closely follows the general trend of the single pile. Furthermore, as the pile spacing $s/d$ increases, normalized bending strains of pile groups converge to those of single piles. For $r/H \to \infty$ piles behave as a rigid disk and regardless of boundary condition at the tip, all piles will experience zero total bending strains. The variation of normalized total bending strains with slenderness ratio ($r/H$) implies the presence of two distinct points, local minimum points which minimizes the normalized total bending strains (optimal pile radius) and local maximum points which maximizes the normalized total bending strains. For small values of the slenderness ratio $r/H$, normalized inertial bending strains tend to increase markedly which can be due to dominance of inertial forces. As the slenderness ratio increases, bending strains tend significantly to decrease up to a local minimum point $r/H \approx (r/H)_{min}$ then increase almost linearly up to a local maximum point $r/H \approx (r/H)_{max}$ which can be due to dominance of kinematic interaction. Afterwards gradually decrease beyond the local maximum. This point indicates the presence of a worst-case slenderness ratio in which pile groups may experience bending failure.

Figures 5.42 through 5.44 ($E_p/E_s = 1000$) or Figures 5.45 through 5.47 ($E_p/E_s = 100$) show that when the factor $Fr$ increases, the value of the normalized bending strains in pile groups at local minimum gradually increases. In this case, the local minimum area occurs for small $Fr$ (i.e., $\leq 5 \times 10^{-5}$) within the practical range of $r/H$. This implies the radius that can appropriately minimize the bending strains. The presence of local minimum area is linked to the opposite change in the inertial and kinematic bending strains with $r/H$. It is apparent that the changes in $Fr$ have little effect upon the value of slenderness ratio at local maximum.

By comparing results of figures 5.42 through 5.44 ($E_p/E_s = 1000, \varphi_r = 0, -\pi/2, -3\pi/4$) with those of figures 5.45 through 5.47 ($E_p/E_s = 100, \varphi_r = 0, -\pi/2, -3\pi/4$), it can be noted that at the local minimum

once the phase lag $\varphi_r$ begins to decrease the value of the normalized total bending strains gradually tend to decrease. When $\varphi_r$ becomes closer to $-\pi$, approximately all piles in the group experience zero total bending strain. This implies that by decreasing the value of the phase lag $\varphi_r$ the value of the inertial bending strain and the kinematic bending strain become equal with different signs and subsequently cancel each other. However, being $\varphi_r = -\pi$ in practical engineering may not be realistic because the phase lag $\varphi_r$ probably converges to about $-3\pi/4$ in the case where $T_s/T_g \geq 1$, as described by Murono and Nishimura [5.2].

Figures 5.42 through 5.44 $(E_p/E_s = 1000, \varphi_r = 0, -\pi/2, -3\pi/4)$ and Figures 5.45 through 5.47 $(E_p/E_s = 100, \varphi_r = 0, -\pi/2, -3\pi/4)$, also show the variations in normalized total bending strains with different values of the pile-soil stiffness ratio. These figures imply that the value of the normalized total bending strains at the local minimum point significantly increases as $E_p/E_s$ increases. The reason for this increase can be due to the fact that the increase in the pile-soil stiffness due to the movement of the surrounding soil, as indicated by Equation (2.7), makes the reaction forces in the dynamic Winkler springs apparently increase.

In figures 5.61 through 5.66, the results of parametric studies are shown for 4×4 fixed-tip pile groups. In these figures the local minimums and the local maximums characterized by wavy pattern of the total bending strains appear. This behaviour is the direct consequence of the pile-to-pile interaction between piles. Thus, peaks and valleys appear on the normalized total bending strains curves, which becomes increasingly pronounced as the number of piles in the group increases.

The effects of important parameters ($Fr$, $\varphi_r$, $E_p/E_s$) on the value of local minimum and local maximum slenderness ratios in pile groups can be categorized in the following sections:

### 5.5.11 Effect of factor *Fr*

In order to have further insight into the characteristics of minimum and maximum pile radius in pile groups against variation of the facotr $Fr$ additional results of 1×2, 1×3, 2×2, 3×3 hinged pile groups with different values of phase lag $\varphi_r = 0, -\pi/2, -3\pi/4$ and pile-soil stiffness ratio $E_p/E_s = 100\,, 1000$ are presented in the following figures:

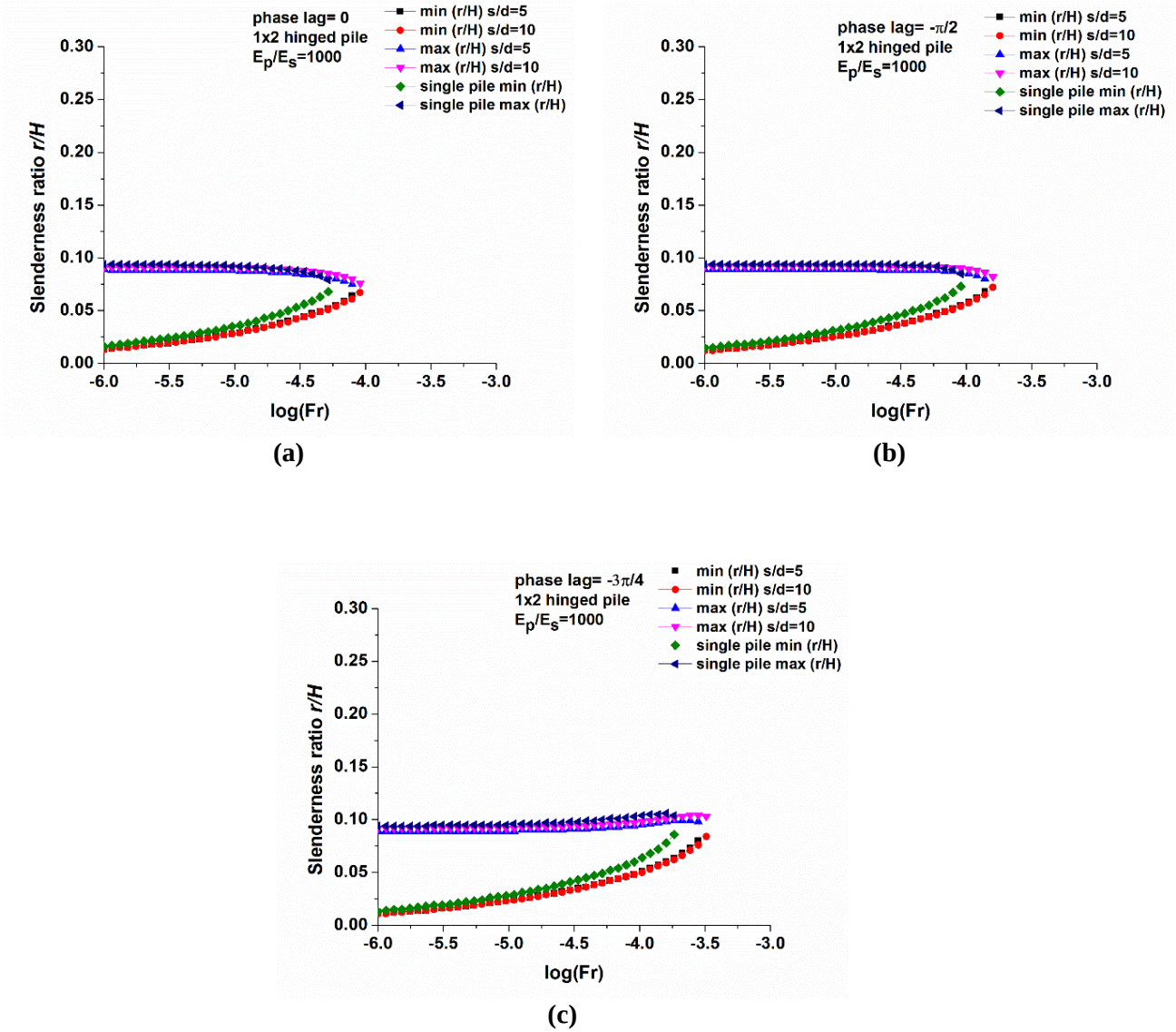


**Figure 5.67:** Variation of minimum and maximum radius of 1×2 hinged pile groups with $Fr$ ($\frac{\rho_p}{\rho_s} = 1.43,\ \upsilon_s = 0.4\,,\ \beta_s = 0.05\,, \frac{E_p}{E_s} = 1000$).

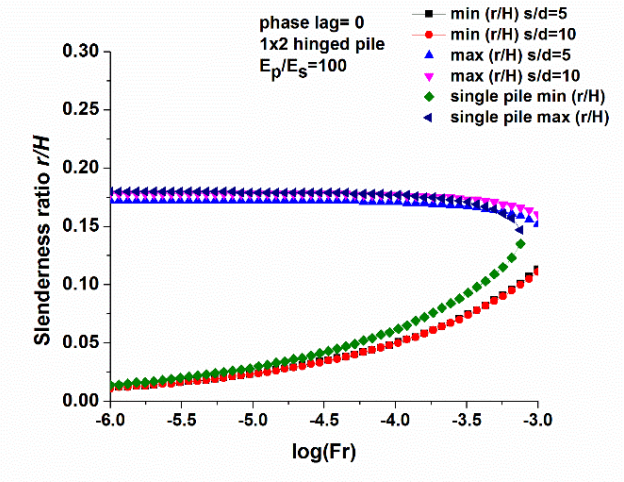


**(a)**

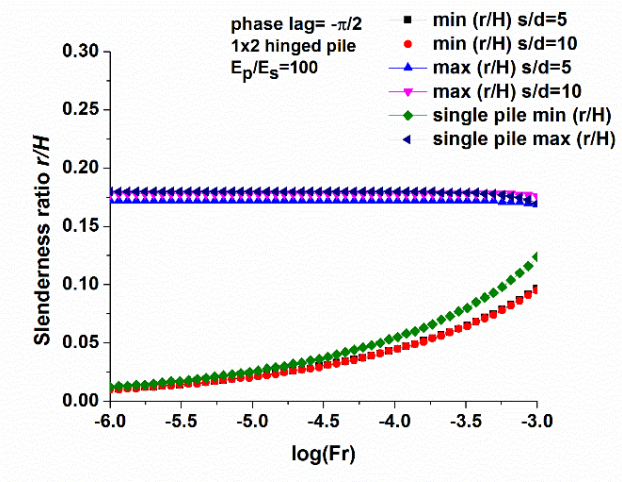


**(b)**

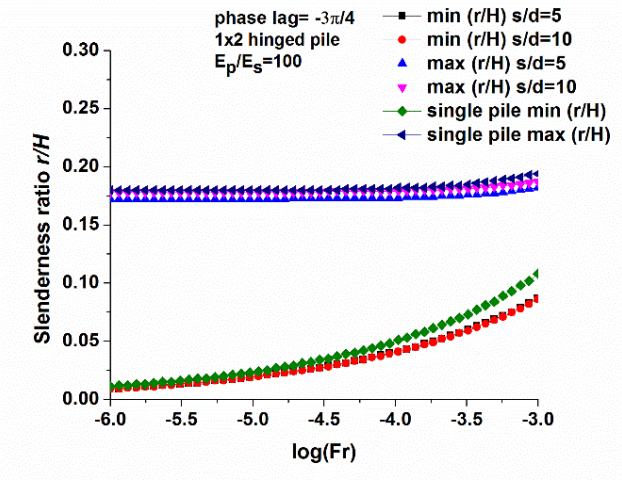


**(c)**

**Figure 5.68:** Variation of minimum and maximum radius of 1×2 hinged pile groups with $Fr$ ($\frac{\rho_p}{\rho_s} = 1.43,\ \upsilon_s = 0.4\ ,\ \beta_s = 0.05\ , \frac{E_p}{E_s} = 100$).

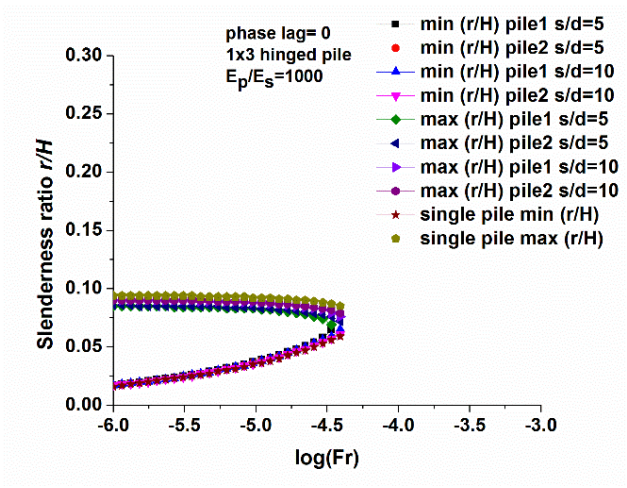


**(a)**

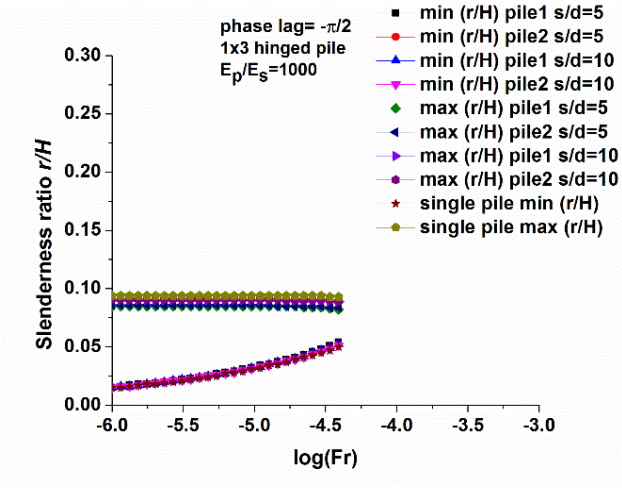


**(b)**

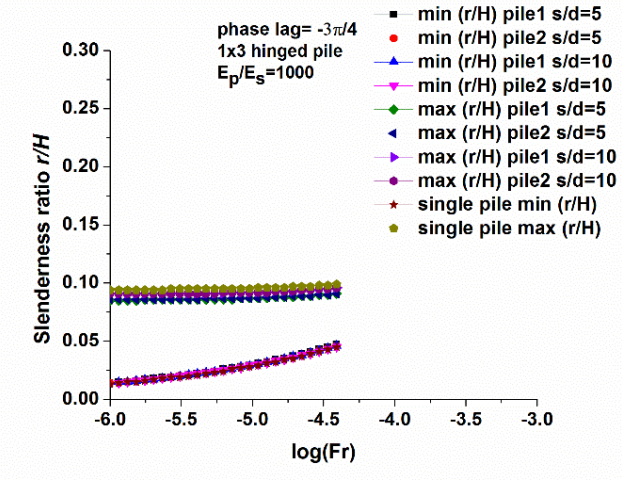


**(c)**

**Figure 5.69:** Variation of minimum and maximum radius of 1× hinged3 pile groups with $Fr$ ($\frac{\rho_p}{\rho_s} = 1.43,\ \upsilon_s = 0.4\ ,\ \beta_s = 0.05\ ,\frac{E_p}{E_s} = 1000$).

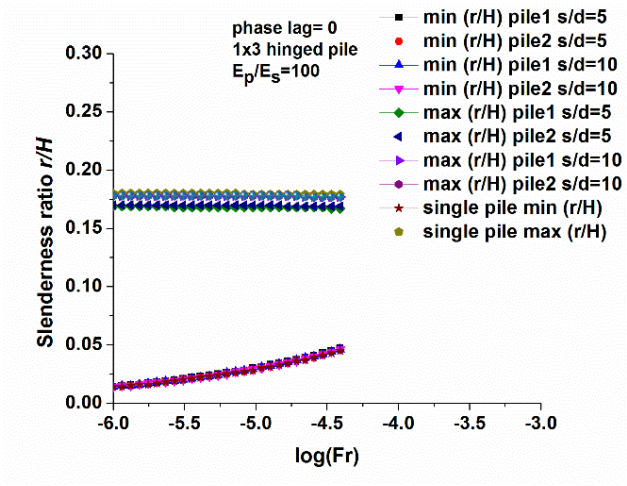


**(a)**

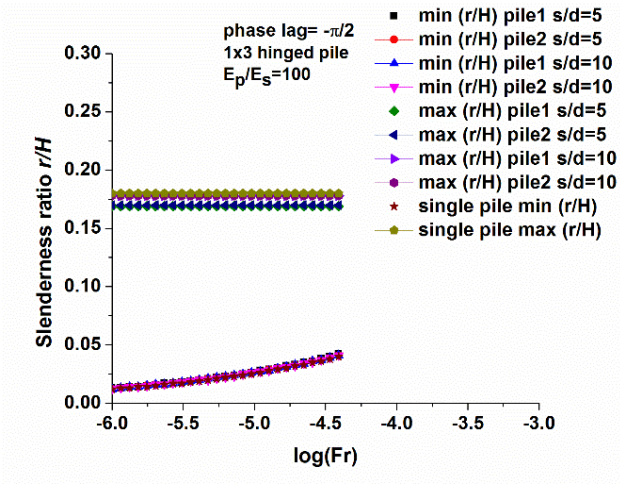


**(b)**

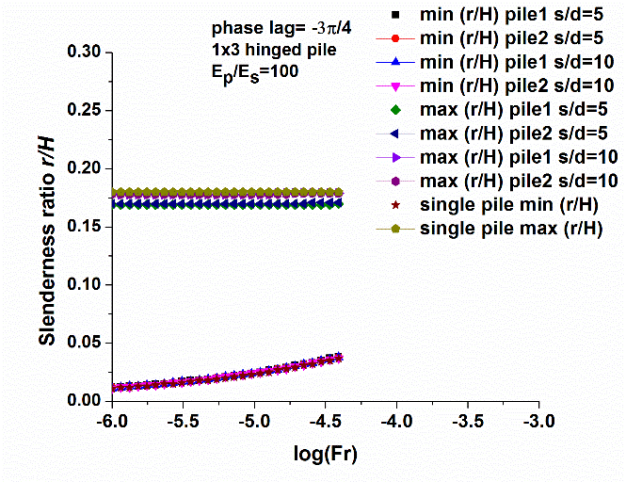


**(c)**

**Figure 5.70:** Variation of minimum and maximum radius of 1×3 hinged pile groups with $Fr$ ($\frac{\rho_p}{\rho_s} = 1.43,\ \upsilon_s = 0.4\ ,\ \beta_s = 0.05\ ,\frac{E_p}{E_s} = 100$).

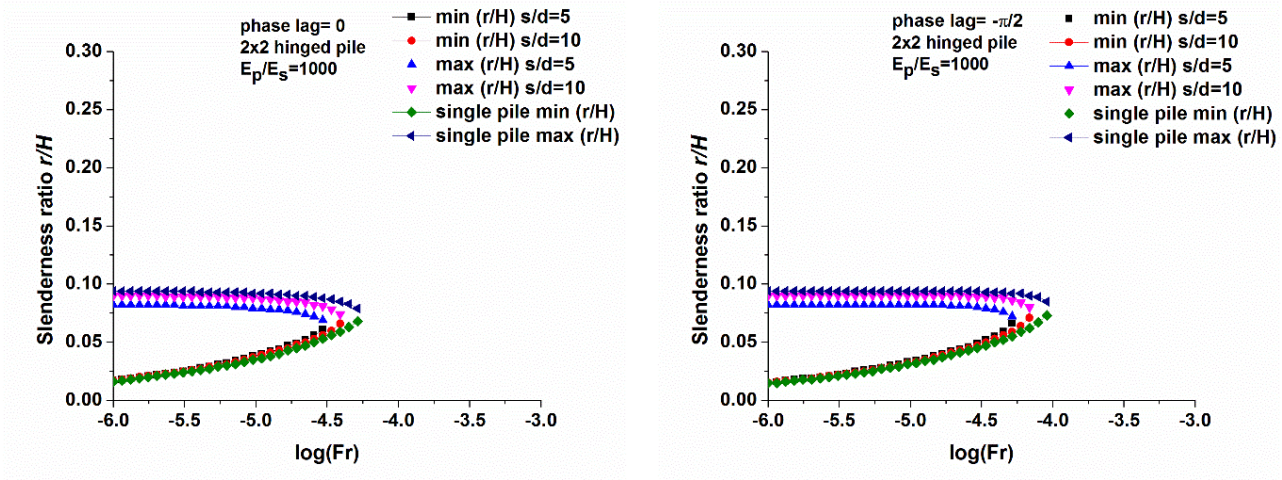


**(a)** **(b)**

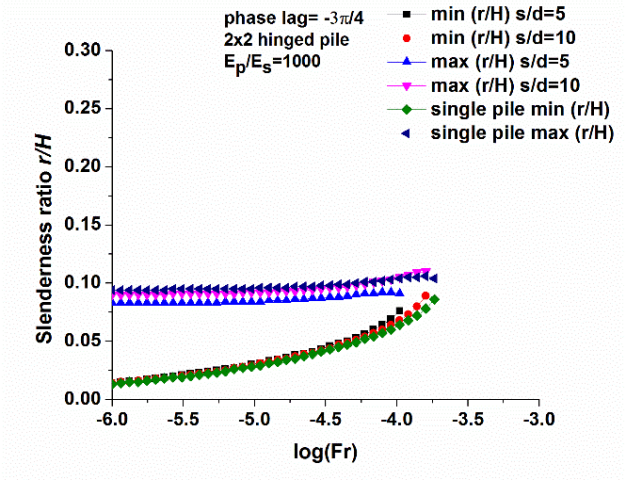


**(c)**

**Figure 5.71:** Variation of minimum and maximum radius of 2×2 hinged pile groups with $Fr$ ($\frac{\rho_p}{\rho_s} = 1.43,\ \upsilon_s = 0.4\ ,\ \beta_s = 0.05\ ,\frac{E_p}{E_s} = 1000$).

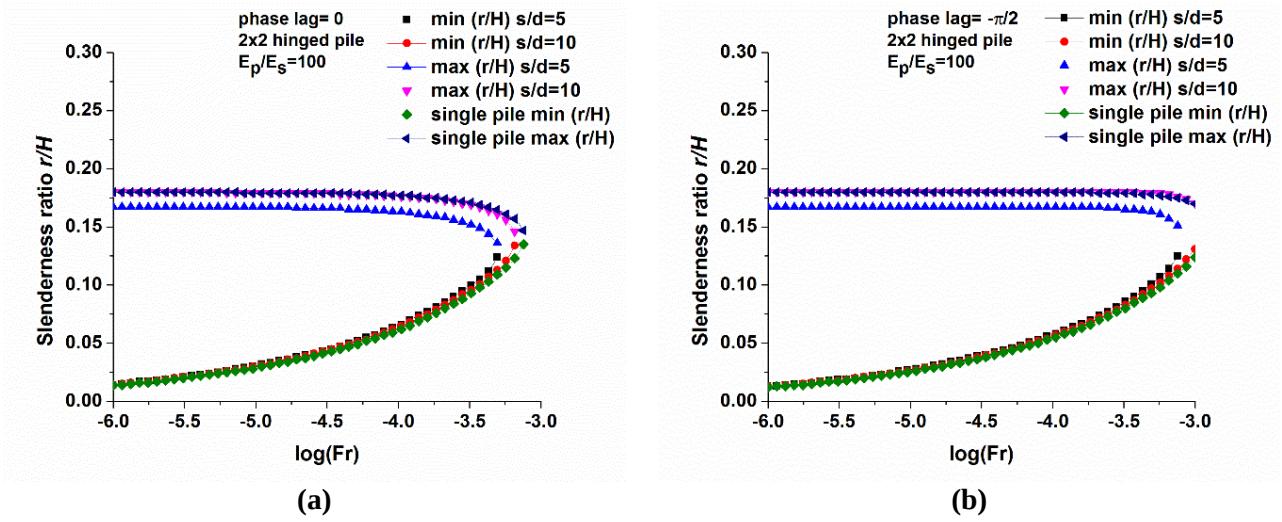


**Figure 5.72:** Variation of minimum and maximum radius of 2×2 hinged pile groups with $Fr$ ($\frac{\rho_p}{\rho_s} = 1.43,\ \upsilon_s = 0.4\ ,\ \beta_s = 0.05\ ,\frac{E_p}{E_s} = 100$).

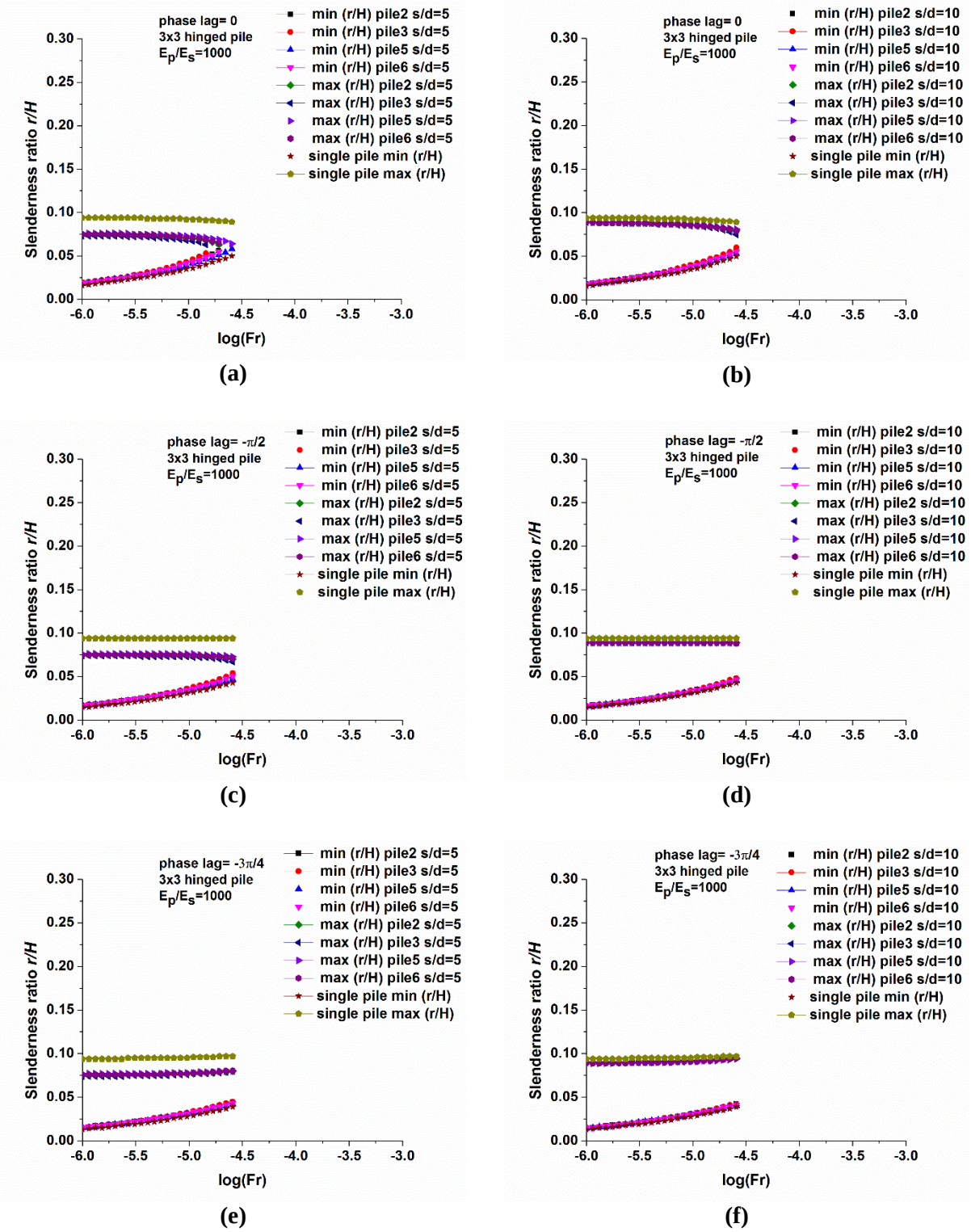


**Figure 5.73:** Variation of minimum and maximum radius of 3×3 hinged pile groups with $Fr$ ($\frac{\rho_p}{\rho_s} = 1.43,\ \upsilon_s = 0.4\ ,\ \beta_s = 0.05\ ,\frac{E_p}{E_s} = 1000$).

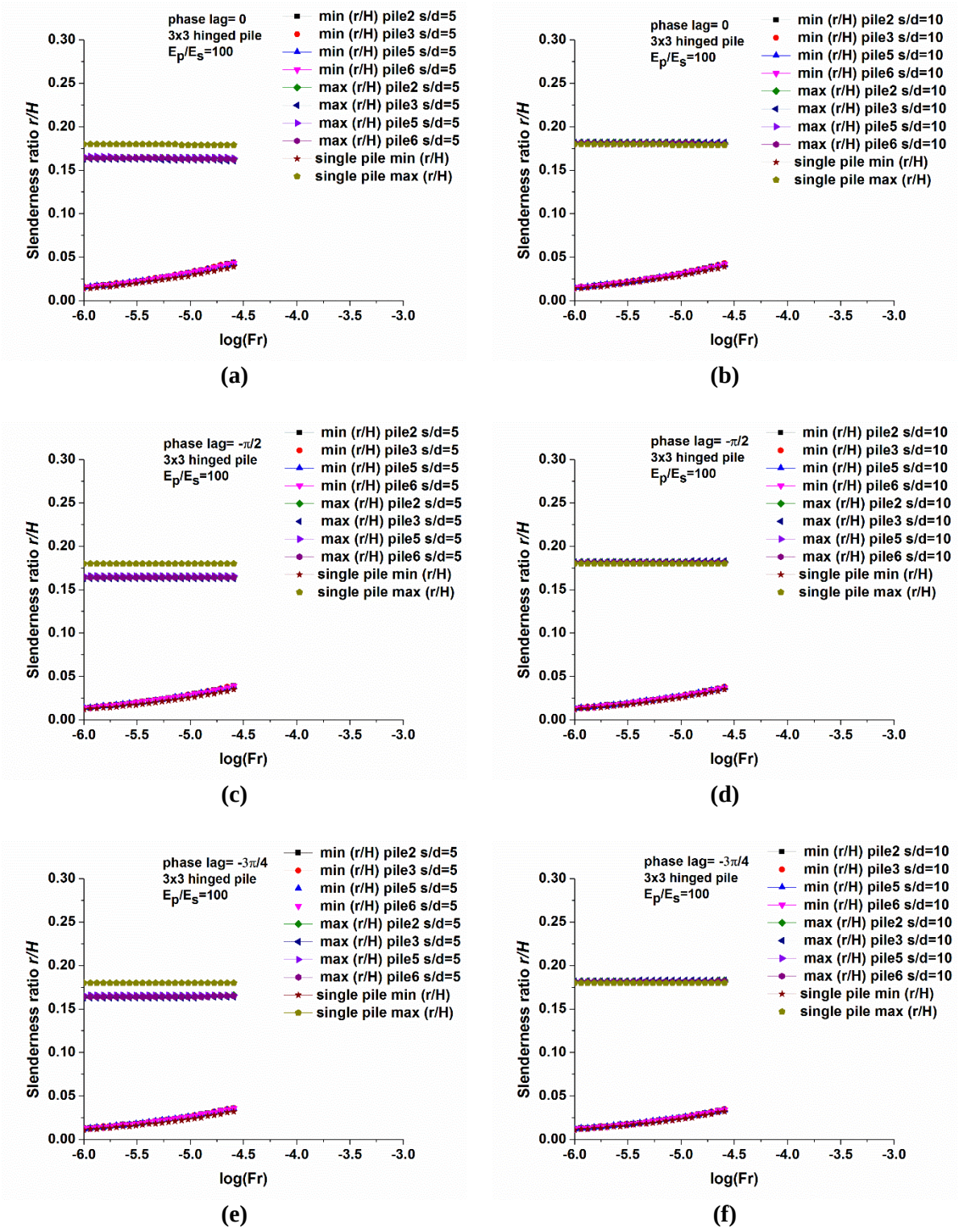


**Figure 5.74:** Variation of minimum and maximum radius of 3×3 hinged pile groups with $Fr$ ($\frac{\rho_p}{\rho_s} = 1.43,\ \upsilon_s = 0.4\ ,\ \beta_s = 0.05\ ,\frac{E_p}{E_s} = 100$).

Figures 5.67 through 5.74, can clearly indicate that the values of the minimum pile radius in pile groups tend to increase gradually as the factor $Fr$ increases. The reason for this can be due to the outcome of inertial bending strains and kinematic bending strains which behave in opposite directions and as a result induce changes in the slenderness ratio associated with the local minimum point. Therefore, the local minimum point tends to move toward larger values of the slenderness ratios as $Fr$ increases. In contrast, as $Fr$ increases (dominance of inertial interaction), the values of the maximum pile radius in pile groups remain approximately unchanged. This can be due to the fact that the value of the slenderness ratio at local maximum point is mainly affected by kinematic interaction. For instance, this behaviour can be clearly seen in figures 5.67 and 5.68. It is also found that the distance between the slenderness ratios associated with the local minimum and the local maximum points tends to decrease as the factor $Fr$ increases. As a result, a local minimum and maximum will be generated for small values of the factor $Fr$ (e.g., $\leq 10^{-4.5}$). It is noted, therefore that the presence of local minimum may largely depend on the value of the factor $Fr$.

### 5.5.12 Effect of phase lag $\varphi_r$

To assist in the understanding the characteristics of minimum and maximum pile radius in pile groups against the variations of the phase lag $\varphi_r$ additional results of 3×3 hinged pile groups with different values of the factor $Fr = 10^{-5}, 5 \times 10^{-5}$ and pile-soil stiffness ratio $E_p/E_s = 100\,, 1000$ are presented in the following figures:

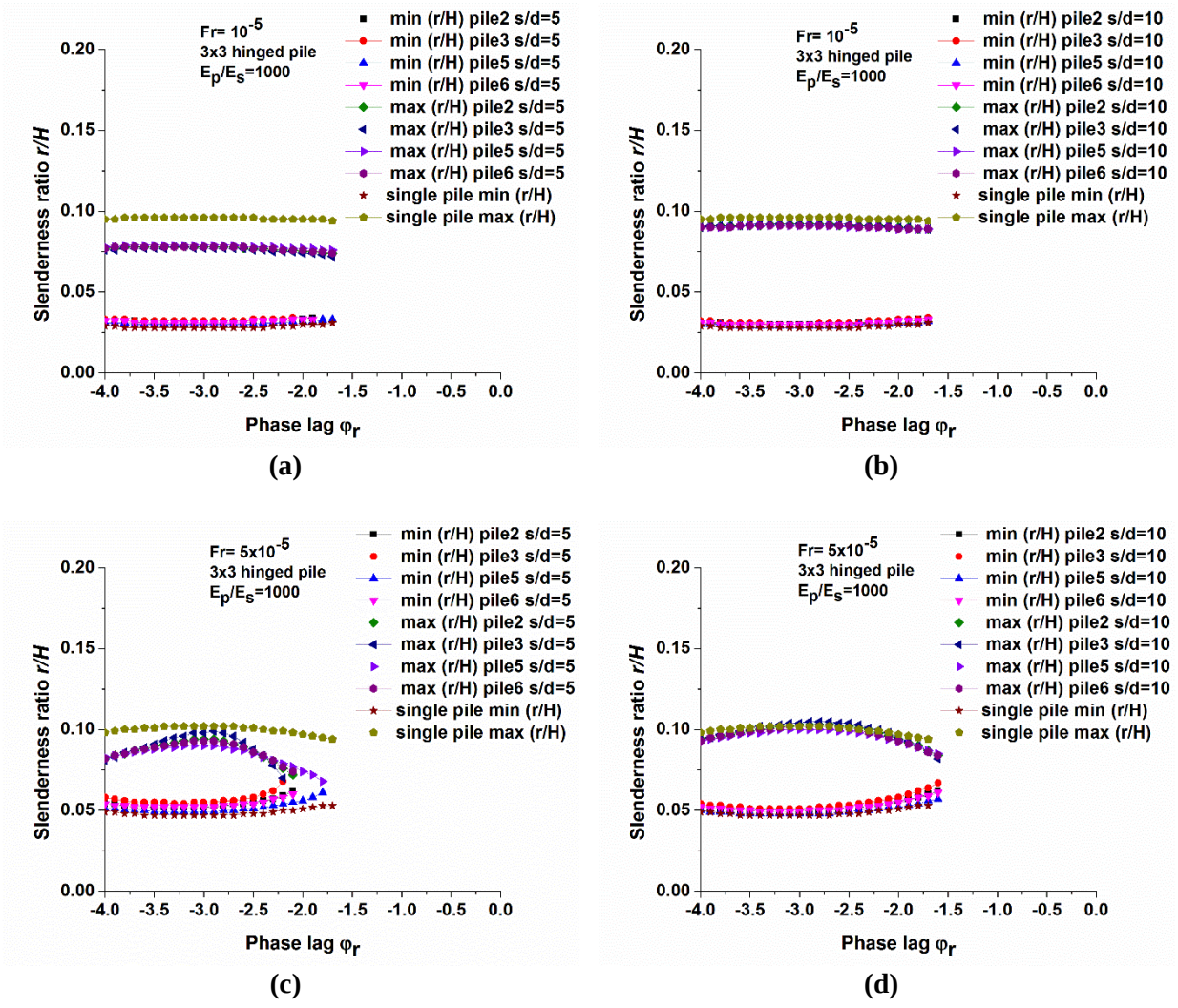


**Figure 5.75:** Variation of minimum and maximum radius of 3×3 hinged pile groups with $\varphi_r$ ($\frac{\rho_p}{\rho_s} = 1.43,\ \upsilon_s = 0.4\ ,\ \beta_s = 0.05\ ,\frac{E_p}{E_s} = 1000$).

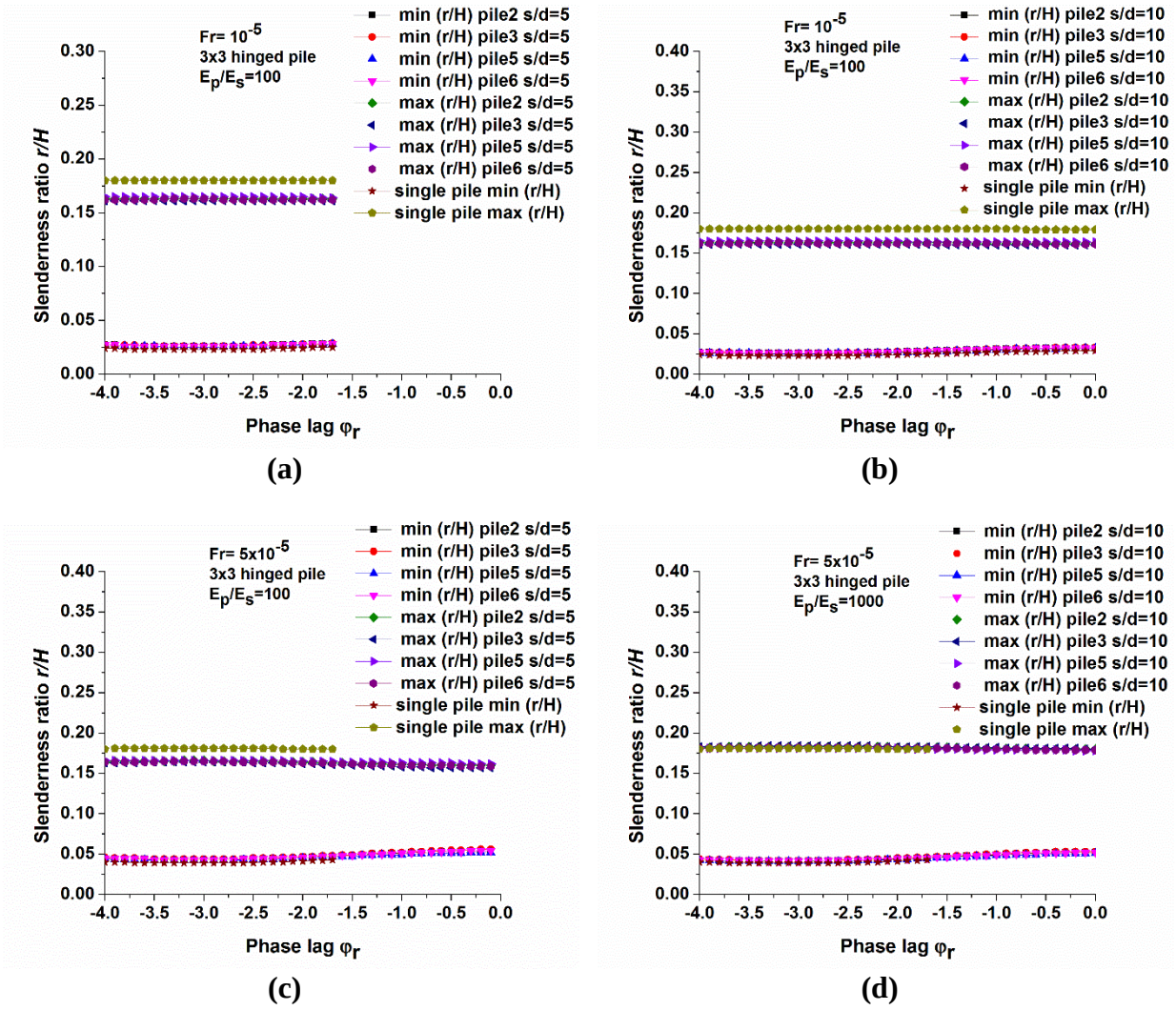


**Figure 5.76:** Variation of minimum and maximum radius of 3×3 hinged pile groups with $\varphi_r$ ($\frac{\rho_p}{\rho_s} = 1.43,\ \upsilon_s = 0.4\ ,\ \beta_s = 0.05\ ,\frac{E_p}{E_s} = 100$).

Despite local deviations in figures 5.75 (c) and (d), it can be concluded the values of the minimum and maximum pile radius in pile groups with variation of the phase lag ranges ($\varphi_r \approx -\pi\ to\ \varphi_r \approx 0$) does not substantially change and can be considered constant. Therefore, the changes in the phase lag $\varphi_r$ have negligible influence upon the minimum and the maximum radius in pile groups. Moreover, as the factor $F_r$ increases the local minimum and local maximum points tend to become equal to each other as one single point.

### 5.5.13 Effect of pile-soil stiffness ratio $E_p/E_s$

To assist in the understanding the characteristics of minimum and maximum pile radius in pile groups against the variations of the pile-soil stiffness ratio $E_p/E_s$ additional results of 3×3 hinged pile groups with different values of the factor $Fr = 10^{-5}, 5 \times 10^{-5}$ and the phase lag $\varphi_r = 0, -\pi/2, -3\pi/4$ have been presented in the following figures:

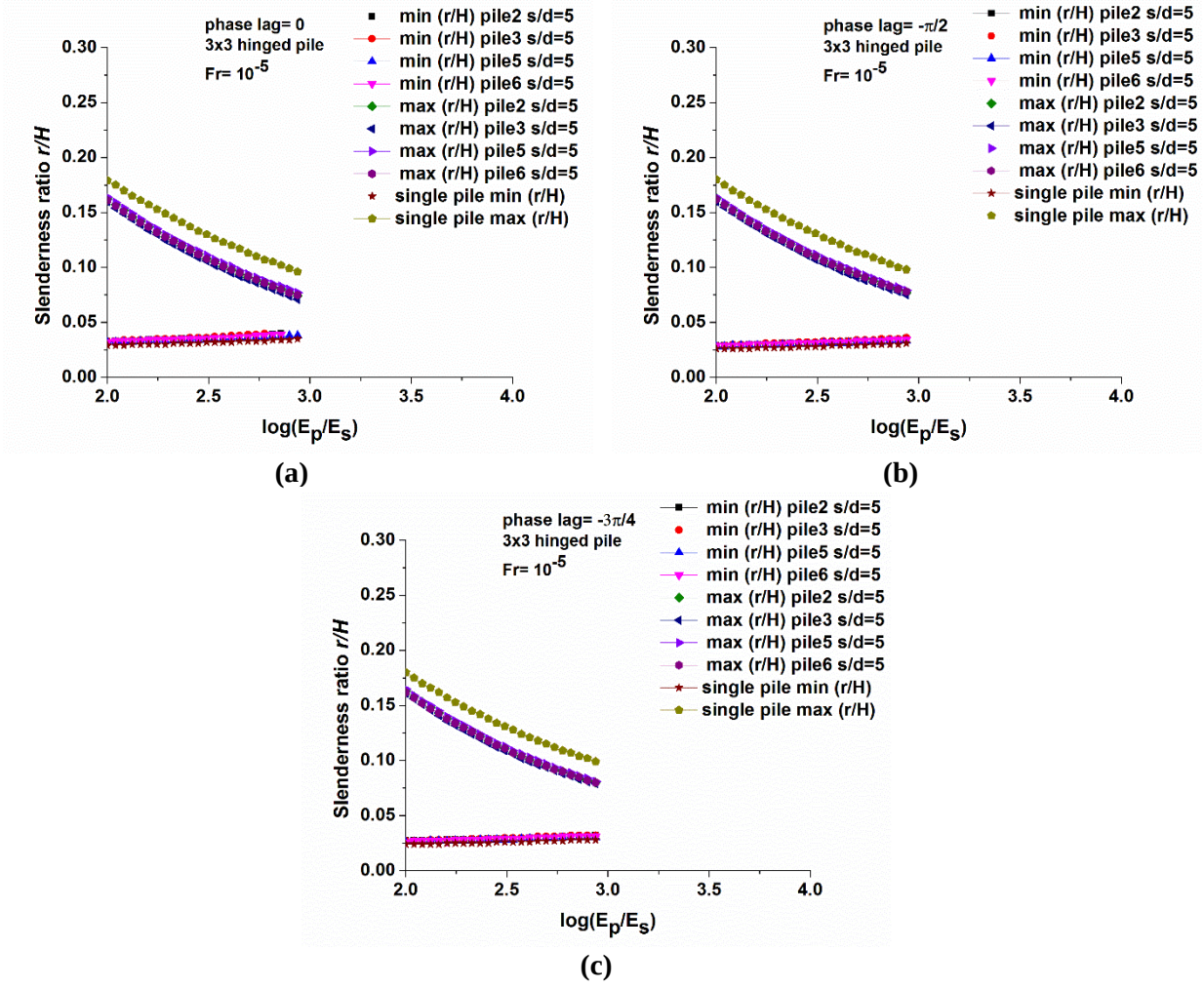


**Figure 5.77:** Variation of minimum and maximum radius of 3×3 hinged pile groups with $E_p/E_s$ $(\frac{\rho_p}{\rho_s} = 1.43,\ \upsilon_s = 0.4\ ,\ \beta_s = 0.05\ , Fr = 10^{-5})$.

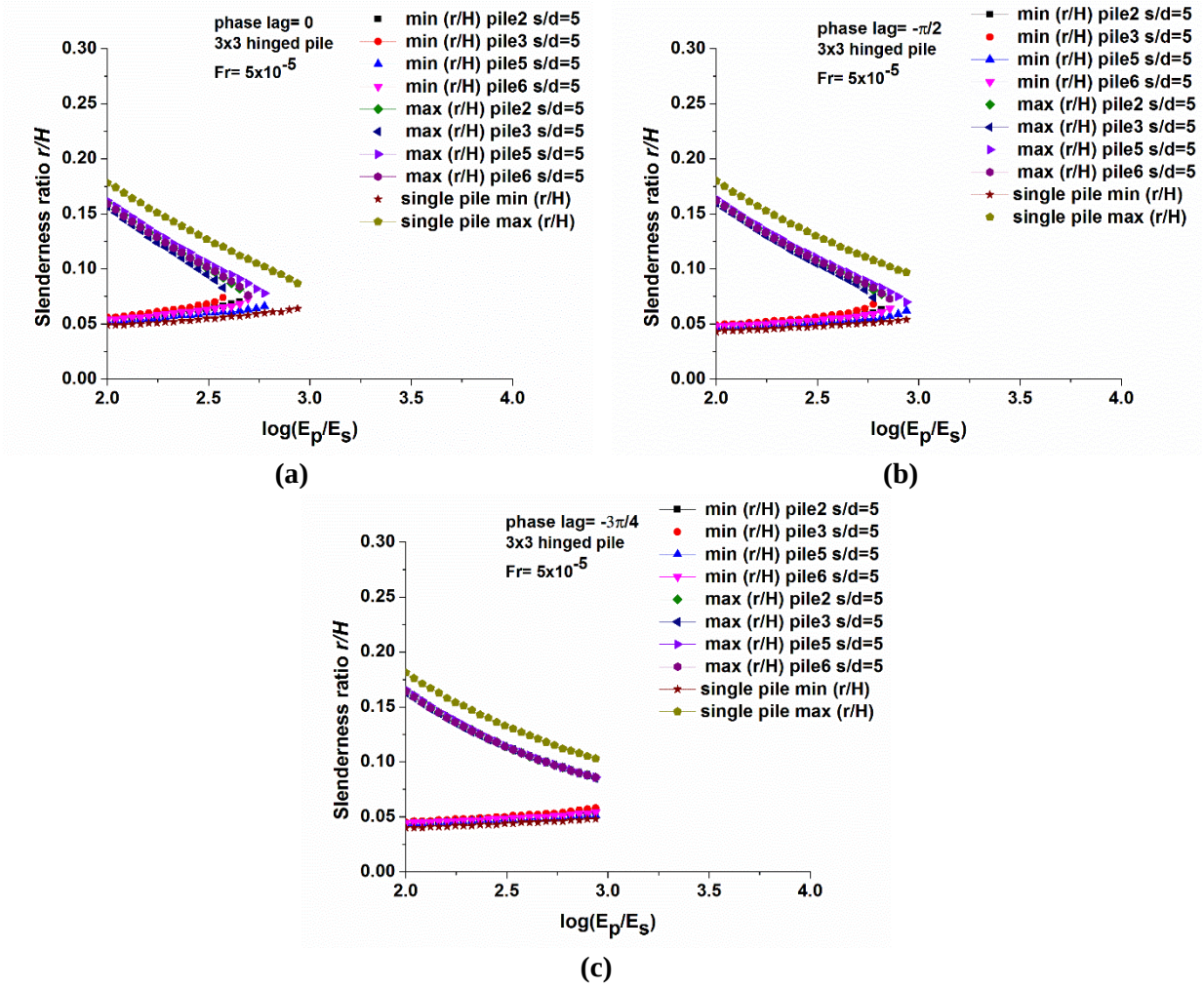


**Figure 5.78:** Variation of minimum and maximum radius of 3×3 hinged pile groups with $E_p/E_s$ ($\frac{\rho_p}{\rho_s} = 1.43,\ \upsilon_s = 0.4\ ,\ \beta_s = 0.05\ , Fr = 5 \times 10^{-5}$).

Figures 5.77 and 5.78 show that the local maximum of bending strains shift substantially to lower values of the slenderness ratio as the pile-soil stiffness ratio $E_p/E_s$ increase. In contrast, as the pile-soil stiffness ratio $E_p/E_s$ increases the values of the minimum pile radius in pile groups remain approximately unchanged. It is also found that the distance between the local minimum and the local maximum tends to decrease as the pile-soil stiffness ratio $E_p/E_s$ increases. As a result, a local minimum and maximum area

will be generated for small values of the pile-soil stiffness ratio $E_p/E_s$ (e.g., $\leq 10^3$). It can be concluded that the changes in the $E_p/E_s$ have negligible effect upon the minimum pile radius in pile groups.

## 5.6 Optimal radius in pile groups and its practical application

By taking the advantage of the local minima of total bending strain, the total bending strain at pile head can be reduced effectively. In this subsection, three methods are proposed to mitigate the bending strains in pile groups by appropriately selecting pile radius. This pile radius is defined as "optimal pile radius" of pile groups. In order to demonstrate the applicability of the method developed in this chapter for optimal pile radius in pile groups, a 3×3 hinged pile groups is considered. The following properties of the system are assumed: $H(=L) = 15\ m$, initial pile diameter $d_0 = 0.5\ m$, the density of the pile $\rho_p = 2.4\ t/m^3$, the ratio of the mass density of the pile $\rho_p$ and the soil $\rho_s$ ($\rho_p/\rho_s = 1.43$), Poisson's ratio $\upsilon_s = 0.4$, pile spacing $s/d = 4$ and material damping $\beta_s = 0.05$. It is assumed that fixed-head piles are simultaneously subjected to the seismic excitation $u_g(t) = u_{g0}e^{i\omega_g t}$ at the bedrock and harmonic head loading $V(t) = V_0 e^{i\omega_g t}$. The frequency of excitation is assumed to be equal to the fundamental frequency of the soil layer $\omega = \omega_g$, the geometry of the pile group is sketched in figure 5.79 (section) and figure 5.80 (plan). Different values of the factor $Fr = 10^{-5}, 2\times10^{-5}, 5\times10^{-5}$, the pile-soil stiffness ratio $E_p/E_s = 100\ , 1000$ and the phase lag $\varphi_r = 0, -\pi/2, -3\pi/4$ are chosen to examine the applicability of the proposed method.

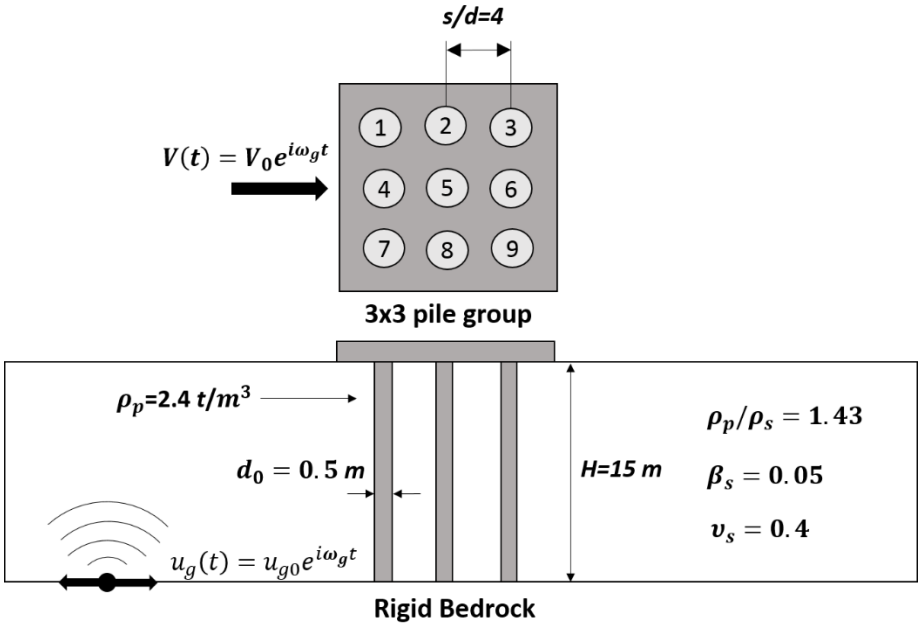


**Figure 5.79:** Cross-section of the 3×3 hinged pile groups and the used soil properties.

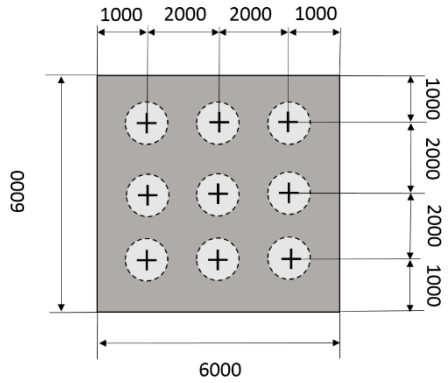


**Figure 5.80:** Plan of the 3×3 hinged pile groups configuration.

### 5.6.1 Ultimate capacity of the pile groups

In order to avoid failure, soil near the surface should have sufficient bearing capacity to support the structural loads. The weight of the superstructure should not surpassed the bearing capacity. Therefore it would be essential to define the weight of the structure based on the compressive ultimate load applied on the top of the pile groups (figure 5.81).

$$(Q_v)_{ult} = Q_p + Q_f \tag{5.21}$$

Where $(Q_v)_{ult}$ is the ultimate bearing capacity of pile, $Q_p$ is the end-bearing capacity, and $Q_f$ is the frictional capacity along the pile perimeter [5.3].

$$Q_p = A_p \sigma'_v N_q \tag{5.23}$$

$$Q_f = pK_s tan\delta \sum_{L=0}^{L=L} \sigma'_{vL}\, \Delta L \tag{5.24}$$

where $N_q$ is the nondimensional bearing capacity parameter and are dependent on the angle of inertial friction of the soil, $\sigma'_v$ is the effective overburden pressure at the pile tip, $A_p$ is the pile tip area, $\sigma'_{vL}$ is the effective vertical stress at a point along the pile length, p is the pile perimeter, $K_s$ is the earth pressure coefficient. for most design purposes, $\delta = 2/3\phi$, $\phi$ is the angle of internal friction. Equation (5.22) may then be rewritten as:

$$(Q_v)_{ult} = Q_p + Q_f = A_p \sigma'_v N_q + pK_s tan\delta \sum_{L=0}^{L=L} \sigma'_{vL}\, \Delta L \tag{5.25}$$

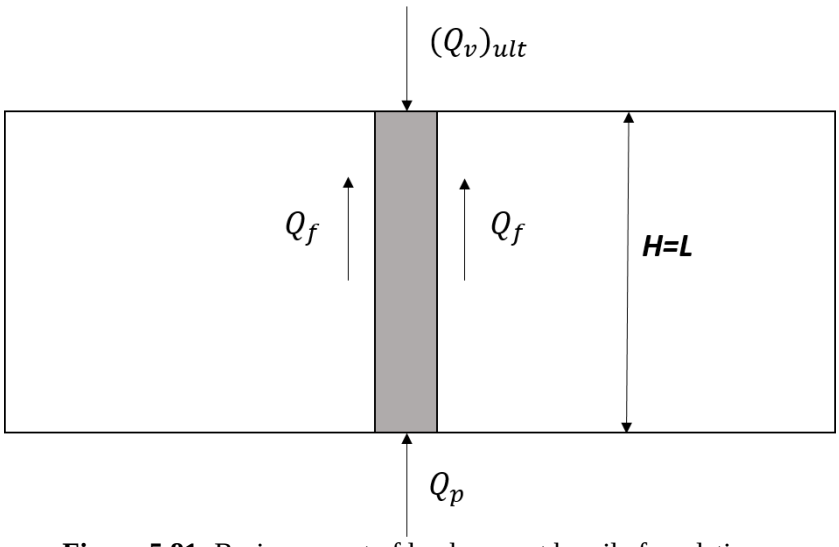


**Figure 5.81:** Basic concept of load support by pile foundations.

It is assumed that the concrete pile is embedded into dry sand, the sand has $\phi = 30^0$ estimate the pile group's allowable load:

$$soil\ density = \gamma_s = 1.6783\ t/m^3 \tag{5.26}$$

$$A_p = \pi/4 * (0.5)^2 = 0.1963\ m^2 \tag{5.27}$$

With reference to [5.3]:

$$N_q = 25 \tag{5.28}$$

$$K_s = 0.5 \tag{5.29}$$

$$\delta = 2/3 * 30^0 = 20^0 \tag{5.30}$$

$$\sigma_v' = 1.6783 * 15 = 27.1745\ t/m^2 \tag{5.31}$$

$$\sum_{L=0}^{L=L} \sigma_{vL}'\, \Delta L = \pi * 0.5 * 0.5 * \tan(20^0) * (0.5 * 1.6783 * 15) * 15 = 188.81 ton \tag{5.32}$$

$$Q_f = \pi * 0.5 * 0.5 * \tan(20^0) * 188.81 = 53.9732 ton \tag{5.33}$$

$$Q_p = \frac{\pi}{4} * (0.5)^2 * 1.6783 * 15 * 25 = 123.575\ \text{ton} \tag{5.34}$$

$$(Q_v)_{ult\ group} = 9 * (Q_p + Q_f) \approx 1600\ ton \tag{5.35}$$

Using a factor of safety, FS , equal to 3

$$(Q_v)_{all\ group} = 1600/3 \approx 533\ ton \tag{5.35}$$

Therefore the weight of the superstructure should be limited by the value of allowable bearing capacity of the pile group. After obtaining total bending strains in each pile, analysis is carried out in reaching the optimal radius in each pile. Three different type of methods are employed to calculate the optimal radius in 3×3 hinged pile group, subsequently each method and corresponding results are discussed.

### 5.6.2 Average method

In this method, the values of the slenderness ratios at local minimum points are averaged by the number of similar piles, for 3×3 pile groups, piles 2,3,5 and 6 are considered for taking the average. By using this

method, optimal pile diameter and pile spacing in pile groups has been obtained for different values of factor $F_r$ ($F_r = 10^{-5}, 2\times10^{-5}, 5\times10^{-5}$) (Table 1) . As shown in figures 5.82 and 5.83, the values of the normalized total bending strains and slendreness ratios corresponding to initial and opimal stage for each pile in the group has been obtained. Moreover, the percent changes between the values of the normalized total bending strains has been calculated (Table 2). For simple case of $F_r = 10^{-5}$, $E_p/E_s = 100$ and the phase lag $\varphi_r = 0$ calculations are given by:

$$(\frac{r}{H})_{opt2} = (\frac{r}{H})_{opt3} = (\frac{r}{H})_{opt6} = 0.033 \tag{5.21}$$

$$(\frac{r}{H})_{opt5} = 0.032 \tag{5.22}$$

$$\text{average}(\frac{r}{H})_{opt} = ((\frac{r}{H})_{opt2} + (\frac{r}{H})_{opt3} + (\frac{r}{H})_{opt5} + (\frac{r}{H})_{opt6})/4 = 0.0328 \tag{5.23}$$

$$d_{opt} = 0.0328 * 15 * 2 = 0.984 \text{ m} \tag{5.24}$$

$$s_{opt} = 4 * \text{d} = 3.936 \text{ m} \tag{5.25}$$

| Phase lag $\varphi_r$ | $Fr\ \times (10^{-5})$ | $E_p/E_s \times (10^2)$ | $d_{opt}(m)$ | $s_{opt}\ (m)$ |
|---|---|---|---|---|
| 0 | *1* | *1* | *0.984* | *3.936* |
| | | *10* | *1.29* | *5.16* |
| | *2* | *1* | *1.23* | *4.92* |
| | | *10* | *Non* | *Non* |
| | *5* | *1* | *1.6425* | *6.57* |
| | | *10* | *Non* | *Non* |
| $-\frac{\pi}{2}$ | *1* | *1* | *0.8775* | *3.51* |
| | | *10* | *1.0725* | *4.29* |
| | *2* | *1* | *1.23* | *4.92* |
| | | *10* | *1.395* | *5.58* |
| | *5* | *1* | *1.4625* | *5.85* |
| | | *10* | *Non* | *Non* |
| $-\frac{3\pi}{4}$ | *1* | *1* | *0.8025* | *3.21* |
| | | *10* | *0.9675* | *3.87* |
| | *2* | *1* | *1.0125* | *4.05* |
| | | *10* | *1.2225* | *4.89* |
| | *5* | *1* | *1.35* | *5.4* |
| | | *10* | *1.68* | *6.72* |

**Table 1:** Optimal pile diameter an pile spacing in 3× 3 hinged pile groups (average method).

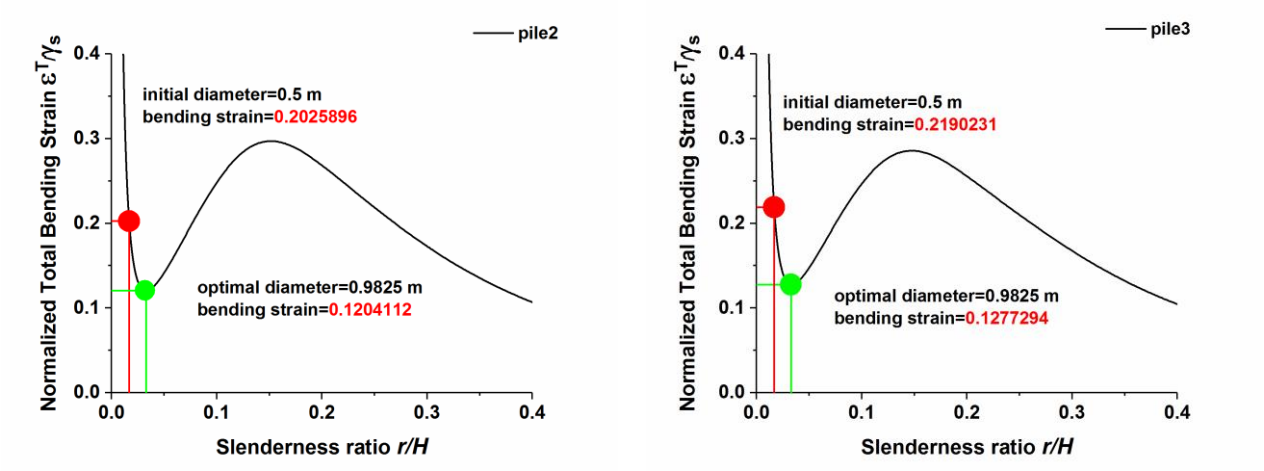


**(a)** **(b)**

**Figure 5.82:** Initial value and optimal value of normalized total bending strains in 3× 3 hinged pile groups (average method)(pile 2 ,3).

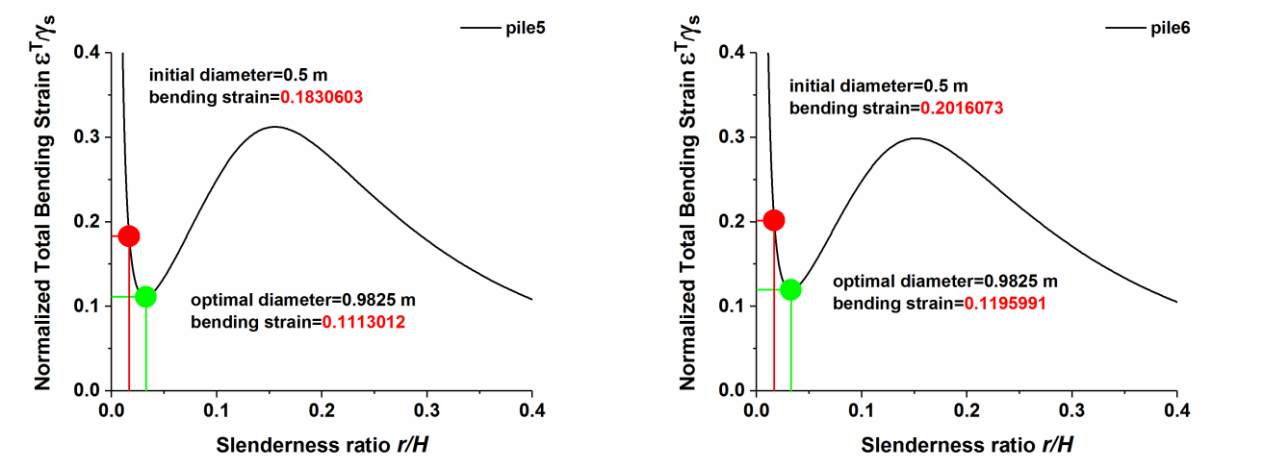


**(a)** **(b)**

**Figure 5.83:** Initial value and optimal value of normalized total bending strains in 3× 3 hinged pile groups (average method)(pile 5 ,6).

| Pile | $(\varepsilon_{pi}/\gamma_s)_0$ | $(\varepsilon_{pi}/\gamma_s)_{opt}$ | Percent change |
|---|---|---|---|
| **2** | 0.2025896 | 0.1204112 | -40.56 |
| **3** | 0.2190231 | 0.1277294 | -41.68 |
| **5** | 0.1830603 | 0.1113012 | -39.20 |
| **6** | 0.2016073 | 0.1195991 | -40.68 |

**Table 2:** Percent changes in the normalized total bending strains between initial vale and optimal values (average method).

### 5.6.3 Weighted average method

In this method, the values of the slenderness ratios at local minimum points are averaged by the number of piles, each value has a specific weight (which is the number of similar piles) assigned to it. By using this method, optimal pile diameter an pile spacing in pile groups has been obtained for different values of factor $F_r$ ($F_r = 10^{-5}, 2\times10^{-5}, 5\times10^{-5}$) (Table 3). As shown in figures 5.84 and 5.85, the values of the normalized total bending strains and slendreness ratios corresponding to initial and opimal stage for each pile in the group has been obtained. Moreover, the percent changes between the values of the normalized total bending strains has been calculated (Table 4). For simple case of $F_r = 10^{-5}$, $E_p/E_s = 100$ and the phase lag $\varphi_r = 0$ calculations are given by:

$$(\frac{r}{H})_{opt2} = (\frac{r}{H})_{opt3} = (\frac{r}{H})_{opt6} = 0.033 \tag{5.26}$$

$$(\frac{r}{H})_{opt5} = 0.032 \tag{5.27}$$

$$\text{average}(\frac{r}{H})_{opt} = (2 * \left(\frac{r}{H}\right)_{opt2} + 4 * \left(\frac{r}{H}\right)_{opt3} + \left(\frac{r}{H}\right)_{opt5} + 2 * \left(\frac{r}{H}\right)_{opt6})/9 = 0.0329 \tag{5.28}$$

$$d_{opt} = 0.0329 * 15 * 2 = 0.987 \text{ m} \tag{5.29}$$

$$s_{opt} = 4 * \text{d} = 3.948 \text{ m} \tag{5.30}$$

| Phase lag $\varphi_r$ | $Fr \times (10^{-5})$ | $E_p/E_s \times (10^2)$ | $d_{opt}(m)$ | $s_{opt}\ (m)$ |
|---|---|---|---|---|
| 0 | *1* | *1* | *0.9870* | *3.9480* |
| | | *10* | *1.32* | *5.28* |
| | *2* | *1* | *1.24* | *4.96* |
| | | *10* | *Non* | *Non* |
| | *5* | *1* | *1.6667* | *6.6667* |
| | | *10* | *Non* | *Non* |
| $-\frac{\pi}{2}$ | *1* | *1* | *0.8833* | *3.533* |
| | | *10* | *1.0867* | *4.3467* |
| | *2* | *1* | *1.24* | *4.96* |
| | | *10* | *1.43* | *5.72* |
| | *5* | *1* | *1.4767* | *5.9067* |
| | | *10* | *Non* | *Non* |
| $-\frac{3\pi}{4}$ | *1* | *1* | *0.8067* | *3.2267* |
| | | *10* | *0.9833* | *3.9333* |
| | *2* | *1* | *1.0167* | *4.0667* |
| | | *10* | *1.2367* | *4.9467* |
| | *5* | *1* | *1.36* | *5.44* |
| | | *10* | *1.7* | *6.804* |

**Table 3:** Optimal pile diameter an pile spacing in 3× 3 hinged pile groups (weighted average method).

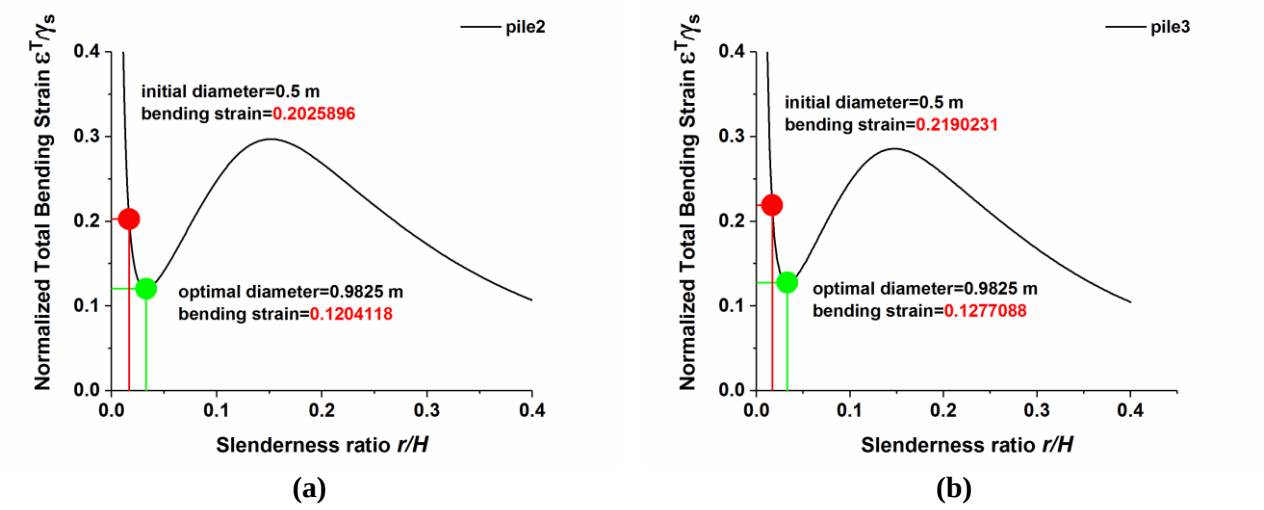


**Figure 5.84:** Initial value and optimal value of normalized total bending strains in 3× 3 hinged pile groups (weighted average method) (pile 2 ,3).

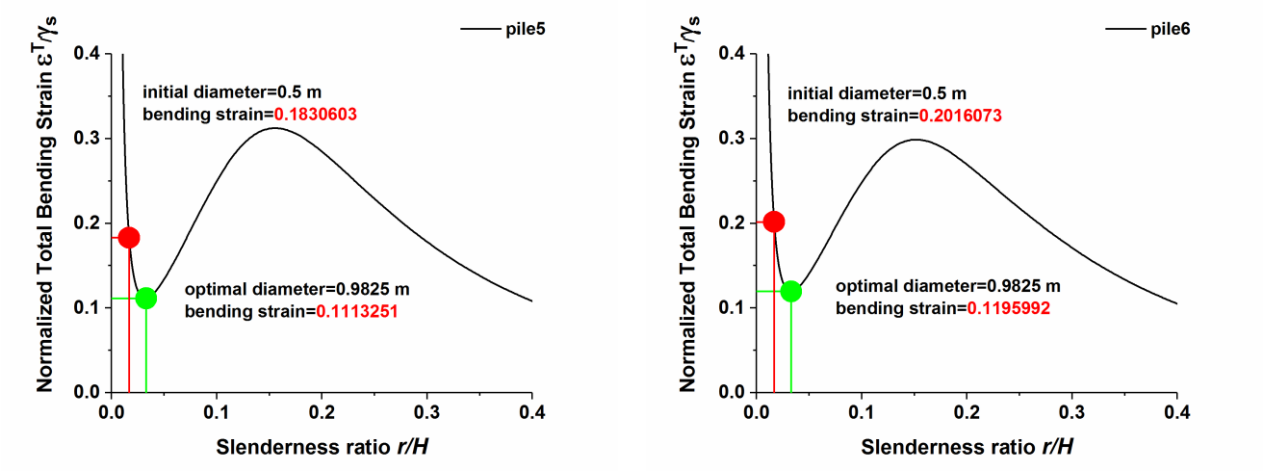


**Figure 5.85:** Initial value and optimal value of normalized total bending strains in 3× 3 hinged pile groups (weighted average method) (pile 5 ,6).

| Pile | $(\varepsilon_{pi}/\gamma_s)_0$ | $(\varepsilon_{pi}/\gamma_s)_{opt}$ | Percent change |
|---|---|---|---|
| **2** | 0.2025896 | 0.1204118 | -40.56 |
| **3** | 0.2190231 | 0.1277088 | -41.69 |
| **5** | 0.1830603 | 0.1113251 | -39.19 |
| **6** | 0.2016073 | 0.1195992 | -40.68 |

Table 4: Percent changes in the normalized total bending strains between initial vale and optimal values (weighted average method).

### 5.6.4 Envelop method

In this method maximum of values of the normalized total bending strains among all piles in each step of analysis are chosen, then the resultant will be the envelope of all maximum vlaues (figure 5.86). By using this method, optimal pile diameter an pile spacing in pile groups has been obtained for different values of factor $F_r$ ($F_r = 10^{-5}, 2\times10^{-5}, 5\times10^{-5}$) (Table 5). As shown in figures 5.87 and 5.88, the values of the normalized total bending strains and slendreness ratios corresponding to initial and opimal stage for each pile in the group has been obtained. Moreover, the percent changes between the values of the normalized

total bending strains has been calculated (Table 6). For simple case of $F_r = 10^{-5}$, $E_p/E_s = 100$ and the phase lag $\varphi_r = 0$ calculations are given by:

$$Max\left\{\frac{\varepsilon_{pi}^{T}(0)}{\gamma_s}\right\} = Max\{\frac{\varepsilon_{p2}^{T}(0)}{\gamma_s}\ \frac{\varepsilon_{p3}^{T}(0)}{\gamma_s}\ \frac{\varepsilon_{p5}^{T}(0)}{\gamma_s}\ \frac{\varepsilon_{p6}^{T}(0)}{\gamma_s}\} \tag{5.31}$$

$$(\frac{r}{H})_{opt} = 0.033 \tag{5.32}$$

$$d_{opt} = 0.033 * 15 * 2 = 0.99 \text{ m} \tag{5.33}$$

$$s_{opt} = 4 * \text{d} = 3.96 \text{ m} \tag{5.34}$$

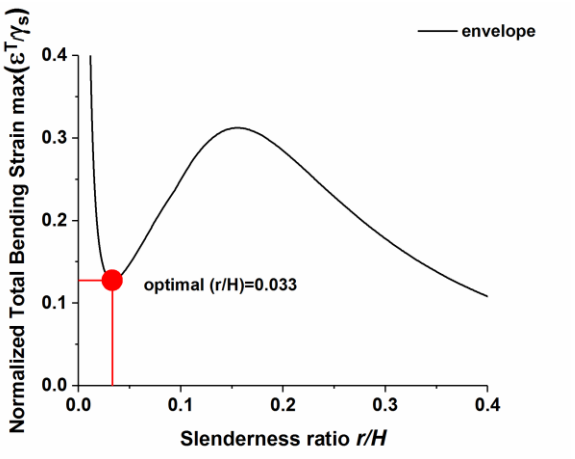


**Figure 5.86:** Optimal diameter of the 3× 3 hinged pile groups with envelope method.

| Phase lag $\varphi_r$ | $Fr \times (10^{-5})$ | $E_p/E_s \times (10^2)$ | $d_{opt}(m)$ | $s_{opt}\ (m)$ |
|---|---|---|---|---|
| 0 | *1* | *1* | *0.99* | *3.96* |
| | | *10* | *1.38* | *5.52* |
| | *2* | *1* | *1.26* | *5.04* |
| | | *10* | *Non* | *Non* |
| | *5* | *1* | *1.71* | *6.84* |
| | | *10* | *Non* | *Non* |
| $-\frac{\pi}{2}$ | *1* | *1* | *0.9* | *3.6* |
| | | *10* | *1.11* | *4.44* |
| | *2* | *1* | *1.26* | *5.04* |
| | | *10* | *1.44* | *5.76* |
| | *5* | *1* | *1.5* | *6* |
| | | *10* | *Non* | *Non* |
| $-\frac{3\pi}{4}$ | *1* | *1* | *0.81* | *3.24* |
| | | *10* | *0.99* | *3.96* |
| | *2* | *1* | *1.02* | *4.08* |
| | | *10* | *1.23* | *4.92* |
| | *5* | *1* | *1.38* | *5.52* |
| | | *10* | *1.7* | *6.804* |

**Table 5:** Optimal pile diameter an pile spacing in 3× 3 hinged pile groups (envelope method).

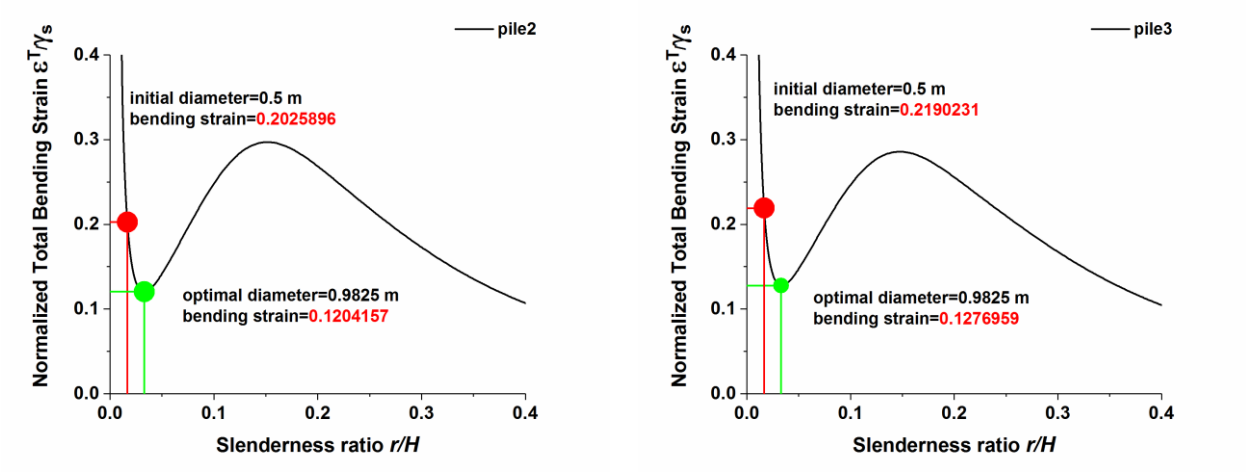


**(a)** **(b)**

**Figure 5.87:** Initial value and optimal value of normalized total bending strains in 3× 3 hinged pile groups (envelope method) (pile 2 ,3).

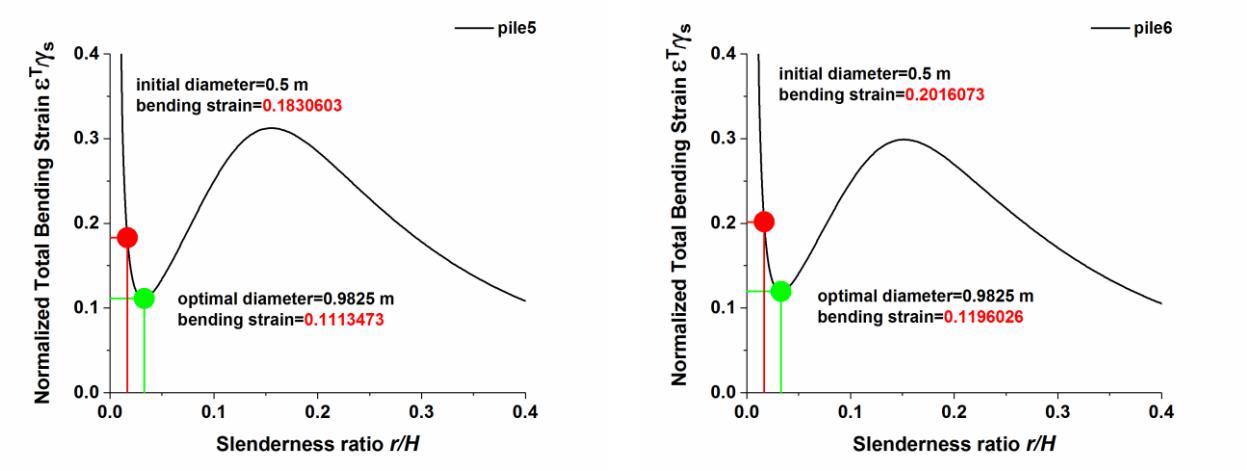


**Figure 5.88:** Initial value and optimal value of normalized total bending strains in 3× 3 hinged pile groups (envelope method) (pile 5 ,6).

| Pile | $(\varepsilon_{pi}/\gamma_s)_0$ | $(\varepsilon_{pi}/\gamma_s)_{opt}$ | Percent change |
|---|---|---|---|
| **2** | 0.2025896 | 0.1204157 | -40.56 |
| **3** | 0.2190231 | 0.1276959 | -41.70 |
| **5** | 0.1830603 | 0.1113473 | -39.17 |
| **6** | 0.2016073 | 0.1196026 | -40.68 |

**Table 6:** Percent changes in the normalized total bending strains between initial vale and optimal values (envelope method).

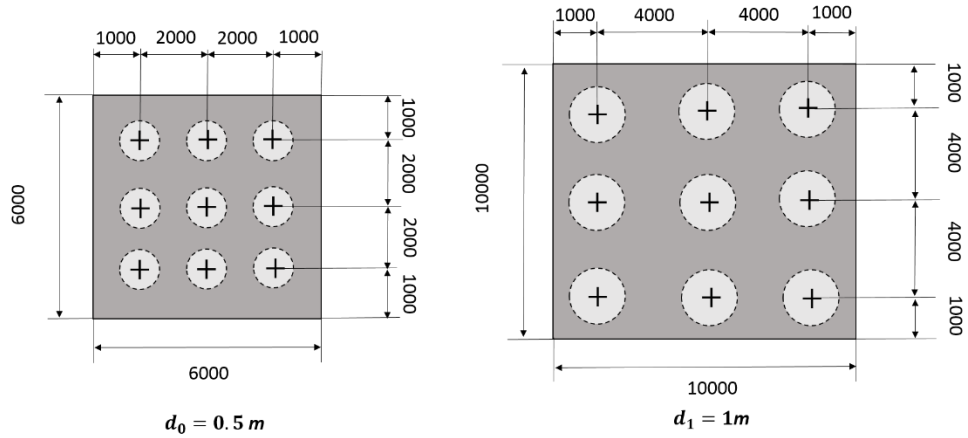


**Figure 5.89:** Initial and optimized configuration of 3×3 hinged pile groups ($\frac{E_p}{E_s} = 100, Fr = 10^{-5}$).

Tables 2,4 and 6 give a comparison of the results obtained by applying three different methods. The percent changes in the values of the normalized total bending indicate that all of them yeild vlues of optimal radius approximately close to each other. In addition, increasing the pile radius makes the spacing between piles in the group increase (figure 5.89). this may increase safety, however, the cost of material and construction will increase. Therefore, optimal radius in pile groups can be defined as the radius in which all piles in the group simultanesouly minimize the total bending strains.

## 5.7 Conclusions

An efficient method has been developed to compute the normalized total bending strains of fixed-head pile groups of finite length embedded in a homogeneous soil layer subjected to both kinematic and inertial harmonic loading. The proposed method allows the total bending strains to be obtained in a closed form formula while using a dynamic Winkler approach in conjunction with an extension to three-dimensions of Novak's plane strain expressions by Mylonakis. The enhanced model is free of the drawbacks of the two-dimensional plane strain model, as it is able to reproduce the cutoff frequency of the soil-pile system. Pile group effect is considered through frequency-dependent interaction factors and the total bending strains are normalized with respect to the mean shear strain of the soil stratum $\gamma_s$. The variation of the normalized total bending strains against slenderness ratio $r/H$ is investigated, revealing valuable insight into the characteristics of the bending strains radius in pile groups. Solutions for pile groups' responses are obtained at the fundamental frequency of the soil stratum.

In pile groups when the slenderness ratios $r/H$ approach zero in all piles, the total bending strains become infinite. Afterwards the total bending strains decrease rapidly up to a local minimum point $r/H \approx (r/H)_{min}$ as the slenderness ratio $r/H$ increases. The local minimum point indicates the presence of optimal case in which bending strains are minimized. After local minimum point, the total bending strains increase almost linearly up to a local maximum point $r/H \approx (r/H)_{max}$. The local maximum point implies

the existence of a particular slenderness ratio $r/H$ that maximizes the total bending strains in pile groups and should, therefore, be avoided.

This chapter shows the normalized total bending strains for various parameters, such as the factor $Fr$, the pile-soil stiffness ratio $E_p/E_s$ and the phase lag $\varphi_r$ indicating the characteristics and the presence of the local minimum and the local maximum in soil-pile group systems. The results of parametric study indicate the dependence of the optimal radius and the optimal bending strains in pile groups on the factor $Fr$, the pile-soil stiffness ratio $E_p/E_s$ and the phase lag $\varphi_r$. As a whole, it appears that the slenderness ratios at local minimum point increases as $Fr$ increases, while the ratios remain unvaried as $E_p/E_s$ and $\varphi_r$ increase. It should be noted that a substantial decrease in the normalized total bending strains at optimal radius would be expected within a range of small $E_p/E_s$ and $Fr$. Moreover, this decrease seems to be more significant for small values of the phase lag $\varphi_r$.

Three different approaches (average, weighted average and envelope) are provided for estimating the optimal radius in pile groups that minimize the normalized total bending strains simultaneously. Each of them can be considered applicable for engineering purposes.

## References


[5.1] Mylonakis, G., Di Laora, R., Mandolini, A. (2014) The Role of Pile Diameter on Earthquake-Induced Bending. In *Perspective on European Earthquake Engineering and Seismology*,. Springer Vol 1. 533-556.

[5.2] Murono, Y., and Nishimura, A. (2000) Evaluation of seismic force of pile foundation induced by inertial and kinematic interaction. *Proceeding,12th world Conference on Earthquake Engineering*, New Zealand, No.1496.

[5.3] Prakash, S., and Sharma, H. (1990) Pile Foundations In Engineering Practice. *John Wiley & Sons*.

# CHAPTER 6

# CONCLUSIONS AND RECOMMENDATIONS FOR FUTURE RESEARCH

## 6.1 Main conclusions

The following summarize some of important findings of this study. As detailed conclusions are provided at the end of each chapter; only major findings are discussed here.

**In chapter 3** , Inertial interaction in soil-pile group systems was analytically investigated through an improved plain strain model by combining the concepts of Winkler support and frequency-dependent interaction factors. The proposed method yields the variation of normalized inertial bending strains with slenderness ratio $r/H$ at the head of fixed-head pile groups resting on rigid base, embedded in a homogeneous viscoelastic soil stratum. Analysis was carried out for different boundary conditions in fundamental frequency of the soil layer. Rigorous numerical solutions based on coupled finite elements-boundary elements (FE-BE) were employed to validate the predictions of the proposed method. It was founded that the proposed method convincingly match with the numerical results for soil-pile group systems.

**In chapter 4** , a theoretical method was developed for the analysis of fixed-head pile groups in a homogeneous viscoelastic soil stratum over a rigid base under vertical impinging seismic shear waves in fundamental frequency of the soil layer. Within the framework of improved plain strain model and frequency-dependent interaction factors, a solution was developed to quantify the variation of normalized kinematic bending strains with slenderness ratio $r/H$ at the head of each pile in pile groups with different tip conditions. It was concluded that:

- Results of normalized kinematic bending strains in pile groups follow closely corresponding results obtained from rigorous FE-BE solutions.

- The combined influence of pile-soil stiffness ratio $E_p/E_s$, pile spacing $s/d$ and the number of piles *N* on normalized kinematic bending strains in pile groups are investigated. It was founded that for slenderness ratios $r/H$ below the location of the maximum, the kinematic bending strains of the piles in a group can always be approximated by that of the single pile regardless of pile group configurations. Moreover practical range of slenderness ratio $r/H$ might be from 0.01 to 0.1. Within that range, the normalized kinematic bending strains may increase almost linearly.

**In chapter 5** , a theoretical method was derived for the analysis of fixed-head pile groups in a homogeneous viscoelastic soil stratum over a rigid base under simultaneous effect of superstructure forces (inertial interaction) and vertically-propagating shear waves (kinematic interaction). Different tip conditions (hinged and fixed) have been taken into account. With an understanding the importance of fundamental frequency of the soil layer, such specific frequency was targeted in this chapter. Normalized total bending strains were expressed in terms of slenderness ratio $r/H$. In order to investigate the fundamental characteristics of normalized total bending strains in pile groups, the effects of important parameters (the factor $Fr$, the pile-soil stiffness ratio $E_p/E_s$ ,the phase lag $\varphi_r$, pile spacing s/d and the number of piles *N*) were considered. The main conclusions of this chapter are:

- Obtained results imply the presence two extreme points, local minimum points which minimizes the normalized total bending strains (optimal pile radius) and local maximum points which maximizes the normalized total bending strains.

- The factor $Fr$, the pile-soil stiffness ratio $E_p/E_s$ and the phase lag $\varphi_r$ have strong influence on the presence of the optimal radius and the optimal bending strains in pile groups. Optimal points are more easily generated as $Fr$ and $E_p/E_s$ becomes smaller. In addition, the normalized bending strains at the local minimum points gradually decrease as the phase lag $\varphi_r$ decreases. It appears

that the value of the slenderness ratios at local minimum points increases as $Fr$ increases, while the ratios remain unvaried as $E_p/E_s$ and $\varphi_r$ increase.

- Three different methods can be used for estimating the optimal radius in pile groups. Each of them can be applied for engineering purposes.

## 6.2 Limitations

Notwithstanding the usefulness and practical appeal of this study is limited by simplifying assumptions of linearity in soil and the pile material, of a perfectly contact between soil and pile, and the adoption of the superposition principle for pile-to-pile interaction. Therefore, revisions are required in presence of strongly non-linear effects in the soil. In order to calculate the optimal pile radius in cases when the local minimum and local maximum disappear, increasing the pile dimatere would be appropriate solution to decrease the total bending strains. However, this solution increases the value of optimal pile radius and pile spacing $s/d$ in pile groups, subsequently, this makes the piles become large-diameter shafts and the cost of materials and construction methods may increase. By increasing the number of piles in pile groups, local minimums and maximums appear on the normalized total bending strains curves, therefore use of optimal pile radius concept for pile groups may leads to erroneous results.

## 6.3 Recommendations and future research

Recommendations for future research include: (i) incorporation of the non-linearity of the soil into the models, (ii) incorporation of inhomogeneity or layered soil deposits in analysis of lateral pile motion, (iii) extension of the analysis in time domain through FFT algorithms to establish a criteria for optimal pile radius in pile groups, (iv) extension of the method for soil-pile groups systems under impinging P or Rayleigh waves, (v) incorporate the contribution of superior modes of vibration in the case of deeper soil deposits.